

# Effect of stochastic material properties on the structural response of laminated composite materials

following the building block approach



Athanasios Droutsas



# Effect of stochastic material properties on the structural response of laminated composite materials

following the building block approach

By

Athanasios Droutsas

in partial fulfilment of the requirements for the degree of

**Master of Science**

in Offshore & Dredging Engineering

at the Delft University of Technology,  
to be defended publicly on February 26, 2018 at 15:00 PM.

Supervisor:	Prof. dr. ir. M. Kaminski	TU Delft
Thesis committee:	Dr. D.Zarouchas,	TU Delft
	Dr.P.Maljaars	TU Delft
	Dr. D. Schraven,	TU Delft
	Ir. J. Broekhuijsen,	Damen Schelde Naval Shipbuilding

*This version of the thesis is not confidential.*



# Preface

This thesis focuses on the material properties of glass fiber reinforced composites that are used to create large scale components which can be part of a vessel's hull. It is aimed to undergraduate or graduate students as well as professionals who want to take into account the stochastic nature of the material properties especially when they are used for large applications. Generally, it is common to give deterministic values at the material properties and then adjust the design according to partial safety factors. However, this thesis approaches the same problem without the use of partial safety factors and describes a method with which the structural response of a glass fibre laminated composite can be predicted accurately by implementing a statistical analysis on the strength and stiffness properties. The aforementioned method is a combination of statistics and the commonly known "*building block approach*" which provides the necessary steps that have to be followed before a 1:1 scale element can be analysed.

This report goes in pair with its supporting document. Generally, a lot of theories/techniques that are used here are explained in the supporting document. That was done on purpose in order to make this report easily readable. Hence, readers that are not familiar with a topic can visit the respective (sub)chapter in the supporting document and find the academic background of the theory that was implemented. A merge of the two documents would lead to a lengthy report that would be tedious and cumbersome.

To conclude, this report along with its supporting document, covers the design of small scale coupons, their manufacturing, their testing, their statistical analysis and the prediction of the structural response of large scale specimens using FEM along with the verification from experiments. Both analytical calculations using Matlab and finite element analyses using Ansys are implemented. On the other hand, at this report, one wouldn't find detailed information regarding the different production methods and the environmental factors which can have a noticeable effect on the composite's material properties.

*A. Droutsas Author  
Delft, February 2018*

# Acknowledgements

I feel obliged to acknowledge the help of certain people without whom, the implementation of this thesis wouldn't be possible. Firstly, from TUDelft's side, I would like to thank the head of my examination committee, Mirosław Lech Kaminski, whose input was crucial for my thesis and his feedback led to the substantial amelioration of the thesis' content. Moreover, I would like to thank Dimitrios Zarouchas who was my daily supervisor and he was always present when I needed him, giving me clear and particular directions. Our regular meetings helped me to express my ideas in a more consistent way and he was always there to discuss and support my planning regarding the development of such a complex topic. Finally, I would like to thank Daan Schraven who was my daily supervisor at the project management part of this thesis and helped me significantly towards the preparation of it.

This thesis was performed as part of a bigger project regarding the construction of Mine Counter Measure Vessels which is being performed by Damen Schelde Naval Shipbuilding (DSNS). Hence, I couldn't do else but recognise the enormous support that I had from the company's side and more specifically, the help I had by Joep Broekhuisjen who was my daily supervisor. Our meetings were of critical importance as he imparted to me vital information about the execution of such a multifaceted project. His input clarified the company's requirements from this project and helped me not to deviate from the core of the problem that had to be answered. Furthermore, I would like to thank my colleagues, Cedric Verhaeghe and Marcel Elenbaas who were always available to give me an experienced approach on the construction of structures made of composite materials.

Last but not least, I would like to thank my family as well as my girlfriend Marlies for their remarkable support during the pressing period up to the completion of this thesis.

# Contents

Preface .....	i
Acknowledgements.....	ii
Contents .....	iii
List of Figures .....	iv
List of Tables .....	vi
Nomenclature .....	viii
Abstract .....	xi
Chapter 1: Introduction.....	1
1.1 Thesis' objective .....	2
1.2 Approach towards thesis' objective .....	3
Chapter 2: Small Scale Coupons .....	5
2.1 Design of Coupons .....	5
2.1.1 Tensile tests .....	6
2.1.2 Compressive coupons .....	7
2.1.3 Shear tests .....	8
2.2 Preparation of Panels.....	9
2.3 Tests description.....	10
2.3.1 Tensile tests .....	10
2.3.2 Compressive Tests .....	11
2.3.3 Shear Tests .....	12
2.3.4 Strain gauges.....	13
2.4 Experimental results for small scale coupons.....	13
2.4.1 Strength Properties.....	13
2.4.2 Stiffness Properties.....	14
2.4.3 Fiber Volume, density tests.....	14
2.5 Discussion of small scale coupon test results .....	14
Chapter 3: Statistics.....	17
3.1 Assign distributions to the material properties .....	18
3.2 Verification of the Matlab model .....	23
3.3 Generate correlated variables .....	26
3.4 Bootstrap Method.....	29
Chapter 4: Large Scale Specimens.....	31
4.1 Manufacturing of large Scale Specimens .....	31
4.1.1 Monolithic Panels.....	31
4.1.2 Sandwich Panels .....	32
4.2 Modelling of large scale specimens' experiments.....	33
4.2.1 Introduction of Imperfections.....	34
4.2.2 Modelling of Non-linear Static Analysis .....	37
4.2.3 Results of non-linear Static Analysis .....	40
4.2.4 Calibration for the horizontal forces.....	44
4.2.5 Non-linear Static analysis, Results with linear springs.....	46
4.2.6 Discussion of the results for the non-linear static analysis with springs, deterministic model.....	49

4.2.7 Introduction of stochastic nature of material properties .....	50
Chapter 5: Conclusions .....	57
Chapter 6: Project Planning .....	61
6.1 MCMV Project – Basic Information.....	62
6.1.1 Hull’s Structural Elements.....	62
6.1.2 Superstructure’s Structural Elements .....	65
6.2 Cost house.....	67
6.3 Cost comparison between steel and composite structure.....	73
6.4 Project Planning/Cost Estimation .....	76
6.4.1 Stochastic analysis for time and costs .....	78
6.5 Conclusions .....	86
Chapter 7: Recommendations.....	88
7.1 Recommendations for the technical part.....	88
7.2 Recommendations for the Integrated Design Management.....	89
References .....	90
Appendix A .....	92
Appendix B .....	93
B.1 Manufacturing of Panels .....	93
B.2 Received panels from Applus+ .....	95
B.3 Construction of Coupons .....	96
Appendix C .....	97
C.1 Test set-ups .....	97
C.1.1 Tensile Test Set-Up.....	97
C.1.2 Compressive Test Set-Up .....	98
C.1.3 Shear Test Set-Up .....	99
C.2 Testing devices .....	100
C.2.1 Tensile Test device (in German).....	100
C.2.2 Compressive Test device (in German) .....	102
C.2.3 Hydraulic Grips.....	104
C.2.4 Shear Test device .....	107
Appendix D .....	109
Appendix E .....	110
Appendix F .....	121
Appendix G .....	122
Appendix H.....	123
Appendix I.....	124
Appendix K .....	127
Appendix IDM-A.....	128

## List of Figures

Figure 1-1: Stan Pilot 2205 FRP, Damen Shipyards Group <sup>[3]</sup> .....	1
Figure 1-2: Visby Convert, Source: Ref [4].....	1
Figures 3-1:Cumulative distribution Functions, Experimental Data .....	22

Figure 3-2: CDFs, Experimental Data, PhD dissertation, Case: $X_T$ .....	26
Figure 3-3: Workflow, Generate correlated variables for samples that follow different distributions .....	27
Figure 3-4: Correlated random variables, $S_{11T}$ & $E_{11}$ .....	28
Figure 3-5: Correlated random variables, $S_{22T}$ & $E_{22}$ .....	28
Figure 3-6: Correlated random variables, $S_{12}$ & $G_{12}$ .....	28
Figure 3-7: Bootstrap Method, Distribution of the mean Values.....	30
Figure 4-1: 3 point bending test, monolithic panel.....	33
Figure 4-2: Geometry of panels (left figure), boundary conditions (right figure).....	34
Figure 4-3: Cases of boundary conditions for the introduction of imperfections.....	35
Figure 4-4: 1 <sup>st</sup> monolithic Panel 1 <sup>st</sup> mode, Case:1.....	36
Figure 4-5: 1 <sup>st</sup> monolithic Panel 2 <sup>nd</sup> mode, Case:1.....	36
Figure 4-6: 1 <sup>st</sup> monolithic Panel 3 <sup>rd</sup> mode, Case:1.....	36
Figure 4-7: Initial Imperfections, Non-normalized(left) and normalized(right) values.....	37
Figure 4-8: Boundary conditions and introduction of loading.....	38
Figure 4-9: Vertical force-displacement curves, 1 <sup>st</sup> sandwich Panel.....	41
Figure 4-10: Vertical force-displacement curves, 2 <sup>nd</sup> sandwich Panel.....	42
Figure 4-11: Vertical force-displacement curves, 1 <sup>st</sup> monolithic Panel.....	42
Figure 4-12: Vertical force-displacement curves, 2 <sup>nd</sup> monolithic Panel.....	43
Figure 4-13: Left Support, zoom-in, 2 <sup>nd</sup> monolithic panel.....	43
Figure 4-14: Combin14 spring element <sup>[31]</sup> .....	44
Figure 4-15: Monolithic specimen, top view with springs (left), rotating support(right).....	46
Figure 4-16: Vertical force-displacement curves, 1 <sup>st</sup> sandwich Panel, for comparison.....	47
Figure 4-17: Vertical force-displacement curves, 2 <sup>nd</sup> sandwich Panel, for comparison.....	47
Figure 4-18: Vertical force-displacement curves, 1 <sup>st</sup> monolithic Panel, for comparison.....	48
Figure 4-19: Vertical force-displacement curves, 2 <sup>nd</sup> monolithic Panel, for comparison.....	48
Figure 4-20: Photo of 2 <sup>nd</sup> monolithic panel before it was unmounted from the testing frame, obvious introduction of horizontal forces.....	50
Figure 4-21: Vertical force displacement curve, 1 <sup>st</sup> sandwich panel.....	52
Figure 4-22: Vertical force displacement curve, 2 <sup>nd</sup> sandwich panel.....	52
Figure 4-23: Vertical force displacement curve, 1 <sup>st</sup> monolithic panel.....	53
Figure 4-24: Vertical force displacement curve, 2 <sup>nd</sup> monolithic panel.....	53
Figure 6-1: Chapter's Workflow.....	61
Figure 6-2: Concept Design.....	62
Figure 6-3: Structural Elements, Panels.....	62
Figure 6-4: Hull, graphical representation.....	63
Figure 6-5: Hull's shell panels.....	63
Figure 6-6 Hull's deck panels.....	64
Figure 6-7: Hull's bulkhead panels.....	64
Figure 6-8: Superstructure's elements.....	65

Figure 6-9: Top view of superstructure's shells .....	66
Figure 6-10: Steel hull mould (in segments).....	69
Figure 6-11: SIGMA 7513 .....	75
Figure 6-12: Structural elements of SIGMA 7513.....	75
Figure 6-13: Unexpected delays .....	83
Figure 6-14: Total costs breakdown, Production in the Netherlands .....	84
Figure 6-15: : Total costs breakdown, Production in Turkey .....	85

## List of Tables

Table 2-1: Testing Plan .....	5
Table 2-2: Test machine for tensile tests .....	11
Table 2-3: Test machine for compression tests.....	12
Table 2-4: Test Machine for Shear Tests .....	13
Table 2-5: Strength Properties, Experimental Results .....	13
Table 2-6: Strength Properties, Experimental Results .....	14
Table 2-7: Fiber Volume & density Experimental Results .....	14
Table 2-8: Correlation of properties extracted from the same results.....	15
Table 3-1: Properties included in the statistical Analysis.....	17
Table 3-2: Chosen Distributions .....	19
Table 3-3: Results from MLE.....	20
Table 3-4: Results from Kolmogorov-Smirnov goodness of fit criterion.....	22
Table 3-5: Distributions that best fit the experimental data .....	23
Table 3-6: Randomly chosen experimental results, PhD dissertation <sup>[9]</sup> .....	24
Table 3-7: Comparison of PhD results with Matlab model, Data: Tensile strength with loading at 0° .....	25
Table 3-8: Comparison of PhD results with Matlab model, Data: In plane Poisson's Ratio with loading at 0° .....	26
Table 4-1: Materials used for the construction of the monolithic panels.....	32
Table 4-2: Materials used for the construction of the sandwich panels .....	32
Table 4-3: Material Properties for 100 simulations .....	51
Table 6-1: Typical thicknesses of hull's shell panels .....	64
Table 6-2: Typical thicknesses of hull's deck and bulkhead panels .....	65
Table 6-3: Superstructure's panels .....	66
Table 6-4: Ship's Geometrical Parameters .....	67
Table 6-5: Material Cost Parameters .....	68
Table 6-6: Scrap rates & resin absorption.....	68
Table 6-7: Non-recurring costs.....	69
Table 6-8: Steel hull mould cost.....	69

Table 6-9: Costs for the foundations of the vessel .....	70
Table 6-10: Unstiffened hull production, activities and man-hours (outer shell) .....	71
Table 6-11: Unstiffened bulkhead/decks production, activities and man-hours.....	71
Table 6-12: Deck/Bulkhead fixation in the hull, activities and man-hours.....	72
Table 6-13: Unstiffened superstructure production, activities and man-hours.....	72
Table 6-14: Peel preventer application, activities and man-hours .....	73
Table 6-15: Labor rates .....	73
Table 6-16: Ship's Geometrical Parameters .....	74
Table 6-17: Steel structure, rough approximation .....	74
Table 6-18: Man-hours explained, steel structure .....	75
Table 6-19: Non-recurring costs for steel structure, explanation .....	75
Table 6-20: Composite Structure, rough approximation .....	76
Table 6-21: Cost Comparison, Steel-Composite Structure .....	76
Table 6-22: Production of Decks/Bulkheads, difference between Gantt chart and reality .....	77
Table 6-23: Triangular distribution <sup>[19]</sup> .....	78
Table 6-24: Assumed Triangular distributions .....	80
Table 6-25: Activities with distributions other than type #1 .....	81
Table 6-26: Total Cost and time needed .....	83

# Nomenclature

$A_{ij}$	Extensional stiffness matrix
ASM	American Society for Metals
ASTM	American Society for Testing and Materials
$B_{ij}$	Axial-Bending coupling stiffness matrix
cdf	cumulative density function
CLT	Classical Lamination Theory
$D_{ij}$	Bending stiffness matrix
DMO	Defense Material Organization
DSNS	Damen Schelde Naval Shipbuilding
FAW	Fiber Aerial weight
FEA	Finite Element Analysis
$G_{12}$	Shear Modulus in “1”, “2” plane
$G_{23}$	Shear Modulus in “2”, “3” plane
$G_{13}$	Shear Modulus in “1”, “3” plane
GRP	Glass reinforced polymers
icdf	Inverse cumulative function
LV	Last visited(references)
pdf	probability density function
QI	Quasi-Isotropic
VARTM	Vacuum Assisted Resin Transfer Molding

## Greek Letters

$\gamma_{12}$	Engineering shear strain in the “1” , “2” plane
$\gamma_{23}$	Engineering shear strain in the “2” , “3” plane
$\gamma_{13}$	Engineering shear strain in the “1” , “3” plane
$\gamma_{xy}$	Engineering shear strain in the “x” , “y” plane
$\gamma_{yz}$	Engineering shear strain in the “y” , “z” plane
$\gamma_{xz}$	Engineering shear strain in the “x” , “z” plane
$\epsilon_1$	Axial Strain at principal (“1”) direction
$\epsilon_2$	Transverse Strain, lateral to principal (“2”) direction
$\epsilon_3$	Strain at the vertical (“3”) direction
$\epsilon_{12}$	Tensor shear strain in the “1” , “2” plane
$\epsilon_{23}$	Tensor shear strain in the “2” , “3” plane
$\epsilon_{13}$	Tensor shear strain in the “1” , “3” plane
$\epsilon_{xy}$	Tensor shear strain in the “x” , “y” plane
$\epsilon_{yz}$	Tensor shear strain in the “y” , “z” plane
$\epsilon_{xz}$	Tensor shear strain in the “x” , “z” plane
$E_1$	Elastic modulus in the “1”-direction, (Axial)
$E_2$	Elastic modulus in the “2”-direction, (Transverse)
$E_3$	Elastic modulus in the “3”-direction, (Vertical)
$\nu_{12}$	Poisson’s ratio for transverse strain in “2” direction when stresses in the “1” direction
$\nu_{23}$	Poisson’s ratio for transverse strain in “3” direction when stresses in the “2” direction
$\nu_{13}$	Poisson’s ratio for transverse strain in “3” direction when stresses in the “1” direction
$\sigma_1$	Normal stress in the “1” direction
$\sigma_2$	Normal stress in the “2” direction

$\sigma_3$	Normal stress in the “3” direction
$\sigma_x$	Normal stress in the “x” direction, (Axial)
$\sigma_y$	Normal stress in the “y” direction, (Transverse)
$\sigma_z$	Normal stress in the “z” direction, (Vertical)
$\tau_{12}$	Shear stress in the “1” , “2” plane
$\tau_{23}$	Shear stress in the “2” , “3” plane
$\tau_{13}$	Shear stress in the “1” , “3” plane
$\tau_{xy}$	Shear stress in the “x” , “y” plane
$\tau_{yz}$	Shear stress in the “y” , “z” plane
$\tau_{xz}$	Shear stress in the “x” , “z” plane

# Abstract

The version of the thesis below is the non-confidential one. The initial, confidential version contained sensitive information regarding the materials used for the construction of the hull of Mine Counter Measure Vessels and as a result some information has to be omitted. For values shown as *XX* please contact Joep Broekhuijsen ([J.Broekhuijsen@damennaval.com](mailto:J.Broekhuijsen@damennaval.com)) . However, this thesis contains all the parts of the initial document that have an added academic value.

This report, which from now and onwards will be called the main body of the thesis, covers the core of the problem that has to be solved. Generally, the aim of this thesis is to investigate a laminated composite's structural response, made of FRP, when its material properties are assumed stochastic instead of deterministic. The materials shown in this thesis are investigated as part of a bigger project that concerns the construction of several Mine Counter Measure Vessels.

In this document, the main focus is given on the results of experiments and/or analytical calculations whereas the theories/methods used to extract these results are presented in the supporting document. As a result, readers that are familiar with statistics, classical lamination theory, FEA modeling among others, can easily read this report without coming across knowledge that they already have. In general, this document covers the writer's contribution to academics whereas the supporting document gives an extensive explanation on what was used in this document. Below, a brief explanation is given on what can be found at each individual chapter.

At chapter 1(introduction), one can find a brief description about what a composite material is, along with some modern applications in the marine industry. Moreover, the procedure that was followed throughout the thesis towards the thesis' objective is depicted concisely which gives the frame of work to readers.

At chapter 2, the coupon testing procedure is showed, including the design, the manufacturing, the cutting and the testing of the small scale coupons. The procedure is unveiled step by step while it is supported by the figures shown in Appendices **A – E**. At the end of the chapter the experimental results are presented along with a discussion about them. In total the testing plan included 15 tests for each one of the in plane properties and 6 tests for the shear out of plane properties. The testing plan also included density tests along with fiber volume tests that were implemented to verify if the coupons were manufactured according to the designs.

At chapter 3, the experimental results are used as input for the statistical analysis. The maximum likelihood estimates is being used to determine the parameters of 9 distributions that were chosen as the most probable ones to describe each individual material property. Then, the distribution that best fits to each material property is determined through the Kolmogorov-Smirnov goodness of fit criterion. The results of the model built by the writer are verified with a PhD where the same procedure was used. Then, the inputs for the FEA model were generated in Matlab where the Cholesky decomposition method is used because it was desired to take into account the correlation of the material properties that were extracted from the same experiments.

The 4<sup>th</sup> chapter concerns the large scale specimens. Information about their design and their production is given which is supported by Appendices **F - G**. Then the focus is given on the finite element modelling of

these panels. By using as inputs the output from the statistical analysis, the structural response of large laminated composite panels and more specifically of 2 monolithic and 2 sandwich panels under 3 point bending is predicted within a 95% confidence interval and is being compared with the experimental results.

At chapter 5, the conclusions are presented regarding the procedure that was followed in the previous chapters.

At chapter 6, an approach from the project's management perspective is given by comparing the total costs of an a-magnetic steel structure with one made of composite materials. The cost comparison is made in an aggregate level which is followed by the detailed planning/cost estimation of a composite's hull & superstructure manufacturing where the stochastic nature of the time needed for each activity is included. At the end of this chapter the conclusions of this study are presented

Finally, at chapter 7, recommendations for future work are presented which can lead to amendment of the procedure followed at both the technical part (chapters 1-5) and the financial one (chapters 6-7).

# Chapter 1: Introduction

The need of more and more sophisticated structures has led to the extensive research for the development of new materials or the amelioration of the existing ones. A “family” of these materials is called composite materials as they are the product of a combination between at least two different materials with distinct properties. In a more scientific way, “*a composite material is a structural material that consists of two or more combined constituents that are combined at a macroscopic level and are not soluble in each other*”<sup>[1]</sup>. The next step is to define these two materials which can vary according to the specific application for which they will be used.

During this thesis, an investigation is implemented only on composite materials made of continuous fibers embedded in a matrix. This type of material is found in many variations at structures around us, in several industries such as the automotive, aerospace and of course the marine industry among others. Its attractive strength and stiffness properties among many other that they have, has led to thorough research in order to fully understand its structural behavior and as a result nowadays we encounter more and more applications of this material. A whole book can be written on the applications of composite materials, but that would be tedious and outside of the scope of this thesis. Hence, this thesis focuses on composite materials that are used in the marine industry and more specifically for the construction of the hull and superstructure of a Mine Counter Measure Vessel (MCMV). The introduction of composites in the marine industry started in 1965<sup>[2]</sup> and since then, the production of composite offshore structures has increased dramatically. A modern application of composite structures in the marine industry constructed by Damen Group is given in figure 1-1 whereas in figure 1-2 one of the most famous examples of vessels made of composite materials (sandwich panels with carbon fibers) is shown which is part of the Swedish Visby class.



Figure 1-1: Stan Pilot 2205 FRP, Damen Shipyards Group<sup>[3]</sup>



Figure 1-2: Visby Converté, Source: Ref [4]

DSNS is part of the Netherlands-based Damen Group, which designs and builds ships of various types and purposes, including military and civilian ships, tugs, offshore support vessels, yachts and ferries<sup>[3]</sup>. Inside this

group, DSNS focuses on the construction of special vessels (for example fishery research vessels, Antarctic research vessels etc) and mainly on the construction of military vessels. Hence, due to the fact that this thesis was implemented as part of the preparation from DSNS' side for a potential order of MCMVs from the Royal Dutch Navy, focus is given on the composite materials that will be used for such a vessel. One of the main reason that this material is opted for MCMVs, has to do with its low magnetic field which renders them invisible to magnetic mines. More information about the significance of the up to date MCMVs is given in the subchapter 1.1 of the supporting document. There, it is also explained the current status of the Dutch MCMVs and the collaboration with the Belgian and French Navy. Last but not least, it is expected that the procedure for the replacement of the current MCMVs, i.e. the Alkmaar Class vessels, will start in the Spring 2018 as at least Belgian authorities have already decided to proceed with the acquisition of 6 new vessels.

As it was explained in the previous paragraph, the materials under investigation at this thesis will be used for the construction of MCMVs. As the first step at the well-known in the aerospace industry *building block approach* (subchapter 1.4 in the supporting document), it was decided that the most cost effective solution would be to design the hull with monolithic panels and the superstructure with sandwich panels in order to be light and provide the vessel with better stability. A combination of XX fibers with XX resin and with a fiber volume  $V_f = XX\%$  will be used for the construction of the load-carrying elements. Regarding the sandwich panels, the core will be made of XX which is a partially linked, structural cellular XX foam, developed for marine applications among others. Readers that are interested into the details of the fibers and the resin are suggested to read subchapters 1.2-1.3 of the supporting document which accompanies this thesis.

## 1.1 Thesis' objective

It is pretty significant to define from the start what is the purpose of this thesis. The aim is to create an "algorithm" which can be used to predict the structural behavior of large composite monolithic and sandwich panels under 3 point bending within a certain confidence level. Towards this goal, small scale coupons have to be tested in order to define the material properties of the composite under investigation and then statistically analyze the experimental results in order to take into account the stochastic nature of the material properties. To put it in other words, it is desired to investigate the effect of stochastic material properties on the structural response of large composite panels. As a result, instead of having one structural response for a specific type of loading, a spectrum of structural responses will be extracted which will be based on the stochasticity of the material properties themselves. By checking the width of the aforementioned spectrum, conclusions can be made of this algorithm's adequacy to predict the response of the large composite panels and its capability of avoiding the expensive and time consuming mid-scale tests. Furthermore, a model able to take into account the stochasticity of the material properties combined with a model that does the same for the loading conditions can potentially lead to thinner/cheaper structural elements when comparing with the design by the norms that inherently have big safety factors.

## 1.2 Approach towards thesis' objective

Towards the completion of the objective that is described above, a sequence of steps has to be followed. By keeping the building block approach as the basic theory of the analysis, the specific composition of the composite material has to be decided which in that case is composed of XX fibers embedded in XX resin with a  $V_f = XX\%$  (supporting document [4.1.1.2](#)). Then, as part of the block 3 of the building block approach (supporting document [1.4.1.3](#)), 87 small scale coupon tests should be performed in order to define the in-plane as well as the out-of plane strength and stiffness properties of the composite material under investigation. Moreover, towards the acquisition of knowledge of the composite material, density tests have to be implemented and then fiber volume tests, which determine the quality of the produced coupons. The next step is to implement a statistical analysis on the material properties in order to assign the distribution that best fits to each one of them and include any potential correlation between them. Up to this point, all the necessary steps have been performed for the preparation of the FEM analyses that would define the success of the thesis' outcome. Hence, as the last step, a finite number of simulations will be run in Ansys where each simulation will use a different combination of material properties; each one of these combinations will be an aftereffect of the statistical analysis. To conclude, I hope that readers have a clear, brief idea about what they should expect in the coming chapters of the thesis.



# Chapter 2: Small Scale Coupons

During this chapter, the preparation of the coupons that were tested is given along with their experimental results. The testing plan included 15 tests for each one of the in-plane material property as well as 6 tests for each one of the out-of plane shear properties. The details of the testing plan are shown in the following table:

Quantity	Test	Norm	In order to define:
15	Tensile 0°	ASTM D3039	$S_{11T}, E_{T,11}, \nu_{12}$
15	Tensile 90°	ASTM D3039	$S_{22T}, E_{T,22}, \nu_{21}$
15	Compressive 0°	ASTM D3410	$S_{11C}, E_{C,11}, \nu_{12}$
15	Compressive 90°	ASTM D3410	$S_{22C}, E_{C,22}, \nu_{21}$
15	Shear 1 – 2	ASTM D7078	$S_{12}, G_{12}$
6	Shear 1 – 3	ASTM D7078	$S_{13}, G_{13}$
6	Shear 2 – 3	ASTM D7078	$S_{13}, G_{13}$
12	Fiber Volume	ASTM D3171	$V_f$ (Check quality)
12	Density	ASTM D792	$\rho$

Table 2-1: Testing Plan

## 2.1 Design of Coupons

The first step towards the experiments is to design the coupons. This procedure is a complex one and the respective norms shown in the above table give a lot of freedom to the researchers. The writer studied thoroughly the literature and came across several examples on the web. Readers that are interested to see the work from other researchers are suggested to read the Ref. [5-10,21] and specially to visit Ref [11] where a big database of hundreds of experiments is freely available, where coupons are tested with different fiber volumes, dimensions, loading orientations in both static and fatigue loading. As it is mentioned by many researchers, the design of coupons is more of an art rather than a standard explicitly defined procedure. Hence, the writer used as his basis the building block approach and designed the coupons in such a way in order to be as more representative as possible of the materials used for the large scale specimens. For that reason, all the coupons where designed with the same fiber mat as the one used for the large scale specimens. To further elaborate on that, the large scale specimens were built with XX(Appendix A) and the

coupons that have unidirectional fiber mats, i.e. the tensile and compressive coupons, were designed with UDXX. The in plane shear tests were designed with EBXSXX (Appendix A). Furthermore, the resin that was used in both cases was exactly the same, i.e. XX (Appendix A). Of course, the designed fiber volume was also exactly the same between the small scale coupons and the large specimens which was equal to  $V_f = XX\%$ . Regarding the length, width and thickness of the coupons, the norms explicitly define the desired dimensions only for the shear tests. The design of the tensile and compressive tests is up to the researcher that has to be careful in order to avoid unwanted failures as it is explained below.

### 2.1.1 Tensile tests

The tensile coupons with fibers at  $0^\circ$  and  $90^\circ$  were the ones that were designed first. By taking into account what was above mentioned, the design procedure led to the coupons shown in figure 2-1 and 2-2 of the supporting document. Prior to giving the green light for the manufacturing of the coupons, certain checks had to be made in order to avoid unwanted failures. Due to the way that the load is introduced into the tensile coupons, the latter have to be tabbed. The main reason behind that is that untabbed coupons will lead to a case where the grips are directly attached to the tensile coupons and that could hurt the coupons and as a result alter the results. These tabs which, are shown in figures 2-1 and 2-2 of the supporting document, have to be adhesively bonded on the coupons. It is intuitive that if the adhesive fails, we will not be able to extract the maximum strength of the coupons. Hence, the norm defines a check that has to be made prior to the manufacturing of the coupons which is:

$$L_{min} = \frac{F^{tu} \cdot h}{2 \cdot F^{su}} \quad (2.1.1)$$

$L_{min}$  = minimum required bonded tab length, mm

$F^{tu}$  = ultimate tensile strength of coupon material, MPa

$h$  = coupon thickness, mm

$F^{su}$  = ultimate shear strength of adhesive, coupon material, or tab material (the lowest), MPa

The ultimate tensile strength of the coupon is not yet known (that's the reason of performing these tests) but from previous/similar experiments, it is expected to be around  $F^{tu} = XX \text{ MPa}$ <sup>[22]</sup>. The thickness of the coupon is defined by taking into account the fiber volume and the number of layers which in the case of both tensile and compressive tests is equal to 4. The number of layers is not defined in the ASTM D3039<sup>[12]</sup> and it is up to the researcher to define the exact amount and the 4 layers were chosen because they lead to realistic and close to the literature designs. As a result, the nominal thickness of the coupons is  $h = XX \text{ mm}$ . The Hysol EA 9394 adhesive has, according to Ref. [15], ultimate shear strength  $F^{su} = 29.6 \text{ MPa}$  and as a result:

$$L_{min} = \frac{F^{tu} \cdot h}{2 \cdot F^{su}} = XX \text{ mm} \leq 70 \text{ mm}$$

The above check is satisfied which means that according to the norm ASTM D3039<sup>[12]</sup> the usage of this adhesive will not lead to unwanted failures which was verified from the results. The unwanted failures can be

seen in the aforementioned norm and generally we want to avoid failures with modes “*XXT*” or “*XXB*” when the failure occurred between the tabs. The first “*X*” corresponds to failure type, the second “*X*” corresponds to failure area and the third letter corresponds to failure location according to ASTM D3039<sup>[12]</sup>.

**Note:** The choice of the adhesive should be done with attention. It should be strong enough to satisfy the above relationship and at the same time its cure temperature should be lower than the heat distortion temperature of the resin itself. Otherwise, the resin will lose its properties and it will become “softer” during the curing of the adhesive.

In subchapter 2.1 of the supporting document the readers can find a detailed analysis of the tensile coupons’ design which is followed by a FEM model in subchapter 2.1.1 of the same document. The writer built this FEM model as part of his research to check the effect of various parameters (such as the dimensions of the coupons and the adhesive, the way that the end of the tab is treated etc.) into the distribution of stresses for the case of tensile coupons with fibers parallel to the loading axis because it is the critical one. Briefly, the structural stress concentration was examined at the tab end and the distribution of the shear stresses along the adhesive’s length for various dimensions and configurations of the tab end. The model shown at subchapter 2.1.1 of the supporting document corresponds to the final one on which the final design was based.

### 2.1.2 Compressive coupons

The design of the compressive coupons followed the same rationale with the tensile ones. The same fiber mat was used (4 layers of UDXX), the same resin (XX) and the same fiber volume  $V_f = XX\%$ . The adhesive that connected the tab was the same (XX) but here there is no need to check a potential adhesive failure because the checks for the tensile coupons which are more critical are satisfied. Taking this into account, the compressive tests were designed as shown in pictures 2-12 and 2-13 of the supporting document.

However, attention should be given in different failure modes according to the norm ASTM D3410<sup>[13]</sup> for the case of compressive coupons. Firstly, the free length should be long enough to allow stress decay to uniform uniaxial compression and minimize Poisson restraint effects due to grips. At the same time, the free length should be small enough in order to avoid buckling prior to crushing of the coupon due to compression. Basically, it is desired to avoid any loss of stiffness that could be the aftereffect of the coupons’ buckling. For that reason, the norm suggests that the free lengths should be between 12 mm and 25 mm and for that reason a free length of 20 mm was opted in this thesis. Furthermore, the norm provides a semi-empirical formula to check a potential buckling of the coupon which is shown below:

$$h_{coup} \geq \frac{l_g}{0.9069 \cdot \sqrt{\left(1 - \frac{1.2F^{cu}}{G_{xz}}\right) \left(\frac{E^c}{F^{cu}}\right)}} \quad (2.1.2)$$

Where:

$h_{coup}$  = specimen thickness, [mm]

$l_g = \text{length of gage section, [mm]}$

$G_{xz} = \text{through the thickness shear modulus, [MPa]}$

$F^{cu} = \text{ultimate compressive Strength, [MPa]}$

$E^c = \text{longitudinal modulus of elasticity, [MPa]}$

According to the values that are available from previous/similar experiments from Ref. [13]:

$$h_{coup} \geq \frac{l_g}{0.9069 \cdot \sqrt{\left(1 - \frac{1.2F^{cu}}{G_{xz}}\right) \left(\frac{E^c}{F^{cu}}\right)}} = XX \checkmark, \text{ for fibers at } 0^\circ$$

$$h_{coup} \geq \frac{l_g}{0.9069 \cdot \sqrt{\left(1 - \frac{1.2F^{cu}}{G_{xz}}\right) \left(\frac{E^c}{F^{cu}}\right)}} = XX \checkmark, \text{ for fibers at } 90^\circ$$

Due to the fact that the above relationships are satisfied (nominal thickness,  $h = XX \text{ mm}$ ), the norm allows for construction of the compressive coupons with that dimensions.

The writer considered relevant to do a further buckling analysis by creating a FEA model in order to ensure that buckling of the coupons will be avoided. This analysis is shown in detail at subchapter 2.1.1 in the supporting document and readers are suggested to read it if they want to get a better understanding of the procedure. Briefly, what was done there, was an elastic buckling analysis in order to define the mode shapes and the critical buckling load which was followed by a non-linear static analysis where imperfections were included and which were based on the 1<sup>st</sup> mode shape (because it is the most conservative). The FEA model showed that for various realistic imperfections, the compressive coupons will fail much earlier before the initiation of loss of stiffness due to buckling (see figure 2-20 in the supporting document) which is something that is desired.

### 2.1.3 Shear tests

The dimensions of the shear tests are defined by the respective norm, i.e. ASTM D 7078<sup>[14]</sup>. Only the thickness is to be defined by the researcher. Hence, the writer determined the thickness of the coupons for the in plane shear tests to be equal to the ones of the tensile coupons and compressive coupons. Hence, 4 layers of EBXS XX were used for their construction with of course  $V_f = XX\%$ . On the other hand, due to the peculiarity of the out of plane shear tests, their thickness was decided to be equal to  $h_{xz,yz} = 4 \text{ mm}$ . That was done on purpose, because as it is shown later, these coupons were extracted by cutting a plate with  $56 \text{ mm}$  of thickness. As a result, a round number was opted instead of the thickness of  $h = XX \text{ mm}$  that was used for the rest of the coupons because it would be easier for the technicians to achieve the desired thickness. Also, the out of plane shear coupons were designed with UD XX fiber mats and the cutting orientation will define the plane at which the properties will be extracted. The final designs are shown in figures 2-22 until 2-24 in the supporting document.

## 2.2 Preparation of Panels

The design of the small scale coupons is shown in detail at subchapters [2.1-2.4](#) of the supporting document and is briefly explained above. This analysis resulted in the design of the panels showed in figures [2-25](#) until [2-30](#) which show the FRP plates from which the small scale coupons were extracted along with the plates that led to the construction of the necessary tabs. Generally, the plates were cut into the correct dimensions towards the preparation of the coupons showed in figures [2-1](#), [2-2](#), [2-12](#), [2-13](#), [2-22](#), [2-23](#), [2-24](#) of the supporting document.

To further clarify the procedure, the first step of the experimental procedure is to produce the panels shown in figures [2-25](#) until [2-30](#) of the supporting document. These panels were produced in October 2017 at KVE<sup>[16]</sup> (Hague, the Netherlands) while Bureau Veritas<sup>[17]</sup> (Rotterdam, the Netherlands) was present during the manufacturing to verify the quality of the produced panels and make sure that the respective norms are followed (see supporting document chapter [2](#)). At this point it should be mentioned that due to the lack of proper fiber mats, instead of using UXX, the fiber mat that was used for coupons with unidirectional fibers was UNIEXX (Appendix A). For example, for the tensile coupons, instead of 4 plies of UDXX, 8 plies of UNIEXX were used for the construction of the panels. Then, the produced panels were sent to a certified lab and more specifically to Applus<sup>[19]</sup>, (Bremen, Germany, see certifications at Ref. [\[18\]](#)). There, they were cut according to the designs shown in figures [2-1](#), [2-2](#), [2-12](#), [2-13](#), [2-22](#), [2-23](#), [2-24](#) of the supporting document and a part of the panels at the perimeter was scrapped because we expect manufacturing imperfections close to the edges of panels due to non-homogeneous transferring of the resin (this is pretty evident at the thick panel used for the out of plane shear properties, figures [Appendix B](#)). The scrapped part is showed with red diagonal lines under the legend margin for cuts.

Through the figures [B-1](#) until [B-12](#) the readers can visualize the procedure followed by KVE<sup>[16]</sup> for the preparation of the panels. At this point, a comment should be added for the thick panel shown in figure [B-9](#) as it is obvious that there is a white spot on the top surface where the resin hasn't been transferred properly. This issue was solved as it is shown in figure [B-10](#) by locally penetrating the vacuum bag and letting air to flow in the panel. This effect allowed the transferring of resin towards the white spot and this procedure is shown in figure [B-10](#).

Now, the first step is finished, as the panels have been manufactured. Prior to sending them to Applus<sup>[19]</sup>, (Bremen, Germany) the panels were cured overnight at room temperature and then they were demoulded and postcured at  $XX^{\circ}C$  for  $XXh$ . The readers can visualize in [Appendix B](#) the composite plates which were sent from KVE to Applus<sup>+</sup>. Now, let's focus in figure [2-25](#) of the supporting document and more specifically at the tensile tests with fibers at  $0^{\circ}$  direction. The first cutting procedure led to a big block with magenta color with a total width  $15 \times 25 = 375 \text{ mm}$  and a length of  $250 \text{ mm}$  and it was done with a water-cooled diamond plated cutter. Readers can see in figure [B-13](#) of [Appendix B](#) that the plate was impressed with lines that defined the cutting area and verify that it was the same as the one defined in figure [2-25](#) of the supporting document. Then, as shown in figure [2-29](#) of the supporting document the tabs were cut in long strips which were used for tensile tests. At this point it should be mentioned that the tabs were made of a symmetric section with 4 plies of EBXS XX with the same resin and fiber volume. As shown in the same figure, the first strip included tabs with numbers between 1 – 15, the second strip had numbers between 16 – 30 and so on.

Then, the strips of tabs were adhesively bonded on the tensile coupons at the correct positions using Hysol EA 9394 (see supporting document subchapter [2.1](#)) and then, after the curing of the adhesive ( $70^{\circ}C$  for 70 minutes with  $40 - 60kPa$ ), the end of the tabs was machined with an inclination 1:4 in order to have a soft introduction of the load from the tabs on the tensile coupons and avoid high stress concentrations at the same locations. The last step of the preparation included the cutting of this tabbed block into the individual tensile coupons as shown in figure [2-1](#) of the supporting document. The same procedure was followed for the rest of the tabbed coupons with the only exception of the compression coupons which do not have machined edges at the tabs.

The resultant coupons that are ready to be tested can be seen in the figures in [Appendix B](#).

As far as the shear coupons are concerned, the absence of tabs meant that they just have to be cut into the correct dimensions as shown in figures [2-22](#) until [2-24](#) of the supporting document. However, the laboratory in Bremen doesn't have the necessary apparatus for the implementation of tests according to ASTM D 7078<sup>[13]</sup> which meant that after the preparation, the panels were sent to Applus<sup>+</sup><sup>[18]</sup> in Barcelona, Spain in order to be cut and tested.

Apart from the material properties, in figures [2-25](#) until [2-28](#) of the supporting document, the positions of the coupons that will be tested for fiber volume as well as for the density are shown and purposely they were chosen in various positions at the initial panels in order to check the uniformity of the panels that were produced. These positions are also visible in [Appendix B](#). All the fiber volume tests should show a fiber volume  $V_f = XX\%$  under the assumption that the manufacturing procedure was perfect.

## 2.3 Tests description

Now, the second phase of the small scale coupon testing is finished as the coupons have obtained their final form and they are ready to be tested. The writer believes that prior to the presentation of the experimental results it is pretty significant to depict more details about the small scale tests regarding the apparatus, the load introduction and the way that the results were extracted.

### 2.3.1 Tensile tests

Static tensile load is applied for determining the Elastic tensile modulus, plain tensile strength and Poisson ratios of the material under investigation. The specimens are loaded by means of hydraulic grips with shear load introduction. The total length of specimens according to the writer's designs was  $250\text{ mm}$  with a free length of  $110\text{ mm}$ . The tests have been implemented in room/dry conditions.

The specimen is loaded at a constant crosshead rate of  $2.0\text{ mm/min}$  until failure. A Biaxial extensometer installed in middle of the free length of the specimen and is used for strain measurement with a gauge length of  $25\text{ mm}$ . According to the writer's requirement, also biaxial strain gauges are bonded at middle of both faces back to back. Grid b is transversal and grid a is longitudinal. During the test, time, load, crosshead

displacement and strain of both, extensometer and strain gauges signals are measured. Modulus is calculated between 1000 and 3000 microstrains as it is defined by the norm ASTM D3039<sup>[12]</sup>.

Table 2-2 shows the main characteristics of the Electromechanic Universal Test Machine for tensile test.

Brand	Zwick GmbH
Model	148400/01 – Retroline
Series	104050 0388 with Dossier Nr. 138628
BKW internal reference	MP 008700
Load cell capacity	250 kN
Load cell last calibration date	November 2017 (annual interval), (Nro.34102 – D-K-15216-01-00-2017-11)
Load cell calibration class	0.5 % acc. to ISO 7500-1
Machine crosshead last calibration date	November 2017 (annual interval),( Nro.34103 – D-K-15216-01-00-2017-11)
Crosshead calibration class	0.5 % acc. to DIN EN ISO 9513
Extensometer	MTS System, GmbH, Biaxial 632.85F 10419691 MP009500
Last calibration	November 2017 (annual interval),( Nro.34103 – D-K-15216-01-00-2017-11)
Strain gauges Type, lot, k-Factor	1-XY91-3/120, Lot, 812078215, k-factor a=2,05 b=2,03 1-XY91-3/120, Lot, 812078215, k-factor a=2,04 b=2,03
Adhesive	Z70
Amplifier	Spider 8-30, HPM, MP006900
Last calibration date	February 2016 (biannual Interval)

Table 2-2: Test machine for tensile tests

More information about the testing device for tensile coupon tests along with photos from the test setup is given in [Appendix C](#).

### 2.3.2 Compressive Tests

Static compression load is applied to the specimen to determine the Elastic compression modulus and plain compression strength of the material under investigation. The test is performed in the HCCF tool with combined load introduction (shear and end loading). Clamping length (upper and lower) is 65 mm (complete tab length) and free length of 20 mm according to writer's definition to minimize/avoid the buckling. The used grips have soft load introduction to avoid early failure of the specimen due to high stress concentration at the beginning of the clamping length. The tests have been implemented in room/dry conditions.

The specimen is loaded at a constant crosshead rate of 1.0 mm/min until failure. Extensometers in this test are biaxial strain gauges (T-rosettes) installed back to back in the middle of the free length of the specimen. Grid a is transversal and grid b is longitudinal. During the test, time, load, crosshead displacement and strain of strain gauges is recorded. Modulus is calculated between 1000 and 3000 microstrains (ASTM D3410<sup>[13]</sup>).

Brand	Zwick GmbH
Model	Z250
Series	150101/2001
Load cell capacity	250 000 N
Load cell last calibration date	November 2017 (annual interval), (Nro.34110 – D-K-15216-01-00-2017-11)
Load cell calibration range	0.5 kN to 200 kN
Load cell calibration class	0.5 % acc. to ISO 7500-1
Machine crosshead last calibration date	November 2017 (annual interval),( Nro.34111 – D-K-15216-01-00-2017-11)
Crosshead calibration class	0.5 % acc. to DIN EN ISO 9513
Strain gauges Type, lot, k-Factor	1-XY91-3/120, Lot, 812078215, k-factor a=2,05 b=2,03 1-XY91-3/120, Lot, 812078215, k-factor a=2,04 b=2,03
Adhesive	Z70
Amplifier	Spider 8-30, HPM, MP006900
Last calibration date	February 2016 (biannual Interval)

Table 2-3: Test machine for compression tests

More information about the testing device for compressive coupon tests along with photos from the test setup is given in [Appendix C](#).

### 2.3.3 Shear Tests

Static shear load is applied to the specimen to determine the Elastic Shear modulus and plain Shear strength of the material under investigation. The tests have been implemented in room/dry conditions and they were conducted under displacement control with a testing speed of 2.0 mm/min.

A XY91 stacked T rosette (HMB) measuring strains at  $\pm 45^\circ$  to the loading axis was placed in the middle of each specimen. Later, the specimen was fixed into the two-rail fixture using spacing blocks. Each half of the fixture contained three bolts to secure the specimen during loading. A bolt torque of 55 N – m was applied in each bolt using a dynamometer key (Stahlwille). Finally, the assembled fixture was placed in the testing machine to start loading.

Brand	MTS
Model	810 MTS
Series	0088543
Applus internal reference	10-WI-013
Load cell capacity	100kN
Load cell last calibration date	10-july 2017 (annual interval)
Load cell calibration class	Class 0.5 (ISO 7500-1)
Machine crosshead last calibration date	03-july 2017 (annual interval)

Crosshead calibration class	Class 1 acc. to EN ISO 9513
Extensometer	-
Last calibration	-
Strain gauges Type, lot, k-Factor	1-XY91-3/350 HBM; lot 812079285; k-factor a=2,07 b=2,06
Adhesive	M-BOND 200 and M-COAT, MICRO Measurements
Amplifier	MX1615, HBM
Last calibration date	10-may-17

Table 2-4: Test Machine for Shear Tests

More information about the testing device for shear coupon tests along with photos from the test setup is given in [Appendix C](#).

### 2.3.4 Strain gauges

For tensile and compression, Strain gauges has been applied at both faces:

- Rosette/Strain gauge 1: smooth face/side (**long1** for longitudinal strain and **trans1** for transversal strain)
- Rosette/Strain gauge 2: rough face/side (**long2** for longitudinal strain and **trans2** for transversal strain)

Recommendation for future projects from Applus<sup>+</sup>: when strain gauges are required, we recommend as much as possible to produce laminates with flat/smooth surface as possible to ensure a good surface preparation and strain gauge bonding.

## 2.4 Experimental results for small scale coupons

On 5<sup>th</sup> of February 2018, Applus<sup>+</sup><sup>[18]</sup> sent to DSNS the report concerning the small scale coupons. This report had a length of 315 pages and the writer decided to include only the core of the information in this report. As a result, the information that was assumed to be of significant importance is shown in this subchapter and is accompanied with [Appendix D](#) and [Appendix E](#).

### 2.4.1 Strength Properties

	$S_{11T}$ [MPa]	$S_{11C}$ [MPa]	$S_{22T}$ [MPa]	$S_{22C}$ [MPa]	$S_{12}$ [MPa]	$S_{13}$ [MPa]	$S_{23}$ [MPa]
Average	XX	XX	XX	XX	XX	XX	XX
Standard Deviation	XX	XX	XX	XX	XX	XX	XX
CoV	2.53%	4.85%	2.84%	3.42%	8.03%	3.09%	4.59%

Table 2-5: Strength Properties, Experimental Results

## 2.4.2 Stiffness Properties

	$E_{11}$ [GPa]	$E_{22}$ [GPa]	$G_{12}$ [GPa]	$G_{13}$ [GPa]	$G_{23}$ [GPa]	$\nu_{12}$ [-]
Average	XX	XX	XX	XX	XX	XX
Standard Deviation	XX	XX	XX	XX	XX	XX
CoV	2.67%	4.20%	20.30%	10.11%	10.93%	2.86%

Table 2-6: Strength Properties, Experimental Results

## 2.4.3 Fiber Volume, density tests

	Plate <i>i</i> Figure 2.25	Plate <i>ii</i> Figure 2.26	Plate <i>iii</i> Figure 2.27	Plate <i>iv</i> Figure 2.28
$V_f$ [%] Average	XX	XX	XX	XX
$\rho$ [g/cm <sup>3</sup> ], Average	XX	XX	XX	XX

Table 2-7: Fiber Volume &amp; density Experimental Results

## 2.5 Discussion of small scale coupon test results

To begin with, the writer is satisfied with the manufacturing of the coupons, the testing procedure and as a result with the outcome of the experiments. The main reason is that the obtained strength and stiffness properties have high and realistic values when comparing to results that are available to the literature. Especially, the high compressive strength which was extracted for both the coupons with  $0^\circ$  and  $90^\circ$  fiber orientation, means that the coupons were designed appropriately and buckling wasn't initiated. By comparing the resultant compressive strengths with the ones available at Ref. [11] where a big database of experimental results is available, it is evident that even if the rest of the properties are similar between this thesis' experimental results and the ones available there, the compressive strengths shown in table 2-5 are significantly higher. The main reason is that here, instead of using antibuckling-devices, it was opted to use a small free length which was checked by the FEA model shown in subchapter 2.2.1 of the supporting document. Another reason for the satisfaction over the experimental results comes from the fact that the Coefficient of Variation (CoV) is pretty small in most of the cases (less than 5%). This is of great importance for potential designers because small CoVs mean that they can know with better accuracy the material properties of a structure that they will design. Of course, it should be mentioned that the results of the individual properties were extracted from the same plate (for example all the tensile coupons with fibers at  $0^\circ$  were extracted from the same plate). However, again by checking in the literature, the CoVs tend to be higher even for the case where the coupons were extracted from the same plate. Small CoVs lead to the conclusion that the manufacturing procedure was performed appropriately and the imperfections were spread uniformly in terms of space. Last but not least, all the failure modes were acceptable which resulted to taking into account all the experiments and by not depicting outliers.

Another point that should be mentioned here, is that the writer explicitly asked for numbering the coupons in the way that it is shown in the figures [2.25](#) until [2.28](#) of the supporting document in order to give the opportunity to other researchers to use these experiments for research towards the spatial variability of the material properties as it is recommended in the last chapter of this thesis. Of course, the writer understands the importance of including as much information as possible regarding these tests and for that reason, in [Appendix D](#), readers can find the results for every individual coupon. Specifically, readers can find strength and stiffness properties of each coupon, load-displacement curves for tensile and compressive coupons as well as stress strain curves for the shear tests. Moreover, in [Appendix E](#), readers can find photos of the broken coupons and verify that unwanted failures were avoided.

Prior to presenting the next chapter, a comment should be made about plate *iii* ([2.27](#) of supporting document) due to a possible mal-manufacturing. It is obvious in table [2-7](#) that the fiber volume is significantly higher than the required one ( $V_f \approx XX\%$  instead of  $V_f = XX\%$ ) which led to a much higher Shear Modulus than the expected one ( $G_{12,ave} = XX \text{ Gpa}$  instead of an expected Shear Modulus of  $G_{12,exp} = XX \text{ GPa}$ ) and a big spread of the results. The high fiber volume was expected due to the fact that the thickness of the coupon was smaller than the designed one (table [D-8](#)) where the placed fibers were exactly as designed. It seems that the Shear strength  $S_{12}$  was left almost unaffected because the results are close to the expected ones. A possible cause is that the in plane shear failure is dominated by both fibers and matrix and a potential increase of the fiber volume doesn't necessarily lead to a proportionate increase of the shear strength; something which is not valid for the shear modulus.

Furthermore, the correlation between the properties that were extracted from the same tests was not the expected one. These correlations can be seen below:

	$S_{11T} - E_{11}$	$S_{22T} - E_{22}$	$S_{12} - G_{12}$
Correlation	-0.49	0.43	-0.36

Table 2-8: Correlation of properties extracted from the same results

For example, the correlation between the tensile strength and the elastic modulus in the direction parallel to the fibers is  $cor = -0.49$ . Intuitively, one could expect that both behaviors are fiber dominated and a negative correlation wouldn't make sense. However, a possible cause is that the fiber strength  $S_{11T}$  is mostly dependent on the amount of fibers in the coupon but the Elastic Modulus  $E_{11}$  is dependent on both the amount of fibers and the adhesion between fibers and matrix. A potential sizing of the fibers (relative slippage between fibers and matrix) will change the Elastic modulus much more than the tensile strength. Another cause has to do with the values that are correlated. The elastic modulus is defined at the start where the behavior is linear but to our surprise, the tensile tests with fibers at  $0^\circ$  showed a small non linearity towards the end of the stress strain curves for some coupons. Another reason has to do with the note from Applus+ as shown [here](#). The coupons had one smooth surface and the other was a little bit rougher as a result of the manufacturing procedure. Applus+ had to slightly grind the rough surface and then mount the strain gauges. As it was explained earlier, the Elastic Modulus was calculated by taking into account the stress level at 1000 and 3000 microstrains as defined from the norm ASTM D3039<sup>[12]</sup>. The average value of the strain gauges at the 2 surfaces was used for the calculation of the Elastic Modulus and deviations between the top and bottom gauges were noticed. These three reasons can justify a negative correlation and can be used also for the

---

negative correlation of the in plane shear tests where the case is even more complex due to the inherent nature of the loading.

Note for the experiments: The quality of the experimental procedure was verified by Bureau Veritas<sup>[17]</sup>. Their Dutch department witnessed the manufacturing of the panels at KVE<sup>[16]</sup>, their German department witnessed the compressive and tensile tests in Bremen and their Spanish department witnessed the shear tests in Barcelona. Applus+, both in Barcelona<sup>[20]</sup> and in Bremen<sup>[18]</sup> are certified laboratories and in their report they included all the certifications regarding their testing capabilities but they are not included here because the writer assumed that the report would become unnecessarily lengthy. KVE<sup>[16]</sup> was selected as the manufacturer of the panels because they were the ones that designed the large scale specimens and according to building block approach, as many factors as possible should be kept constant between the different blocks(subchapter 1.4 of the supporting document).

# Chapter 3: Statistics

The next step of this thesis is to implement a statistical analysis of the experimental results for the small scale coupon tests in order to include the stochastic nature of the material properties. As part of this procedure, a specific distribution has to be assigned to each one of the material properties and then random variables should be generated from these distributions that will be used as inputs for the FEA models which are presented at the next chapter.

In order to avoid any confusions between the material properties that were part of the statistical analysis and the properties shown in table 2-1, below the properties that were analyzed in this chapter are shown:

Properties in the Statistical Analysis	Corresponding Properties in table 2-1	Number of tests
$S_{11T}$	$S_{11T}$	15
$E_{11}$	$E_{T,11}$	15
$S_{11C}$	$S_{11C}$	15
$\nu_{12}$	$\nu_{12}$	15
$S_{22T}$	$S_{22T}$	15
$E_{22}$	$E_{T,22}$	15
$S_{22C}$	$S_{22C}$	15
$S_{12}$	$S_{12}$	15
$G_{12}$	$G_{12}$	15

Table 3-1: Properties included in the statistical Analysis

The rest of the properties shown in 2-1 were not used in the statistical analysis because they are not used as inputs for the FEA models. For example, the elastic modulus in the direction parallel to fibers is defined with one value in FEM, for both the tensile and compressive case. To further elaborate on that, Ansys v.17 gets one value as input for  $E_x$  and it doesn't make any distinction between  $E_{11T}$  and  $E_{11C}$ . In this thesis, the values extracted from the tensile tests were used for the definition of the elastic modulus in both the parallel and perpendicular directions.

The average values of the properties  $S_{13}$ ,  $S_{23}$ ,  $G_{13}$  and  $G_{23}$  were used as inputs for the FEA models because only 6 tests were implemented per property which are not enough for a statistical analysis. Moreover, the out-

of plane Poisson's ratios are explained in subchapter [2.5](#) of the supporting document. More information on the material properties as they were modelled in the FEA model, is provided at the next chapter, [here](#).

For the properties shown in table [3-1](#), the first step of the statistical analysis is to assign a distribution to each material property. This procedure is presented below.

### 3.1 Assign distributions to the material properties

Several distributions were assumed to be the potential ones for the characterization of the material properties which are presented at table [3-2](#). The choice of these distributions is the product of literature study by the writer along with the addition of some distributions from other areas of study (such as economics, communication theory) that are not frequently used for the characterization of composite material properties but they seemed as promising ones. An extensive explanation of the assumed distributions is given at subchapter [3.1](#) of the supporting document. These distributions are:

Distribution	Probability Density Function, pdf
Normal	$f(x; \mu, \sigma) = \frac{1}{\sigma\sqrt{2\pi}} \exp\left[-\frac{1}{2}\left(\frac{x-\mu}{\sigma}\right)^2\right],$ $-\infty < \mu < \infty$ $\sigma > 0$ $-\infty < x < \infty$
Gamma	$f(x; \alpha, b) = \frac{1}{b^\alpha \Gamma(\alpha)} x^{\alpha-1} \exp\left(-\frac{x}{b}\right),$ $x \geq 0$ $\alpha, b > 0$
Log-Normal	$f(x; \mu, \sigma) = \frac{1}{\sigma x \sqrt{2\pi}} \exp\left[-\frac{1}{2}\left(\frac{\ln x - \mu}{\sigma}\right)^2\right],$ $\mu > 0$ $\sigma > 0$ $x > 0$
Weibull	$f(x; k, \lambda) = \frac{k}{\lambda} \left(\frac{x}{\lambda}\right)^{k-1} \exp\left[-\left(\frac{x}{\lambda}\right)^k\right],$ $x \geq 0$ $k, \lambda > 0$
Nakagami	$f(x; \mu, \omega) = 2 \cdot \left(\frac{\mu}{\omega}\right)^\mu \frac{1}{\Gamma(\mu)} x^{2\mu-1} \exp\left(-\frac{\mu}{\omega} x^2\right),$ $\mu \geq 0.5$ $\omega > 0$ $x > 0$
Logistic	$f(x; \mu, \sigma) = \frac{\exp\left(\frac{x-\mu}{\sigma}\right)}{\sigma \left[1 + \exp\left(\frac{x-\mu}{\sigma}\right)\right]^2},$ $-\infty < \mu < \infty$ $\sigma > 0$ $-\infty < x < \infty$
Rician	$f(x; s, \sigma) = I_0\left(\frac{x s}{\sigma^2}\right) \frac{x}{\sigma^2} \exp\left[-\left(\frac{x^2 + s^2}{2\sigma^2}\right)\right],$ $s \geq 0$ $\sigma > 0$ $x > 0$

Minimum Extreme Value	$f(x; \mu, \sigma) = \frac{1}{\sigma} \exp \left\{ \frac{x - \mu}{\sigma} - e^{\frac{x - \mu}{\sigma}} \right\}, \quad \begin{array}{l} \sigma > 0 \\ -\infty < x < \infty \end{array}$
Maximum Extreme Value	$f(x; \mu, \sigma) = \frac{1}{\sigma} \exp \left\{ -\frac{x - \mu}{\sigma} - e^{-\frac{x - \mu}{\sigma}} \right\}, \quad \begin{array}{l} \sigma > 0 \\ -\infty < x < \infty \end{array}$

Table 3-2: Chosen Distributions

It is obvious that all these distributions require two parameters in order to be fully described. The writer created a Matlab model (version: R2016b) to calculate these parameters by using as inputs the experimental results shown in tables D-1 until D-5 and by implementing the Maximum Likelihoods Estimates method which is presented at subchapter 3.2 of the supporting document. Briefly, with the MLE method one can find the most probable parameters of each distribution and for each material property that could result to the experimental data after a random sampling. The basis of the theory is that the result from every individual coupon is independent of the result of the previous/next coupon's result. This is a valid assumption because factors such as the wearing of the test devices is not taken into account and generally there is no reason for one coupon to have any influence on another coupon. In a mathematical form, this assumption can be translated into:

$$P(x_1 - \varepsilon, X_1, x_1 + \varepsilon, \dots, x_n - \varepsilon, X_n, x_n + \varepsilon) \approx f_{\theta}(x_1) \cdot f_{\theta}(x_2) \cdot \dots \cdot f_{\theta}(x_n) \cdot (2\varepsilon)^n \quad (3.1.1)$$

because the intersection of independent events is equal to the product of the individual probabilities.

The goal is to define the parameters of the probability density function for each one the 9 different  $f_{\theta}$  and for each material property which can maximize the probability that is shown in eq. 3.1.1. This is achieved by defining a likelihood function and trying to maximize it.

$$L(\theta) = f_{\theta}(x_1) \cdot f_{\theta}(x_2) \cdot \dots \cdot f_{\theta}(x_n) \quad (3.1.2)$$

A common trick that is used at this point, is to take the natural logarithm of the likelihood function because it makes the calculations much less complex.

$$\ell(\theta) = \ln(L(\theta)) \quad (3.1.3)$$

The main reason for this action has to do with the inherent property of the natural logarithms that  $\ln(a \cdot b) = \ln(a) + \ln(b)$ . The last step of this procedure is to maximize the log-likelihood function by taking its derivatives towards the two parameters that define each distribution

$$\frac{\partial \ell(par_1, par_2)}{\partial par_1} = 0$$

$$\frac{\partial \ell(par_1, par_2)}{\partial par_2} = 0 \tag{3.1.4}$$

For the case of the normal distribution  $par_1 = \mu$  and  $par_2 = \sigma$  whereas for the Weibull distribution  $par_1 = k$  and  $par_2 = \lambda$  (and so on for the rest of the distributions as they are all fully defined with 2-parameters)

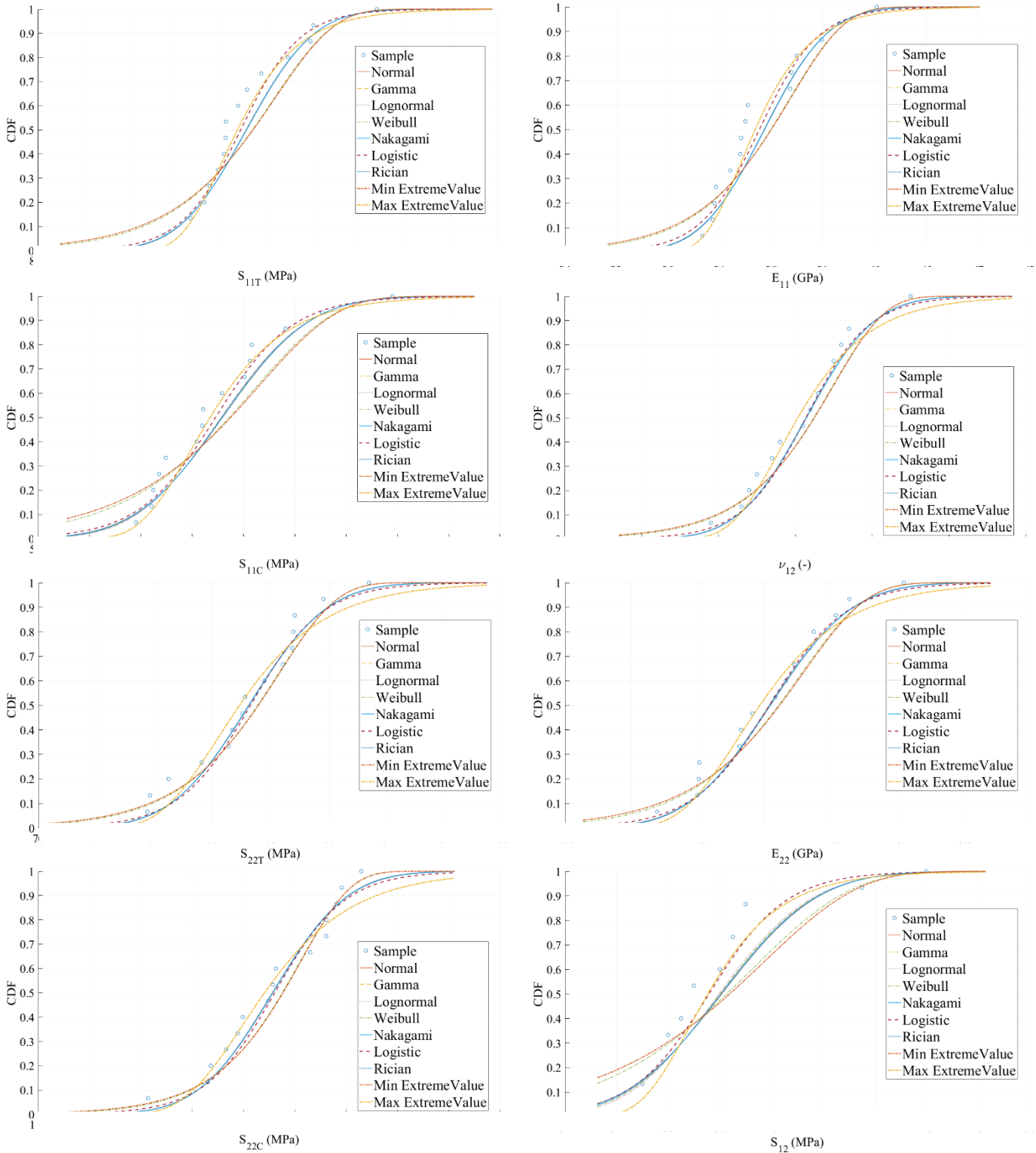
This procedure was modelled in Matlab (version: R2016b) and the model generated the following parameters.

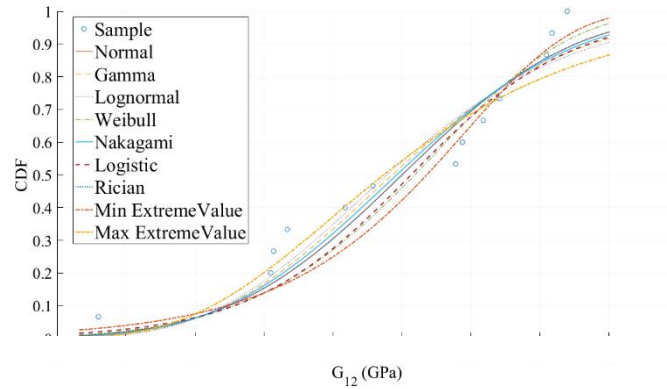
	<i>Normal</i> ( $\mu, \sigma$ )	<i>Gamma</i> ( $\alpha, b$ )	<i>Lognormal</i> ( $\mu, \sigma$ )	<i>Weibull</i> ( $k, \lambda$ )	<i>Nakagami</i> ( $\mu, \omega$ )	<i>Logistic</i> ( $\mu, \sigma$ )	<i>Rician</i> ( $s, \sigma$ )	<i>Min Extr</i> ( $\mu, \sigma$ )	<i>Max Extr</i> ( $\mu, \sigma$ )
$S_{11T}$ (MPa)	XX	XX	XX	XX	XX	XX	XX	XX	XX
$E_{11}$ (GPa)	XX	XX	XX	XX	XX	XX	XX	XX	XX
$S_{11c}$ (MPa)	XX	XX	XX	XX	XX	XX	XX	XX	XX
$\nu_{12}$ (-)	XX	XX	XX	XX	XX	XX	XX	XX	XX
$S_{22T}$ (MPa)	XX	XX	XX	XX	XX	XX	XX	XX	XX
$E_{22}$ (GPa)	XX	XX	XX	XX	XX	XX	XX	XX	XX
$S_{22c}$ (MPa)	XX	XX	XX	XX	XX	XX	XX	XX	XX
$S_{12}$ (MPa)	XX	XX	XX	XX	XX	XX	XX	XX	XX
$G_{12}$ (GPa)	XX	XX	XX	XX	XX	XX	XX	XX	XX

Table 3-3: Results from MLE

Note: The results at table 3-3 correspond to the results shown at table 3-2 at the supporting document. Furthermore, for the avoidance of any confusion, the Maximum Extreme Distribution has negative values for all the material properties at the mean parameter, "μ" because the same probability distribution function is used for the minimum and maximum case in the matlab model. To put it simply, the maximum extreme distribution is equal to the minimum one when all the inputs have values with opposite signs.

A visualization of the results from the MLE method along with the experimental results is shown below:





Figures 3-1: Cumulative distribution Functions, Experimental Data

However, with this procedure no indication is given about the goodness of fit of the extracted distributions. Hence, another way should be found in order to define which of the extracted distributions can best describe each material property. Towards this goal, the Kolmogorov-Smirnov goodness of fit criterion was used as shown in detail at subchapter 3.3 of the supporting document. Briefly, with this method one finds the vertical distance between each experimental value from the sample and each cumulative distribution, i.e. the vertical distance between the blue circles and the cumulative distributions as shown in the figures above. For every individual distribution, the focus is given only to the maximum vertical distance which is shown as "D" at figure 3-3 of the supporting document and then this value is "translated" into a confidence level "α" as shown below:

$$D^* = \left( \sqrt{n} + 0.12 + \frac{0.11}{\sqrt{n}} \right) D$$

$$\alpha = 2 \sum_{j=1}^{\infty} (-1)^{-j} \exp(-2j^2 D^{*2}) \tag{3.1.5}$$

Normally, one should find only the value "D" and then use tables to extract the confidence level "α". However, if "D" is between some values in the tables, extrapolation has to be used. In order to avoid the usage of tables, the writer modelled the analytical equations above which resulted to the following "α" values:

	Normal (μ, σ)	Gamma (α, b)	Lognormal (μ, σ)	Weibull (k, λ)	Nakagami (μ, ω)	Logistic (μ, σ)	Rician (s, σ)	Min Extr (μ, σ)	Max Extr (μ, σ)
<i>S<sub>11T</sub></i>	0.654	0.664	0.670	0.552	0.659	0.838	0.654	0.535	0.943
<i>E<sub>1</sub></i>	0.372	0.384	0.390	0.330	0.378	0.573	0.372	0.326	0.758
<i>S<sub>11C</sub></i>	0.894	0.912	0.922	0.600	0.903	0.979	0.894	0.508	0.912
<i>ν<sub>12</sub></i>	0.999	0.998	0.998	0.968	0.999	0.993	0.999	0.956	0.932
<i>S<sub>22T</sub></i>	0.991	0.989	0.988	0.928	0.990	0.988	0.991	0.910	0.761
<i>E<sub>2</sub></i>	0.950	0.947	0.945	0.996	0.948	0.951	0.950	0.991	0.965
<i>S<sub>22C</sub></i>	0.854	0.857	0.858	0.896	0.855	0.879	0.854	0.869	0.957
<i>S<sub>12</sub></i>	0.297	0.358	0.393	0.128	0.324	0.854	0.297	0.096	0.908
<i>G<sub>12</sub></i>	0.625	0.535	0.503	0.781	0.570	0.752	0.622	0.785	0.598

Table 3-4: Results from Kolmogorov-Smirnov goodness of fit criterion

At table 3-4, the levels of significance for each distribution and for each material property are shown. As it is explained in depth at subchapter 3.3 of the supporting document, if a value in the above table is higher than a predefined level of significance  $\alpha_0 = 5\%$ , then it is assumed that this distribution can describe adequately the corresponding material property as we fail to reject the null hypothesis. At table 3-4, it is obvious that all the distributions can describe all the material properties adequately as all the values are higher than 0.05. However, the distribution that best fits every corresponding property is presented with red color and a summary of both the MLE method and the Kolmogorov-Smirnov criterion is given below:

	<i>Distribution</i>	<i>1<sup>st</sup> parameter</i>	<i>2<sup>nd</sup> parameter</i>	<i>significance level , <math>\alpha</math></i>
$S_{11T}$ (MPa)	<i>Max Extreme</i> ( $\mu, \sigma$ )	XX	XX	0.943
$E_1$ (GPa)	<i>Max Extreme</i> ( $\mu, \sigma$ )	XX	XX	0.758
$S_{11C}$ (MPa)	<i>Logistic</i> ( $\mu, \sigma$ )	XX	XX	0.978
$\nu_{12}$ (-)	<i>Normal</i> ( $\mu, \sigma$ )	XX	XX	0.999
$S_{22T}$ (MPa)	<i>Normal</i> ( $\mu, \sigma$ )	XX	XX	0.991
$E_2$ (GPa)	<i>Weibull</i> ( $k, \lambda$ )	XX	XX	0.996
$S_{22C}$ (MPa)	<i>Max Extreme</i> ( $\mu, \sigma$ )	XX	XX	0.957
$S_{12}$ (MPa)	<i>Max Extreme</i> ( $\mu, \sigma$ )	XX	XX	0.909
$G_{12}$ (GPa)	<i>Min Extreme</i> ( $\mu, \sigma$ )	XX	XX	0.785

Table 3-5: Distributions that best fit the experimental data

**Note:** The fact that all the distributions can adequately describe all the material properties means that a correct choice was made when the family of distributions was chosen. As it is shown later at figure 3-2, a wrong choice of distribution would lead to a rejection of the null hypothesis and as a result this distribution is not capable of describing adequately the respective material property

## 3.2 Verification of the Matlab model

At this point, it is deemed appropriate to verify the Matlab model that was used for the extraction of the results showed in table 3-5. Towards that goal, a PhD dissertation was found with the title: “Reliability determination for the design of structures made by composite materials” [21] where the same procedure was followed. An explanation of what was implemented there would be a tedious procedure and outside of the scope of this thesis. However, the experimental results from this PhD dissertation were used as inputs for the same statistical analysis and the results between the dissertation and the matlab model were compared.

Many experiments were performed towards the completion of the aforementioned dissertation and some of them were randomly chosen here which are shown below:

$X_T$ (MPa)	$\nu_{xy}$ (-)
44.08	0.453
44.45	0.455
41.85	0.597
40.74	0.448

36.69	0.469
43.23	0.578
37.02	0.486
40.91	0.511
41.31	
42.94	
40.78	
39.04	
39.61	
41.78	
38.92	
40.64	
37.94	
38.00	
39.31	

Table 3-6: Randomly chosen experimental results, PhD dissertation<sup>[9]</sup>

The experimental results in table 3-6 were extracted when Carbon-Epoxy laminates with  $\pm 55^\circ$  layup were tested in tension (loading at  $0^\circ$ ). The maximum likelihood estimates and the Kolmogorov-Smirnov criterion were used for the statistical analysis which resulted

	$X_T$			
	MLE		Kolmogorov-Smirnov criterion, $\alpha$	
	PhD results	Matlab	PhD results	Matlab
<i>Normal</i> ( $\mu, \sigma$ )	40.49 2.210	40.486 2.207	0.975	0.975
<i>Gamma</i> ( $\lambda, \eta$ )	8.3 335.930	8.3 336.412	0.954	0.955
<i>Lognormal</i> ( $\mu, \sigma$ )	3.7 0.055	3.7 0.055	0.941	0.942
<i>Weibull</i> ( $k, \lambda$ )	41.54 19.89	41.54 19.88	0.970	0.969
<i>Nakagami</i> ( $\mu, \omega$ )	-	84.33 1.64E+03	-	0.966
<i>Logistic</i> ( $\mu, \sigma$ )	-	40.47 1.31	-	0.964
<i>Exponential</i> ( $\lambda$ )	-	40.48	-	1.1E-06
<i>Rician</i> ( $s, \sigma$ )	-	40.43 2.21	-	0.975

<i>Min Extr</i> ( $\mu, \sigma$ )	41.6 2.08	41.6 2.08	0.941	0.938
<i>Max Extr</i> ( $\mu, \sigma$ )	39.39 2.02	39.39 2.02	0.658	0.66

Table 3-7: Comparison of PhD results with Matlab model, Data: Tensile strength with loading at 0°

It is obvious that the results from the PhD dissertation almost perfectly match with the Matlab results which verifies the built model. Small differences between the results can be attributed to the fact that not all the decimals are included in the statistical analysis in Matlab because the used input was taken from the dissertation's corresponding report where a small amount of numbers is given after the decimal point. All the input data included in the Matlab model had only two decimals whereas in the PhD, the input was extracted after performing calculations on the experimental results which leads to many numbers after the decimal point. To further clarify it, the tests lead to force-strain displacements from which the material properties should be extracted after calculations.

Note: In table 3-2, the pdf of the Gamma distribution is presented at the same form as it is included in Matlab. However, in the PhD dissertation, its pdf is given as:

$$f(x; \lambda, \eta) = \frac{\lambda^\eta}{\Gamma(\eta)} x^{\eta-1} \exp(-\lambda x), \quad \begin{array}{l} x \geq 0 \\ \lambda, \eta > 0 \end{array}$$

Hence, the parameters shown in table 3-7 correspond to  $\lambda, \eta$  respectively, whereas the parameters shown in table 3-3 correspond to  $\alpha, b$ .

#### End of Note

The aforementioned comparison was implemented for the in-plane Poisson's ratio  $\nu_{xy}$  too:

	$\nu_{xy}$			
	MLE		Kolmogorov-Smirnov criterion, $\alpha$	
	PhD results	Matlab	PhD results	Matlab
<i>Normal</i> ( $\mu, \sigma$ )	0.5 0.055	0.5 0.054	0.740	0.762
<i>Gamma</i> ( $\lambda, \eta$ )	178.00 88.890	177.43 88.647	0.809	0.811
<i>Lognormal</i> ( $\mu, \sigma$ )	-0.70 0.11	-0.70 0.11	0.816	0.833
<i>Weibull</i> ( $k, \lambda$ )	0.525 9.15	0.525 9.15	0.697	0.696
<i>Nakagami</i> ( $\mu, \omega$ )	-	21.81 0.253		0.78

<i>Logistic</i> ( $\mu, \sigma$ )	-	0.49 0.03		0.86
<i>Rician</i> ( $s, \sigma$ )	-	0.50 0.06		0.763
<i>Min Extr</i> ( $\mu, \sigma$ )	0.529 0.057	0.529 0.057	0.634	0.648
<i>Max Extr</i> ( $\mu, \sigma$ )	0.475 0.038	0.475 0.038	0.896	0.888

Table 3-8: Comparison of PhD results with Matlab model, Data: In plane Poisson’s Ratio with loading at 0°

From the above table, it is again obvious that the Matlab model is correct. The main reason for adding this comparison is to show the influence of decimals when less data are used as inputs (at table 3-6, 19 values for  $X_T$  and 8 values for  $\nu_{xy}$ ).

Prior to the presentation of the next subchapter, it is worth mentioning that improper choice of distributions can lead to the rejection of the null hypothesis as presented in the subchapter 3.2 of the supporting document. For example, the exponential distribution is incapable of describing the stochastic nature of the material properties as it is evident from its  $\alpha$  value shown in table 3-7. Hence, it is allowed to accept all the distributions for the stochastic analysis of the tensile strength  $X_T$ , except from the exponential one because its  $\alpha$  value is  $\alpha = 1.01E - 06$ ; much smaller than the predefined level of significance  $\alpha_0 = 5\%$ . A visualization of this fact is given below

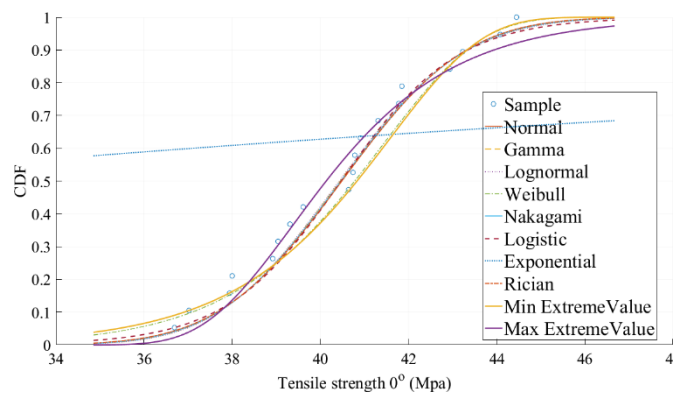


Figure 3-2: CDFs, Experimental Data, PhD dissertation, Case:  $X_T$

To conclude, in this subchapter it is proved that the Matlab model, which is based on the theory presented in subchapters 3.1-3.3 of the supporting document, can verify the results from the PhD dissertation at Ref.[9].

### 3.3 Generate correlated variables

The next step in the statistical analysis is to create material property inputs that will be used in the FEA. A trivial way to do that is to simply generate random samples with values between 0 and 1 from a uniform distribution,  $U(0,1)$  and then find the inverse cumulative function at these values from the distributions presented in table 3-5. However, in that way a potential introduction of the correlation between the material

properties wouldn't be possible and it is intuitive that for example properties that are dominated from the same mechanisms will have correlated properties as we saw at subchapter 2.5. Hence, a different method to generate correlated variables was implemented and is extensively explained in subchapter 3.4 of the supporting document. A brief, visual representation of this method is given below:

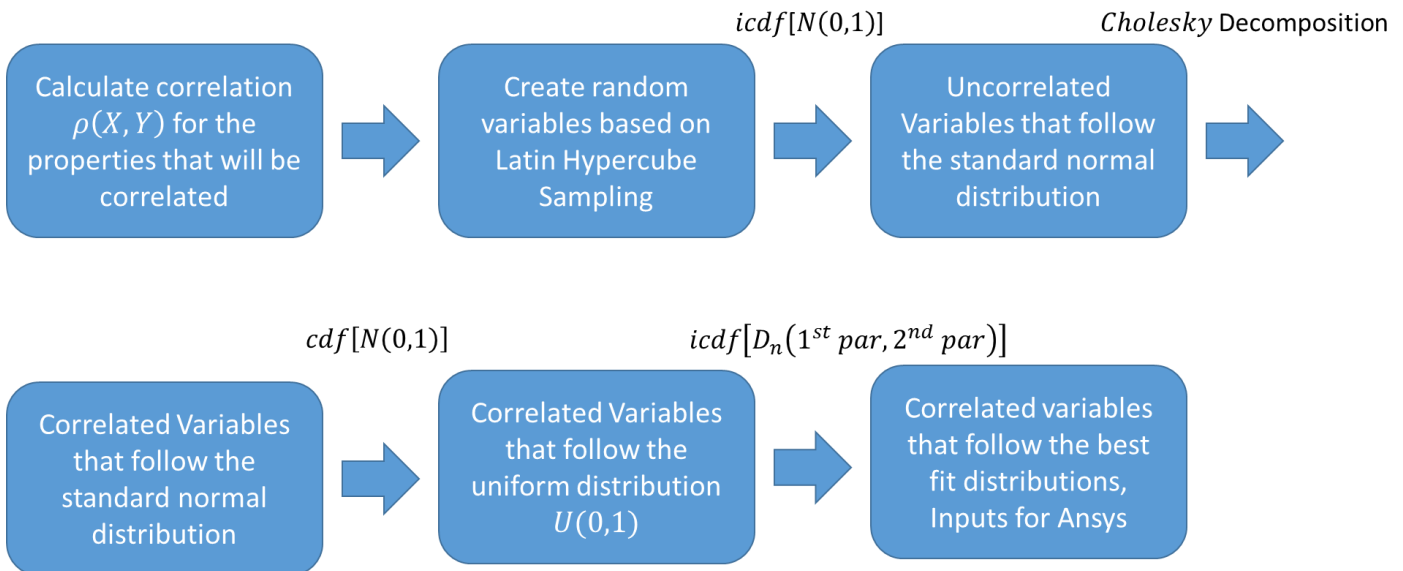


Figure 3-3: Workflow, Generate correlated variables for samples that follow different distributions

Briefly, what is shown in the figure above, is the procedure to create a pre-defined amount of variables that are correlated and still follow the distributions with the parameters shown in table 3-5. The first step is to create 100 random values between 0 and 1 for each material property based on the Latin Hypercube Sampling. Then, by taking the inverse cumulative function of the standard normal distribution at the values of the random variables which were defined previously, we end up with uncorrelated variables that follow the standard normal distribution. Then, by using the Cholesky transformation and by using as input the variance-covariance matrix  $Q$  as shown in eq. 3.4.7 of the supporting document, we end up with correlated variables that follow the standard normal distribution. Then, we take the cumulative distribution of these correlated variables and we end up with variables that are correlated and follow the Uniform distribution. As the last step, we take the inverse cumulative function of the distribution that best fits to each material property as shown in the table 3-5 and we end up with values that are both correlated and still follow the desired distributions.

In this thesis, the properties that are correlated are only the ones that were derived from the same experiments. This means that only the correlations  $\rho(S_{11T}, E_1)$ ,  $\rho(S_{22T}, E_2)$  and  $\rho(S_{12}, G_{12})$  have been introduced in the analysis, but only if the correlation from the experimental data is higher than a predefined correlation, i.e.  $|\rho_{exp}| > 0.05$ . However, this method works fine even when more properties are to be correlated. The only input that this method needs is the correlation of the material properties that it is desired to be taken into account. If, instead of two, more properties are to be correlated, the only change is that the variance-covariance matrix will be  $Q = [n \times n]$  with  $n \geq 2$ . As it is shown in the last chapter where recommendations for future work are presented, it could be of great research interest to define a way in order to correlate the material properties that come from different tests such as the correlation between tensile and compressive strengths.

Another critical information is the amount of variables that it is desired to be generated. The exact amount is derived from the way the FEM analysis was performed. For reasons presented in the next chapter, the amount of generated variables was decided to be 100. Then, the workflow shown in figure 3-3 was modeled in Matlab and it was added to the Matlab model which is presented in subchapters 3.1-3.2.

In figures 3-4 until 3-6, the results from the aforementioned addition to the Matlab code are presented. Each blue circle in these figures represents the input material properties in the FEM analysis for one model run. Hence, 100 realizations mean that the Ansys model was run 100 times and each time with different material properties.

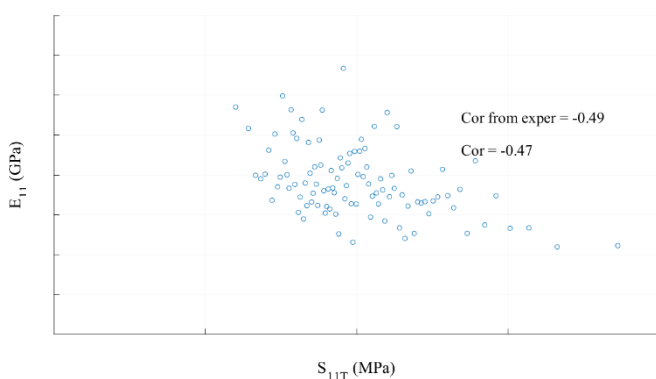


Figure 3-4: Correlated random variables,  $S_{11T}$  &  $E_{11}$

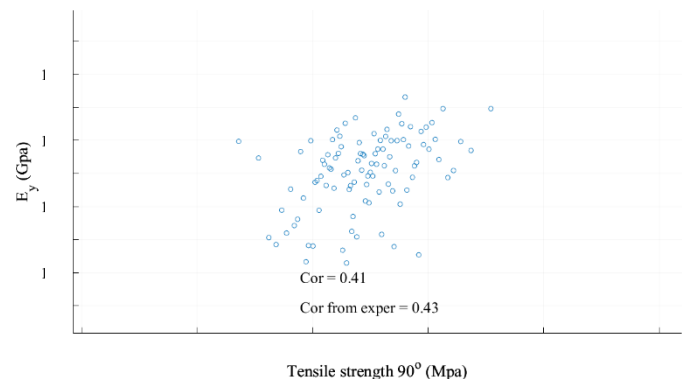


Figure 3-5: Correlated random variables,  $S_{22T}$  &  $E_{22}$

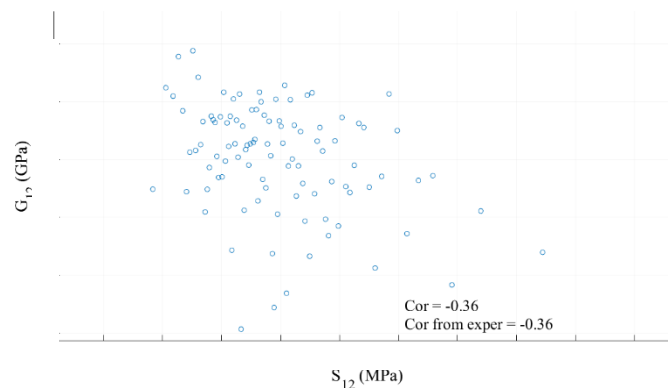


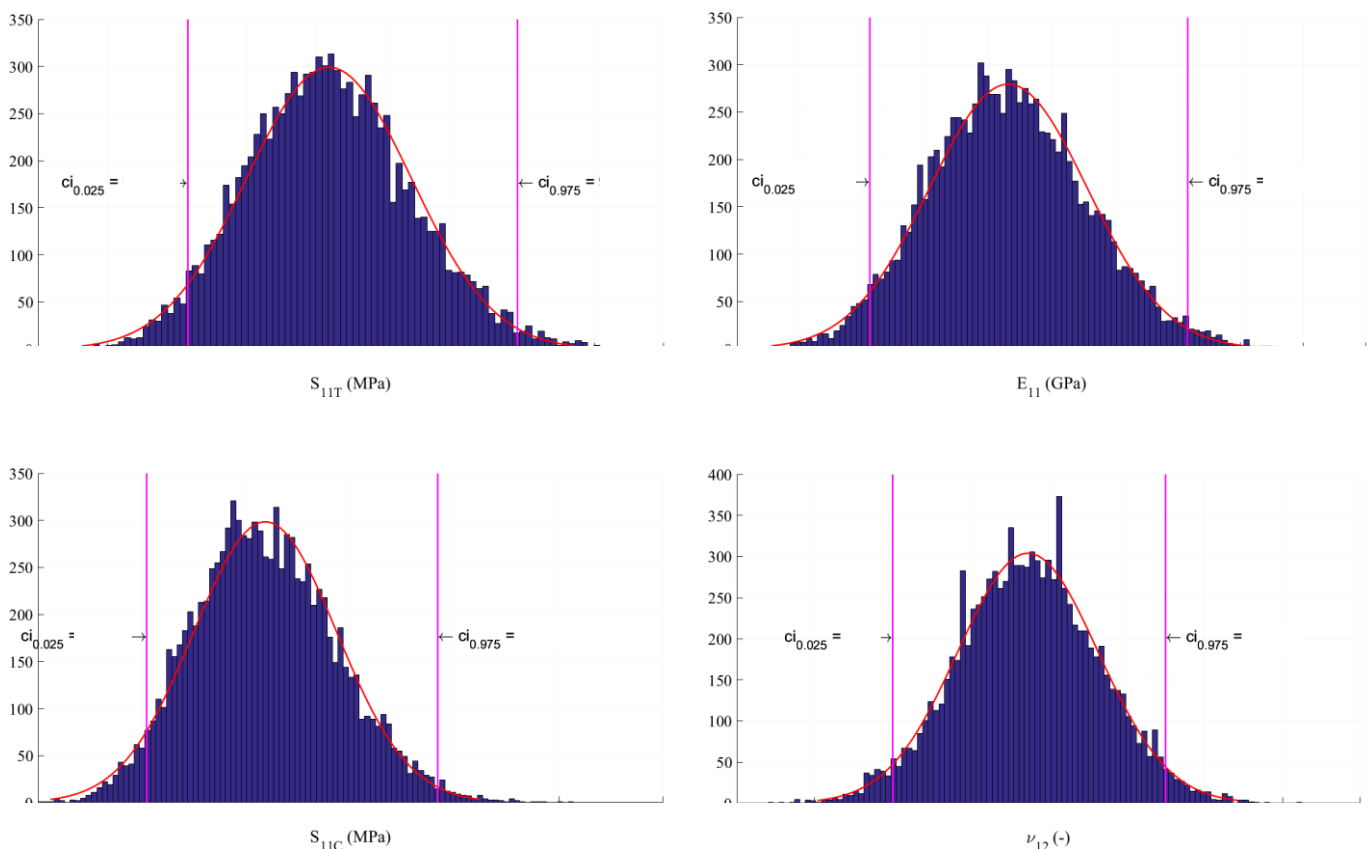
Figure 3-6: Correlated random variables,  $S_{12}$  &  $G_{12}$

At figure 3-4, it is obvious that there is strong negative correlation between the tensile strength and the elastic modulus in the fibers' direction. A perfect correlation ( $\rho = \pm 1$ ) would mean that all the blue circles would lie on a straight line. Moreover, it is obvious that the modelled method leads to desirable results as the initial correlation (Cor from exper in the above figures) between the experimental results for the tensile strength and elastic modulus is almost the same as the one for the generated variables (Cor in the above figures). Furthermore, it should be noted that the tensile strength still follows the Maximum extreme distribution,  $MaxExtr(-XX,XX)$  and the elastic modulus still follows the Maximum extreme distribution too,  $MaxExtr(-XX,XX)$  which means that no information was lost during the aforementioned method. Experienced with this procedure readers, can notice this claim by looking carefully at figure 3-4. Of course, the same holds for the rest of the correlated properties, i.e. for the couples of  $S_{22T}$  &  $E_{22}$  and  $S_{12}$  &  $G_{12}$ .

## 3.4 Bootstrap Method

This subchapter is included mostly for academic reasons and for readers who want to avoid the statistical analysis presented in this chapter and at the respective subchapters [3.1-3.4](#) of the supporting document.

In many applications, mostly for simplicity reasons, engineers do not take into account the stochastic nature of the composites' material properties and they just use their mean values. Hence, in this subchapter a method is presented which allows the usage of the mean values with a high level of certainty that in reality they will lie between a certain interval. This method is called the Bootstrap method and is explained in detail at subchapter [3.5](#) of the supporting document. It is based on the fact that if 15 new tests will be implemented for the same in plane material properties, the new mean values will be different that the ones extracted from the experiments showed in subchapter [2.4](#). Hence, this method leads to the estimation of a specific parameter such as the mean value " $\mu$ " for the whole expected population instead of just the  $\mu$  of the given sample and was implemented to take into account the distribution of the mean values for each material property. For 10000 Bootstrap samples for each material property, the results are:



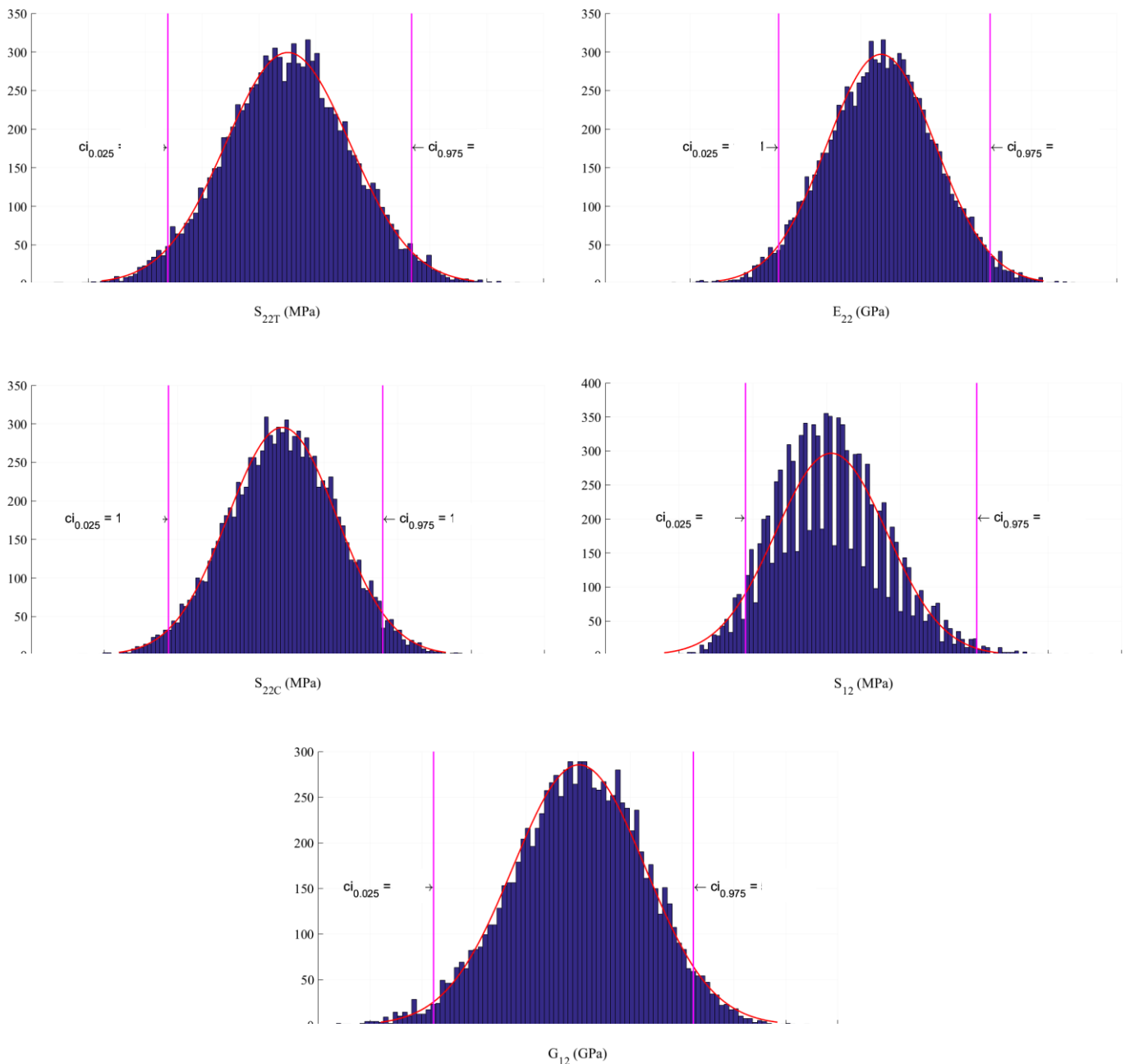


Figure 3-7: Bootstrap Method, Distribution of the mean Values

The above figures can provide important information to engineers that want to use the mean values of the material properties for their analyses. For example, it can be extracted with a confidence level equal to 95%, that the mean value of the tensile strength in the direction parallel to the fibers is between  $XX MPa$  and  $XX MPa$ . Furthermore, the low limit i.e.  $ci_{0.025} = XX MPa$  means that there is only 2.5% probability that the tensile strength's mean will be below this value and as a result it can be used for a conservative design. The same method can be used for the evaluation of mean values with 1%, 5%, 10% probability of not exceedance. To conclude, the red line in the above figures, show the adequacy of the normal distribution to describe the distribution of the mean values.

# Chapter 4: Large Scale Specimens

In this chapter, focus is given on the large scale specimens. As it was mentioned at the start of this thesis, (subchapter 1.2) the thesis' objective is to develop an algorithm which would be capable of predicting the structural response of large monolithic and sandwich panels within a certain level of confidence. The previous chapters, even if they were tedious and time-consuming, they were just the preparation that led to the inputs for this chapter's calculations. In this chapter, readers can find information regarding the manufacturing of the large scale specimens, the 3-point bending experimental results as well as the comparison of these results with finite element models. The FEA models were built in such a way in order to take into account the stochastic nature of the composite's material properties.

The main reason behind the execution of the large scale specimens is the DMO, which was interested in estimating the structural response of large scale monolithic and sandwich specimens that are aimed to be used for the construction of MCMVs. The geometry of the panels shown in this chapter is characteristic of the plates that will be present in the vessel's hull and superstructure, between two consecutive primary stiffeners. DMO wanted to check which panel configuration will result to the best structural behavior and for that reason they ordered the designs of monolithic, sandwich and hat-stiffened panels. The latter are not examined in this thesis due to our lack of input data, due to their complexity during the manufacturing procedure and due to the big amount of different materials that was used.

## 4.1 Manufacturing of large Scale Specimens

Following what was mentioned in the previous paragraph, DMO<sup>[24]</sup> requested from Solico<sup>[33]</sup> (with DSNS<sup>[3]</sup> being the intermediate) to design the monolithic and the sandwich panels which are shown in Appendix F. The designs were sent to KVE in January 2017 and KVE produced them in the same month. Of course, the fiber volume of the large scale specimens was designed to be equal to  $V_f = XX\%$ . That fiber volume also defined the fiber volume of the small scale coupon tests because it was desired to avoid any violation of the building block approach and more specifically any violation by passing from block 3 to block 4.

### 4.1.1 Monolithic Panels

Release Agent: XX
Lay-up: XX (Appendix A)
Peel-ply: XX

Flownet: XX
Vacuum bag: XX
Resin: XX

Table 4-1: Materials used for the construction of the monolithic panels

Firstly, the XX layers of XX EQXXX were laid up on an aluminium tool as shown in figure G-1. This lay-up was then covered with peelply and flownet. A central runner was applied on top, with two secondary runners next to that. Vacuum outlets were placed along the long sides at the bottom of the laminate, at about XX cm spacing. Then all is vacuum bagged, leak tested and left under full vacuum overnight. Infusion was performed the next day. Then, the resin was mixed and the infusion was started which is shown in figure G-2. When the resin flow front has passed the secondary runners, the inlets for those runners were opened as well. Infusion pressure was initially set at XX mbar. When the resin had reached all outlets, the pressure was increased in steps of XX mbar to XX mbar. After XX minutes, the resin inlets were closed and the laminate was left to cure overnight. The next day, the morning, the laminate was demoulded and process consumables were removed. Then, the panels were postcured in the same postcure cycle. The KVE autoclave was used for this postcure. All panels were placed in the autoclave in such a way that adequate airflow all around each panel was guaranteed, ensuring an even temperature distribution. The temperature logs of are compiled in figure G-3.

According to the manufacturer(KVE), the overall impregnation was perfect, with no visible dry spots or voids. The resulting thickness was XXmm and the panels were trimmed to XXxXXmm manually using a water-cooled diamond plated cutter.

#### 4.1.2 Sandwich Panels

For many marine applications, sandwich panels in hulls and decks are infused in one shot. There, the core is either perforated or grid/scored, to allow resin the flow from upper skin through the core to the lower skin laminate. In this case, with the very high core, and with this type of resin, it was decided to use a solid, impermeable core and infuse both skins separately. This avoids an enormous resin uptake of the core, and the associated exothermic reaction of the resin in the core which potentially damages the core. Due to the long lead-time of the core, an off-the-shelf XX mm core was selected, which was bonded in XX layers to the required XX mm using XX resin, and a vacuum bag to compress the core during cure.

Release Agent: XX
Lay-up: XX
Core: XX
Peel-ply: XX
Flownet: XX
Vacuum bag: XX
Resin: XX

Table 4-2: Materials used for the construction of the sandwich panels

The panel was infused from both sides, so the lay-up started with a runner with flownet, peelply, glass, core, glass, peelply, flownet and finally runners on top too. The infusion was from 1 long side of the panel to the other long side, as shown in figures G-4, G-5 and G-6. Infusion pressure was initially set at XXmbar. When the resin had reached all outlets, the pressure was increased in steps of XXmbar to XXmbar. After XX minutes, the resin inlets were closed and the laminate was left to cure overnight. The next day, the morning,

the laminate was demoulded and process consumables were removed. The post curing occurred simultaneously with the monolithic panels which is described above.

According to the manufacturer, the impregnation of both skins is good, with no visible dry spots or voids. The resulting thickness was  $XX$  mm. The panels were trimmed to  $XX \times XX$  mm manually using a water-cooled diamond plated cutter.

The resultant monolithic and sandwich panels can be seen in figures G-7 and G-8.

## 4.2 Modelling of large scale specimens' experiments

In the previous subchapter, the procedure towards the construction of 2 monolithic panels and 2 sandwich panels were shown. These panels, when they were in their final form, were sent to TNO where they were tested in 3 point bending. Generally, in this subchapter, the aim is to model in a FEA model (Ansys v17.1) the experiment shown in the following figure:

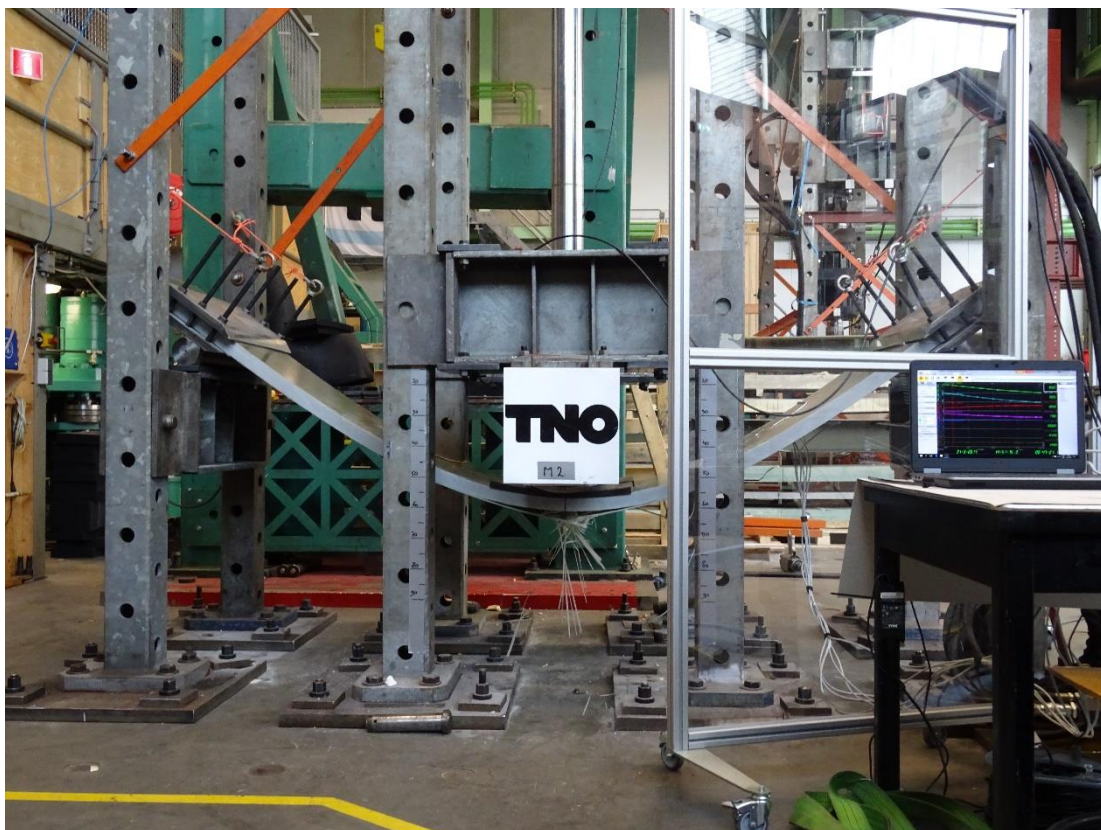


Figure 4-1: 3 point bending test, monolithic panel

In figure 4-1, one of the two monolithic panels are shown a little bit after it sustained its maximum vertical load at the middle of the plate which led to its ultimate failure. This figure is helpful towards the preparation of the FEA model regarding its boundary conditions and the applied load. By looking carefully in the above figure and combining it with the figure 4-2, the following conclusions can be made:

- Only 1/4 of the panel will be modelled due to the symmetric loading/geometry as shown by the red dashed lines of figure 4-2. The part that will be modelled is lightly shaded with green colour.
- The part of the panel that lies at the left of the left support will be discarded as there is no interest in this area. This part is shown in figure 4-2 and lies at the left of the green dashed line. The same holds for the part of the panel that lies at the right of the right support (right of purple dashed line). These parts are lightly shaded with purple colour.
- It is assumed that any horizontal force at the panel will just lead to the rotation of the cylinder which supports the panel (blue colour, figure 4-2, right). As a result, the supports at the end are assumed to be simple supports which means that they are free to rotate as well as able to freely slide towards the longitudinal direction of the panel

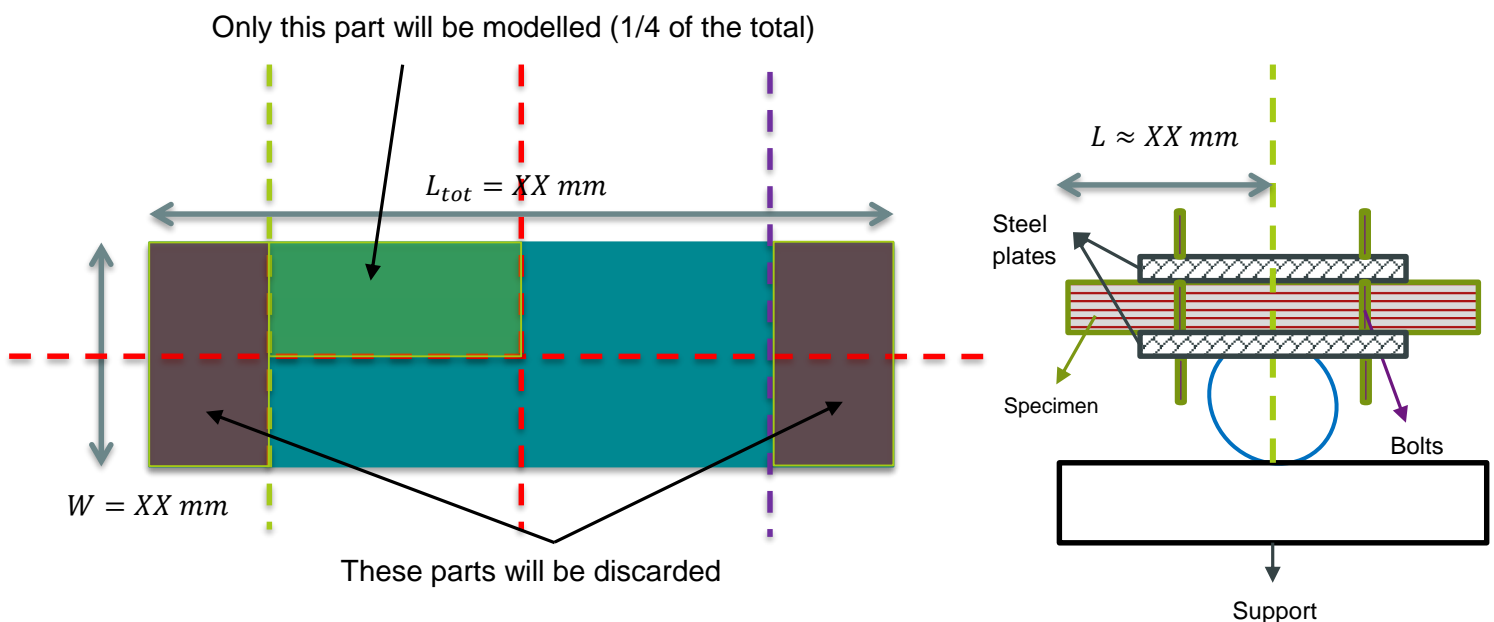


Figure 4-2: Geometry of panels (left figure), boundary conditions (right figure)

Note for the large scale experiments: Prior to the presentation of the FEA models for large scale specimens, the writer considers significant to make a discussion about their experimental results. Unfortunately, TNO didn't provide DSNS with a report where all the information would be included because DMO was its official customer. Only some figures were provided to DSNS along with the vertical force - vertical displacement curves which are shown and discussed in Appendix H. Readers that are interested to see how the large specimens failed and get some comments on that, are suggested to read this Appendix.

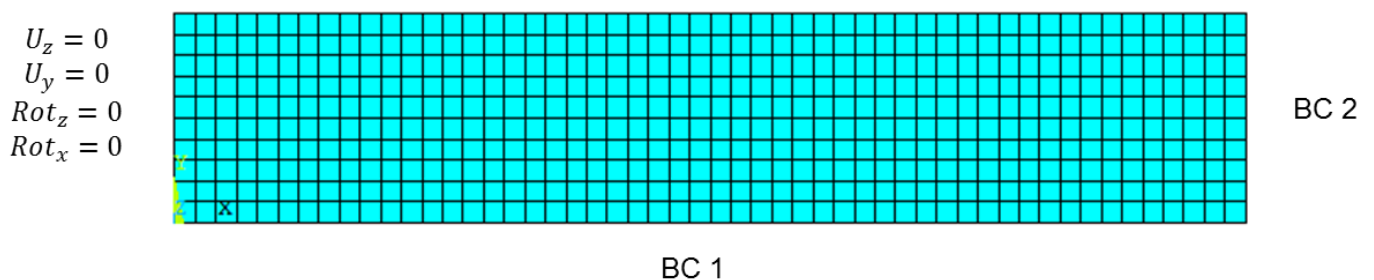
### 4.2.1 Introduction of Imperfections

For this simulation, the writer considered proper to introduce imperfections in the FEA model. In this subchapter this procedure is depicted which is based on the assumption that the imperfections can be simulated as the summation of many different mode shapes<sup>[26, 27]</sup>. One model was made for each panel due

to different geometries as shown in [Appendix H](#) which results to 4 models in total; 2 for monolithic and 2 for sandwich panels.

The element type that was used here is again shell181; information regarding this element type can be found in subchapter [2.2.1](#) of the supporting document. The only difference is that here the integration option was changed from fully integrated elements with compatible modes to reduced integrated ones with hourglass control. That was done in order to save computational time because later it is shown that a big amount of simulations should be run and this option can save a significant amount of time (days in our case) without losing any accuracy at the results. Regarding the lay-up of the sections, the FEM models were built in accordance to [Appendix H](#) and subchapter [4.1](#) where the details of the sections are given (plies' lay-up, number of plies, thickness of the section, thickness of the core for the sandwich panel). The way that the lay-up was defined in the model was the same with the one presented at subchapter [2.2.1.1](#) of the supporting document. The material properties were introduced in the model through a linear, elastic, orthotropic material for the composite parts and with an isotropic material for the sandwiches' core. The assigned values were the ones that are shown in table [2-6](#) for the composite parts and for the sandwiches' core the assigned values can be found in figure [A-8](#). The out-of plane Poisson ratio was based in the formulas shown in subchapter [2.5](#) of the supporting document and the out of Plane elastic modulus was assumed to be equal to the one at the weak direction, i.e.  $E_{22} = E_{33}$ .

Special attention should be given to the boundary conditions as by taking into account the symmetries of the geometry, certain mode shapes can be lost. For example, by taking into account the Case 1 of the figure [4-3](#) (BC1: Symmetric and BC2: Symmetric), the vertical displacement will be free at the two sides and as a result the anti-node modes will be lost (nodes with zero vertical displacement at these sides). For that reason, 4 cases of boundary conditions should be taken into account as they are shown below:



- |        |              |           |
|--------|--------------|-----------|
| Cases: | 1. BC1: Sym  | BC2: Sym  |
|        | 2. BC1: Asym | BC2: Sym  |
|        | 3. BC1: Sym  | BC2: Asym |
|        | 4. BC1: Asym | BC2: Asym |

Figure 4-3: Cases of boundary conditions for the introduction of imperfections

The length of the above model varies from model to model because the free span is not the same for all the panels as presented in [Appendix H](#). Of course in every case, it is assumed to be equal to the free span divided by 2, whereas the width in all the models was equal to  $W = XX/2 = XX \text{ mm}$ .

As the last step, a small displacement was introduced at the nodes with coordinates  $x = 0$ , i.e. at the left end and an elastic buckling analysis was run. As it is probably already clear by now, this elastic buckling analysis doesn't aim to define the critical buckling load but it is used as a mean to extract the mode shapes.

The first 3 buckling modes for the 1<sup>st</sup> monolithic panel with total free span  $L = XX \text{ mm}$  and for the 1<sup>st</sup> of the 4 Cases is shown in the figures below:

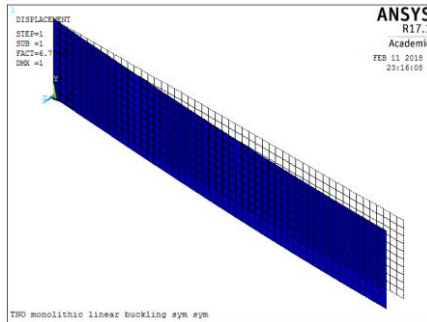


Figure 4-4: 1<sup>st</sup> monolithic Panel 1<sup>st</sup> mode, Case:1

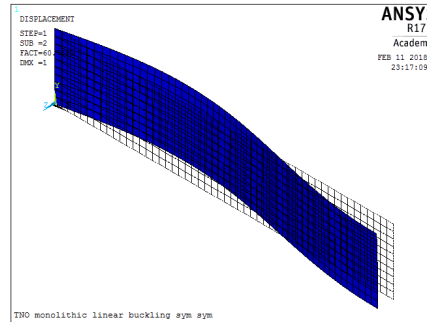


Figure 4-5: 1<sup>st</sup> monolithic Panel 2<sup>nd</sup> mode, Case:1

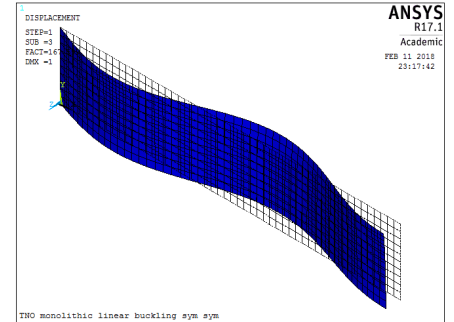
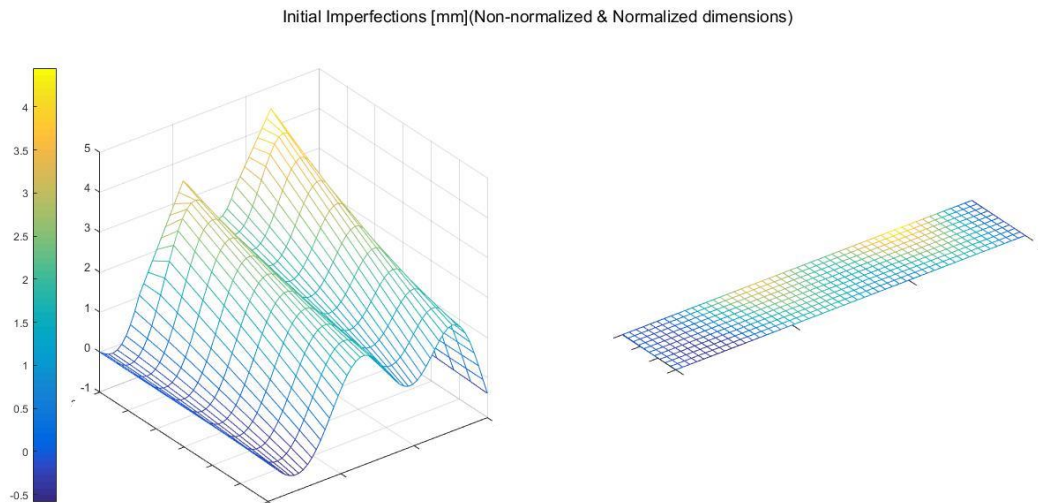


Figure 4-6: 1<sup>st</sup> monolithic Panel 3<sup>rd</sup> mode, Case:1

The next step is to determine how the imperfections will be defined. There are various ways to introduce imperfections in a model and in this thesis it was decided to use one of most commonly used ways where the imperfections are defined by the summation of a finite amount of different modes. Hence, the initial vertical displacement of each node is defined as:

$$y(k) = \sum_{i=1}^4 \sum_{j=1}^5 C \cdot y_{mode\ i,j}(k) \quad (4.2.1)$$

In eq. 4.2.1 one can see the way that the imperfections were introduced. For each case ( $i = 1 \dots 4$ ) as shown in figure 4-3 and for each mode ( $j = 1 \dots 5$ ) the resultant mode shape is multiplied with a factor  $C$ . The main reason is that the mode shapes do not give actual values of the vertical displacement but normalized ones. To further clarify that, if the vertical displacements of figure 4-4 were plotted the maximum displacement at the nodes with  $x = XX/2$  (because half the length and width were modelled) will show a value of 1 and the rest of the nodes will have vertical displacements with values between  $-1$  and  $1$ . Only the relative difference between the nodes has to be taken into account. Hence, these normalized values have to be multiplied with a factor that will assign specific units to imperfections ( $mm$  in this case) and then they can be included to a static analysis as it shown in the following chapters. For the case of the monolithic panels this factor " $C$ " was determined to be equal to  $C = h/50$  where " $h$ " is the total thickness of the monolithic panels.



**Figure 4-7: Initial Imperfections, Non-normalized(left) and normalized(right) values**

The final result of adding 20 different modes, i.e. 5 modes for 4 different cases, and multiplying them with the factor  $C = h/50 = XX \text{ mm}$  is shown in figure 4-7 for the case of the 1<sup>st</sup> monolithic panel. In this figure at the left, it is shown that a wavy shape is the outcome of adding so many different modes and at the right the same figure is shown but with normalized dimensions (pay attention to the axes' values to verify the difference). Furthermore, it is obvious that the biggest imperfections happen at the free edge that is something which is desired because in reality, the biggest imperfections are expected at the edges as we saw with the case of the thick panel during the manufacturing of the out-of plane shear coupons, figure B-10. Finally, the level of the imperfections as introduced in the FEA model is realistic when it is compared with actual measurements at the thickness of the panels as shown in figure I-1 in Appendix I.

The exact same way was followed for the determination of the imperfections for the rest of the panels except from the fact that  $C = h_{sandwich}/100$  for the sandwich panels because they have much thicker sections. In Appendix I, the 20 modes that were used for the determination of the imperfections for the 1<sup>st</sup> monolithic panel are shown. Due to the fact that the differences in mode shapes cannot be seen with naked eye, only the modes used for the 1<sup>st</sup> monolithic panel are shown there.

### 4.2.2 Modelling of Non-linear Static Analysis

The next step is to run a non-linear static analysis. The panel is again modelled with reduced integrated shell181 elements; the lay-up and the material properties were defined in the way that is shown above at subchapter 4.2.1 (mean values for the strength and stiffness properties according to table 2-5 and 2-6 respectively). The boundary conditions and the loading are defined as shown in the figure below:

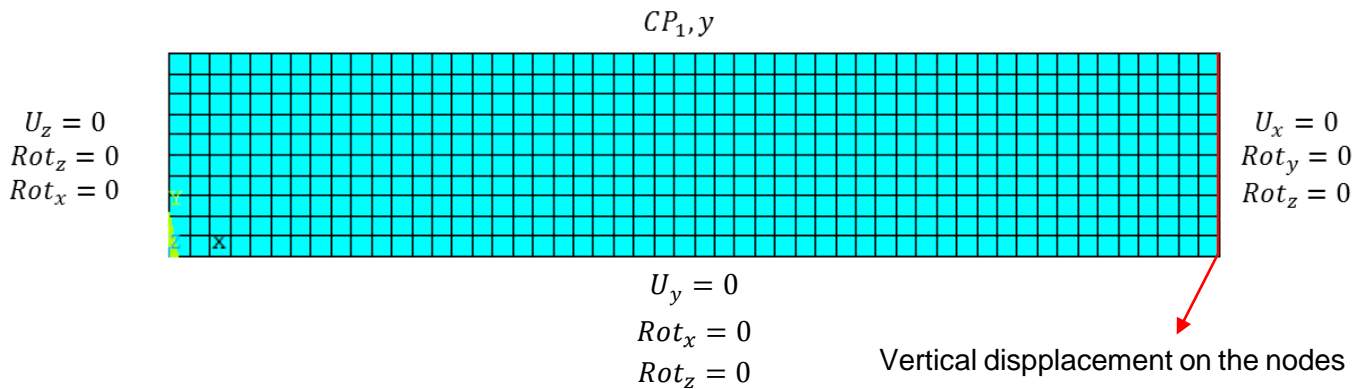


Figure 4-8: Boundary conditions and introduction of loading

The loading is modelled as vertical displacement at the midspan of the panel which corresponds at the right end of the model under the assumption that only 1/4 of the panel was modelled. The vertical displacement is incrementally increased in 100 steps from 0 to the maximum vertical displacement for each panel as shown in [Appendix H](#). Of course, the geometric non-linearities were included by introducing the command `nlgeom,on` in Ansys v.17.1. The academic background of the non-linearities can be found in Ref. [28] and more specifically about composite structures at Ref. [26].

Special attention should be given at the damage initiation and damage propagation criteria. In contrast with the elastic buckling analysis, for the non-linear static analysis a way has to be defined in order to let the model know when a ply fails and what happens after its failure. The ply fails when a failure criterion is met and the damage propagates according to the instant ply discount method. The failure criteria used in the FEA models are extensively explained at subchapter [4.3](#) of the supporting document and the progressive damage analysis is explained at subchapter [4.4](#) of the supporting document. The writer considered also significant to include the theory about the mechanics of composite structures which is presented in subchapter [4.1](#) and [4.2](#) of the supporting document. In that way, readers are suggested to read the chapter [4](#) of the supporting document and get a full view about the structural response of a composite structure under various loading conditions. Of course, readers that are familiar with the mechanics and failure of composite materials can skip this suggestion.

#### 4.2.2.1 Failure Criteria

Several failure criteria were implemented which are dependent on the nature of the composite structure's failure. These failure criteria are shown below:

Failure in Fiber Tension (Hashin Criterion)	$\left(\frac{\sigma_1}{S_{11T}}\right)^2 + \left(\frac{\tau_{12}}{S_{12}}\right)^2 + \left(\frac{\tau_{23}}{S_{23}}\right)^2 < 1, \quad \sigma_1 > 0$
Failure in Fiber Compression (Max. Stress Criterion)	$\sigma_1 < S_{11C}$

<p>Matrix Failure (Puck's Criterion)</p>	$\text{Mode A: } I_{MF,A} = \sqrt{\left(\frac{\tau_{12}}{S_{12}}\right)^2 + \left(1 - p_{6t} \frac{S_{22T}}{S_{12}}\right)^2 \left(\frac{\sigma_2}{S_{22T}}\right)^2} + p_{6t} \frac{\sigma_2}{S_{12}}, \text{ if } \sigma_2 \geq 0$ $\text{Mode B: } I_{MF,B} = \frac{1}{S_{12}} \left[ \sqrt{\tau_{12}^2 + (p_{6c}\sigma_2)^2} + p_{6c}\sigma_2 \right], \text{ if } \begin{cases} \sigma_2 < 0 \\ \left  \frac{\sigma_2}{\tau_{12}} \right  \leq \frac{F_{2A}}{F_{6A}} \end{cases}$ $\text{Mode C: } I_{MF,C} = \frac{S_{22C}}{\sigma_2} \left[ \left(\frac{\tau_{12}}{2(1+p_{2c})S_{12}}\right)^2 + \left(\frac{\sigma_2}{S_{22C}}\right)^2 \right], \text{ if } \begin{cases} \sigma_2 < 0 \\ \left  \frac{\sigma_2}{\tau_{12}} \right  \geq \frac{F_{2A}}{F_{6A}} \end{cases}$
--	--

The Hashin criterion was opted as the criterion for the determination of the fiber tensile failure due to the fact that it takes into account the influence of the in plane and out of plane shear stresses on the fiber failure. The effect of the shear stresses has been observed to have a noticeable effect on the tensile fiber failure as it is explained in the respective subchapter in the supporting document along with its references. The simplest failure criterion was opted for the compressive failure of the fibers, i.e. the Maximum stress criterion, because the determination of the compressive strength during the small scale testing, takes into account effects such as micro-buckling of fibers, kinking and crushing of fibers. For that reason, it should be noticed that the Puck Criterion, the Hashin Criterion and the Max. Stress criterion have exactly the same formula when the failure due to compression in the fibers' direction is to be considered. The Puck Criterion was opted for the determination of failure initiation when the matrix is considered for both tensile and compressive loading due to its sophisticated model. Puck combined phenomenological observations with in depth knowledge regarding composite's fracture and he developed the above shown criteria. He separates the failure criterion in two loading cases; one corresponds to matrix tension (mode A) and the second corresponds to matrix compression but the latter takes also into account the relative ratio of the compressive and the in plane shear stress. It is a pretty complex criterion and for that reason it is explained in depth in subchapter 4.3.2 of the supporting document. However, one should also define the fitting parameters when he uses the Puck's criterion which in the case of glass fibres are  $p_{6t} = 0.3$ ,  $p_{6c} = 0.25$ ,  $p_{2c} = 0.2$ <sup>[29]</sup>.

#### 4.2.2.2 Progressive damage modelling

Up to now, the way that a failure is initiated has been defined which occurs when the respective failure criterion is met for one of the four specific failure modes (fiber tension, fiber compression, matrix tension and matrix compression). However, the next question is still open. What happens when a ply fails at one of these modes? The answer is given at the subchapter 4.4 of the supporting document. Briefly, it is assumed that the elements' plies can be in 2 distinct statuses. They can be either undamaged or damaged. As the vertical displacement is incrementally increased, more and more stresses are developed at the structure. At one point, one (or more) of the aforementioned criteria is met and the failed ply changes its status to damaged only for the mode that has failed. The damaged ply, from now and on, will have a reduced stiffness matrix due to the mode that has failed and it can be reduced even more if at the following loading steps other failure modes are initiated too. The reduced stiffness matrix is shown below:

$$[Q]_d = \begin{bmatrix} \frac{S_{11}}{1-d_f} & S_{12} & S_{13} & 0 & 0 & 0 \\ S_{21} & \frac{S_{22}}{1-d_m} & S_{23} & 0 & 0 & 0 \\ S_{31} & S_{32} & \frac{S_{33}}{1-d_m} & 0 & 0 & 0 \\ 0 & 0 & 0 & \frac{S_{44}}{1-d_s} & 0 & 0 \\ 0 & 0 & 0 & 0 & \frac{S_{55}}{1-d_s} & 0 \\ 0 & 0 & 0 & 0 & 0 & \frac{S_{66}}{1-d_s} \end{bmatrix}^{-1} \quad (4.2.2)$$

$$d_f = \begin{cases} d_f^+, & \text{if } \lambda_f^+ > 0 \\ d_f^-, & \text{if } \lambda_f^- > 0 \end{cases}$$

$$d_m = \begin{cases} d_m^+, & \text{if } \lambda_m^+ > 0 \\ d_m^-, & \text{if } \lambda_m^- > 0 \end{cases}$$

$$d_s = (1 - d_f^+)(1 - d_f^-)(1 - d_m^+)(1 - d_m^-)$$

Of course the values of the damage variables  $d_i^\pm$  have to be defined in the model. According to Ref. [30], “a good agreement between experimental results and numerical predictions” can be obtained when the damage variables take the values:  $d_f^+ = 0.93, d_f^- = 0.86, d_m^+ = 0.8, d_m^- = 0.6$ . Finally, the values of  $\lambda_i^\pm$  define the loading orientation. If the fibres fail in tension, the damage variable  $d_f$  becomes equal to  $d_f^+$  whereas if they fail in compression  $d_f = d_f^-$ . Then, the value of the  $d_f$  is used to determine the reduced stiffness of the failed ply by calculating the inverse of the compliance matrix as shown in eq (4.2.2). Regarding the core of the sandwich panels it was decided to assume  $d_f^+ = 1.0, d_f^- = 1.0, d_m^+ = 1.0, d_m^- = 1.0$  which corresponds to full loss of stiffness when a ply fails and the damage initiation criterion is the maximum stress criterion. The reason behind this choice is that in sandwich panels the core is responsible of carrying the shear forces whereas the skin are responsible for carry the bending moments and as a result the stress at the core is not complex and there is no need for sophisticated failure criteria.

### 4.2.3 Results of non-linear Static Analysis

By taking into account what was presented in subchapter 4.2.2 and by introducing the imperfections as shown in subchapter 4.2.1 the vertical force-displacement curve for the first sandwich panel is shown below:

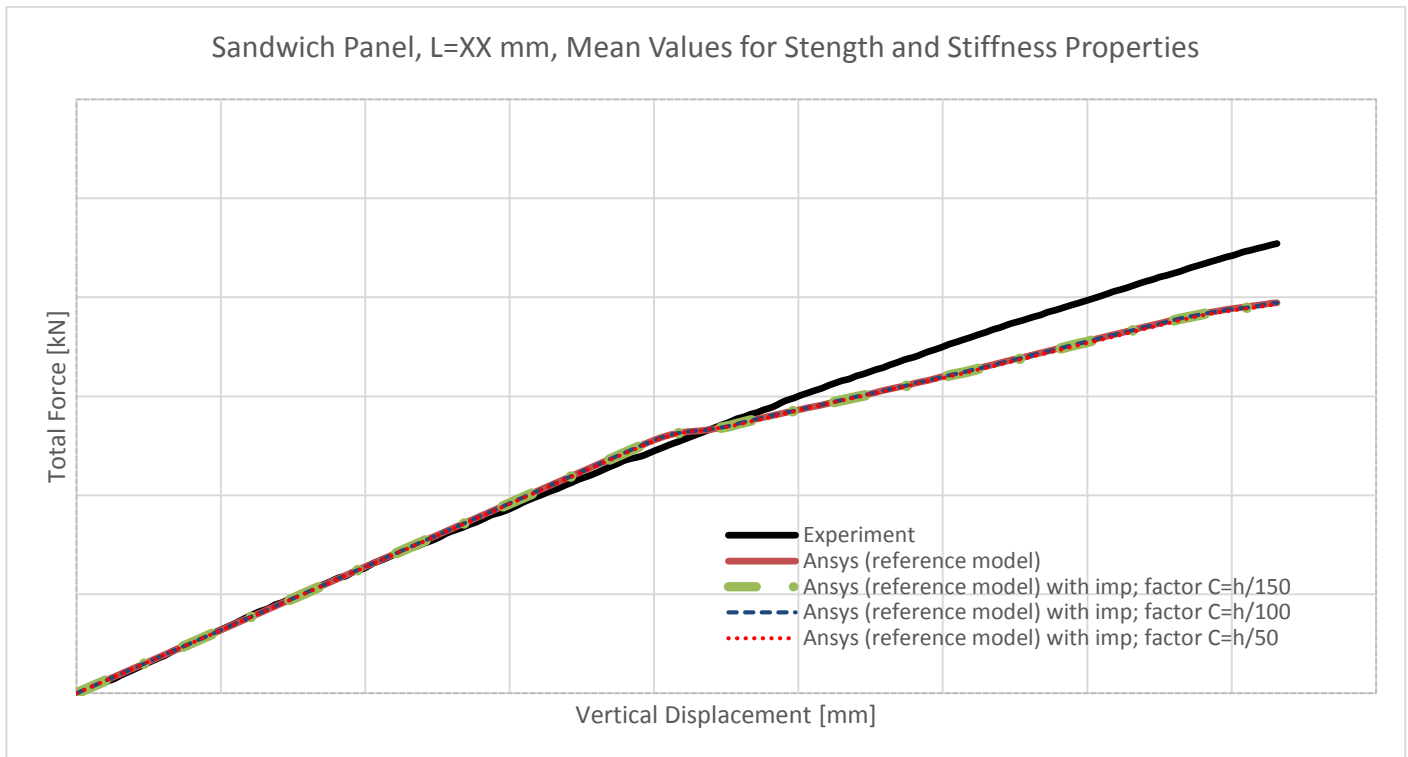


Figure 4-9: Vertical force-displacement curves, 1<sup>st</sup> sandwich Panel

Firstly, from the figure above it is obvious that the level of the imperfections has a negligible influence on the structural response of the panel. This is something that was expected due to the nature of the load. For example, if instead of vertical displacement the loading was introduced as horizontal displacement, the effect of imperfections would be noticeable. However, the vertical load lead to a sagging shape for the panels and as a result the influence of the imperfections is negligible. That was the case for the rest of the panels and in order to avoid a lengthy report with unnecessary information, this effect is omitted from now and onwards.

Secondly, the fact that the plate *iii*, which was manufactured for the in-plane shear tests, had a much higher fibre volume ( $V_f \approx XX\%$  instead of  $V_f = XX\%$ ) led to a significantly higher Shear modulus than the expected one. The influence of the shear modulus is much higher on the sandwich panels than the monolithic panels as it is shown later (figures below). This is pretty evident for the 2<sup>nd</sup> sandwich panel which is shown below. At the “elastic” regime, the sandwich panels show an increased stiffness and the main reason for that has to do with the shear modulus as it is shown in the conclusions. However, for the rest of the thesis, the in plane shear properties were assumed to be the ones that were extracted from the experiments. It is known at the writer that the best scenario would require to repeat the in-plane shear tests where the fiber volume would be equal to  $V_f = XX\%$  but that was impossible due to time constrains.



Figure 4-10: Vertical force-displacement curves, 2<sup>nd</sup> sandwich Panel

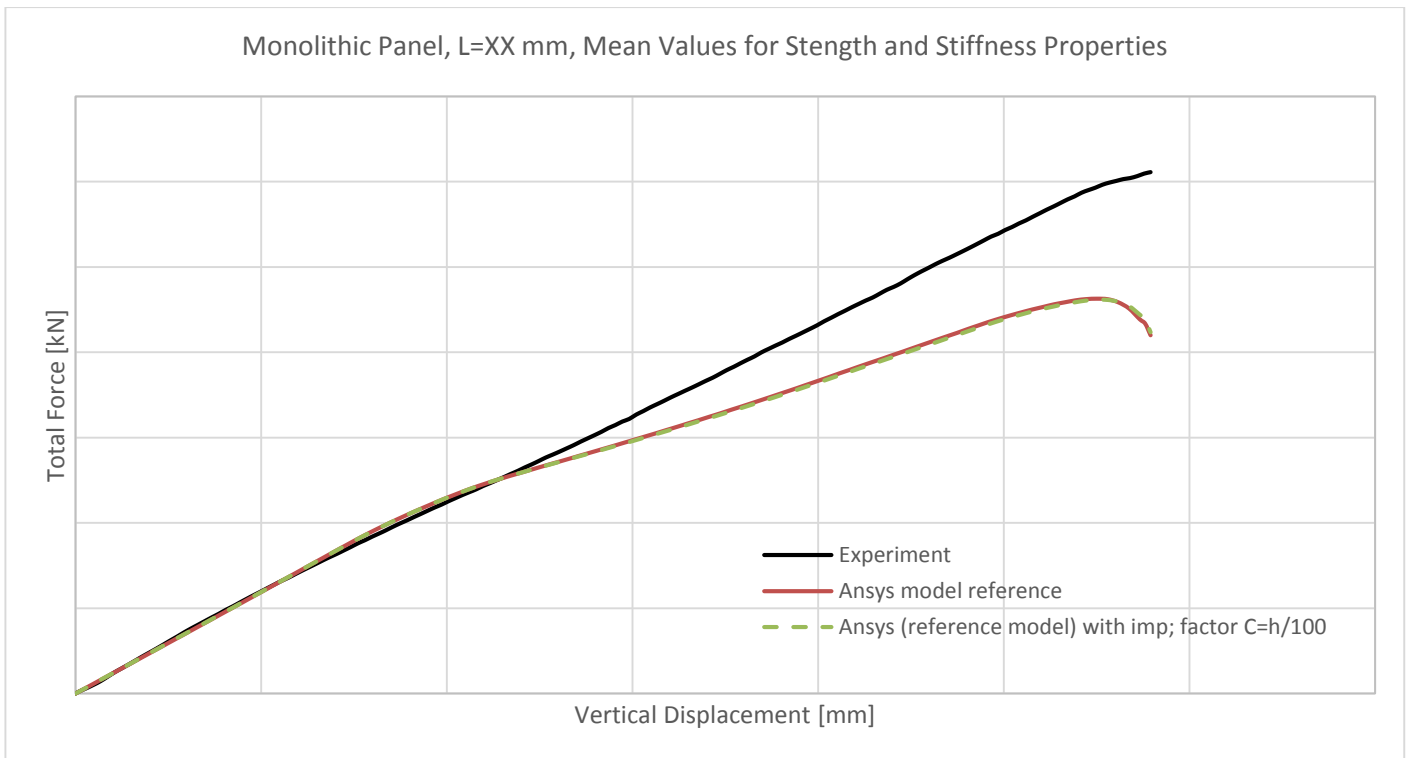


Figure 4-11: Vertical force-displacement curves, 1<sup>st</sup> monolithic Panel

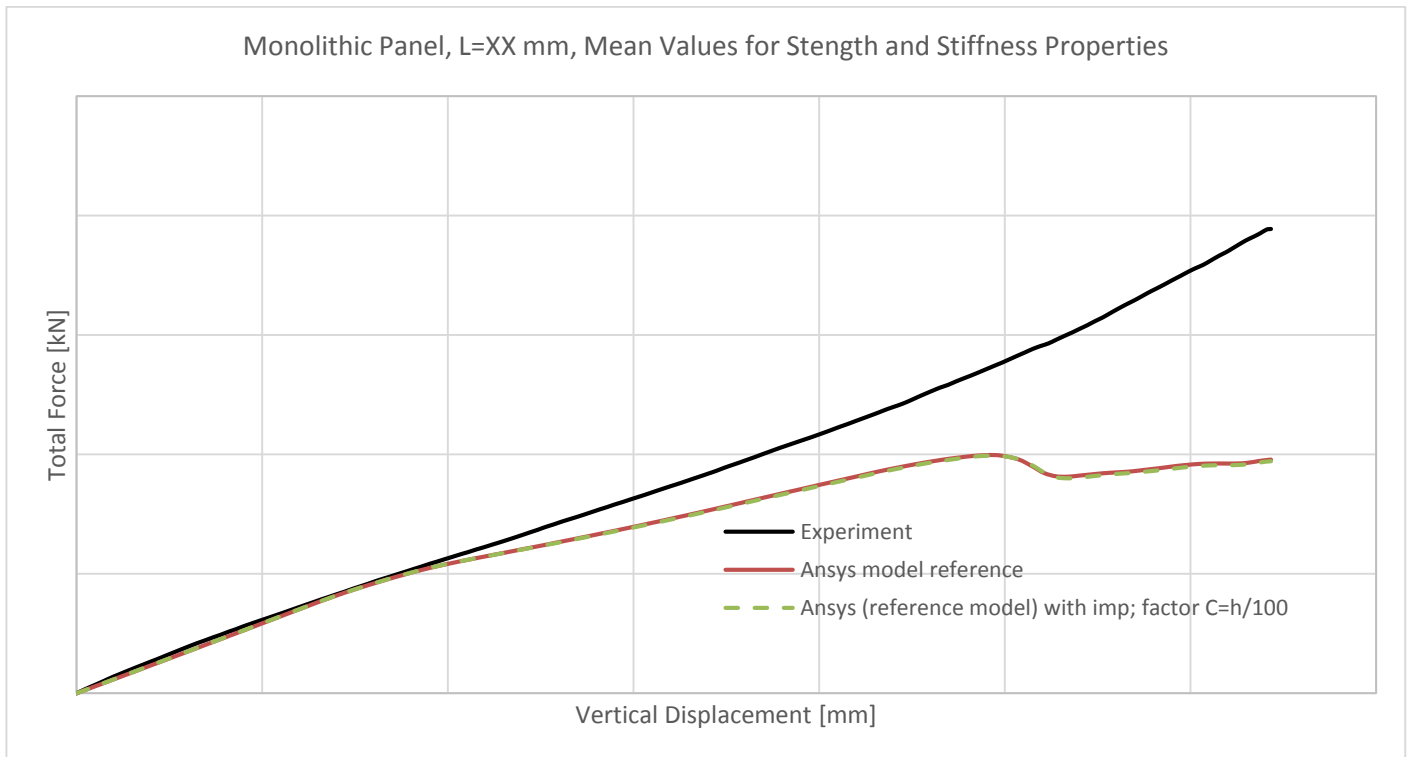


Figure 4-12: Vertical force-displacement curves, 2<sup>nd</sup> monolithic Panel

It is noticed that after one point, the stiffness of the modelled panels is much lower than the one at the experiment. This effect is intense for the case of the monolithic panels. Hence, the writer had to rethink about the definition of the boundary conditions. Special attention was given then at the way that the support was modelled.

By checking carefully the images shown in [Appendix H](#), it was obvious that the assumption that the left end of the figure 4-8 is free to slide horizontal, i.e.  $U_x = free$ , doesn't correspond to reality. Below, a zoom-in of the figure H-4 is implemented at the support

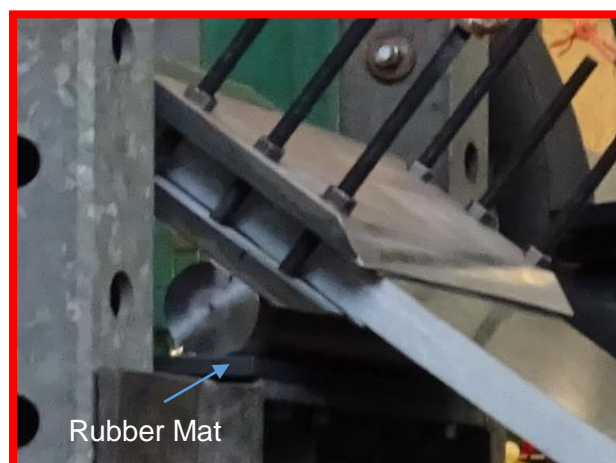


Figure 4-13: Left Support, zoom-in, 2<sup>nd</sup> monolithic panel

By looking at figure 4-12, it is safe to claim that some horizontal forces are present during the experiment. For example, the friction between the cylinder and the rubber mat would certainly produce horizontal forces

and one should also take into account the influence of the rest of the developing frictions such as the ones between the panel and the lower/upper steel plate or the ones between the cylinder and the lower steel plate. Furthermore, due to the vertical pressure from the panel to the cylinder, it is highly possible that a dent was created below the cylinder. Hence, during the cylinder's rotation, it has to rotate out of the dent which creates extra horizontal forces. Generally, the influence of the absence of horizontal forces due to the defined boundary conditions was evident in Ansys too. By the time that the models and the experiments start to deviate, in Ansys models the horizontal displacements at the supports were growing with higher rate comparing to the start of the analysis. Hence, the writer considers significant to find a way in order to introduce the effect of horizontal forces.

#### 4.2.4 Calibration for the horizontal forces

The best way to take into account the effect of the horizontal forces is to model the support as it was in the experiment. Volume elements can be used for the cylinder with an isotropic material (steel) and shell elements for the rubber mat and the steel plates that are placed on top and below the panel. Furthermore, the steel rods can be modelled with bar elements in Ansys. However, there are two significant obstacles that led to the avoidance of such a model. Firstly, all the characteristic of the contacts such as the friction coefficient should be known but these values are unknown to the writer. Secondly, as it is shown later, 100 time-consuming analysis were run when the stochastic nature of the material properties was taken into account. Hence, the idea of modelling exactly the support was dropped off and a simpler, alternative solution had to be found.

The solution that was found, included the introduction of linear horizontal springs. As it is shown in the figure below, linear horizontal springs were introduced at the left end of the panels. These springs were introduced in Ansys v.17.1 through the command `et,2,14` and the spring element is:

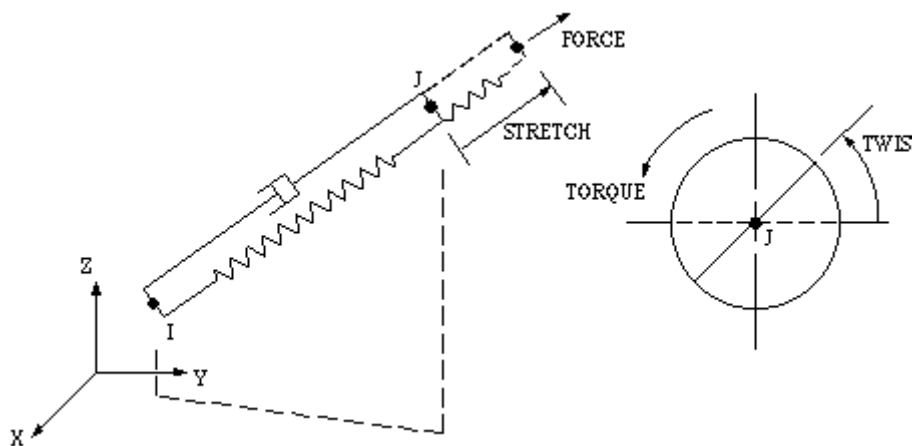


Figure 4-14: Combin14 spring element<sup>[31]</sup>

COMBIN14 has longitudinal or torsional capability in one, two, or three dimensional applications. The longitudinal spring-damper option is a uniaxial tension-compression element with up to three degrees of freedom at each node: translations in the nodal x, y, and z directions. No bending or torsion is considered. The torsional spring-damper option is a purely rotational element with three degrees of freedom at each node:

rotations about the nodal x, y, and z axes but this capability is not used for this application. No bending or axial loads are considered.

The only information that is missing is the spring's stiffness. For its definition the following steps were used:

- Run the analysis without springs
- Find the maximum  $u_x$  at location  $x = 0$
- Find the maximum vertical force,  $F_V$ , from the experiment (it is assumed that in reality, the loading conditions are known)
- Find the maximum horizontal force  $F_X$  by multiplying  $F_V$  with the friction coefficient (unknown yet)
- Apply the formula  $F_X = K \cdot u_x$  to find the stiffness of the springs

Up to now, the friction coefficient is unknown and it was decided to calibrate it according to one of the two sandwich panels and apply the " $\mu$ " to the other panel too. The determined friction coefficient was  $\mu = XX$  for the sandwich panels. Furthermore, due to the fact that the deformed shape is totally different for the monolithic panels along with the fact that they can sustain much higher vertical displacements at the midspan, the friction coefficient for the monolithic panels was decided to be different than the one for the sandwich panels. Furthermore, due to the cylindrical shape of the support, for high horizontal displacement it is expected to get noticeable vertical displacements at the left end too. This effect is shown in figure 4-13 as well as at the figure 4-15 (right). As a result, it was decided that the monolithic panels will have a different friction coefficient than the sandwich panels which would be equal to  $\mu = XX$

The introduction of the linear springs can initiate a big discussion about the way that the boundary conditions should be introduced in FEA models in order to represent the reality as much as possible. Many questions can be raised such as why it was decided to use linear springs and not non-linear ones. Also, one can question even the mathematical function of the non-linear springs in terms of assuming 2<sup>nd</sup>, 3<sup>rd</sup> or even higher order of polynomial for the correct representation. It is obvious that in the framework of this thesis, such a study would be tedious and it would cover the material for a whole new thesis. That's why in the recommendations for future work, it is suggested to implement a study only at the supports in order to verify the accuracy of the method that is used here.

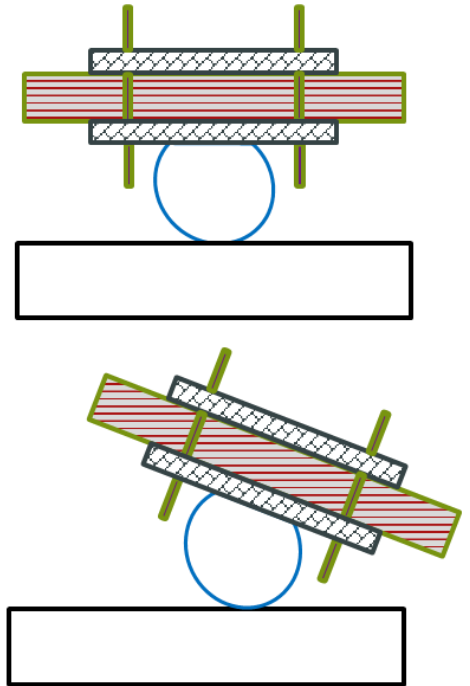
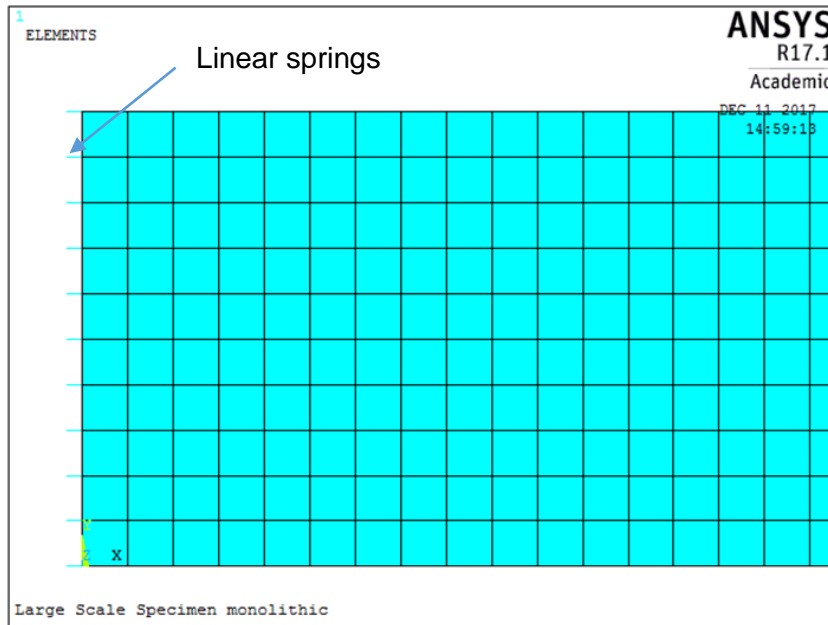


Figure 4-15: Monolithic specimen, top view with springs (left), rotating support(right)

#### 4.2.5 Non-linear Static analysis, Results with linear springs

From the figures below, it is obvious that taking into account the effect of the horizontal forces was something that had to be done. The fact that at the “elastic” part the force-displacement curves with and without springs almost coincide, means that at the start of the experiments the horizontal displacements are negligible and they do not lead to significant horizontal forces. However, for both the sandwich and the monolithic panels, it is shown that after one point, the absence of horizontal forces would mask the final results and lead to discrepancies between the experimental force-displacement curves and the resultant ones from the FEA models.

Below, the force-displacement curves are shown as they were derived from the experiments and they are compared with the results from the Ansys models without and with (calibrated) springs.

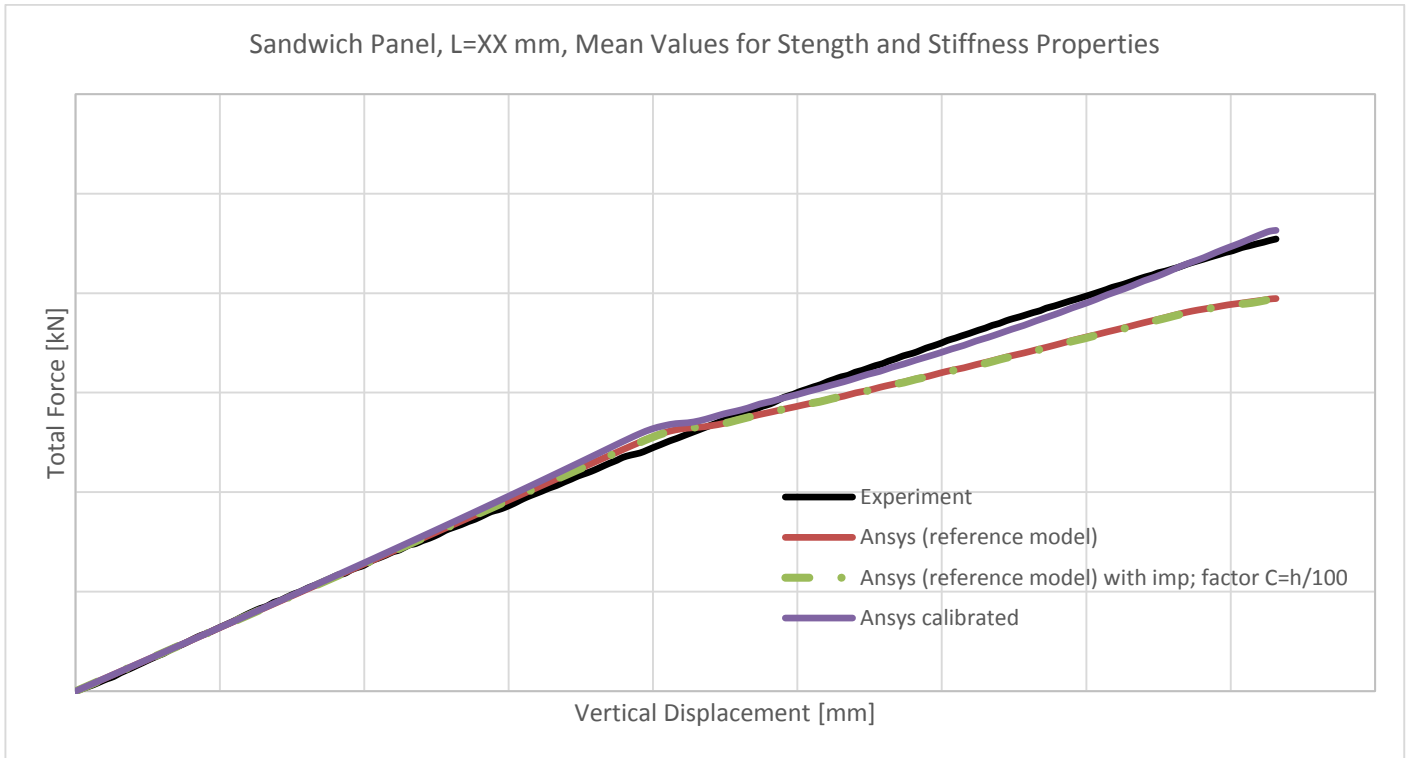


Figure 4-16: Vertical force-displacement curves, 1<sup>st</sup> sandwich Panel, for comparison

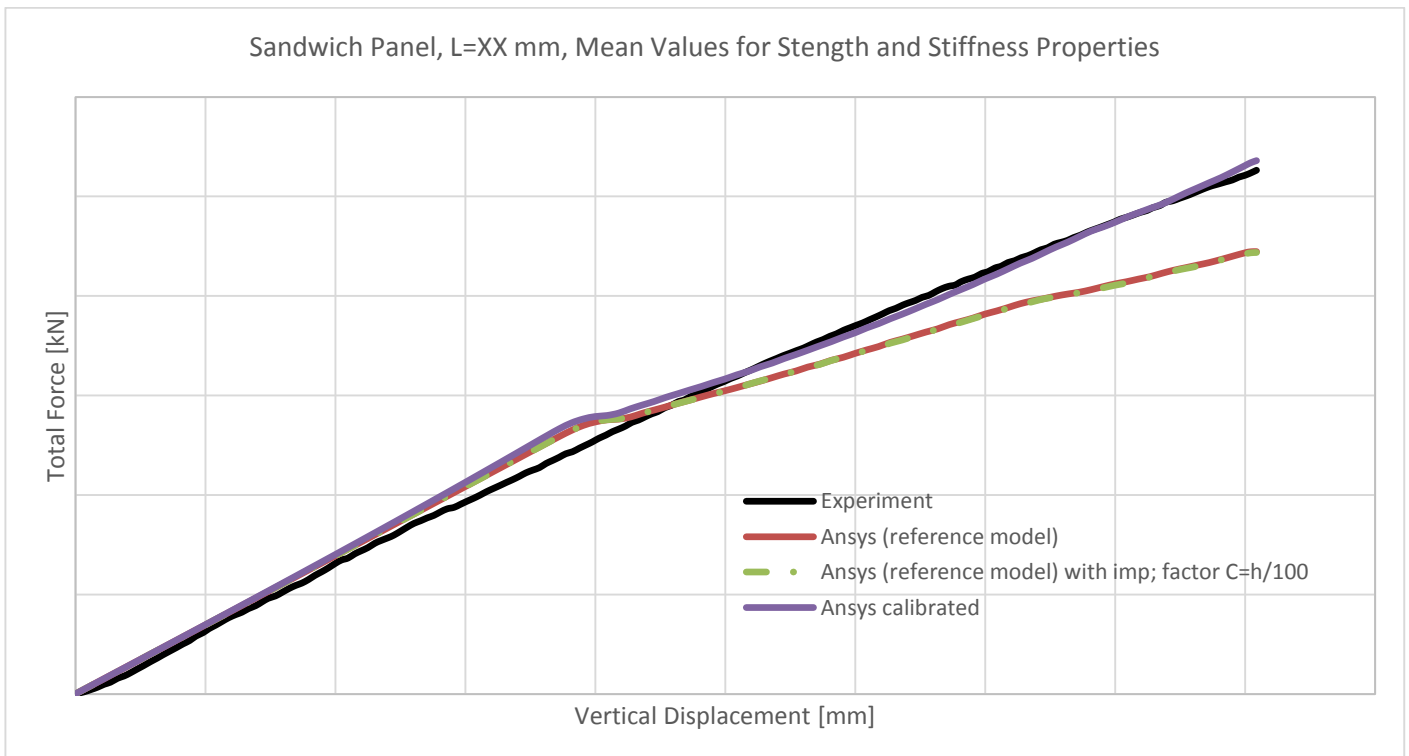


Figure 4-17: Vertical force-displacement curves, 2<sup>nd</sup> sandwich Panel, for comparison

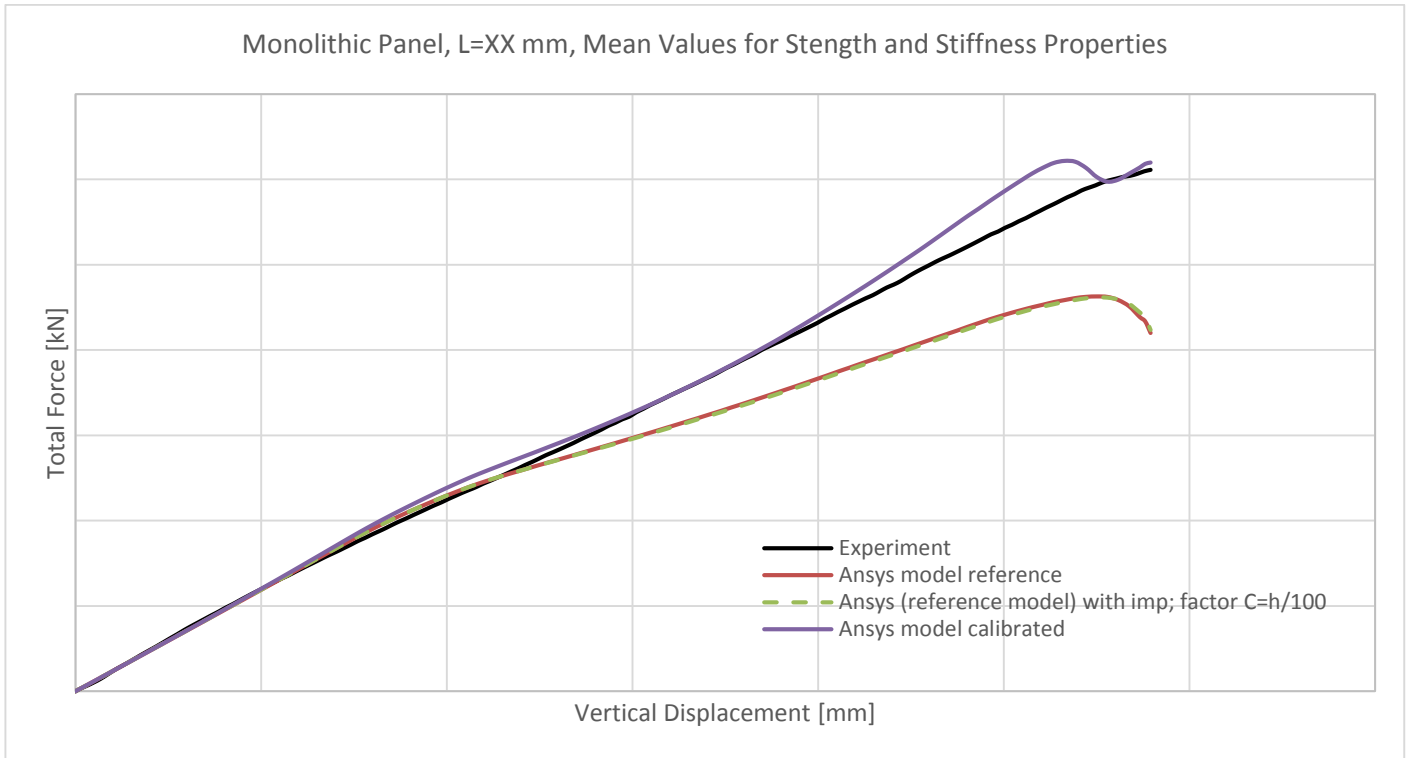


Figure 4-18: Vertical force-displacement curves, 1<sup>st</sup> monolithic Panel, for comparison

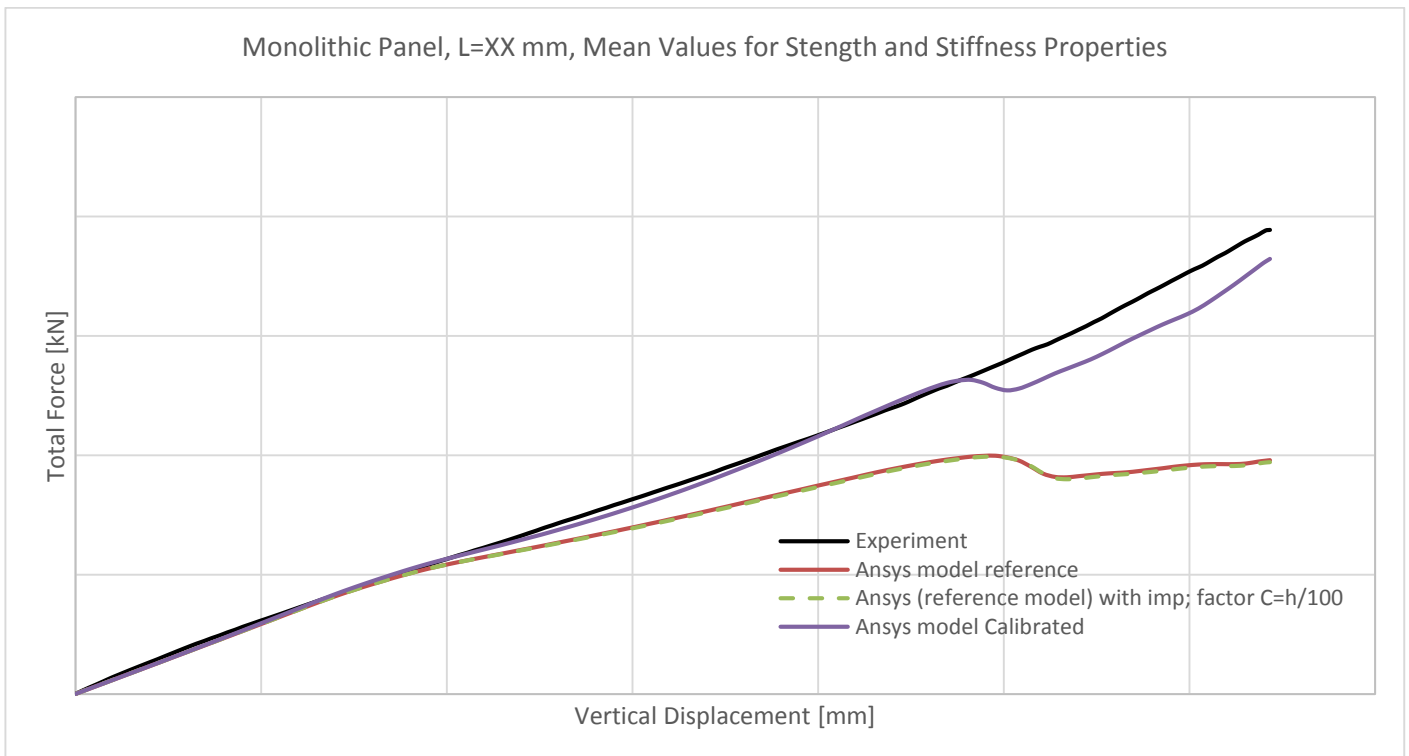


Figure 4-19: Vertical force-displacement curves, 2<sup>nd</sup> monolithic Panel, for comparison

### 4.2.6 Discussion of the results for the non-linear static analysis with springs, deterministic model

The writer considers it significant to discuss the results that are shown in figures 4-16 until 4-19 before the next models are presented where the stochastic nature of the material properties is introduced.

Firstly, a comment should be made regarding the method that is introduced for the progressive damage modelling. As it is explained in subchapter 4.2.2.2, the model recognizes 2 distinct statuses for each element's plies, namely damaged or undamaged. This is a simplification of what happens in reality because it is known that plies can be partially damaged and more sophisticated models should be introduced. As it is explained at subchapter 4.4 of the supporting document, these sophisticated models which are based on energy criteria, do take into account the case where a ply is partly damaged. To put it simply, readers can think that the status of each element's ply in this thesis' method is either 0 or 1 but there are other methods where the status can take all the values between 0 and 1. As it is mentioned in the supporting document, these methods require extra tests for the definition the energy dissipated per unit area for the 4 damage modes along with tests for determining their viscous damping coefficients. Due to the fact that these tests would expand the testing plan and the costs significantly, they were not implemented. However, their omission can be noticed in the figures above. For example, both sandwich panels have increased stiffness for a vertical displacement up to  $XX\text{ mm}$  and after that the models seem to follow adequately the experimental results. This fact leads to 2 conclusions. Firstly, for vertical displacements between 0 and  $XX\text{ mm}$  of the sandwich panels the plies could be partially damaged and as a result the resultant curve from the FEA models seems to be higher than it should be. Of course, the high assumed Shear Modulus should also be taken into account as a factor of this deviation. Moreover, the effect of the assumed progressive damage modelling is also evident at the 1<sup>st</sup> monolithic panel at figure 4-18 where for vertical displacements approximately at  $XX\text{ mm}$ , it is obvious that the some of the primary/load carrying plies are with an undamaged status. The inclusion of partly damaged plies would significantly ameliorate the structural response of this panel for vertical displacements around  $XX\text{ mm}$ .

The 2<sup>nd</sup> conclusion is that the damage variables that were taken from Ref. [30] produce satisfying results as the post-damaged behaviour of all the panels seem to verify the experimental results.

Another significant question arose to the writer for the case of the 2<sup>nd</sup> monolithic panel shown in figure 4-19. As it can be easily observed there, for vertical displacements higher than approximately  $XX\text{ mm}$  there is constantly a difference of  $XX\text{ kN}$  of the total vertical force between the Ansys model and the one produced by the actuator. This confused the writer as there was no reason for such a discrepancy if we take into account that the rest of the panels have well defined/predictable structural behavior. Then, instead of looking for amendments at the Ansys models, the writer implemented forensic engineering in order to check what happened during the experiment. As it shown in the figure 4-20, the red arrows point at the curved steel bars which are assumed that are the root of the problem. The technicians from TNO decided to connect the steel bars with the test frame by attaching ropes for reasons unknown to the writer. By checking the length of the ropes, it is highly probable that they were loose during the implementation of the experiment and for small rotations of the cylindrical supports, but when these rotations got bigger the ropes got stretched and as a result extra horizontal forces were introduced in the system. Hence, the ropes were in tension and they

“pulled” the steel bars which resulted in their final curved shape. These ropes were not present at the rest of the panel tests.



Figure 4-20: Photo of 2<sup>nd</sup> monolithic panel before it was unmounted from the testing frame, obvious introduction of horizontal forces

#### 4.2.7 Introduction of stochastic nature of material properties

The next and last step of the analysis is to include the stochastic nature of the material properties. The stochasticity of the material properties is extracted from the small scale experiments as explained at chapter 2. It is worth to be mentioned that the variability of the material properties is being derived from just one panel for each strength and stiffness property and as a result, readers should know that this is the minimum variability that can be taken into account. It is intuitive that if further experiments are performed for the same material properties, the results will be close to the ones that they were obtained here but not exactly the same. Hence, it is expected that the CoVs will increase as a result of the increased standard deviations.

In the figures below, the vertical force-displacement graphs are shown as they were extracted from the experiments and they are compared with both the models with the mean values for strength and stiffness

properties (subchapter 4.2.5) along with the upper and lower bounds of a 95% confidence interval (dashed lines). For the definition of the spectrum of structural responses which defined these two bounds, the table 3-5 was used in combination with the method presented at subchapter 3.3.

To further clarify this, the procedure which is presented at subchapter 3.3 and is supported by the subchapter 3.4 of the supporting document is used here which resulted to the definition of the following material properties:

Simulation #	$S_{11T}$ [MPa]	$E_{11}$ [GPa]	$S_{11C}$ [MPa]	$\nu_{12}$ [-]	$S_{22T}$ [MPa]	$E_{22}$ [GPa]	$S_{22C}$ [MPa]	$S_{12}$ [MPa]	$G_{12}$ [GPa]
1	XX	XX	XX	XX	XX	XX	XX	XX	XX
2	XX	XX	XX	XX	XX	XX	XX	XX	XX
⋮	⋮	⋮	⋮	⋮	⋮	⋮	⋮	⋮	⋮
100	XX	XX	XX	XX	XX	XX	XX	XX	XX

Table 4-3: Material Properties for 100 simulations

For this thesis 100 simulations were opted to be run in Ansys because this number is big enough to assume that the distributions will be well represented in the values shown in the tables above; this claim is supported even more by the choice to use the Latin Hypercube Sampling method which is an efficient sampling method due to its stratified sampling as presented in subchapter 3.4 of the supporting document. Moreover, the computational time played a significant role as 100 simulations required approximately 55 hours to run for each monolithic panel and approximately 11 hours for each sandwich panel. Further increase of the number of simulations would require much more computational time while the increased accuracy wouldn't be of such significance. Of course, the best way to prove this it would be through a convergence analysis but such an analysis would require too much time that wasn't available in this thesis' framework.

In table 4-3 the material properties that were used as inputs to Ansys are shown for some simulations. Readers that are interested to see these values for all the simulations are suggested to visit Appendix K. It should be noticed here that all the material properties follow the distribution that best fits to each one of them according to table 3-5. Furthermore, as shown in subchapter 3.3, the generated random variables have the correlations that were defined by the experiments. More specifically, the values of the tensile strength  $S_{11T}$  have a correlation  $\rho(S_{11T}, E_{11})_{model} = -0.47$  with the Elastic modulus  $E_{11}$  which is pretty close to the one from the experiments ( $\rho(S_{11T}, E_{11})_{exp} = -0.49$ ). This small difference has to do with the method that was followed to correlate the random properties and more specifically has to do with the step where the correlated uniform variables are transformed to variables that follow the distribution that best fits each material property. However, this small deviation is assumed to be negligible for this case and for that reason, this method is accepted. Furthermore, the tensile strength  $S_{22T}$  is correlated with the Elastic modulus  $E_{22}$  with  $\rho(S_{22T}, E_{22})_{model} = 0.41$  whereas the experiments showed a ( $\rho(S_{11T}, E_{11})_{exp} = 0.43$ ). Again, the same reason is responsible for that deviation. Finally, the in plane shear strength is correlated with the in plane shear modulus with  $\rho(S_{12}, G_{12})_{model} = -0.36$  which is exactly the same as the one derived from the experiment.

By keeping all the above into mind, the vertical force displacement curves for all the panels are:

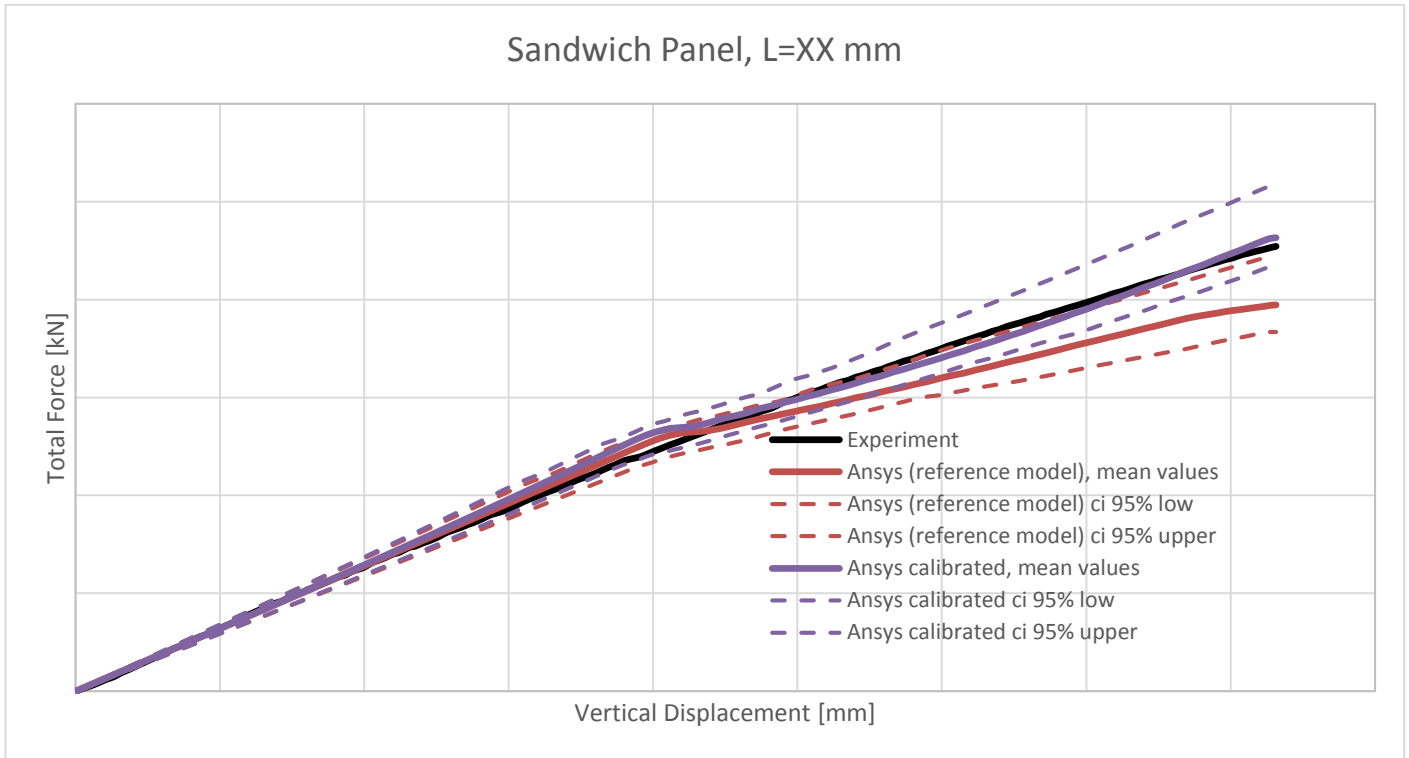


Figure 4-21: Vertical force displacement curve, 1<sup>st</sup> sandwich panel

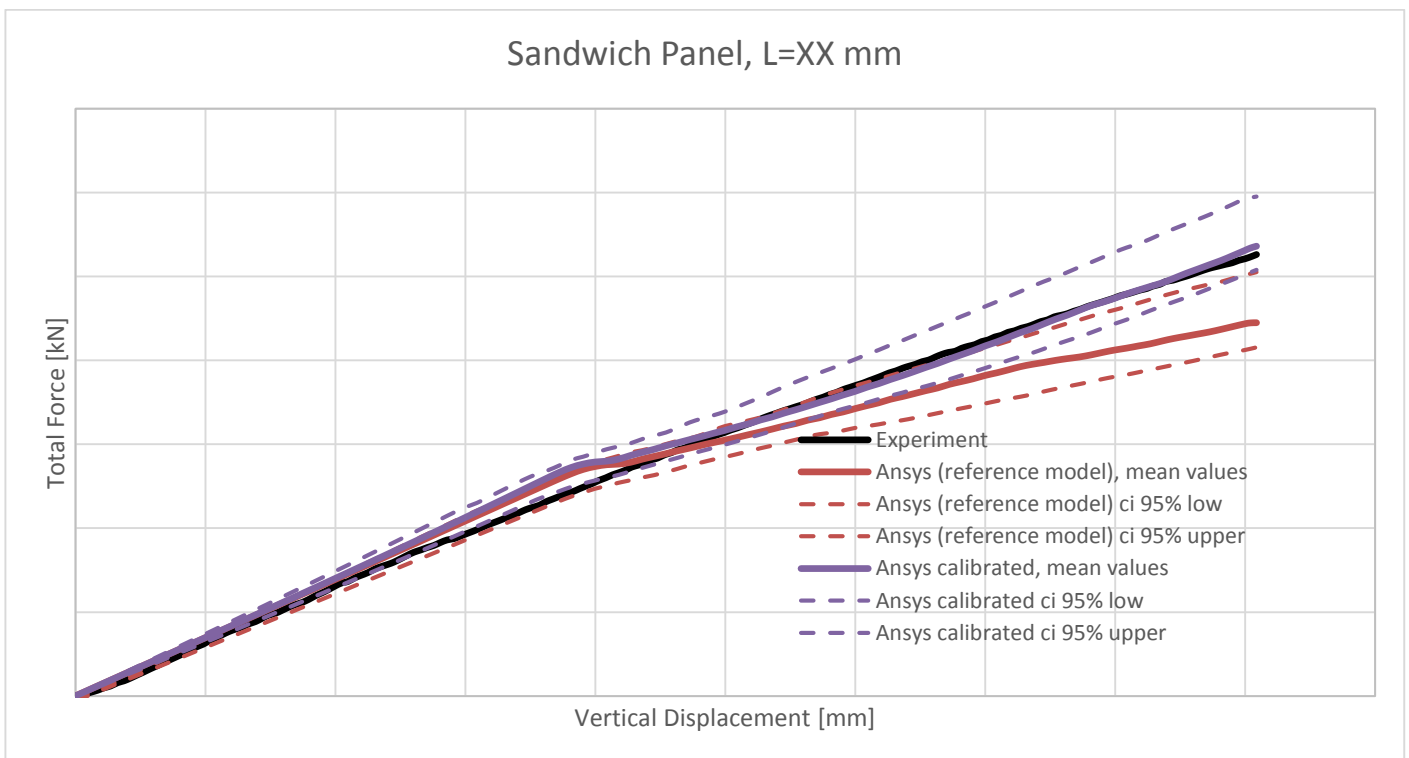
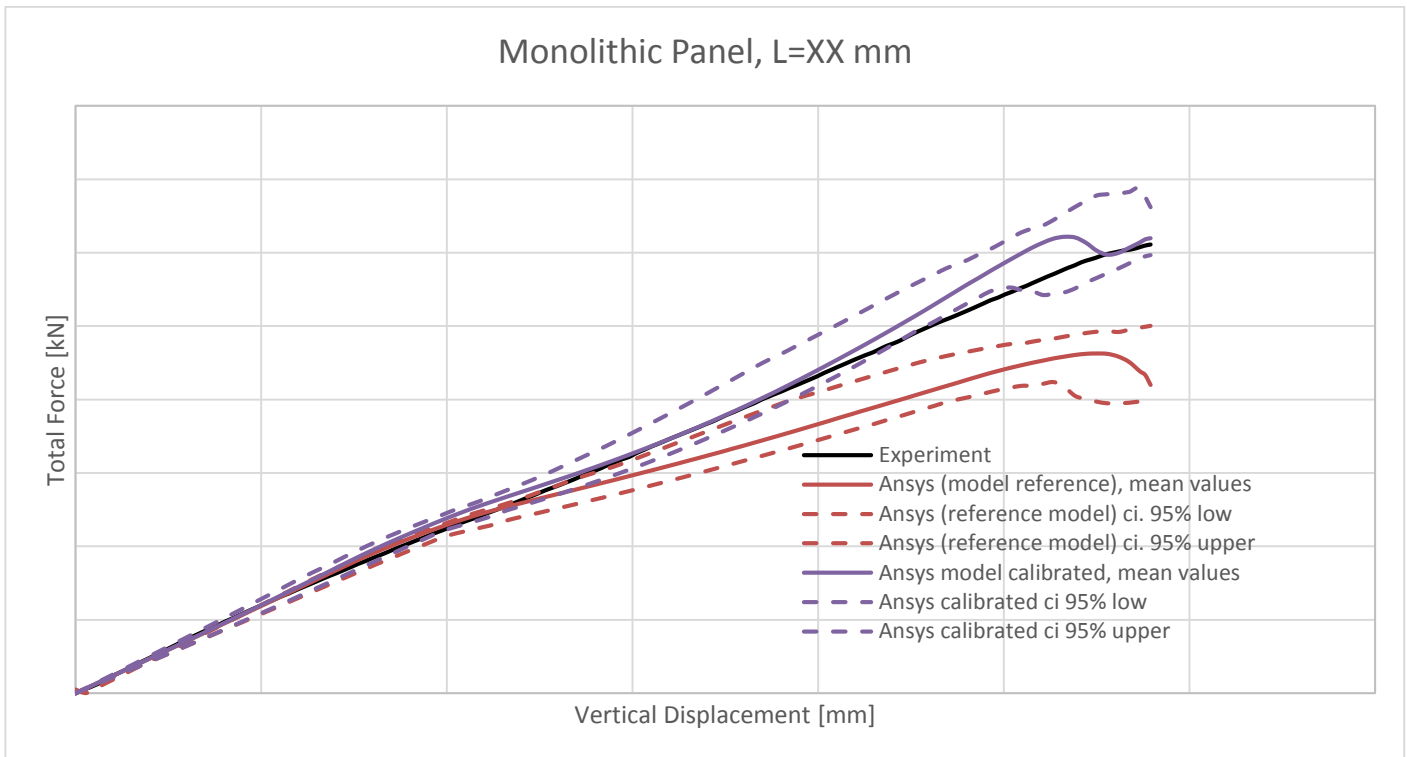
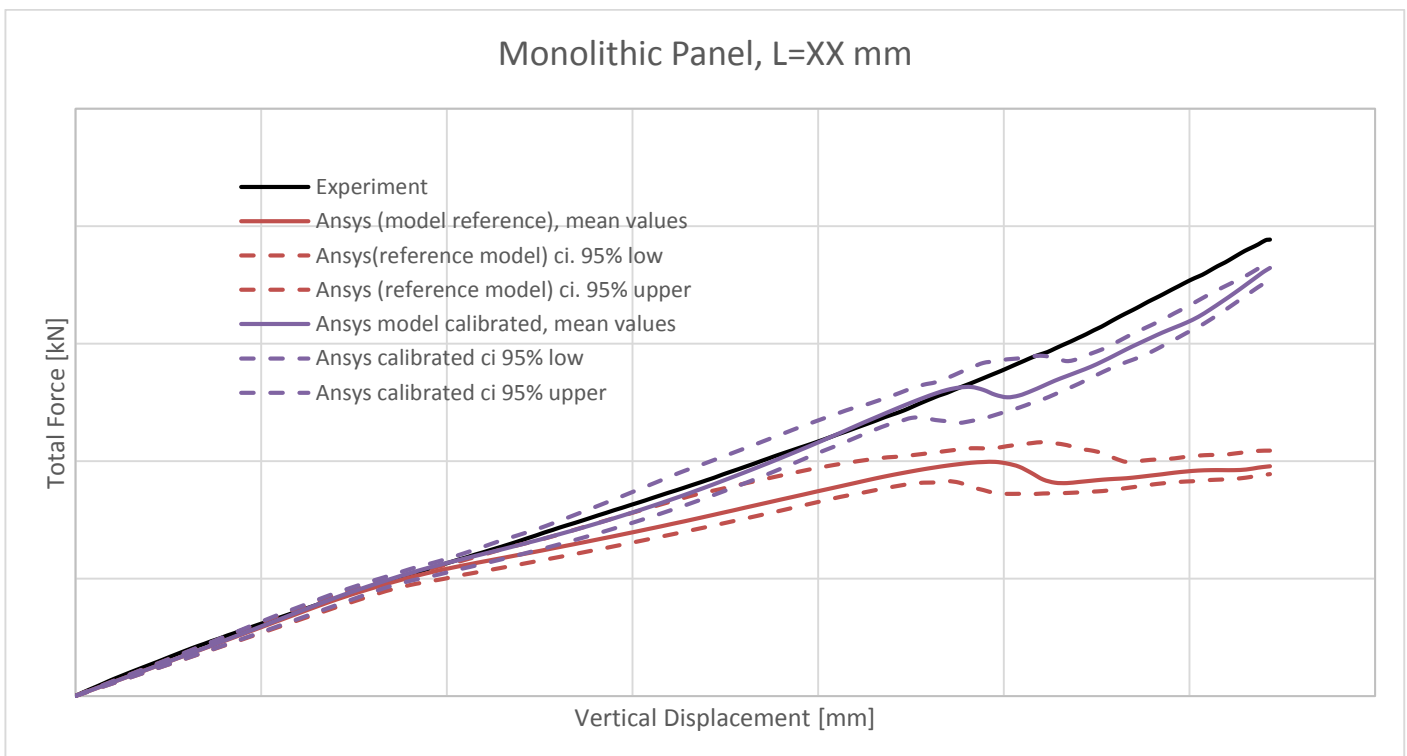


Figure 4-22: Vertical force displacement curve, 2<sup>nd</sup> sandwich panel

Figure 4-23: Vertical force displacement curve, 1<sup>st</sup> monolithic panelFigure 4-24: Vertical force displacement curve, 2<sup>nd</sup> monolithic panel

At the subchapter 1.2, the thesis' objective was defined. There it was explained that with this thesis, it is desired to investigate the effect of stochastic material properties on the structural response of large composite panels. This effect is shown in figures 4-21 until 4-24 and the focus should be concentrated at the purple dashed lines. These lines define the upper and lower bounds of the structural response with a confidence level of 95%. To put it in other words, we are 95% sure that the force-displacement curve of the modelled panels will be in between these two bounds under the assumption that the variability of the material properties is extracted from the small scale coupon tests. Moreover, as it was stated at the start of this subchapter (4.2.7), the variability of each material property is based on the intra-panel variability as all the coupons were extracted from the same panel towards the definition of each individual property. With more coupon tests from different panels, the variability would increase and the 2 bounds would move away from each other.

Regarding the results shown in figures 4-21 until 4-24, it is decided to discuss each panel's results separately.

The first sandwich panel shown in figure 4-21, shows that the force-displacement curve can be predicted accurately within a confidence level of 95% from the start till the end of the experiment. As it shown there, the experimental results (black line) is continuously between the two bounds (purple dashed lines) which proves the adequacy of the model and the "algorithm" that was developed in this thesis.

The second sandwich panel shown in figure 4-22, shows that the force- displacement curve can be predicted accurately for most of the experiment. For vertical deflections of around  $XX\text{ mm}$ , the experimental curve is at maximum 2.5% lower than the lower bound that defines the 95% confidence interval. As it was discussed in the previous subchapters, the main reason for this effect has to do with the high shear modulus that resulted from the coupon tests due to their high fiber volume. Also, it can be concluded that the second panel is more sensitive to the shear modulus than the first one because the latter's model could predict the structural response for these vertical deflections within the confidence level. The main reason for that is that the second sandwich panel had a smaller free span which led to faster development of the shear stresses for the same shear modulus. However, the model should work for a more representative shear modulus as it is shown in the conclusions

The first monolithic panel shown in figure 4-23, shows that the force- displacement curve can be predicted accurately for almost the whole experiment. For vertical deflections around  $XX\text{ mm}$  the experimental curve is at maximum 1.5% below the lower bound that defines the 95% confidence interval. For the reason of this deviation, we should search at the progressive damage modelling. The increase of the steepness at the model's results in this area show that the dominant layers (ones with fibers parallel to the longitudinal direction) are undamaged and the steep loss of stiffness due to their failure occurred exactly after this maximum deviation was noticed. Hence, it is once again supported by the writer that a more sophisticated model should be used for the progressive damage modelling based on continuum damage mechanics.

The second monolithic panel shown in figure 4-24, shows that the force-displacement curve can be predicted accurately for vertical displacement between the start and the ones around  $XX\text{ mm}$ . After this point, the experimental curve is significantly higher than the modelled one and the main reason was explained at subchapter 4.2.6 and it was supported by the figure 4-20. The presence of the ropes which are attached to the test frame were not included in the FEA model because during the definition of the springs' stiffness at the left end of the monolithic panels, the same friction coefficient  $\mu$  was defined for both cases. The only way

to take the ropes into account was to introduce in the FEM model a spring element that would become active after a certain vertical deformation (through the command `eolive`) but again the stiffness should have been defined by the writer who didn't know anything about these ropes. On the other hand, an assumed higher spring stiffness could be used but that would be arbitrary and would lead to higher force-displacement curves for vertical deformation from the start till  $XX$  mm. Last but not least, by carefully looking at the figure 4-24 it is obvious that the upper and the lower bound come close to each other towards the end of the experiment. That is pretty interesting because as it is shown at the table 2-5 and 2-6 the CoVs of the material properties that were included in the statistical analysis are pretty low expect the one that concerns the Shear modulus  $G_{12}$ . What can be extracted from this phenomenon, is that most of the plies with  $\pm 45^\circ$  degrees orientation have failed and the significance of the Shear modulus has become negligible. It is intuitive that low CoVs result to confidence interval bounds that are close to each other and this is obvious for vertical displacements higher than  $XX$  mm.



# Chapter 5: Conclusions

As it was stated at the start of this thesis, the objective was to build a model which would be capable to predict the structural response of large composite panels under 3 point bending within a confidence level of 95%. These large, monolithic and sandwich panels have a length of  $XX\text{ mm}$  and a width of  $XX\text{ mm}$  and they are designed to be part of a MCMV's hull and superstructure. Their dimensions correspond to the real size of a panel which lies between two primary stiffeners. Towards this objective, 3 distinct steps were followed. The first concerned the implementation of small scale coupon tests in order to define the material properties of the composite under investigation. During the second step, a statistical analysis was implemented towards the definition of the stochastic nature of the material properties where the experimental results from the previous step were used as inputs. The third and final step concerned the large scale experiments whose results were compared with both deterministic and stochastic models built in FEM. The conclusions from each one step are:

- The preparation and execution of the small scale coupon tests is a complex and time-consuming activity. Special attention should be given at the design of the coupons and at the goal of the testing plan. Even if the experimental results are satisfying, 2 comments should be made. The first comment has to do with the fibre volume fraction of the in-plane shear coupons. Due to the fact that less resin than needed was introduced in the panel that was designed to extract the in plane shear tests, the panel's fibre volume was much higher than the designed one ( $V_f \approx XX\%$  instead of  $V_f = XX\%$ ). This effect led to a higher than expected Shear modulus  $G_{12}$  which in turn created deviations between the modelled and the experimental results for the large scale specimens, especially for the sandwich panels which were more sensitive to this material property. Hence, the first conclusion is that by taking into account these values the building block approach is violated as by passing from block 3 to block 4 a significant factor such as the fibre volume is altered. The second comment that should be added has to do with the finished surfaces of the coupons. As it was noted by the Applus<sup>+</sup> lab in Bremen, the surface of the coupon at the side of the vacuum bag were rough and they had to be grinded before the strain gauges were mounted. As a result, the strain gauges showed slightly different measurements for the strains between the top and bottom surfaces even for the case of tensile tests which is something unexpected. Then, due to the fact that the strains at one time instant were defined as the average of the two strains at the same time instant, it can be assumed that the Elastic moduli  $E_{11}, E_{22}$  can be slightly changed which can also be part of the reasons for the strong negative correlation between  $S_{11T}$  &  $E_{11}$ . Hence, the 2<sup>nd</sup> conclusion is that the manufacturing procedure should be done with high precision because small manufacturing imperfections such as the finished surfaces can have a noticeable effect on the material properties. At this point it should be mentioned that the writer used all the results from the experiments on the small scale coupons for the rest of the thesis

as they were performed by a certified lab and they were supervised by a certified classification society. However, the writer considered significant to point out the reasons for the potential reasons that led to unexpected results.

- Regarding the statistical analysis, in most of the literature, the Normal, lognormal and Weibull distributions are used to describe the material properties of composites. However, as it is shown in chapter 3, there are other distributions that can describe even better the material properties. Only 3 of the 9 material properties follow one of the aforementioned distributions. There are 4 material properties that follow the Maximum Extreme distribution, 1 that follows the Logistic and the last 1 that follows the Minimum Extreme distribution. Hence, the writer concludes that it is worth investigating more distributions when it is desired to take into account the variability of a material property. Even the rest of the material properties that didn't qualify for a specific material property seem promising as they are able to describe all the material properties but they didn't qualify because another distribution seemed to better fit to each individual material property.
- During the statistical analysis, a method was built to take into account any correlation between the material properties when random variables are to be generated. This method has two advantages. It is independent of the distributions of the material properties for which random variables have to be generated and there is no restriction on how many materials properties can be correlated. This method was verified in this thesis as the resultant correlation of the generated variables was pretty close to the one from the experiments and at the same time the generated variables followed the desired distributions.
- Regarding the large scale specimens, the first conclusion concerns the correct modelling of the large scale experiments. Generally, it is desired to model in FEM the experiments in a way that approximates the reality as much as possible and then observe the range of the resultant structural responses due to the variability of the material properties. As it is shown in chapter 4, the boundary conditions have a great effect on the structural response of the large scale specimens. The first assumption that the left end of the models can freely slide at the longitudinal direction and as a result not to develop any horizontal forces proved to be wrong. Hence, the introduction of a way to take into account the developed horizontal forces was necessary and it was implemented by introducing linear springs which is a simplistic but yet satisfying method.
- Another significant but intuitive conclusion, is that the CoVs from the experimental results are linked to the distance between the upper and lower bounds of the confidence interval. It is intuitive that when the variability of the material properties' values is small, the generated random variables will be close to each other and as a result the two bounds will be close to each other. However, it should be mentioned that a large deviation of the experimental results would be unexpected because each material property was extracted from the same plate. If the same experiments are performed for new panels this deviation would increase and this analysis would reduce the bias and it would be more representative of a vessel's hull were plenty of panels are present.
- Due to the high in plane shear modulus as a result of the increased fibre volume at the panel that was used for the in plane shear tests, deviations at the stiffness were found for the "linear" part of the large

scale specimens and more specifically for the sandwich panels. The writer found significant to check the deviation of the in plane shear properties by comparing the existing values with ones that were found in the literature. A characteristic example can be found at Ref. [8] where the resultant shear strength and stiffness properties that were extracted from the experiments were equal to  $S_{12} = XX \text{ MPa}$  and  $G_{12} = XX \text{ GPa}$  respectively (note: the results from the experiments gave  $S_{12} = XX \text{ MPa}$  and  $G_{12} = XX \text{ GPa}$ ). These experiments were made on rectangular specimens with fibres at  $\pm 45^\circ$ , with a tensile loading at  $0^\circ$  direction and there composed of XX fibres, a XX matrix and with a fibre volume  $V_f \approx XX\%$

- As the last conclusion, it is easily observed in figures 4-21 until 4-24 that most of the structural response can be predicted accurately as the experimental curves lie within the bounds that define the 95% confidence level. The main reasons for the small parts that lie outside the upper and lower bound, can be found on the high shear properties and the progressive damage model. As it was stated earlier, new experiments on the in plane shear properties could potentially solve the deviation of the stiffness and improve the results. Furthermore, new experiments are needed to define the fracture energies  $G_I$  and  $G_{II}$  which will make possible the usage of continuum damage modelling where the plies can be partly damaged. For the second monolithic panel in figure 4-24, the main reason that the experimental curve lies outside the confidence interval bounds has to do with the presence of the ropes as shown in figure 4-20. To conclude, this method provided satisfying results and is suggested by the writer. Obviously, the thesis' objective was accomplished as in the figures 4-21 until 4-24 it is easily observed that the effect of the stochastic material properties led to the spectrum of structural responses that lie between the two bounds that define the confidence interval.



# Chapter 6: Project Planning

Up to this point, emphasis was only given on the engineering of the composite materials. However, it is equally important to investigate how the production process and costs are altered when this type of material replaces the steel which is the dominant material in the marine industry nowadays. The changes in the production procedure as well as the differences in the prices of the composite material can lead to noticeable reductions of both the total costs and the required time to manufacture a Mine Counter Measure Vessel (MCMV). The cost differences are investigated in this chapter where two cases are used as inputs. It is assumed as the base of the analysis that both the cases that are examined have to show the same operating capabilities and more specifically they should have low magnetic signal in order to be invisible to magnetic mines. Hence, the first case is a MCMV made of a-magnetic steel and the second case, which will be investigated in depth, is a MCMV made by XX fiber reinforced polymers embedded in a XX matrix with a monolithic structure for the hull and a sandwich structure for the superstructure. Briefly, this specific project is explained in subchapter 1.1 of the supporting document and at this subchapter an extensive analysis is implemented.

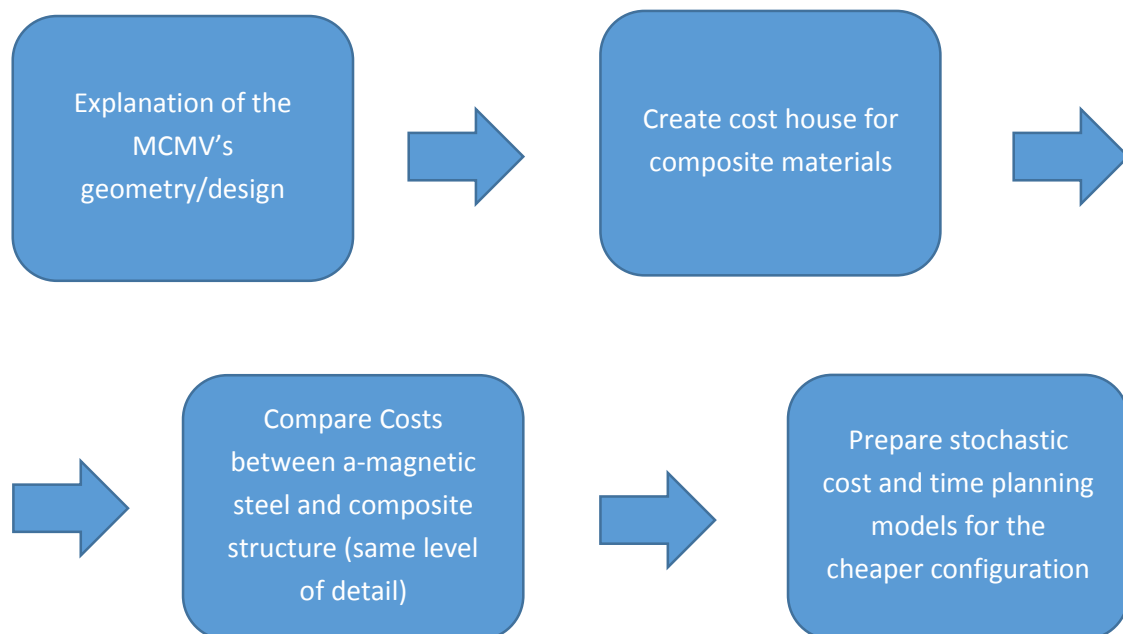


Figure 6-1: Chapter's Workflow

In the figure above, the readers can visualize the workflow that was followed at this chapter. Firstly, the basic information is given to the readers in order to make them familiar with the project. The vessel's dimensions

are presented along with its structural elements. Significant terms that are used for the rest of the chapter are clarified such as the hull, the superstructure, the bulkheads and the decks which are also visualized through the provided figures. After delivering the base for the establishment of a common “language”, a cost house is presented regarding the construction of composite structures. There, the readers can become familiar with the activities that have to be followed for the construction of the hull and the superstructure of the vessel through the provided tables. These tables show the costs of the materials that are needed for a composite structure along with the time that each activity takes which indirectly plays a significant role because the time needed multiplied with the workers’ wage leads to the labor cost that has to be added to the rest of the costs. Then, a cost comparison between two alternatives is made and more specifically between an a-magnetic steel structure and a composite one. This comparison is made in an aggregate level due to lack of input for the a-magnetic steel. Hence, a “zoom-out” of the cost house is performed and the same structure is compared in terms of costs when the a-magnetic steel and composite materials are used at the same level of detail. This comparison showed that the vessel can be significantly cheaper when it is made of composite materials and as a result this option is opted to be investigated in depth. Hence, the next and last step is to make a time and cost planning estimation for the construction of the vessel’s hull and its superstructure as they were presented at the first step (subchapter 6.1). What makes this analysis intriguing is that the stochastic nature of the time needed for the activities is taken into account and as a result the planning is treated from a statistical approach. Prior to the presentation of the first step, it is significant to define the aim of this study. What is attempted to be done here is to provide to the project planners with a tool, with which they can accurately predict the time and cost for the implementation of such so complex projects within certain probability levels. With this tool they will be able to predict the probability of completing the project (or various stages of it) within a certain confidence interval. In that way, they will be able to define aggressive or conservative strategies depending on the characteristics of the projects for which they have make cost and time estimations.

## 6.1 MCMV Project – Basic Information

### 6.1.1 Hull’s Structural Elements

At subchapter 6.1 one can find a schematic representation of the vessel in order to make the rest of the analysis more comprehensive. It provides the foundation of chapter 6 as it gives a graphical representation of the individual structural elements that compose the whole structure.



Figure 6-2: Concept Design

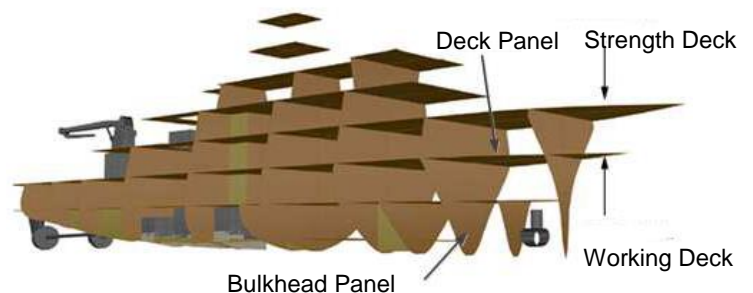


Figure 6-3: Structural Elements, Panels

A breakdown of the panels shown in figure 6-3 is following and these panels are separated into three groups: the shell panels, the bulkhead panels and the deck panels. The shell panels will be infused all together in two consecutive infusions; specifically, the following procedure should be followed:

- Create the steel hull mould (subchapter 6.2)
- Prepare it for the infusion
- Placement of the fibres onto the mould
- 1<sup>st</sup> and 2<sup>nd</sup> Resin Shots

The resultant product of this procedure is shown in figure 6-4 below (without the horizontal decks)



Figure 6-4: Hull, graphical representation

Towards the construction of the hull, the hull's decks and the bulkheads should be constructed separately and then be adhesively bonded on the hull's shell. The final result (figure 6-4) will be the hull which runs from the keel up to and including the strength deck as shown in figure 6-3. The individual shell, deck and bulkhead panels are shown below:

Confidential. Contact: J.Broekhuijsen@damennaval.com

Figure 6-5: Hull's shell panels

In the figure above it is shown that specific codes have been given to each panel, something that was necessary for their structural design. Each shell panel has its' specific code, length (L\_SP=Length Shell Panel) and height (H\_SP=Height Shell Panel) be stored in a database. Then, a certain material configuration is given to the panels which for this thesis is assumed to be a monolithic structure for all the panels belonging to the hull. As a last step, certain thicknesses have been assigned to each panel which play a significant role to the structural analysis of the composite sections.

# Of Panel	Panel's code	Thickness [mm]
1	XX	XX
2	XX	XX
⋮	⋮	⋮
XX	XX	XX

Table 6-1: Typical thicknesses of hull's shell panels

Following the same rationale, the hull's decks and bulkheads are presented below:

Confidential. Contact: J.Broekhuijsen@damenaval.com

Figure 6-6 Hull's deck panels

Confidential. Contact: J.Broekhuijsen@damenaval.com

Figure 6-7: Hull's bulkhead panels

# Of Panel	Panel's code	Thickness [mm]
1	XX	XX
2	XX	XX

⋮	⋮	⋮
XX	XX	XX
XX	XX	XX
XX	XX	XX
⋮	⋮	⋮
XX	XX	XX

Table 6-2: Typical thicknesses of hull's deck and bulkhead panels

The thicknesses shown in tables 5-1 & 5-2 are the result of the structural analysis according to Lloyds Register<sup>[38]</sup> which used as inputs the material properties from the experimental results, under the assumption that the hull has a monolithic structural configuration and under the assumption that the loads follow the specifications of the same Lloyds Register rules<sup>[38]</sup>. An extensive explanation on the derivation of the loading conditions or the general background of the structural engineering is far beyond the scope of this thesis and as a result, it is not presented here. However, the readers should know that the different panels' thicknesses that were taken into consideration are based on preliminary structural calculations and they correspond to realistic values.

### 6.1.2 Superstructure's Structural Elements

Confidential. Contact: J.Broekhuijsen@damennaval.com

Figure 6-8: Superstructure's elements

A schematic representation of the superstructure is shown in figure 6-8. The tool that was built for the structural analysis of the hull wasn't used for the superstructure as the given loading conditions affect only the hull. The superstructure under investigation was the result of previous research in the company and here it is taken as given. To clarify this, the activities needed for the construction of the superstructure are taken into account in the analysis shown in chapter 6.4 but the panels needed for its construction haven't been optimized in terms of thickness. To conclude, the readers should know that the superstructure is assumed as a big block composed of horizontal (superstructure's decks) and vertical (superstructure's shell/bulkheads) panels with a sandwich configuration and thicknesses of both the core and the skins that represent realistic values. A top view of the superstructure's decks is shown in figure 6-9; the superstructure's shells are placed at the perimeter of the decks and the bulkheads provide vertical barriers between the superstructure's rooms.

Confidential. Contact: J.Broekhuijsen@damennaval.com

Figure 6-9: Top view of superstructure's shells

Typical geometric characteristics of the superstructure's panels are shown below:

# Of Panel	Length	Breadth	Area	$h_{skin}$ [mm]	$h_{core}$ [mm]
XX (shell)	XX	XX	XX	XX	XX
XX(shell)	XX	XX	XX	XX	XX
⋮	⋮	⋮	⋮	⋮	⋮
XX(shell)	XX	XX	XX	XX	XX
XX (bulkhead)	XX	XX	XX	XX	XX
XX (bulkhead)	XX	XX	XX	XX	XX
XX (deck)	XX	XX	XX	XX	XX
XX (deck)	XX	XX	XX	XX	XX
⋮				⋮	⋮
XX (bulkhead)	XX	XX	XX	XX	XX

Table 6-3: Superstructure's panels

Now that the geometrical configuration of the vessel is defined, a financial analysis should be implemented to check if it is cost effective to use composite materials as the loading carrying structural elements for the given MCMV.

In summary, the vessel's main geometrical characteristics are given below:

Ship Parameter	Value (m)
Length Overall	XX
Rule Length	XX
Depth	XX
Breadth	XX
Deck Height 1	XX
Deck Height 2	XX
Deck Height 3	XX
Minimum walk-through height	XX

Table 6-4: Ship's Geometrical Parameters

## 6.2 Cost house

The first step of the analysis is to gather data regarding the prices that are related to the construction of the MCMV. The cost data shown below were extracted from an inner report of DSNS<sup>[22]</sup> and are presented in a normalized way because they are confidential. By normalized way, it is meant that all the prices in this chapter do not correspond to real prices, but they are divided by a number defined by the writer. In this way, the relation between the costs is kept constant which allows the comparison between the two cases but the values presented do not correspond to reality.

### Material Cost Parameters

Item	Cost
XX fibers, quasi-isotropic (XX gr/m <sup>2</sup> )	XX €/m <sup>2</sup>
XX fibers, orthotropic (XX gr/m <sup>2</sup> )	XX €/m <sup>2</sup>
XX fibers, quasi-isotropic (XX gr/m <sup>2</sup> )	XX €/m <sup>2</sup>
XX fibers, orthotropic (XX gr/m <sup>2</sup> )	XX €/m <sup>2</sup>
XX, uni-directional (XX gr/m <sup>2</sup> )	XX €/m <sup>2</sup>
XX resin (inc.hardener) – infusion	XX €/kg
XX (inc.hardener) – hand lamination	XX €/kg
Consumables: peel-ply, bleeder, breather, mesh, spiro tubing, assembly, placement, control of vacuum bag etc., incl. scrap rate, excl. resin absorption	XX €/m <sup>2</sup>
Release agent	XX €/m <sup>2</sup>
Skin coat	XX €/m <sup>2</sup>
Gel coat (only for hull)	XX €/m <sup>2</sup>
Peel-ply	XX €/m <sup>2</sup>
Preparation of fibers: cutting into correct dimensions	XX €/kg

Fillet material/adhesive XX (connections)	XX €/kg
Pultruded glass rod(-for glass pins) XX mm diameter, sanded & treated	XX €/m
Bleeder/peel ply for vacuum bagging of the core	XX €/kg
Core material: (XX)	XX €/m <sup>3</sup>
Core material: (XX)	XX €/m <sup>3</sup>
Marking of decks, bulkheads	XX €

Table 6-5: Material Cost Parameters

Apart from the material costs, a correct estimation for the expenses towards the construction of MCMV should also include the costs derived from the scrap rate, the resin that is absorbed by the neighboring materials during manufacturing, the garbage costs, the non-recurring costs, the cost for the steel mould, the costs for the foundations of the vessel as well as the labor costs.

### Scrap rates & resin absorption

Production Activity	Resin Absorption	Scrap rate
Peel ply	XX kg/m <sup>2</sup>	XX%
Placement of fibers in hull mould	–	XX% Overlap XX% Scrap
Placement of fibers on infusion table	–	XX% Overlap XX% Scrap
Placement of fibers for connection laminate	–	XX% Overlap XX% Scrap
Consumables for infusion: mesh, breather, spiro tubing, vacuum bag, peel ply	XX kg/m <sup>2</sup>	XX% Scrap
Infusion of sandwich deck/bulkhead: resin absorption of balsa core	XX kg/m <sup>2</sup>	–
Connection laminate (hull-deck, hull-bulkhead)	–	XX%

Table 6-6: Scrap rates &amp; resin absorption

**Garbage costs:** The garbage costs are dependent on many parameters such as the regulations, location of production and the type of material that has to be disposed. As a rule of thumb which is close to reality, the garbage costs are assumed to be 5% of the total material costs.

### Non-recurring Costs

Description	Cost €
Vacuum equipment ( <i>capacity</i> = 2 * 100 m <sup>3</sup> /hour)	XX
leak detectors (5)	XX
spray/polish equipment	XX
chopper spray equipment	XX

crane cradles for peel ply/fibre	XX
fibre preparation/cutting table	XX
Storage racks for fibres	XX
upper mould flange for fibre fixation	XX
infusion equipment: 2 resin mixing machines ( $\sim XX \text{ kg/min each}$ ) & 1 degassing machine	XX
cutting table, 2 stationary routers & milling heads (5)	XX
adhesive application machines (2)	XX
grinders, dust extraction	XX
diamond saw with special rail	XX
Vacuum table: $12 \text{ m} \times 20 \text{ m}$ (5)	XX
wooden templates for core cutting	XX
vacuum-picker for crane	XX
waterjet cutting machine	XX
Small tooling: 12 toolboxes	XX
Scaffolding: inside & outside of the mould	XX
Positioning lasers	XX
<b>Total Costs</b>	<b>XX</b>

Table 6-7: Non-recurring costs

### Steel Hull mould

Item	Weight	Cost Price	Material	Labor
Hull mould for $L = XX \text{ m}$	$XX \text{ tons}$	$XX \text{ €}$	$XX\%$	$XX\%$

Table 6-8: Steel hull mould cost



Figure 6-10: Steel hull mould (in segments)

The costs for the foundations of the vessel can be derived only when the final design is ready to be implemented. For this analysis, the foundations are assumed to be the same as the ones of the Alkmaar's class vessels and their total costs, including the labor, are:

#### Alkmaar foundation Costs

Item	Cost €
Stainless steel material cost	XX
Aluminum material costs	XX
Adhesive material costs	XX
Adhesive labor costs	XX
<b>Total Costs</b>	<b>XX</b>

Table 6-9: Costs for the foundations of the vessel

A total amount of XX stainless steel foundations was included, consisting of insert and backing plates which are bonded to the structure. This represents a total weight of approximately XX tons and a total area of approximately XX m<sup>2</sup>. Also XX aluminium foundations were retrieved, representing a total weight of almost XX kilogram and a total area of almost XX m<sup>2</sup>.

The following parameters are applied during the cost and weight calculation:

- Isobond is used as adhesive
- A bonding thickness of XX mm is assumed
- An average labour rate of XX h/m<sup>2</sup> hours is assumed

*Note:* The costs shown at table 5-5, 5-7, 5-8, 5-9 correspond to prices as they extracted from the suppliers in February 2015. Later, in subchapters 6.4, these values were adjusted for inflation according to the respective year that the production was initiated

It is quite intuitive that a big part of the total cost for such a project would be derived from the labor costs. The estimation of the exact time needed for the completion of this project is a tedious procedure and here is calculated as the sum of all the individual tasks that have to be done prior to the construction of a MCMV. A detailed analysis towards the estimation of the lead time is given in subchapter 6.4. The individual tasks along with their time needed to be performed, are presented below and they are calculated as mean man-hours needed and not as the total time that will be needed in reality. For example, the removal of the hull from the mould is presented as XX man-hours (table 5-10). However, in reality this procedure takes approximately XX days. Later (subchapter 6.4), it is explained that this procedure requires the collaboration of many workers and if for example it is assumed that XX workers are involved in the procedure, a total XX/XX = XX hours (or two working days) are needed. To clarify this, the reader should know that the values below represent total man-hours and not the time that will be needed in reality because the latter is dependent on the amount of workers that are assigned to each specific task.

### Unstiffened laminate hull construction – Monolithic panels – outer shell

Step	Activity	Man-hours
1	Assembly of partial hull moulds into integral hull mould, including levelling of the integral mould	<i>XX h</i>
2	placement of scaffolding (inside & outside of the mould)	
3	Making the mould air tight & control of the vacuum tightness	<i>XX h</i>
4	Application of release agent into the mould	<i>XX h/m<sup>2</sup></i>
5	Placement of skin coat & application of gel coat	<i>XX h/m<sup>2</sup></i>
6	Finishing skin coat with peel ply	<i>XX h/m<sup>2</sup></i>
7	Placement of the fibres in the mould & fixation of the fibres to the upper mould flange	<i>XX h/m<sup>2</sup></i>
8	Consumables: peel-ply, bleeder, breather, mesh, spiro tubing, assembly, placement, control of vacuum bag etc., incl. scrap rate, excl. resin absorption	<i>XX h/m<sup>2</sup>/layer</i>
9	Placement of consumables: bleeder, breather, spiro tubing, assembly/ placement/ control of vacuum bag	<i>XX h/m<sup>2</sup></i>
10	Resin infusion: 1 <sup>st</sup> shot & 2 <sup>nd</sup> shot	<i>XX h</i>
11	Removal of consumables	<i>XX h</i>
12	Trimming of upper edge of the hull	<i>XX h/lin. m</i>
13	Removal of hull out of the mould	<i>XX h</i>

Table 6-10: Unstiffened hull production, activities and man-hours (outer shell)

When the activities shown in table 5-10 are completed, the hull is not ready yet. That's because the hull includes everything from the keel to the strength deck. Hence, the next step is to manufacture the decks and bulkheads and the sequence of the activities that has to be followed is shown below:

### Unstiffened laminate superstructure construction/ Sandwich panels

Step	Activity	Man-hours
1	Preparation of infusion table	–
2	Placement of the fibres onto the infusion table	<i>XX h/m<sup>2</sup>/layer</i>
3	Placement of consumables	<i>XX (~all in)</i>
4	Infusion	
5	Removal of superstructure's deck/bulkhead from infusion table	
6	Cleaning of infusion table	
7	Cutting panels to correct size with water jet cutting machine	

Table 6-11: Unstiffened bulkhead/decks production, activities and man-hours

When the bulkheads and the decks are prepared, they have to be fixed on the outer shell. The resultant product will form the hull which includes the structural elements from the keel until the strength deck.

### Deck/Bulkhead fixation in the hull

Step	Activity	Man-hours
1	Lining out and fixation of deck/bulkhead in the hull ~without adjustment	<i>XX h/panel</i>
2	Adhesive bonding and filleting (R50) of the connection: on two sides	<i>XX h/lin. m</i>
3	Hand lamination of connection laminate (hull-deck, hull-bulkhead): on two sides	<i>XX h/layer/lin. m</i>

Table 6-12: Deck/Bulkhead fixation in the hull, activities and man-hours

When the activities shown in tables 5-10 until 5-12 are finished, the hull is ready. Then, the superstructure has to be completed and attached to the hull in order to get all the structural elements of the vessel. At this point, it should be reminded that the foundations are part of the structural elements but in this thesis they are assumed to have a fixed value for their construction (table 5-9) regardless the length of the vessel and the lay-up of the composite materials which form the hull. Nonetheless, the foundations' contribution to the total cost is negligible (subchapter 6.4) and as a result this assumption will not lead to significant deviation from the reality.

As it is stated in the introduction of this chapter, the superstructure of the vessel will be made of sandwich panels and more specifically, with skins made of the same composite material (same composition, i.e.  $V_f$ , fiber mats, resin etc.) and with a *XX mm* balsa core. The production activities in that case slightly change and they are presented below:

### Unstiffened laminate superstructure construction/ Sandwich panels

Step	Activity	Man-hours
1	Preparation of infusion table	–
2	Placement of the fibres onto the infusion table	<i>XX h/m<sup>2</sup>/layer</i>
3	Preparation of core: core is already drilled & grooved. Only the geometry needs to be cut out.	<i>XX h/m<sup>2</sup></i>
4	Placement of the core onto the infusion table	<i>XX h/m<sup>2</sup></i>
5	Placement of the fibres onto the infusion table	<i>XX h/m<sup>2</sup>/layer</i>
6	Placement of consumables	<i>XX h/m<sup>2</sup> (~all in)</i>
7	Infusion	
8	Removal of superstructure's deck/bulkhead from infusion table	
9	Cleaning of infusion table	
10	Cutting panels to correct size with water jet cutting machine	

Table 6-13: Unstiffened superstructure production, activities and man-hours

For the completion of the superstructure and its fixation in the hull, the activities shown in table 5-13 have to be followed. Last but not least, in this study, the peel preventers were included which are made of circular glass pins with a diameter of *XX mm* and a length of *XX mm* placed at intermediate distances of *XX cm*. They

are used at all deck-hull and bulkhead-hull connections and they are applied in order to delay delamination. The activities for their application are shown below:

#### Peel preventer application

Step	Activity	Man-hours
1	Drilling of holes, placement of glass pens & application of the adhesive	<i>XX h/lin.m</i>
2	Hand lamination of cover laminate on both sides	<i>XX h/layer/lin.m</i>

Table 6-14: Peel preventer application, activities and man-hours

Tables 5-10 until 5-14 present the activities that have to be followed along with the total man-hours needed for their completion. The total amount of hours needed for the construction of the vessel times the labor rate will result to the total labor cost. The latter value will then be added with the costs shown in table 5-5 until 5-9 in order to extract the total cost assigned to this phase of the project. The labor rates are:

#### Labor Rates

Building Location	Labor rate
The Netherlands	<i>XX €/h</i>
Turkey	<i>XX €/h</i>

Table 6-15: Labor rates

Two different building locations were considered in this study, one in the Netherlands and one in Turkey (in Antalya, Damen has production facilities) in order to check how much the total cost will be reduced if it is decided to build the vessel in Turkey.

In subchapter 5.2, a cost house is presented for the case where the MCMV is built by composite materials. All the values shown in this subchapter's tables are a result of extensive research by a conglomerate of companies and more specifically by DSNS<sup>[3]</sup>, Airborne<sup>[32]</sup>, Solico<sup>[33]</sup>, CompoConsult and Polyworx<sup>[34]</sup>.

## 6.3 Cost comparison between steel and composite structure

Prior to the implementation of a detailed analysis for a vessel made of composite materials, it should be proved that it is possible to get reduced total costs when comparing with its a-magnetic steel counterpart. The comparison in this subchapter is being implemented in an aggregate level as it shown below.

From a list with various MCMVs that can be ordered by DMO<sup>[35]</sup>, one was chosen which will be the item of investigation for the whole chapter and the structural elements' geometry is presented in subchapter 6.1. The vessel's basic geometrical parameters are given again in the following table:

Ship Parameter	Value (m)
Length Overall	<i>XX</i>
Rule Length	<i>XX</i>

Depth	XX
Breadth	XX
Deck Height 1	XX
Deck Height 2	XX
Deck Height 3	XX
Minimum walk-through height	XX

Table 6-16: Ship's Geometrical Parameters

DSNS<sup>[11]</sup> has long experience in the production of military vessels. Hence, even without an extensive study for a MCMV made by steel, it is possible to extract approximate values that correspond to the production of such a vessel. Based on the data from Sigma class corvettes and frigates for the weight calculation, it can be extracted that for a vessel with the parameters shown in table 5-16, the vessel will have the following characteristics:

	Description	Parameter	Reference
Material	Austenitic stainless steel XX	XX €/kg	Quotation Outokumpu <sup>[36]</sup> , Germany
Total Weight	Hull & Superstructure included	XX tons	Inner report form DSNS <sup>[22]</sup>
Welding material	XX (about XX% of the total weight)	XX €/kg	Estimated by DSNS <sup>[22]</sup>
Labor	Man-hours/ton, hull	XX h/ton	Estimation Damen <sup>[22]</sup> & Exotech <sup>[37]</sup>
	Man-hours/ton, superstructure		
	Labor rate inc. facilities (in the Netherlands)	XX €/h	Estimated rate by DSNS <sup>[22]</sup>
Other costs	Non recurring costs	XX €	Estimated by DSNS <sup>[22]</sup>

Table 6-17: Steel structure, rough approximation

It is deemed significant to clarify how the man-hours and the non-recurring costs were extracted. The rest of the data were straight-forwardly extracted from the references shown in table 5-17.

The base for the analysis that results in the aforementioned man-hours value is the normal grade A or AH steel. By excluding the small steelwork and outfitting:

#### Man-hours, explanation, steel structure

	Normal steel [h/ton]	Factor for a-magnetic steel	a-magnetic steel [h/ton]
Steel cutting & bending	XX	XX	XX
Steel assembling	XX	XX	XX
Welding	XX	XX	XX
Finishing	XX	XX	XX

<b>Total</b>	<b>XX</b>	<b>–</b>	<b>XX</b>
--------------	-----------	----------	-----------

Table 6-18: Man-hours explained, steel structure

Factors for a-magnetic steel are estimated based on the fact that there is much more deformation due to welding. This can be managed by using less heat input resulting in additional welding layers, which give more welding hours and more time needed for stretching. Furthermore, the learning curve is not considered separately, but is included in the baseline value, i.e. at the values shown at the column under normal steel in table 5-18. At last, the non-recurring costs for the steel structured are explained below:

#### Non-recurring costs for steel structure, explanation

Description	Cost €
Cleaning existing building facilities(no contact with carbon steel is allowed)	XX
Replacing magnetic lifters with vacuum lifters.	XX
Cover all working surfaces (rollers, laser cutters bending machines) with suitable materials or replace with stainless steel alternatives.	XX
Plasma cutter to be cleaned thoroughly.	XX
All small tools used for carbon steel to be replaced by new tools.	XX
Cover all blocks, beds etc. with suitable materials like wood, rubber or plastic material.	XX
Personal protection against welding gasses	XX
Welding Qualifications	XX
<b>Total</b>	<b>XX</b>

Table 6-19: Non-recurring costs for steel structure, explanation



Figure 6-11: SIGMA 7513

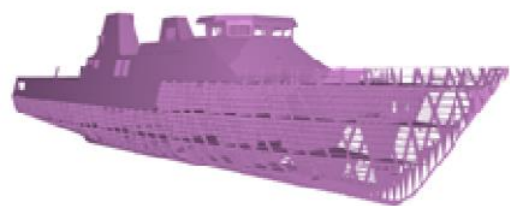


Figure 6-12: Structural elements of SIGMA 7513

At the same level of detail, the costs shown in table 5-17 were found for the case where composite materials are used for the hull and the superstructure. Based on values from Ref. [22]

	Description	Parameter
Material	Monolithic laminate: XX fibers(XX EQX-QI) embedded in a XX matrix, hull	XX €/kg
Material	Sandwich laminate: XX fibers(XX EQX-QI) embedded in a XX matrix at skins, XX core, superstructure	XX €/kg

Total Weight	Hull	XX tons
Total Weight	Superstructure	XX tons
Connections	Connections between decks/ bulkheads/ superstructure and hull	XX €/lin. m
Labor	Man-hours/ton, hull	XX h/ton
	Man-hours/ton, superstructure	XX h/ton
	Labor rate inc. facilities (in the Netherlands)	XX €/h
Other costs	Non recurring costs	XX €

Table 6-20: Composite Structure, rough approximation

The values shown in table 5-20 are dependent on the thickness of the laminates which in turn is dependent on the loading conditions. The structural engineering behind these analytical calculations is way out of the scope of this thesis as it is said before. However, it is worth-mentioning that the aforementioned costs concern structural details that meet the structural capacity which the ship should have according to Lloyd's Register<sup>[18]</sup>.

Based on the tables 5-17 & 5-20, a gross calculation of the total costs for the two cases can be performed:

$$Cost_{steel} = XX \text{ €}$$

$$Cost_{composite} = XX \text{ €}$$

\* approximately 1000m is the total length of connections

\*\* foundations

Construction Material	Total Cost [ $10^3\text{€}$ ]
Steel Structure(A-magnetic steel)	XX
Composite Structure	XX

**Reduction = 29%**

Table 6-21: Cost Comparison, Steel-Composite Structure

The comparison showed in table 5-21, makes it evident that a vessel made by the aforementioned compositions of composite materials can lead to significantly lower total costs (29% lower as shown in the table). Hence, it is of interest to implement a detailed analysis where the costs and the lead times are calculated with an excessive level of accuracy based on the cost house presented in subchapter 6.2.

## 6.4 Project Planning/Cost Estimation

The first step of this subchapter is to estimate the total time needed for the implementation of all the activities shown in tables 5-10 until 5-14. In order to make the analysis simpler without losing any detail, the activities are separated between these that have to be performed towards the construction of the hull (everything between keel and strength deck) and these towards the construction of the superstructure. For the case that only one worker will perform all the activities for the hull construction, a Gantt Chart was prepared. This chart, includes all the information presented at tables 5-10 until 5-12 and 5-14(optional to include) and it will be the

base of this analysis. As inputs, laminates are used which are capable to carry the loads in which the vessel is expected to be exposed according to Ref. [22] and Ref [38]. Hence, at figure A-1 in Appendix IDM-A, this Gantt chart (made in Microsoft Visio) is shown in order to make the readers familiar with the procedure that is followed in this subchapter. As it is intuitive, with only one worker as manpower, the project would last for many years and more specifically, according to the given input, such a project would last *XX* years and *XX* months under the assumption that every day has 8 working hours and that each week has 5 working days.

However, such an analysis would be incomplete because more than one workers deal with each activity as well as there are activities that can be implemented at the same time. Generally, after discussing with experts in DSNS with experience in shipbuilding with composite materials, it was decided that the construction of the vessel's outer shell defines the critical path and that its bulkheads and decks can be constructed simultaneously. The same holds for the superstructure which can be built independently and then fitted to the vessel's hull. Apart from that, discussions with the same experts resulted to the assignment of the number of workers shown in figures A-2 & A-3 of Appendix IDM-A.

Starting with the hull construction that is showed in figure A-2, the reader can get a complete picture of the activities that have to be performed prior to the construction of the vessel's hull. The time needed for each activity is also depicted in the Gantt chart and some activities were added in order to get a more realistic situation. For example, the time needed for the transportation of the steel mould (because it will be built in Galati, Romania) as well as the time needed to be spent between activities were added, among others. The procedure shown in figure A-2 resulted in a total time of *XX* months and *XX* days and when experts were asked to give an approximate value for the construction of such a hull, their answer was: *approximately a year*. That shows that the detailed analysis that is implemented here meets our expectations regarding the lead time of this project.

Note for figure A-2: The floating activities shown in figure A-2 correspond to the construction of the decks and the bulkheads. Limitations in the program that was used for the preparation of the Gantt chart didn't allow to show the exact way that these activities will be performed. A visual way is given in the table below which corresponds better to reality

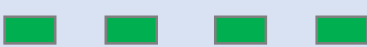
Activity	Modelled	In reality
Placement of fibres: cutting into correct dimensions		
Placement of Consumables/ Infusion/ Removal of deck or bulkhead from infusion table/ Cleaning the infusion table/ Cutting the deck or bulkhead to correct size with water jet cutting machine		

Table 6-22: Production of Decks/Bulkheads, difference between Gantt chart and reality

As it is shown in the right column of table 5-22, the fibers will be prepared in batches of 5 panels (because the production facility has 5 vacuum tables according to non-recurring costs) and then these panels will be infused. After that, the panels will be either stored or they will be directly fitted in the hull.

End of Note

Following the same rationale, the activities leading to the production of the superstructure are shown in figure A-3 of Appendix A. As a general overview of the project, figure A-4 is shown in Appendix A; as it is depicted there, the activities with a red color are the ones for which no detailed analysis was implemented in this thesis and the whole project planning will be ready when an analysis with the same level of detail will be performed for these activities too. The grey activities correspond to the total time needed for the production of the vessel which resulted from figures A-2 & A-3 for the hull and the superstructure respectively; for the rest of this chapter, focus will be given only to these two figures.

The next step of the analysis is to include the probabilistic nature of the time needed for the activities. This is shown in the following subchapter.

### 6.4.1 Stochastic analysis for time and costs

It is intuitive that when it is being said that for example the time needed for the activity: “*Placement of fibers: cutting into correct dimensions*” is equal to  $XX \text{ h/layer/m}^2 = XX \text{ min/layer/m}^2$ , in reality the actual time needed will be around this value but not exactly this. Hence, it was decided to introduce the probabilistic nature of all these activities by assigning triangular distributions to each one of them. The probability and cumulative density function for the triangular distribution is given below:

Distribution	Pdf	Cdf
Triangular	$f(x; a, b, c) = \begin{cases} \frac{2(x-a)}{(c-a)(b-a)}, & a \leq x \leq b \\ \frac{2(c-x)}{(c-a)(c-b)}, & b < x \leq c \\ 0, & x < a \text{ or } x > c \end{cases}$	$f(x; a, b, c) = \begin{cases} 0, & x < a \\ \frac{(x-a)^2}{(c-a)(b-a)}, & a \leq x \leq b \\ 1 - \frac{(c-x)^2}{(c-a)(c-b)}, & b < x \leq c \\ 1, & c < x \end{cases}$

Table 6-23: Triangular distribution<sup>[19]</sup>

The choice of the triangular distribution was not straight forward. Literature study has been implemented and the purpose of including the stochastic nature of the activities comes from the fact that there is always uncertainty in these kind of activities regarding the time needed to be performed. There were several distributions that could be used but the triangular distribution was opted for its characteristics. Firstly, the chosen distribution should be “enclosed” between two boundaries in order to obtain realistic values. To put it in another way, let’s assume that the aforementioned activity follows a normal distribution. As it is shown later, for the implementation of the statistical analysis, 100000 simulations were run in Matlab. In case that the normal distribution was used, some of these simulations would have assigned pretty small (it could be even negative) values for the time needed for such an activity. Of course, if the standard deviation of the normal distribution was reduced drastically, this effect would not be significantly possible but in that case most of the values would be around the mean value of the distribution and the statistical analysis would lose its purpose. Distributions that do not allow the choice of negative values such as the Weibull could be used too, but the determination of its parameters would be a cumbersome procedure and would require an extensive study by itself. Nonetheless, problems will arise concerning the right tail of the distributions, because by following the same rationale as the one for the left tail, it would be probable to have unrealistic

high values for the time needed of an activity. As a result, the triangular distribution was opted for its simplicity, the fact that it is bounded between two barriers and the fact that its parameters can be evaluated empirically.

At this point it should be made clear that the statistical analysis includes the stochastic nature only of the time needed for the implementation of the activities and not of the material's costs. That was done on purpose because an extensive study<sup>[22]</sup> made by DSNS for the determination of the individual costs and as a result it is assumed that these values are deterministic and that there is no reason to further complicate the analysis by including any kind of stochasticity for these values. The costs have just been adjusted for inflation due to the fact that the study was performed in 2015.

The next step was to decide the parameters of the assumed triangular distributions. It was decided to include 6 different triangular distributions that were assigned to several activities. The probability density function (pdf) of these 6 types are shown below and the reason behind this choice is given below the following table.

Type	Pdf
1	<p>Value in figures in Appendix</p> <p>Most Probable Value (MPV)</p> <p><math>a = 0.8 \cdot MPV</math> <math>b</math> <math>c = 1.6 \cdot MPV</math></p>
2	<p>Value in figures in Appendix</p> <p>Most Probable Value (MPV)</p> <p><math>a = 0.8 \cdot MPV</math> <math>b</math> <math>c = 1.4 \cdot MPV</math></p>

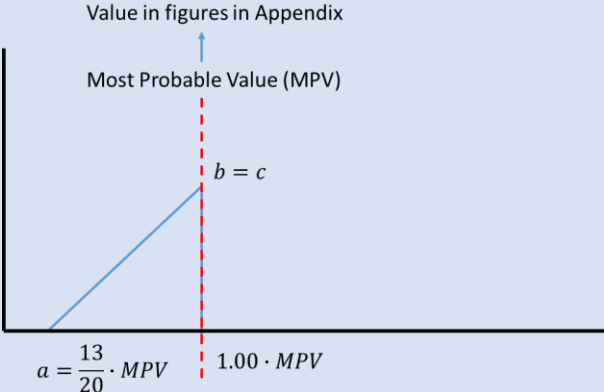
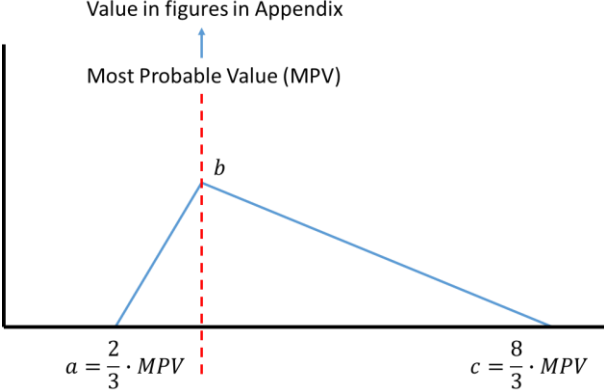
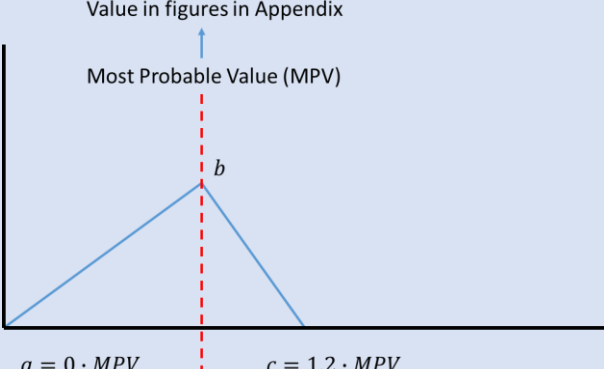
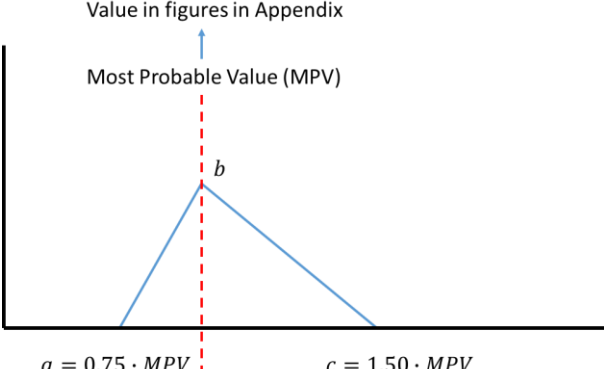
3	 <p>Value in figures in Appendix</p> <p>Most Probable Value (MPV)</p> <p><math>b = c</math></p> <p><math>a = \frac{13}{20} \cdot MPV</math>     <math>1.00 \cdot MPV</math></p>
4	 <p>Value in figures in Appendix</p> <p>Most Probable Value (MPV)</p> <p><math>b</math></p> <p><math>a = \frac{2}{3} \cdot MPV</math>     <math>c = \frac{8}{3} \cdot MPV</math></p>
5	 <p>Value in figures in Appendix</p> <p>Most Probable Value (MPV)</p> <p><math>b</math></p> <p><math>a = 0 \cdot MPV</math>     <math>c = 1.2 \cdot MPV</math></p>
6	 <p>Value in figures in Appendix</p> <p>Most Probable Value (MPV)</p> <p><math>b</math></p> <p><math>a = 0.75 \cdot MPV</math>     <math>c = 1.50 \cdot MPV</math></p>

Table 6-24: Assumed Triangular distributions

Explanation of table 5-24:

The parameters for the 6 triangular distributions shown above have been decided after consulting experts in the area of shipbuilding with the usage of composite materials and more specifically the usage of glass fiber reinforced polymers for the construction of the loading carrying elements, i.e. the hull's and superstructure's components. For better understanding of the procedure, the readers are suggested to read and understand the sequence of the activities shown in figure A-2, A-3 as well as the tables 5-10 until 5-14 which provide the input for the former figures.

Activity	Type
Assembly of partial hull moulds into integral hull mould, including levelling of the integral mould	2
Transportation of the mould	2
Make the mould air tight & control of the vacuum tightness	2
Lining out and fixation of deck/bulkhead in the hull	2
Removal of the hull out of the mould	2
Resin infusion 1 <sup>st</sup> and 2 <sup>nd</sup> shot	3
Removal of consumables	3
Bureaucracy and inspection of mould	4
Inspection of air tightness	5
Time needed between activities	6

Table 6-25: Activities with distributions other than type #1

The nature of each of the individual activities defined the parameters of the respective distribution that was assigned to each activity. All the activities were assigned with the triangular distribution type #1 except from the ones that are shown in table 5-25. A further explanation is given below for the rationale used towards the determination of the distribution's parameters.

- Distribution Type #2

This distribution type was used for 5 activities which are shown in table 5-25. The first activity with the name: "Assembly of partial hull moulds into integral hull mould, including levelling of the integral mould" lasts for  $XX$  manhours according to table 5-10 and can be found at figure A-2 as activity #1. This value, as explained in table 5-24 represents the "b" value which is the most probable one. Of course, according to elementary statistics, the probability of obtaining exactly  $XX$  manhours for this activity is equal to zero as a certain interval of values has to be defined in order to get a probability higher than zero, i.e.  $P(MPV - \varepsilon < X < MPV + \varepsilon) > 0$ . By having a long discussion with the aforementioned experts in the company, it was decided that the minimum amount of time needed for this activity is approximately 80% of this value whereas the maximum amount of time is equal to 140% of this value. As it is shown in the suggested future research, an extensive study has to be implemented for the definition of these parameters based on historical data of various shipyards, which for this thesis was not available. As an alternative, discussions were made with experts who know in depth this procedure and their input was used for the statistical analysis. To conclude, a rule of thumb was used to assign this type of distribution to several activities which uses as input the most probable value as shown in tables 5-10 until 5-14 and figures A-1 and A-2. If this most probable value is high, then this type of distribution was assigned; hence, the 5 activities with high most probable values were assigned with type #2 distribution.

- Distribution Type #3

This distribution type was assigned to two activities: “*Resin Infusion 1<sup>st</sup> and 2<sup>nd</sup> shot*” as well as “*Removal of consumables*”. By taking as granted the amount of employees shown in figure A-2, this distribution took into account the physics of these activities. Both activities cannot last longer than two working days because the resin will thicken and that would create problems. For the activity: “*Resin Infusion 1<sup>st</sup> and 2<sup>nd</sup> shot*” the resultant hull’s shell will not have the desired quality at the connection between the 1<sup>st</sup> and 2<sup>nd</sup> resin shot while if the consumables are removed after XX working days, the thickened resin will make this activity too difficult. Hence, this type was adjusted in a way that these activities will last at maximum XX working days and for that reason, in table 5-24 the most probable value “*b*” according to table 5-10 is equal to the maximum value “*c*”. Regarding the left end with the value of  $a = 13/20$ , this value was decided because the minimum amount of time that these activities last is approximately a working day (~ XX manhours).

- Distribution Type #4

This distribution type was assigned to the activity: “*Bureaucracy and inspection of mould*”. It is known that when the steel mould is transported to its destination, some bureaucratic work has to be done for the acceptance of the product along with some inspection. According to experts this procedure takes XX working weeks with a minimum amount of XX weeks ( $a = XX$ ) and a maximum amount of XX weeks ( $c = XX$ ). For this reason, the type #4 was assigned to the activity #3 according to figure A-2.

- Distribution Type #5

This distribution type was assigned to the activity: “*Inspection of air tightness*”. It is pretty significant for quality reasons to make the mould air tight and control the vacuum tightness. This activity (#4 at figure A-2) has to be done carefully and its significance requires occasionally inspections. These inspections (#5 at figure A-2) last approximately XX working days with a maximum amount of XX days ( $c = XX$ ) and a minimum amount of zero days ( $a = XX$ ). For this reason, the type #5 was assigned to the activity #5 according to figure A-2.

- Distribution Type #6

This distribution type was assigned to the activity: “*Time needed between activities*”. In the total project, the time that is necessary to be spent between the activities (activity #21 in figure A-2) was decided to be approximately equal to XX working weeks or 10 working days. This value (MPV) takes into account occasions such as moving from one place to another, breaks between the activities, discussions among employees etc. The left end was decided to be XX of the MPV ( $a = XX$ ) and the right equal to XX ( $c = XX$ ); these values are based on recognition and their exact definition is difficult to be made; nonetheless, the chosen values represent realistic cases.

Last but not least, it should be mentioned that the rest of activities follow the triangular distribution type #1. There the left end is decided to be equal to 80% of the most probable values (MPV) shown in tables 5-10 until 5-14 and the right end equal to 160% of the MPV. This choice is based on the fact that activities that last for

a small period of time (small values of MPV) have higher probability to be delayed and on average, these values for the parameters  $a, c$  are assumed realistic according to the experts' experience.

### Expect the unexpected

Distributions are now assigned to all the activities and they have been added to a Matlab model. A last distribution was added which accounted for any unexpected events that can occur during such a complex project. These unexpected events include holidays, potential illnesses, delays from suppliers among many others. The unexpected delays were modelled as a normal distribution that can be either  $N(1 \text{ month}, 1 \text{ week})$  or  $N(2 \text{ months}, 2 \text{ weeks})$  where the 1<sup>st</sup> parameter describes the mean value of the normal distribution and the 2<sup>nd</sup> its standard deviation. If the random sampling leads to a negative value for the unexpected delay, the model was built in a way to assume the delay equal to zero. Again, there are many distributions that can describe such events but the normal was assumed to be the most representative. Especially, by avoiding negative delays, this distribution is opted for modelling random events.

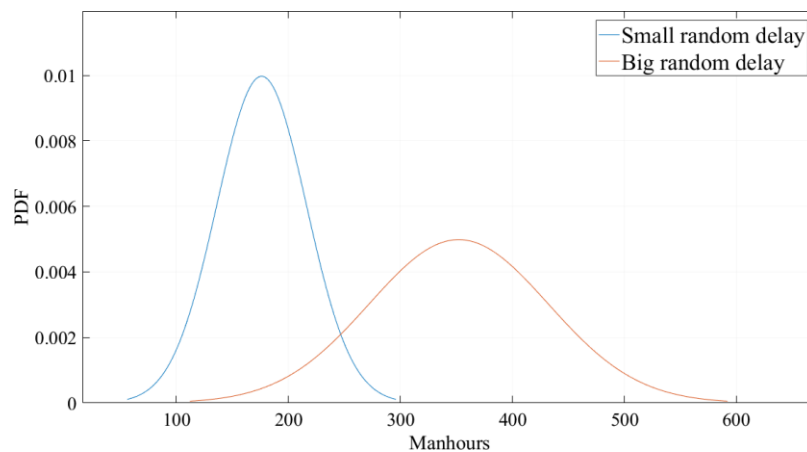


Figure 6-13: Unexpected delays

The last step, is to run a Monte Carlo analysis where all the above distributions are included. For more information about Monte Carlo Sampling (MCS) the reader is suggested to read the subchapter 3.4.1 of the supporting document. The MCS was opted compared to the Latin hypercube(explained in the same chapter) for its simplicity.

After running 100000 simulations in Matlab the resultant total costs and total time needed are:

Total Cost [ $10^3\text{€}$ ]		Total Time [h]
$P_{50} = XX$ (the Netherlands)	$P_{50} = XX$ (Turkey)	$T_{50} = XX^*$
$P_{70} = XX$ (the Netherlands)	$P_{70} = XX$ (Turkey)	$T_{70} = XX^{**}$

Table 6-26: Total Cost and time needed

\* $T_{50} = 2530$  hours, corresponds to  $XX$  year(s),  $XX$  months and  $XX$  days

\*\* $T_{70} = 2621$  hours, corresponds to  $XX$  year(s),  $XX$  months and  $XX$  days

Under the assumption of 8 working hours per day, 5 times per week

The value  $P_{50}$  corresponds to the value where there is a probability of 50% to be exceeded. On the other hand,  $P_{70}$  is the value where there is only 30% chance to be exceeded. Identical notation were used for  $T_{50}$  and  $T_{70}$ . The same model can be used to find the values  $P_{10}$  or  $P_{90}$  with 90% and 10% probability to be exceeded respectively. That is a useful tool for the managers who will decide the offer that the company will make regarding to their economic policy. Conservative thinking will lead to the choice of sale prices based on total costs higher than  $P_{50}$  such as  $P_{70}, P_{90}$  etc. whereas an aggressive economic policy will lead to the opposite result.

If the focus is given to the mean values for the costs, a breakdown of the individual costs will show which parts contribute most. This is shown with the pie charts that are following for the two different production locations.

### TOTAL COSTS BREAKDOWN PRODUCTION IN THE NETHERLANDS

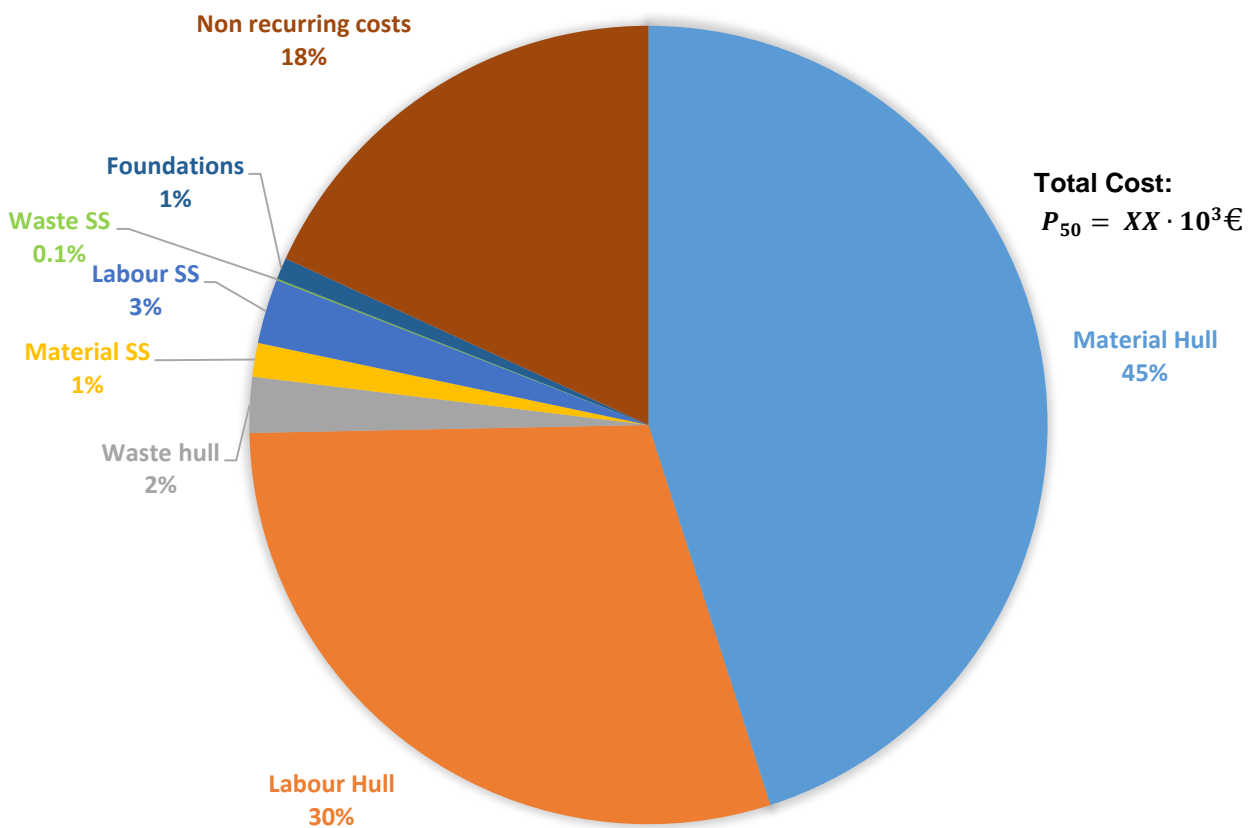


Figure 6-14: Total costs breakdown, Production in the Netherlands

## TOTAL COSTS BREAKDOWN PRODUCTION IN TURKEY

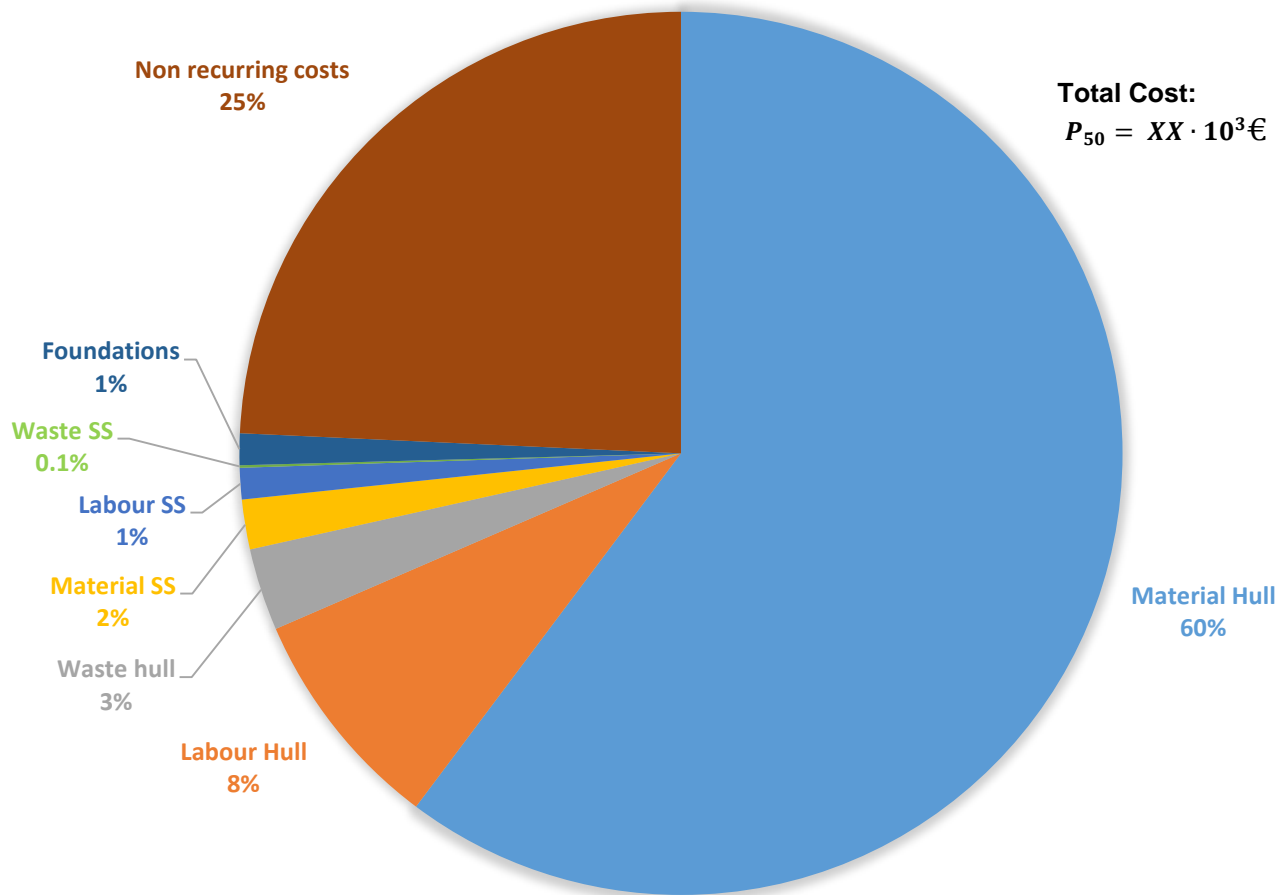


Figure 6-15: : Total costs breakdown, Production in Turkey

At this point it is worth mentioning that this financial study didn't include the:

- Project management (similar for both composite and steel construction)
- Production management
- Facilities (sheds, halls, storage, etc)
- Engineering
- Outfitting
- Ship Equipment
- Launching (similar for both composite and steel construction)
- Commissioning (similar for both composite and steel construction)

## 6.5 Conclusions

In this study a model was built in Matlab which is capable of predicting the time and costs needed within a pre-defined probability of not exceedance. This can be a great tool for project planners because they can say to their clients that they need a timespan higher than  $T_{50}$  when they follow a conservative strategy and smaller than  $T_{50}$  when they follow an aggressive strategy. Also, this model is capable of quantifying the compromise between costs, time and probability of not exceedance. For example, by looking at table 5-26, a project planner can find it preferable to increase the timespan by 3.6% in order to have a disproportionate increase of 20% at the probability of not exceedance in terms of time. To further clarify this, it is known that there is 50% chance of completing the project within  $XX$  working hours and 70% chance of completing it within  $XX$  hours. This small increase of 3.5% at the time planning will make the project planners 20% more sure that the project will be completed within the agreed time. Furthermore, the project planners can investigate the same impact at the costs too. For the same example, a small increase of the estimated costs by 0.27% can lead to an increase of 20% at the probability of not exceedance (from  $P_{50}$  to  $P_{70}$ ) for the case where the construction occurs in Turkey. Last but not least, the same Matlab model is capable of giving the relative costs of the activities as shown in figure 6-14 and 6-15. This can be of great help during the basic engineering phase because the project planners can focus on the factors that contribute more at the costs. For example, for the case of the production in Turkey, it makes sense to pay a lot of attention at the cost of hull's materials because a potential decrease (by finding cheaper suppliers or optimizing the structure) can lead to a significant decrease to the total estimated costs. On the other hand, in figure 6-15, it is shown that it doesn't make sense to pay a lot of attention at the decrease of the superstructure's material costs as they have an almost negligible contribution at the total costs.

To conclude, the objective of this study is accomplished because as it was stated at the introduction of this chapter, a tool was built with which the project planners are able to predict the probability of completing the project (or various stages of it) within a certain confidence interval and within time and cost.



# Chapter 7: Recommendations

## 7.1 Recommendations for the technical part

- By checking the figures 4-21 until 4-24 it is safe to claim that the size effects are not so big when the elastic modulus in various directions are considered. However, this cannot be claimed for the case of the strength properties in various directions because it is not easy to figure out the exact ply and its position when it fails. Hence, it is highly recommended by the writer to implement experiments in order to define the scale effects, i.e. to investigate the decrease of the strength when coupons with bigger dimensions are examined. Furthermore, in the same testing plan, the coupons can be extracted in a way that the correlation of the material properties that are derived from different tests can be included too. Then, by using the writer's method as introduced in subchapter 3.3 random variables with correlations at various properties can be generated and as a result multiple analysis can be run again where the properties will be better correlated
- Another recommendation from the writer concerns the introduction of a more sophisticated model for the progressive damage modelling. Continuum damage mechanics can be used for the prediction of partly damaged plies which reduce incrementally their contribution to the stiffness matrix. Readers that are interested to implement this method should perform further experiments for the determination of viscous damping coefficients and energies dissipated per area unit. They can find relevant information at Ref. [40-41].
- During this thesis it was obvious that a lot of discussion was made for the cylindrical supports of the large scale experiments. It was decided here to use a simplistic model where the horizontal forces were modelled through elastic linear springs. The writer suggests that an extensive study could be made to investigate the effect of the horizontal forces at these and similar experiments and then check the accuracy of the assumed method that was used in this thesis.

---

## 7.2 Recommendations for the Integrated Design Management

- As it is mentioned in the chapter 6.2.1 the values  $a, b, c$  of the triangular distributions were defined after discussions with experts who have extensive experience in the construction of composite vessels and as a result on the time needed for these activities. However, the writer highly suggests to gather data from actual shipyards where these activities were/are performed. In that way the credibility of the model could increase as the values  $a, b, c$  will be defined through historical data and not from simple discussions with individuals. Furthermore, it is of great interest to see how the time and the costs needed for the construction of multiple vessels will lead to a decrease of the cost of a unit vessel due to the learning curve. It is intuitive that if a shipyard constructs multiple vessels, the cost per vessel will be lower comparing to the case where just one vessel was constructed. The writer suggests that a study should be implemented in order to quantify the above qualitative argument.

## References

- [1] Autar Kaw, Mechanics of composite materials, 2<sup>nd</sup> Edition, 2006, ISBN-13: 978-0-8493-1343-1
- [2] Yong Bai, Wei-Liang Jin, Marine Structural Design, 2<sup>nd</sup> Edition, (2016), ISBN: 978-0-08-099997-5
- [3] Damen Shipyards Group, Company's site: <http://products.damen.com/> (LV: 17/ 11/ 2017)
- [4] Swedish Stealth Corvette: "HMS Helsingborg", <https://imgur.com/gallery/jedM68n> (LV: 04/ 02/ 2018)
- [5] Alexandre Landesmanna, Carlos Alexandre Serutia, Eduardo de Miranda Batista, Mechanical Properties of Glass Fiber Reinforced Polymers Members for Structural Applications, Materials Research. 2015; 18(6): 1372-1383, DOI: <http://dx.doi.org/10.1590/1516-1439.044615> (LV: 6/02/2018)
- [6] Sang-Young Kim et al., Mechanical properties and production quality of hand-layup and vacuum infusion processed hybrid composite materials for GFRP marine structures, Int. J. Nav. Archit. Ocean Eng. (2014) 6:723~736, <https://doi.org/10.2478/IJNAOE-2013-0208> (LV: 06/02/2018)
- [7] Yunfu Ou et al, Mechanical Characterization of the Tensile Properties of Glass Fiber and Its Reinforced Polymer (GFRP) Composite under Varying Strain Rates and Temperatures , Polymers 2016, 8, 196; doi:10.3390/polym8050196, <http://www.mdpi.com/journal/polymers> (LV: 06/02/2018)
- [8] K.C. Bacharoudis, PhD Thesis, Stochastic analysis of structures made of composite materials,2014
- [9] J Bai, Advanced Fibre-Reinforced Polymer (FRP) Composites for Structural Applications, 1st Edition, Ch. 13,e- ISBN: 9780857098641,2013
- [10] Leif A. Carlsson, Donald F. Adams, R. Byron Pipes, Experimental Characterization of Advanced Composite Materials, 4th Edition, ISBN-10:1439848580,2014
- [11] Knowledge Centre WMC, <https://wmc.eu/> (LV: 06/02/2018)
- [12] ASTM International, Standard Test Method for Tensile Properties of Polymer Matrix Composite Materials, D3039/D3039M-14, Approved: 15 May 2014, DOI: 10.1520/D3039\_D3039M-14
- [13] ASTM International, Standard Test Method for Compressive Properties of Polymer Matrix Composite Materials, with Unsupported Gage Section by shear Loading, D3410/D410M-03, Approved: 1 Sept 2008,, DOI: 10.1520/D3410\_D3410M-03R08
- [14] ASTM Standard Test Method for Shear Properties of Composite materials by V-notched Rail Shear Method, D7078/D7078M-12, Approved: 15 June 2012,, DOI: 10.1520/D7078\_D7078M-12
- [15] Technical Datasheet, Hysol EA 9394, Epoxy Paste adhesive. Structural paste Adhesive, source: [http://www.northerncomposites.com/docs/default-source/data-sheets/hysol\\_ea\\_9394-en15a40c281cc2688d932fff000006e6f6.pdf?sfvrsn=2](http://www.northerncomposites.com/docs/default-source/data-sheets/hysol_ea_9394-en15a40c281cc2688d932fff000006e6f6.pdf?sfvrsn=2) (LV: 10/ 11/ 2017)
- [16] KVE Composites Group, Company's site: <https://www.kve.nl/> (LV: 20/ 11/ 2017)
- [17] Bureau Veritas, Company's site: <http://www.bureauveritas.nl/> (LV: 20/ 11/ 2017)
- [18] Applus+, Bremen, Germany, Company's site: <https://www.bk-werkstofftechnik.com/> (LV: 20/ 11/ 2017)

- [19] Applus+, Bremen, Germany, Certifications of laboratory that performed the small scale coupon tests, source: <https://www.bk-werkstofftechnik.com/certifications/> (LV: 20/ 11/ 2017)
- [20] Applus+ Laboratories, Barcelona, Spain Company's site: <http://www.appluslaboratories.com>
- [21] D.J. Lekou, PhD thesis, Reliability determination for the design of structures made by composite materials", 2010, [Greek]
- [22] Design Study FRP Construction MCMV, Inner report (confidential), DSNS,2015
- [23] Damen Schelde Naval Shipbuilding, Company's site: <http://www.damen.com/companies/damen-schelde-naval-shipbuilding>, (LV: 27/ 11/ 2017)
- [24] Defence Material Organization, DMO, website: <https://english.defensie.nl/organisation/dmo> (LV: 09/02/2018)
- [25] TNO, Company's site: <https://www.tno.nl/nl/> (LV: 11/ 02/ 2018)
- [26] Lijian Qi, Master Thesis: A Study of the Buckling Behaviour of Stiffened Panels under Compression and Lateral Pressure,2018
- [27] Mesut Tekgoz, Mater Thesis, Strength Assessment of Imperfect Stiffened Panels Using Modified Stress Strain Curves, 2012
- [28] Hughes, Owen F.; Paik, Jeom Kee, Ship Structural Analysis and Design, 2010, e-ISBN: 978-1-61344-140-4
- [29] A. Puck, J. Kopp, M. Knops, Guidelines for the determination of the parameters in Puck's action plane strength criterion, Composites Science and Technology 62 (2002) 371–378, PII: S0266-3538(01)00202-0
- [30] T. E. Tay, G. Liu, V. B. C. Tan, X. S. Sun and D. C. Pham, Progressive Failure Analysis of Composites, Journal of composite materials, Vol. 42, No. 18/2008, DOI: 10.1177/0021998308093912
- [31] Ansys Mechanical User's Guide, help manual v.17.1
- [32] Airborne, Company's site: <http://www.airborne.com/> (LV: 27/ 11/ 2017)
- [33] Solico, Solutions in Composites, Company's site: <https://www.solico.nl/>, (LV: 27/ 11/ 2017)
- [34] Polyworx, Company's site: <http://www.polyworx.com/>, (LV: 27/ 11/ 2017)
- [35] Defence Material Organization, DMO, Website: <https://english.defensie.nl/organisation/dmo>, (LV: 27/ 11/ 2017)
- [36] Outokumpu, Company's site: <http://www.outokumpu.com/en/Pages/default.aspx>, (LV: 27/ 11/ 2017)
- [37] Schelde Exotech, Company's site: <http://www.exotech.nl/en/company>, (LV: 27/ 11/ 2017)
- [38] Lloyds Register: Rules and Regulations for the classification of Special Service Craft, Vol. 6, Pt. 8 , Hull Construction in Composite, July 2014
- [39] Triangular Distribution - MATLAB & Simulink - MathWorks United Kingdom, source: <https://uk.mathworks.com/help/stats/triangular-distribution.html>
- [40] Ever J. Barbero, Mehdi Shahbazi, Determination of material properties for ANSYS progressive damage analysis of laminated composites, Composite Structures 176 (2017) 768–779
- [41] Ever J. Barbero, finite element analysis of composite materials using Ansys®, 2nd Edition, (2014), ISBN-13: 978-1-4665-1690-8

# Appendix A

Confidential. Contact: Joep Broekhuisjen ([J.Broekhuijsen@damennaval.com](mailto:J.Broekhuijsen@damennaval.com))

# Appendix B

## B.1 Manufacturing of Panels



Figure B- 1: Dry fiber mats



Figure B- 2: Dry fiber mat, fibers at 0°



Figure B- 3: Dry fiber mat, fibers at 90°



Figure B- 4: Dry fiber mat, fibers at 0°/90°



Figure B- 5: Dry fiber mat, thick panel, fibers at 0°



Figure B- 6: Resin transferring, VARTM

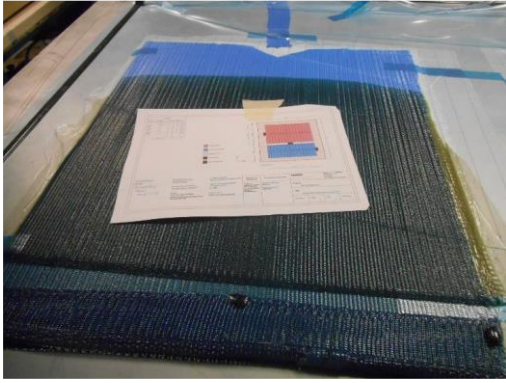


Figure B- 7: Resin transferring, Case: Fibers at 90o



Figure B- 8: Resin transfer finished, Case: Fibers at 0°/90°



Figure B- 9: Resin transfer finished, Case: thick panel

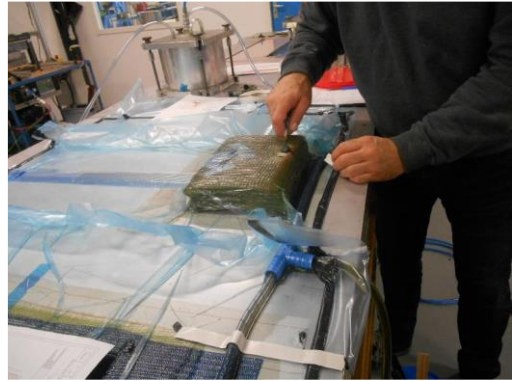


Figure B- 10: Penetration of vacuum bag to let air pass



Figure B- 11: Procedure finished



Figure B- 12: Control of underpressure during VARTM

## B.2 Received panels from Applus+

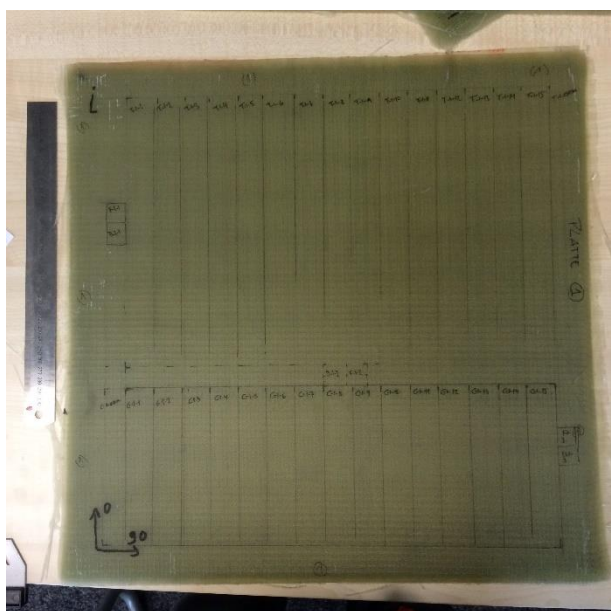


Figure B- 13: Panel i, Fibers at 0°

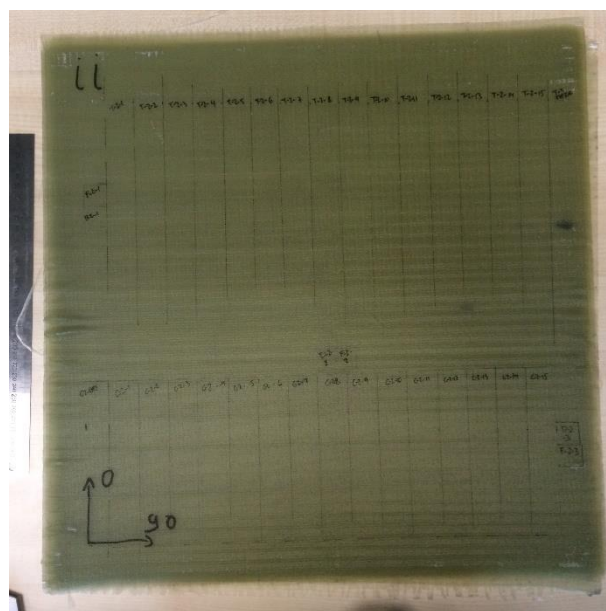


Figure B- 14: Panel ii, Fibers at 90°

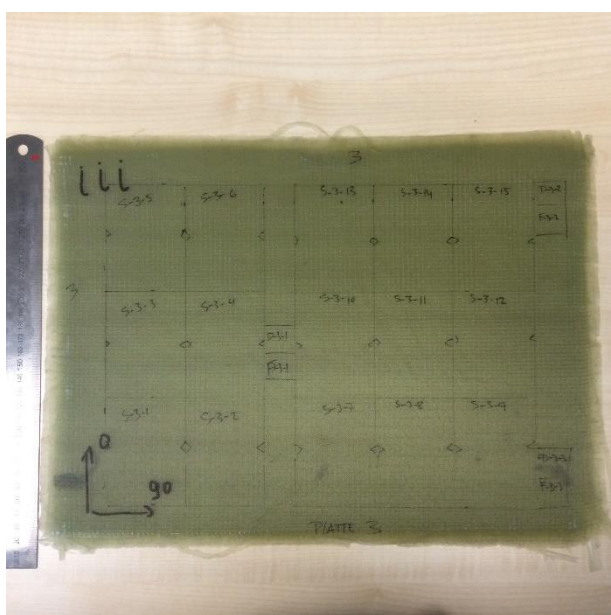


Figure B- 15: Panel iii, Fibers at 0°/90°



Figure B- 16: Panel iv, Fibers at 0°



Figure B- 17: Panel iv, Fibers at 0°



Figure B- 18: Panel iv, Fibers at 0°

## B.3 Construction of Coupons

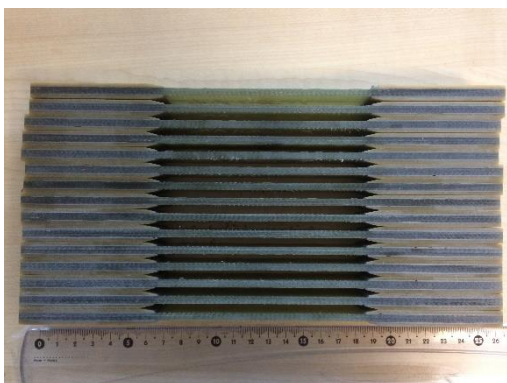


Figure B- 19: Tensile Coupons, Fibers at 0°



Figure B- 20: Random Tensile Coupons, mounted gauges

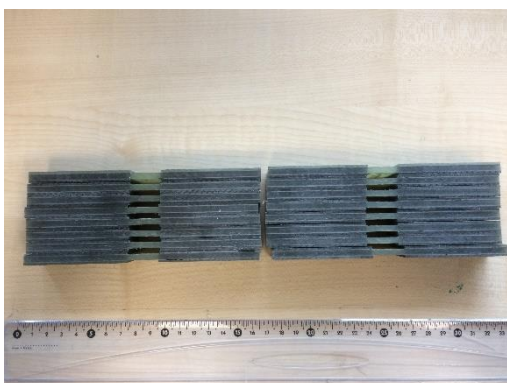


Figure B- 21: Compressive coupons, Fibers at 0°

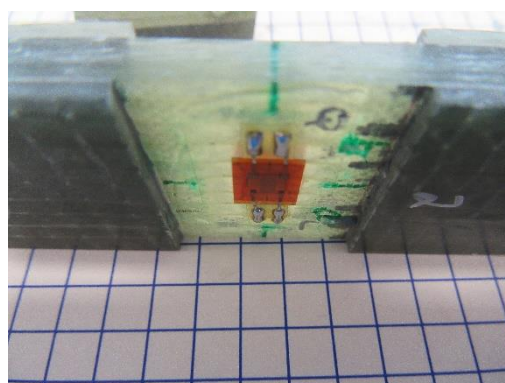


Figure B- 22: Random Compressive Coupon, mounted gauges



Figure B- 23: Random Shear coupon

# Appendix C

## C.1 Test set-ups

### C.1.1 Tensile Test Set-Up



Figure C- 1: Tensile test set-up (1)



Figure C- 2: Tensile test set-up (2)

## C.1.2 Compressive Test Set-Up

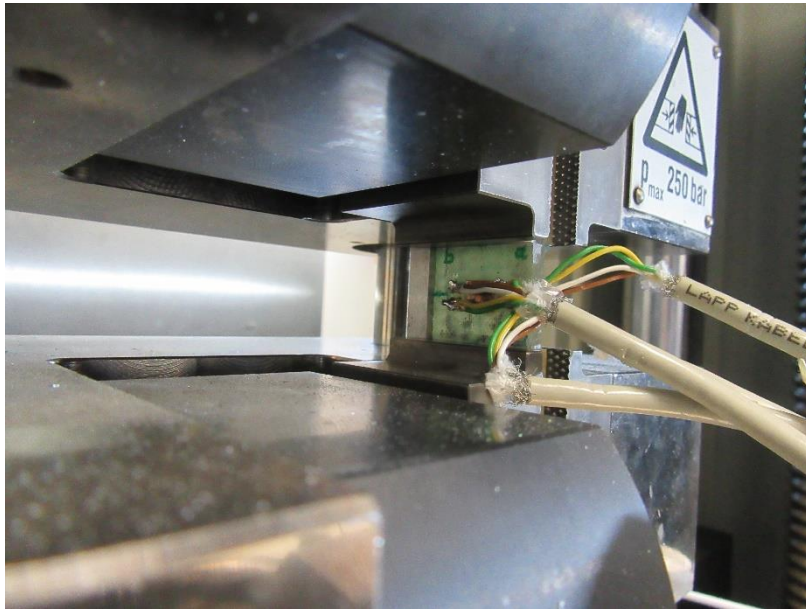


Figure C- 3: Compressive test set-up (1)

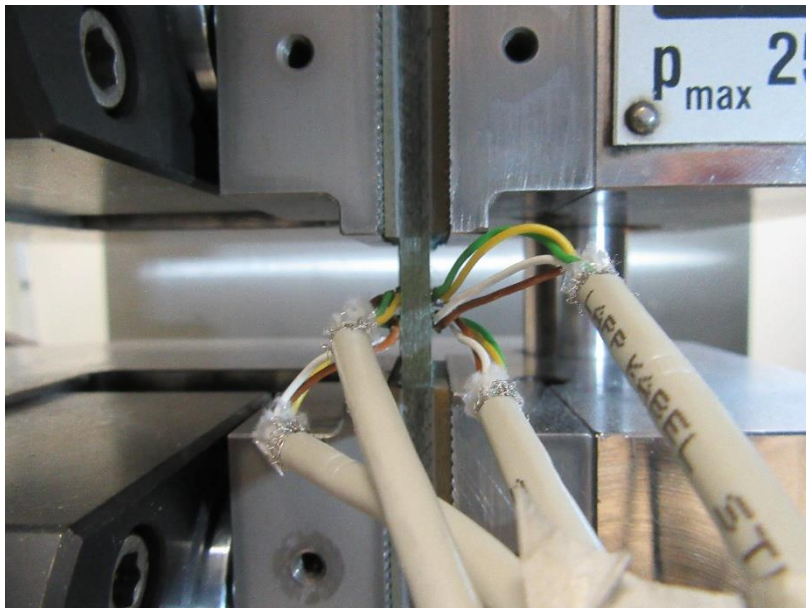


Figure C- 4: Compressive test set-up (2)

### C.1.3 Shear Test Set-Up



Figure C- 5: Shear tests, set up

## C.2 Testing devices

### C.2.1 Tensile Test device (in German)

**Zwick / Roell**

**Zwick**  
Materialprüfung

#### Produktinformation

Ausrichteinheiten, Fmax 50 kN bis 250 kN



Ausrichteinheit in Flanschverbindung montiert zwischen Kraftaufnehmer und Probenhalter



Ausrichteinheit mit Bolzenverbindung direkt auf die Traverse montiert

#### Anwendungsbereich

Die exakte axiale Ausrichtung der Prüffachse der Material-Prüfmaschine ist eine Grundvoraussetzung zur Ermittlung exakter Kennwerte. Insbesondere bei spröden Werkstoffen wie Faserverbundwerkstoffen und verschiedenen Metallen muss die Ausrichtung mit großer Sorgfalt erfolgen.

#### Produktbeschreibung

Die Ausrichteinheit ist ein Justageelement, das zwischen der Traverse der Material-Prüfmaschine und dem Probenhalter bzw. Prüfwerkzeug eingebaut wird. Über Einstellschrauben wird zunächst der Winkelfehler und danach der Achsenversatz justiert. Jeder Fehler kann auf diese Weise einzeln und über die Anordnung justiert werden. Die Anordnung der Einstellschrauben in X- und Y-Richtung erlaubt die Korrektur der Fehler entlang ihrer jeweiligen Wirkrichtung.

#### Vorteile/Merkmale

- Erhebliche Verringerung des Justageaufwands
- Komfortable Justage auch unter Zug- oder Druckbelastung
- Hinreichend großer Stellbereich
- Winkel- und Versatzfehler sind unabhängig voneinander einstellbar
- Feste Verspannung der Ausrichteinheit, so dass das Justageergebnis langfristig erhalten bleibt
- Adaptierbar an Kopf-, Fahr- und Sockeltraversen
- Bei der Kraftstufe 250 kN ist eine Variante mit Flanschschnittstelle erhältlich. Dadurch ist ein kürzerer Prüfaufbau und eine noch höhere Steifigkeit möglich

#### Hinweis zur Alignment-Messung

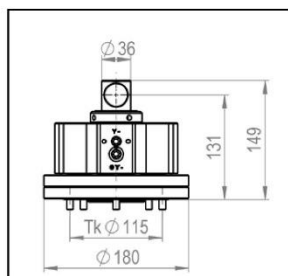
- Die genauen Vorgaben der maximal zulässigen Querbelastungen sind in den jeweiligen Anwendungsnormen festgelegt
- Zum Nachweis der Maschinengenauigkeit muss die Justage im belasteten Zustand über optional erhältliche DMS-applizierte Mess-Normale, Messverstärker und *testXpert*® II Softwareapplikation erfolgen. Die Berechnungsroutinen entsprechen der ASTM E 1012
- Die rein mechanische Justage im unbelasteten Zustand kann über die Anschlussbolzen bzw. über eine im Probenhalter gespannte, geteilte Probe erfolgen

**Produktinformation**

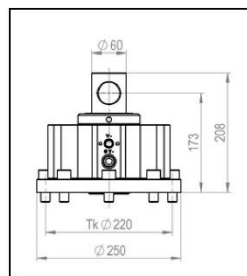
Ausrichteinheiten, Fmax 50 kN bis 250 kN

Artikelnummer	058005	058006	068902
Ausführung	50 kN Bolzen	250 kN Bolzen	250 kN Flansch
In Verbindung mit	AllroundLine	AllroundLine	AllroundLine
Fmax	50 kN	250 kN	250 kN
Anschluss	Bolzen Ø 36 mm	Bolzen Ø 60 mm	Flanschverbindung
Belastungsarten (symmetrisch)	Zug/Druck (statisch)	Zug/Druck (statisch)	Zug/Druck (statisch)
Max. zulässiges Biegemoment auf den Anschlussbolzen/flansch	1 kNm	7,5 kNm	30 kNm
Traversenschnittstelle	Zentrierung D70 8 x M8 auf Tk 115	Zentrierung D70 8 x M16 auf Tk 220	Zentrierung D70 8 x M16 auf Tk 220 <sup>1)</sup> 8 x M16 auf Tk 264
Probenhalterschnittstelle	Bolzen D 36g6	Bolzen D 60g6	Zentrierung D70 8 x M16 auf Tk 220
Versatzkorrektur (X/Y)	± 3 mm	± 3 mm	± 3 mm
Erreichbare Genauigkeit bei Versatzkorrektur	± 0,01	± 0,01	± 0,01
Winkelkorrektur	± 1 °	± 0,7 °	± 0,35 °
Erreichbare Genauigkeit bei Winkelkorrektur	± 0,006 °	0,004 °	0,002 °
Abmessungen			
Gesamthöhe	152 mm	211 mm	145 mm
Bauraumhöhe	111 mm	138 mm	142 mm
Durchmesser	180 mm	250 mm	290 mm
Gewicht	ca. 14 kg	ca. 34 kg	ca. 49 kg
Temperaturbereich	+10... 35 °C	+10... 35 °C	+10... 35 °C

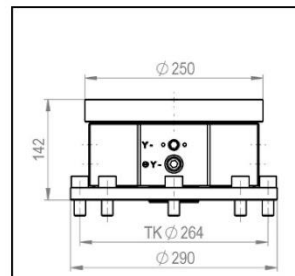
<sup>1)</sup> mit Zwischenflansch



50 kN Ausführung mit Bolzen



250 kN Ausführung mit Bolzen



250 kN Ausführung mit Flanschschnittstelle

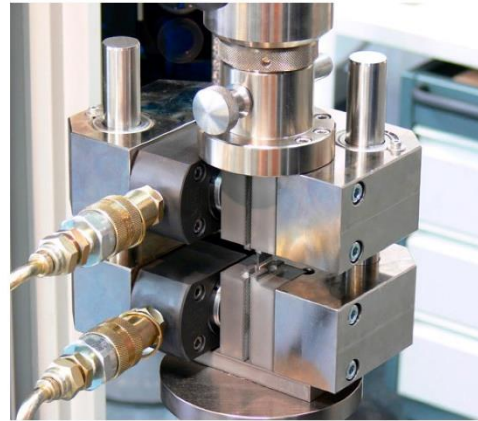
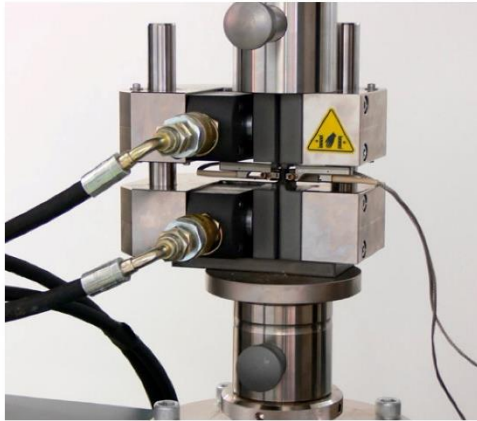
## C.2.2 Compressive Test device (in German)

**Zwick / Roell**

**Zwick**  
Materialprüfung

### Produktinformation

Hydraulische Druckvorrichtung für Verbundwerkstoffe (HCCF)



#### Anwendungsbereich

Diese hydraulische Druckvorrichtung für Verbundwerkstoffe (HCCF - Hydraulic Composites Compression Fixture) wurde für die Bestimmung der Druckeigenschaften entwickelt.

Sie wird für die Prüfung an langfaserverstärkten Verbundwerkstoffen, z.B. kohlestofffaserverstärkten Kunststoffen (CFK) oder glasfaserverstärkten Kunststoffen (GFK) mit unidirektionaler, multidirektionaler oder gewebter Faserverstärkung eingesetzt.

Die Druckvorrichtung eignet sich für „Plain“, „Open Hole“ und „Filled Hole“ Druckversuche mit Krafteinleitung über Klemmung (Shear loading) oder mit einer kombinierten Krafteinleitung mit stirnseitiger Abstützung und gleichzeitiger Klemmung (Combined Loading).

Die verschiedenen Ausführungen der Druckvorrichtung sind für Prüfungen in einem breiten Temperaturbereich einsetzbar.

#### Vorteile/Merkmale

- Die offene Bauweise in C-Form ermöglicht Ihnen einen bequemen Probenwechsel. Außerdem vereinfacht sie den Einsatz von Längenänderungs-Messsystemen
- Durch die Bauweise ist die Probe extrem genau ausgerichtet, Toleranzen aus dem Prüfaufbau werden ausgeschlossen

- Das parallel spannende, hydraulische Klemmprinzip sorgt für stick-slip freie und damit biegefreie Kraftaufbringung mit weitgehend konstanter Verformungsgeschwindigkeit
- Die hydraulische Spannkrafterzeugung garantiert eine zuverlässige und reproduzierbare Probeneinspannung. Die Spannkraft wird gleichmäßig auf die Probe aufgebracht und die Probe wird sicher gespannt
- Die optimierte Probenführung minimiert Messfehler und Streuungen
- Aufgrund reibungsarmer Kugelführungen in der Druckvorrichtung werden Verfälschungen der Messergebnisse durch Reibkräfte minimiert
- Die magnetische Halterung der beweglichen Spannbacken erleichtert Ihnen den Probenwechsel und die Reinigung der Spannflächen

#### Normenliste:

- ISO 14126 - Methode 1 und Methode 2
- prEN 2850 Typ A
- AITM 1-0008
- ASTM D 3410
- ASTM D 6641
- JIS K 7076
- CRAG Methode 400, 401
- Airbus QVA-Z10-46-38
- ASTM C 1358
- Airbus-Dokument X88SP1105735: "Compression plain tests according to AITM 1.0008 A1 and A2 with Zwick HCCF"

**Produktinformation**

Hydraulische Druckvorrichtung für Verbundwerkstoffe (HCCF)

Technische Daten aller Druckvorrichtungen			
Max. hydraulischer Druck	250 bar		
Spannkraft	36,3 kN		
Höhe x Breite x Tiefe	220 x 200 x 150 mm		
Gewicht	27,9 kg		
Max. Einspannlänge	35 mm		
Höhe der Backen	65 mm		
Oberflächenstruktur der Backen	Schuppenraster 1,25 mm, plasmanitriert		
Max. Backenabstand	50 mm		
Erforderliche Klemmlänge <sup>1)</sup>	65 mm		
Bei stirnseitiger Kräfteinleitung in den Probekörper (end loading) ist die Gesamtlänge des Probekörpers wie folgt festgelegt: Gesamtlänge = Einspannlänge + (2 x Höhe der Backeneinsätze)			
Hierzu erforderlich: Backeneinsatz (siehe unten), 2 Anschlussschläuche sind enthalten			
Artikelnummer	060309	060312	060347
Fmax	50 kN	150 kN	250 kN
Anschluss-Ø	36 mm	60 mm	60 mm
Temperaturbereich	- 60 ... + 150 °C	- 60 ... + 150 °C	- 60...+ 150 °C

<sup>1)</sup> Die Kräfteinleitung erfolgt hauptsächlich über die Probenenden. Deshalb ist die Klemmlänge von 65 mm einzuhalten. Abweichende Klemmlängen auf Anfrage

**Zubeh r (je 1 x erforderlich)**

Beschreibung	Artikelnummer
Satz Backeneinsätze für Probekörper z.B. nach AITM 1-0008, prEN 2850 Typ A, ISO 14126 (inkl. Typ B2), ASTM D 3410, ASTM D 6641. Probendicke: 1 ... 5 mm, Probenbreite: bis 36 mm	<b>047320</b>
Satz Backeneinsätze für Probekörper z.B. nach AITM 1-0008, prEN 2850 Typ A, ISO 14126 (inkl. Typ B2), ASTM D 3410, ASTM D 6641. Probendicke: 5 ... 10 mm, Probenbreite: bis 36 mm	<b>047321</b>
Satz Backeneinsätze für Probekörper z.B. nach prEN 2850 Typ A, ISO 14126 (ohne Typ B2), ASTM D 3410, ASTM D 6641. Probendicke: 1 ... 5 mm, Probenbreite: bis 20 mm Geeignet für den Einsatz mit Ansetzaufnehmern.	<b>047322</b>
Satz Backeneinsätze für Probekörper z.B. nach prEN 2850 Typ A, ISO 14126 (ohne Typ B2), ASTM D 3410, ASTM D 6641. Probendicke: 5 ... 10 mm, Probenbreite: bis 20 mm Geeignet für den Einsatz mit Ansetzaufnehmern.	<b>047323</b>
GripControl	<b>087280</b>
Grip Control SA	<b>087281</b>
Paar hydraulische Handpumpen, max. Betriebsdruck 250 bar	<b>048480</b>
Druckplatte, Fmax 250 kN, Ø 136 mm Anschluss unten über Anschlussstück, z.B. Artikelnummer 314658	<b>316581</b>

Temperierkammern in verschiedenen Ausführungen für Tisch- und Stand-Prüfmaschinen bieten wir Ihnen gerne auf Anfrage an. Hierzu beraten wir Sie gerne.

## C.2.3 Hydraulic Grips

**Zwick / Roell**

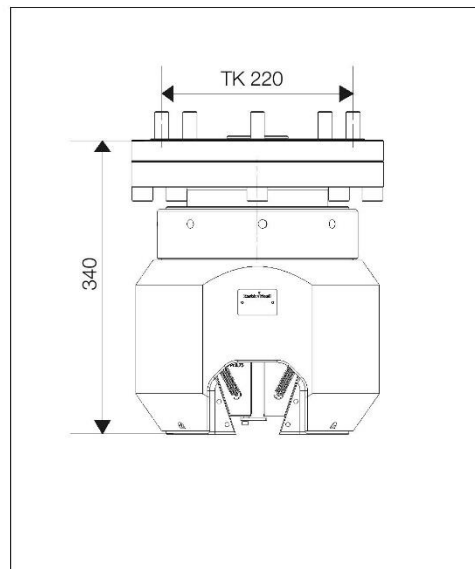
**Zwick**  
Materials Testing

### Product Information

Hydraulic grips type 8594 "body over wedge", Fmax 250 kN



Hydraulic grip for temperature chamber



Hydraulic grip for room temperature

#### Application range

Specimen materials: fiber-reinforced composites, hard and reinforced plastics, ferrous and non-ferrous metals, structural sheet metals, metal-ceramic composites, composites and other materials.

Specimen shape: flat, round

Type of stress: tensile, compression, alternating load

#### Product description

Symmetrically closing hydraulic grips. Positively driven jaws ensure reproducible, precisely axial positioning of the specimen to the tensile axis. The symmetrical design and high stiffness of the main body of the grips make them ideal for tests which require accurate alignment of the specimen to the test axis.

#### Advantages/features

- Excellent, reproducible gripping position and alignment of specimen to test axis; ideal for tests on specimens sensitive to transverse forces
- Suitable for tensile, compression and alternating load tests
- No differential movement of jaws on increase in test load (parallel-clamping grips)
- Symmetrical closing movement of jaws saves set-up time in the event of frequent changes in specimen thickness
- Open design for quick, easy specimen and jaw changes
- Mechanical interface on grips for quick, easy connection of additional test fixtures, load cells and specimen grips
- Unwanted forces acting on the specimen are compensated for during the clamping process by Zwick's 'Force Constant Hold' feature when the grips are used in conjunction with Zwick hydraulic power-packs, *testControl* and *testXpert*® II testing software

**Product Information**

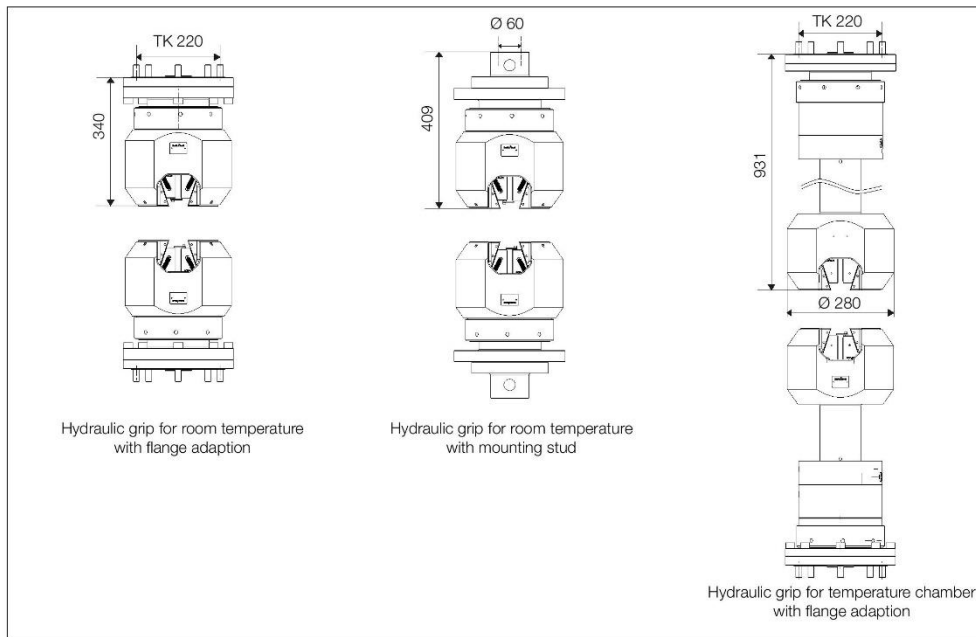
Hydraulic grips type 8594 “body over wedge”, Fmax 250 kN

Item number	072871	072881	071955 <sup>(1)</sup>
Type	8594	8594	8594
Fmax	250 kN	250 kN	250 kN
Functional principle	wedge action	wedge action	wedge action
Max. gripping force (210 bar)	478 kN	478 kN	478 kN
Max. pressure	210 bar	210 bar	210 bar
Height	339,7 mm (open)	408,7 mm	627 mm (below), 931 mm (above)
Outer diameter	280 mm (at head)	280 mm	280 mm
Gripping stroke	according to grip insert	according to grip insert	according to grip insert
Max. opening width	40 mm (flat specimen)	40 mm (flat specimen)	40 mm (flat specimen)
incl. jaws	30 mm (round specimen)	30 mm (round specimen)	30 mm (round specimen)
Specimen gripping	The specimen must be gripped by at least 2/3 of the jaw height.		
Weight per grip (without jaws)	118 kg	113 kg	160 kg (below), 179 kg (above)
Connection interface	flange	mounting stud	flange
Connection diameter	TK 220	60 mm	TK 220
Connection cooling water	-	-	Hose barb 1/4"
Connection condensation water	-	-	Hose barb 1/8"
Temperature range	+4...+35 °C	+4...+35 °C	-70...+250 °C
Scope of supply	1 pair	1 pair	1 pair

**Therefore required**

Hydraulic power pack

<sup>(1)</sup> For grip up to 250° C a connection for cooling water and condensation water required.



All data at ambient temperature.

All rights reserved.

**Product Information**

Hydraulic grips type 8594 “body over wedge“, Fmax 250 kN

**Jaw inserts (1 x required)**

Specimen schape	Design	Jaw width	Jaw high	Hardness	Specimen thickness	Item number
<b>Flat jaw</b>						
Flat	PR 0.75	60 mm	82 mm	56-58 HRC	0 - 12 mm	<b>071996</b>
Flat	PR 0.75	60 mm	82 mm	56-58 HRC	9 - 21 mm	<b>071997</b>
Flat	PR 0.75	60 mm	82 mm	56-58 HRC	18 - 30 mm	<b>075671</b>
Flat	parallel seration 2 mm	60 mm	82 mm	56-58 HRC	30 - 40 mm	<b>075672</b>
Flat	fish scale 1.25 mm	60 mm	82 mm	56-58 HRC	1 - 13 mm	<b>075674</b>
<b>Prism jaw</b>						
Round	parallel seration 1 mm	60 mm	82 mm	56-58 HRC	∅ 6 - 14 mm	<b>075676</b>
Round	parallel seration 1 mm	60 mm	82 mm	56-58 HRC	∅ 14 - 22 mm	<b>075673</b>
Round	parallel seration 1 mm	60 mm	82 mm	56-58 HRC	∅ 22 - 30 mm	<b>075677</b>
Round	parallel seration 2 mm	60 mm	82 mm	56-58 HRC	∅ 14 - 22 mm	<b>084264</b>
Round	parallel seration 2 mm	60 mm	82 mm	56-58 HRC	∅ 22 - 30 mm	<b>084265</b>

Scope of supply: 1 set = 4 pieces  
PR = Pyramid

**Optional Accessories**

Description	Item number
Adapter flange for compression, bending tools for the adaptation of tools up to 250 kN (for example, compression and bending devices), Scope of supply: 1 pair	<b>072701</b>

**Figure C- 8: Tec. Specs Hydraulic Grips**

## Components of the 810 System

### Load Unit Assembly

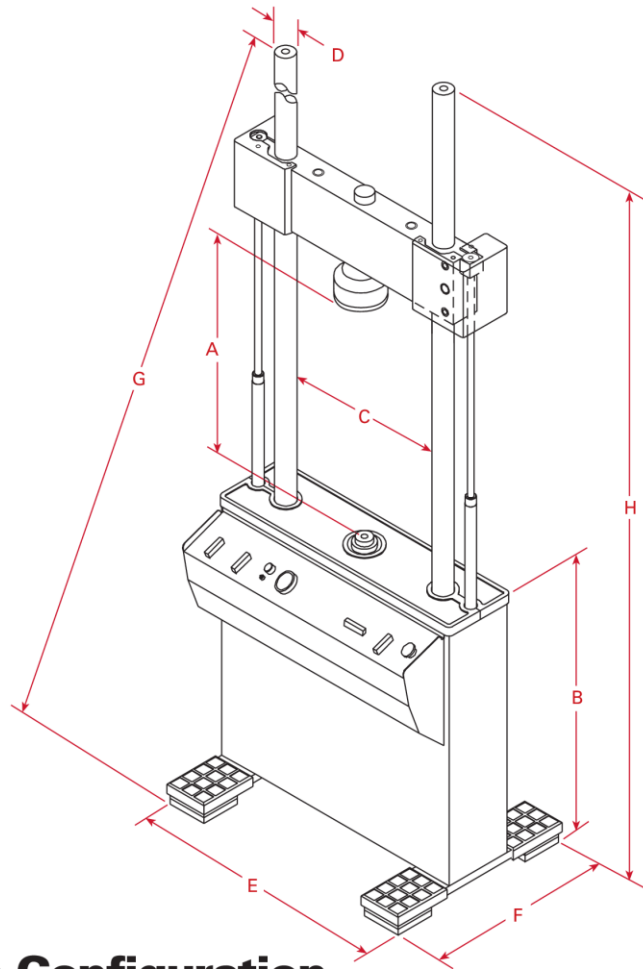
A complete load frame assembly requires the selection of the frame, actuator size, actuator rod/load cell thread, and hydraulic service manifold. The servovalve(s) and other options are selected separately.

The 810 system employs MTS Model 318 load unit assemblies that are force rated up to 500 kN. This floor mounted frame has high axial and lateral stiffness that improves test accuracy and system performance. This load frame is available in a variety of sizes and can be easily configured for many different applications. Please see Performance Curves on page 20 for more details.

Crosshead mounted load cell provides an accurate force reading for measurement and control. The displacement transducer is integral to the actuator for position measurement and control.

Other options such as crosshead mounted actuators, actuator antirotate, hydrostatic bearing actuators, and air isolator pads are available with the 318. Integral actuator design shortens the force train providing higher lateral stiffness. Low friction actuator ensures the best possible test control and resolution.

There are two hydraulic service manifold options for the 318 Load Units. The 298.11 provides OFF/ON pressure control while the 298.12 has OFF/LOW/HIGH pressure control with a controlled pressure transition to and from high pressure.



## Specifications by Frame Configuration

### Load unit specifications

Model	318.10	318.25	318.50
Force capacity (maximum)	100 kN (22 kip)	250 kN (55 kip)	500 kN (110 kip)
Available actuator ratings	15, 25, 50, 100 kN (3.3, 5.5, 11, 22 kip)	100, 250 kN (22, 55 kip)	250, 500 kN (55, 100 kip)
Vertical test space* (A)	1308 mm (51.5 in)	1625 mm (64 in)	2108 mm (83 in)
Working height (B)	889 mm (35 in)	889 mm (35 in)	889 mm (35 in)
Column spacing (C)	533 mm (21 in)	635 mm (25 in)	762 mm (30 in)
Column diameter (D)	64 mm (2.5 in)	76 mm (3 in)	102 mm (4 in)
Base width (E)	864 mm (34 in)	1003 mm (39.5 in)	1245 mm (49 in)
Base depth (F)	610 mm (24 in)	762 mm (30 in)	914 mm (36 in)
Diagonal Clearance (G)	2718 mm (107 in)	3251 mm (128 in)	3835 mm (151 in)
Overall Height (H)	2540 mm (100 in)	3023 mm (119 in)	3581 mm (141 in)
Stiffness†	2.6 x 10 <sup>8</sup> N/m (1.5 x 10 <sup>6</sup> lb/in)	4.3 x 10 <sup>8</sup> N/m (2.4 x 10 <sup>6</sup> lb/in)	7.5 x 10 <sup>8</sup> N/m (4.3 x 10 <sup>6</sup> lb/in)
Weight	500 kg (1100 lb)	910 kg (2000 lb)	1770 kg (3900 lb)

\*Test space is the maximum distance between the load cell and the actuator with the actuator fully retracted.

Optional extended height versions available, add 300 mm (12 inches) to pertinent dimensions.

†Determined at each load unit's full fatigue rating with its crosshead raised 1270 mm (50 in.) above the base plate.

Figure C- 9: Tech Specs, Instron

“The fixture used is a two-rail fixture. Each half of the fixture contains a side rail and two gripping plates that have a high coefficient of friction on the gripping surface. Three bolts apply pressure to each gripping plate to secure the specimen during loading. The fixture is loaded in tension. Spacer blocks, can be used to maintain specimen alignment when installing in the fixture halves.”

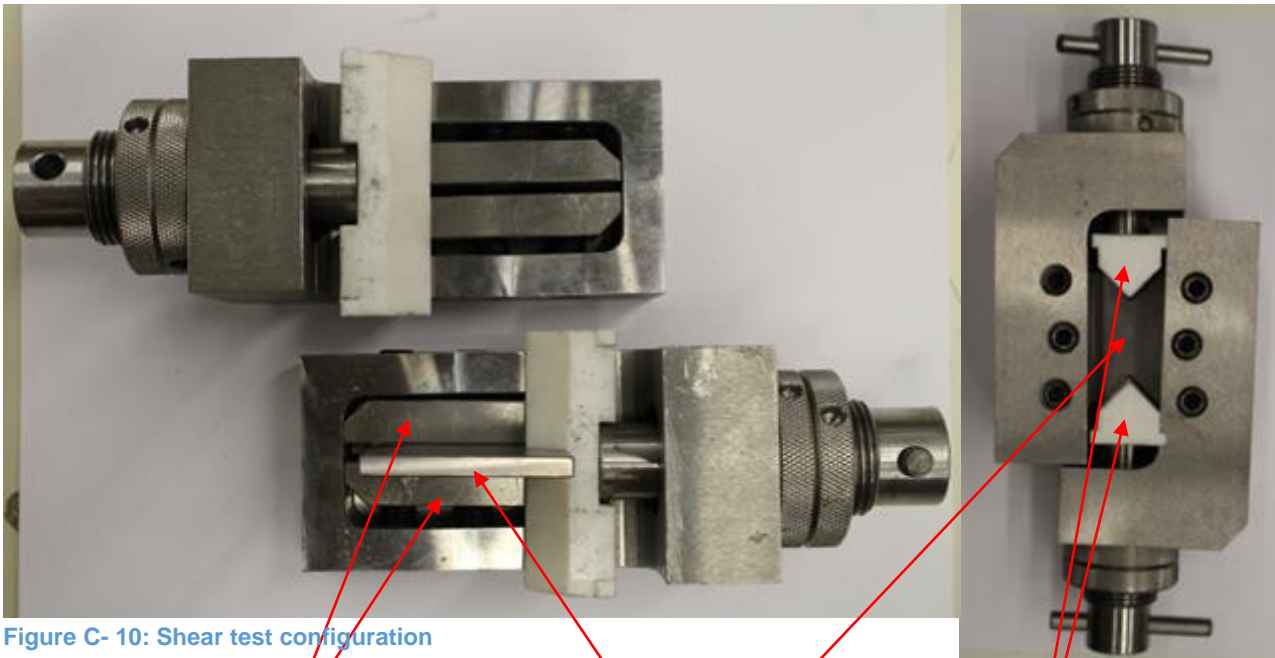


Figure C- 10: Shear test configuration

Gripping Plates

Specimen

Spacers

In general, you can also find additional information in the following link.

<http://www.wyomingtestfixtures.com/Products/a2.html> (LV: 07/02/2018)

# Appendix D

Confidential. Contact: Joep Broekhuisjen ([J.Broekhuijsen@damennaval.com](mailto:J.Broekhuijsen@damennaval.com))

# Appendix E



Figure E-1: Broken tensile coupons, fibers at 0°, Top view



Figure E-2: Broken tensile coupons, fibers at 0°, Side view



Figure E-3: Broken tensile coupons, fibers at 90°, Top view

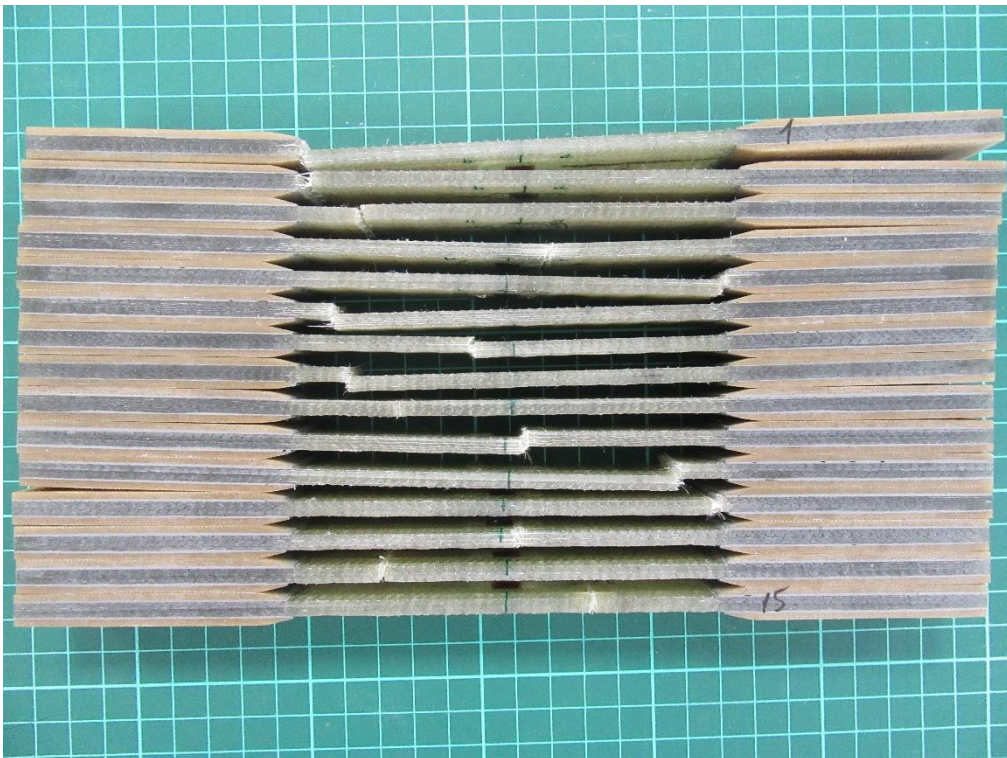


Figure E-4: Broken tensile coupons, fibers at 90°, Side view



Figure E-5: Broken compressive coupons, fibers at 0°, Top view



Figure E-6: Broken compressive coupons, fibers at 0°, Side view

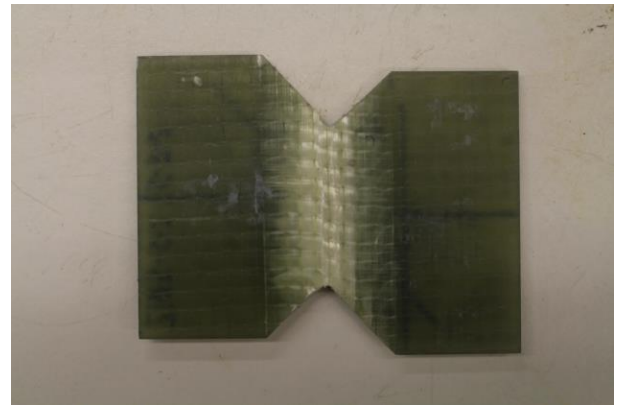
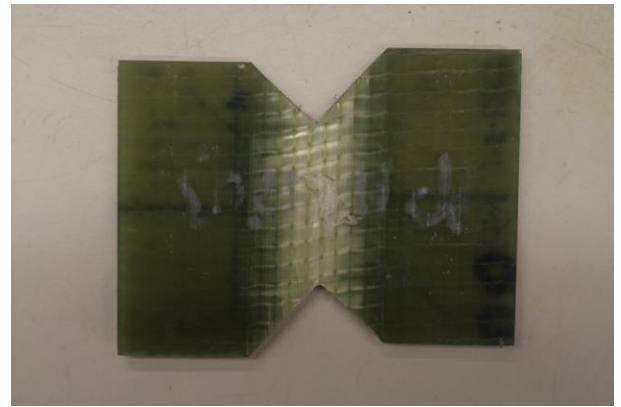


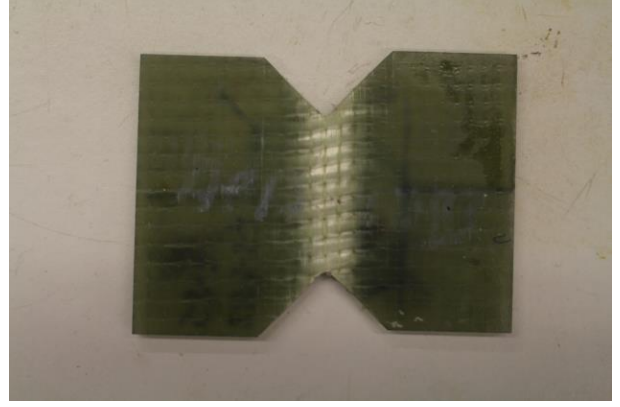
Figure E-7: Broken compressive coupons, fibers at 90°, Top view

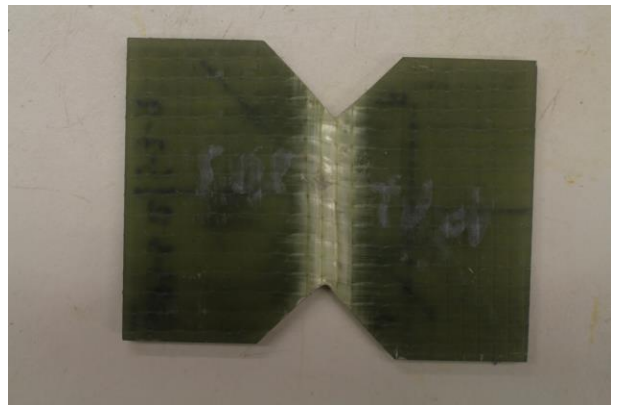
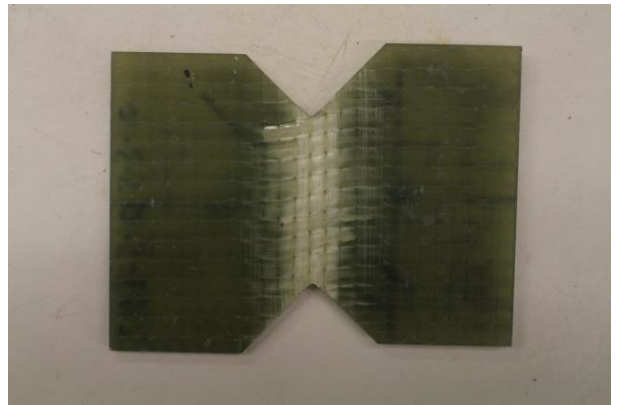


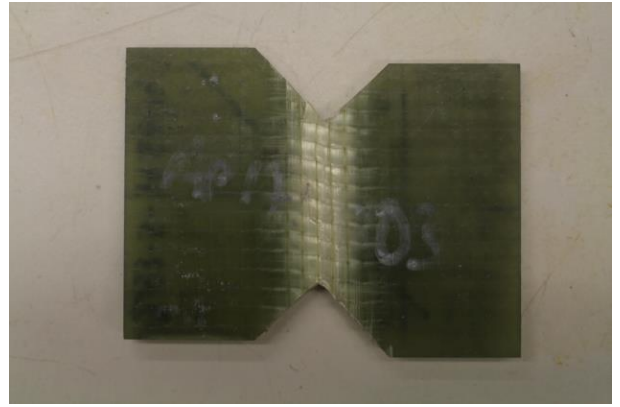
Figure E-8: Broken compressive coupons, fibers at 90°, Top view

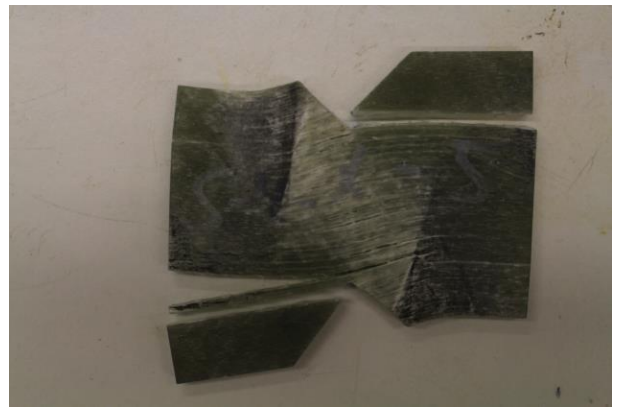
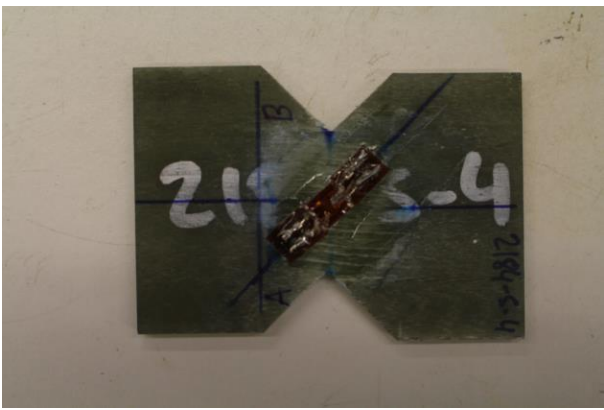
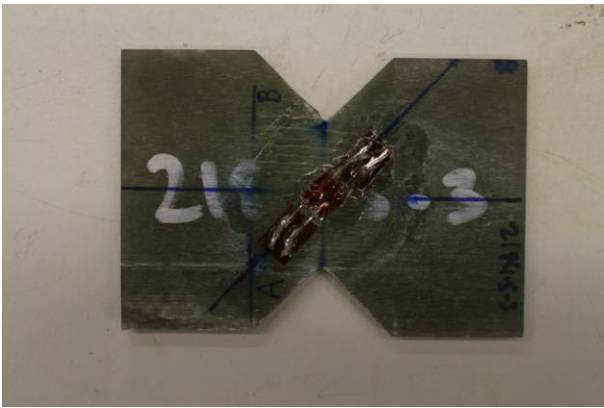
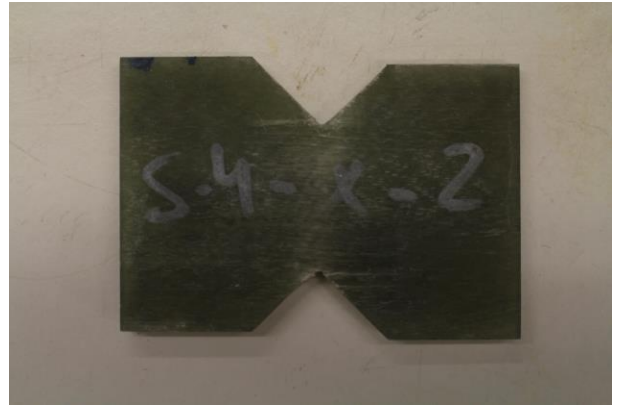
Figure E-9: Broken Shear Coupons

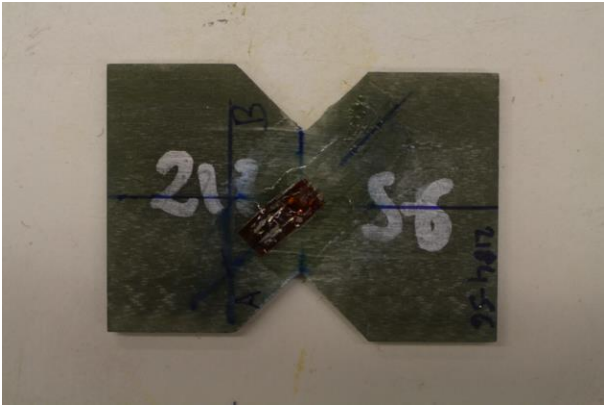


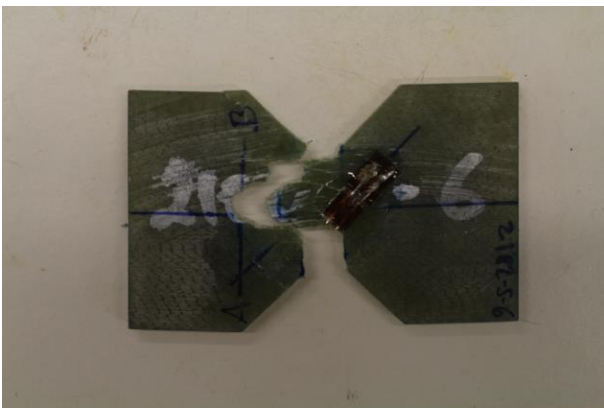
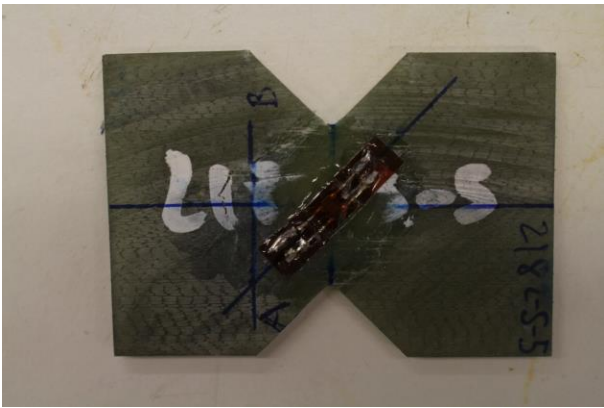
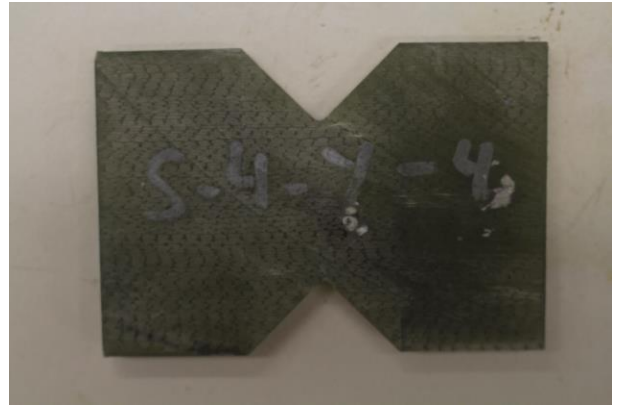












# Appendix F

Confidential. Contact: Joep Broekhuisjen ([J.Broekhuijsen@damennaval.com](mailto:J.Broekhuijsen@damennaval.com))

# Appendix G

Confidential. Contact: Joep Broekhuisjen ([J.Broekhuijsen@damennaval.com](mailto:J.Broekhuijsen@damennaval.com))

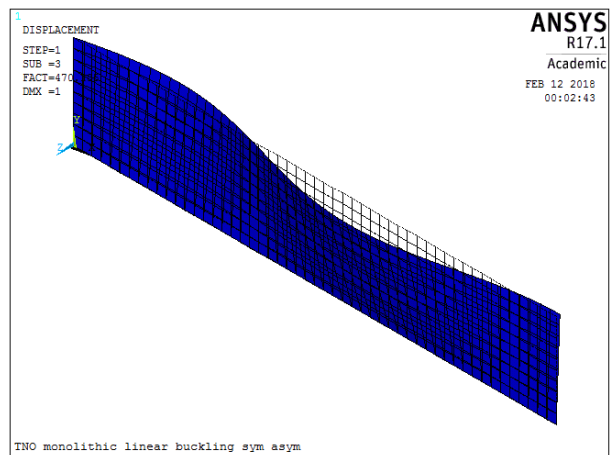
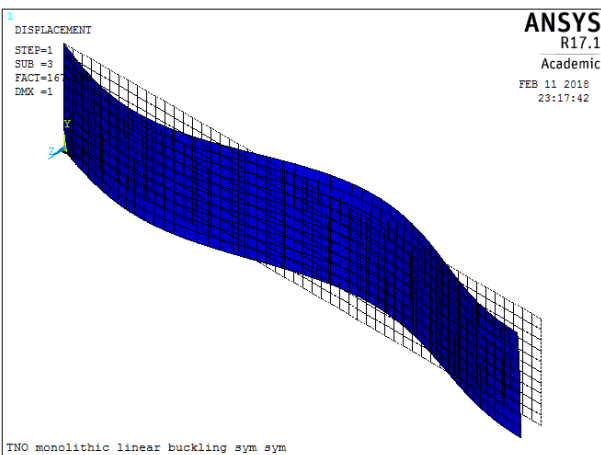
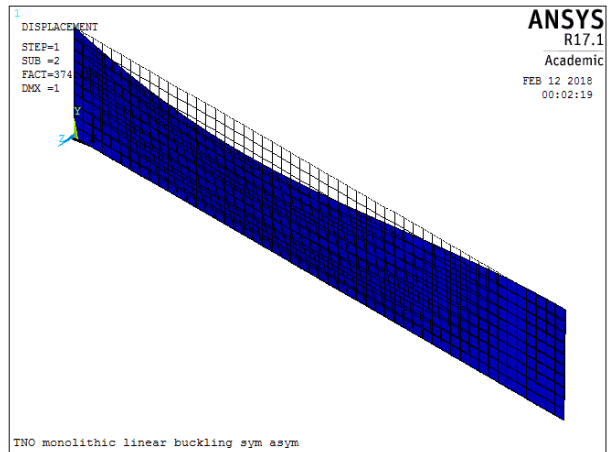
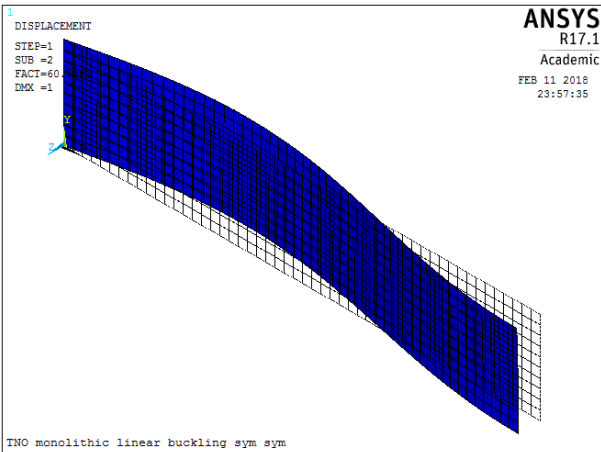
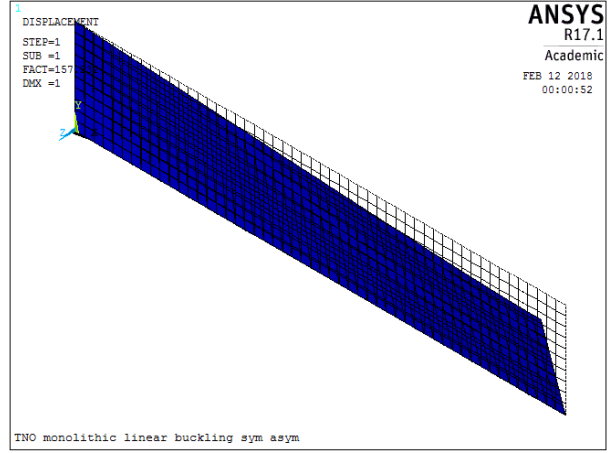
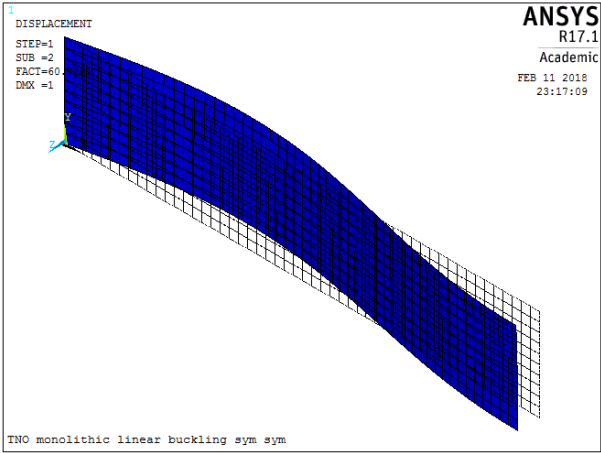
# Appendix H

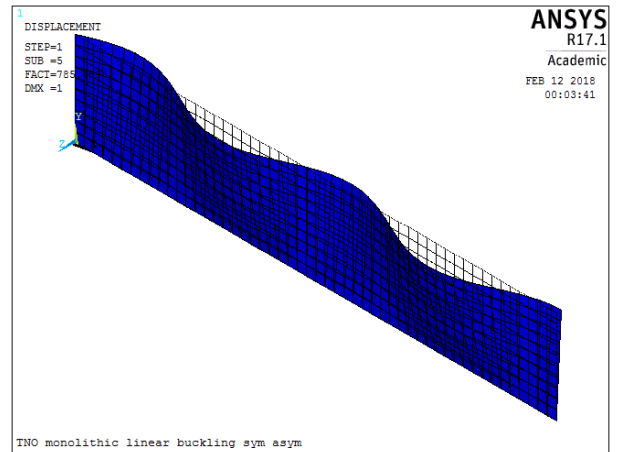
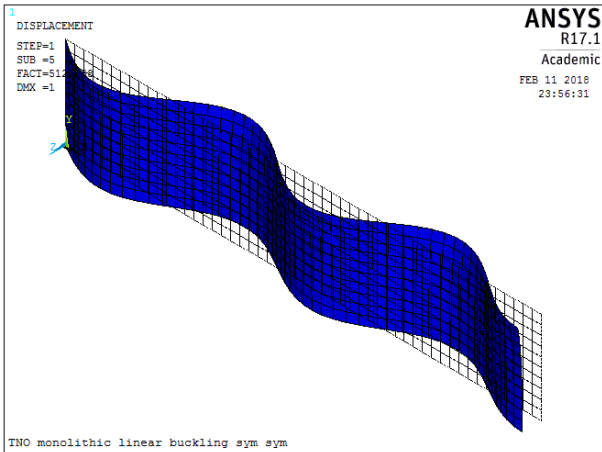
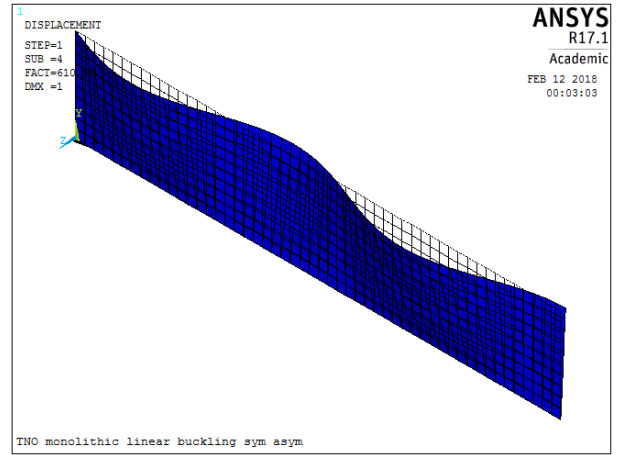
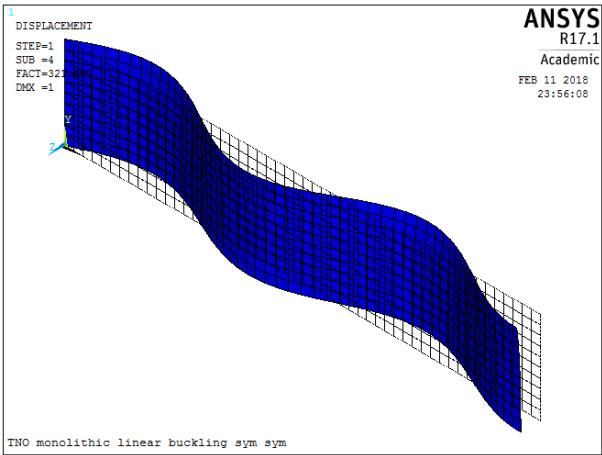
Confidential. Contact: Joep Broekhuisjen ([J.Broekhuijsen@damennaval.com](mailto:J.Broekhuijsen@damennaval.com))

# Appendix I

Case 1 (figure 4-3)

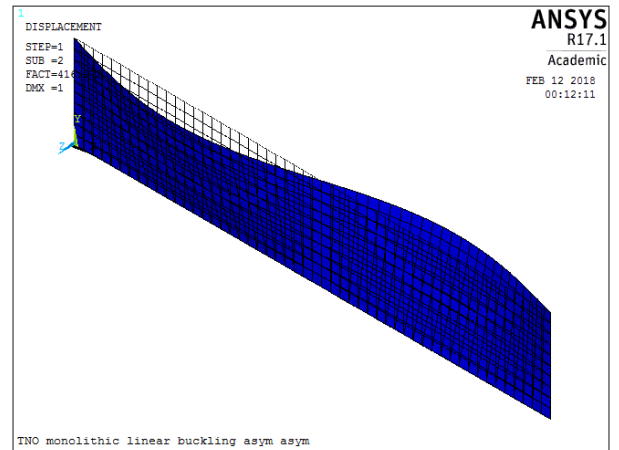
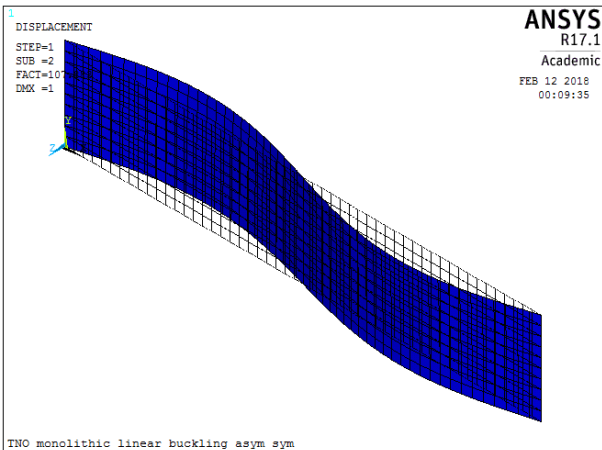
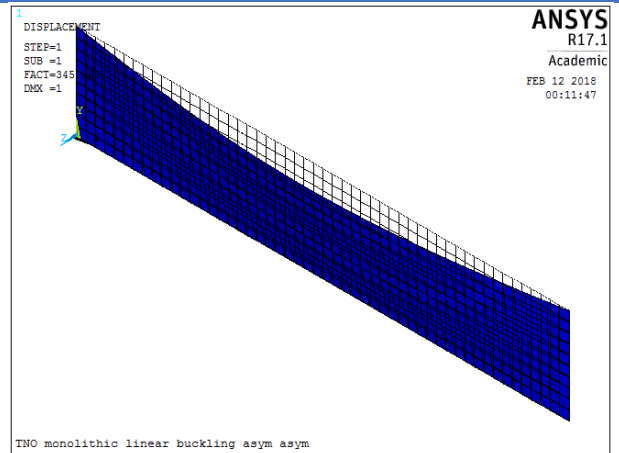
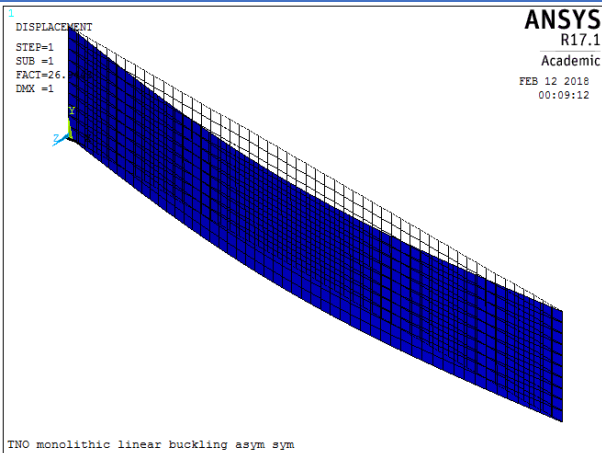
Case 2 (figure 4-3)

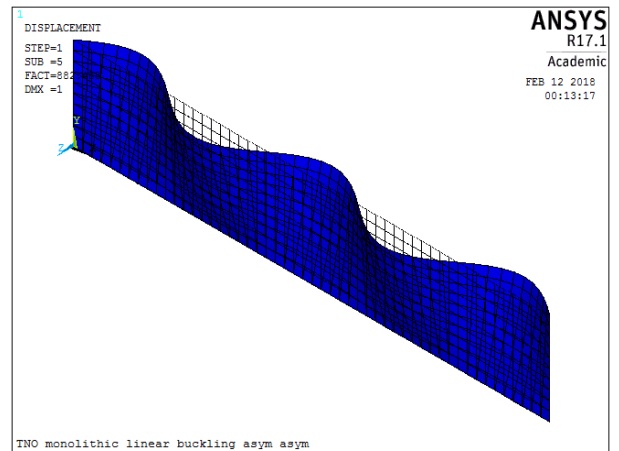
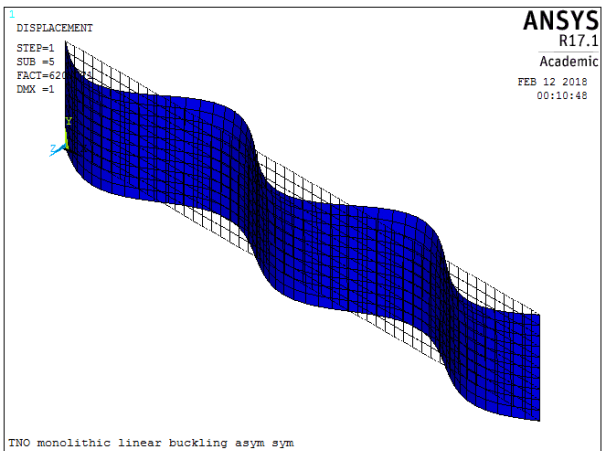
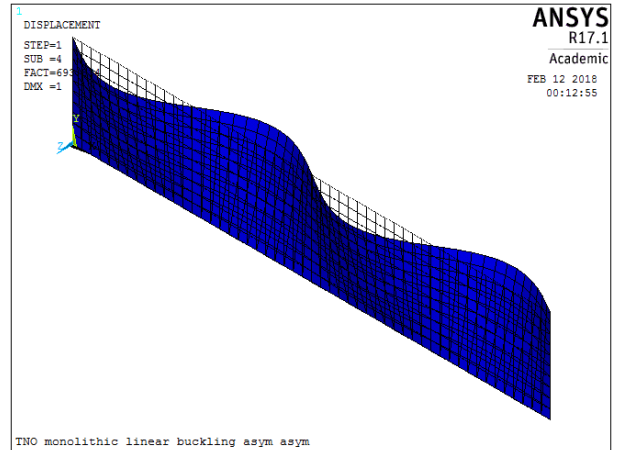
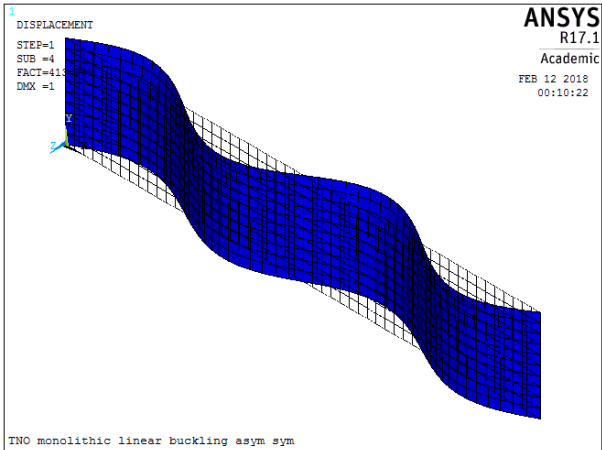
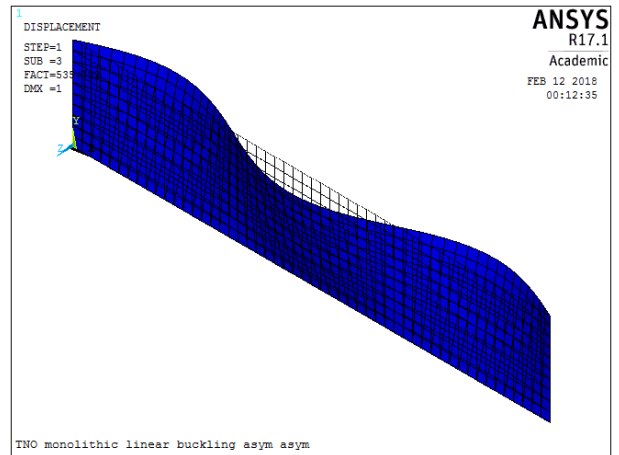
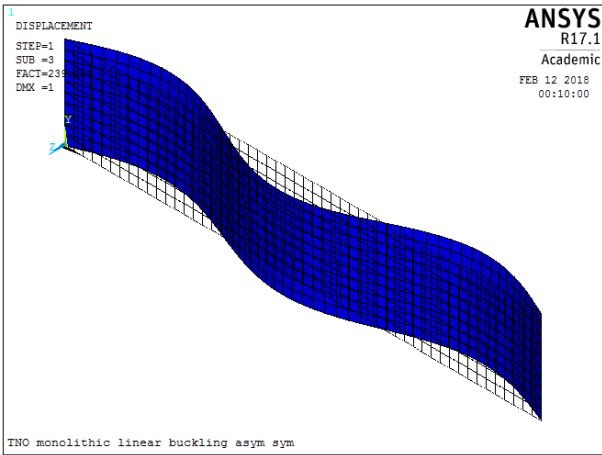




Case 3 (figure 4-3)

Case 4 (figure 4-3)





Confidential. Contact: Joep Broekhuisen ([J.Broekhuisen@damennaval.com](mailto:J.Broekhuisen@damennaval.com))

Appendix I- 1: Measured dimensions at various locations for monolithic panels

# Appendix K

Confidential. Contact: Joep Broekhuisjen ([J.Broekhuijsen@damennaval.com](mailto:J.Broekhuijsen@damennaval.com))

# Appendix IDM-A

Confidential. Contact: Joep Broekhuisjen ([J.Broekhuijsen@damennaval.com](mailto:J.Broekhuijsen@damennaval.com))

# Effect of stochastic material properties on the structural response of laminated composite materials

following the building block approach  
(supporting document)



Athanasios Droutsas



# Effect of stochastic material properties on the structural response of laminated composite materials

following the building block approach  
(supporting document)

By

Athanasios Droutsas

in partial fulfilment of the requirements for the degree of

**Master of Science**

in Offshore & Dredging Engineering

at the Delft University of Technology,  
to be defended publicly on February 15, 2018 at 11:00 AM.

Supervisor:	Prof. dr. ir. M. Kaminski	TU Delft
Thesis committee:	Dr. D.Zarouchas,	TU Delft
	Dr.P.Maljaars	TU Delft
	Dr. D. Schraven,	TU Delft
	Ir. J. Broekhuijsen,	Damen Schelde Naval Shipbuilding

*This version of the thesis is not confidential..*



# Preface

The version of the thesis' supporting document below is the non-confidential one. The initial, confidential version contained sensitive information regarding the materials used for the construction of the hull of Mine Counter Measure Vessels and as a result some information has to be omitted. For values shown as *XX* please contact Joep Broekhuijsen (J.Broekhuijsen@damennaval.com) . However, this thesis contains all the parts of the initial document that have an added academic value.

The main reason behind the preparation of this report is to support whatever has been implemented and presented at the main body of the thesis. It provides the academic background of all the methods used while extensive explanation is given in terms of steps that have to be followed accompanied with examples. In the main body of the thesis, the writer's contribution to academics is depicted; there, many theories/techniques are used that are product of the literature study which has been implemented from the writer. This supporting document explains these theories in order to make readers familiar with certain topics in case they are interested to validate the results shown in the main body of the thesis.

*A. Droutsas Author  
Delft, January 2017*



# Contents

Preface .....	i
Contents .....	iii
List of Figures .....	iv
List of Tables .....	v
Nomenclature .....	vii
Abstract .....	x
Chapter 1: Introduction.....	1
1.1 Necessity of MCMVs to this date .....	1
1.1.1 Danger of sea mines to this day.....	2
1.1.2 MCMV Project.....	2
1.2 Glass-based fibres .....	4
1.3 Matrix.....	5
1.4 Building Block Approach .....	7
1.4.1 Group A: Material property development.....	8
1.4.2 Group B: design-value development .....	10
1.5 References .....	11
Chapter 2: Small Scale Coupons .....	13
2.1 Tensile Tests .....	13
2.1.1 FEA Model for tensile tests .....	17
2.2 Compressive tests .....	23
2.2.1 FEA models for compressive tests.....	27
2.3 Shear tests.....	32
2.4 Fibre volume and density tests.....	37
2.5 Out-of-plane Poisson's ratios .....	37
2.6 References .....	44
Chapter 3: Statistics.....	47
3.1 Chosen distributions .....	47
3.1.1 Normal Distribution .....	47
3.1.2 Gamma ( $\Gamma$ ) distribution .....	49
3.1.3 Log-normal distribution .....	50
3.1.4 Weibull Distribution .....	51
3.1.5 Nakagami distribution .....	52
3.1.6 Logistic .....	53
3.1.7 Rician: .....	53
3.1.8 Extreme value distributions .....	55
3.2 Maximum likelihood estimates .....	55
3.2.1 Loglikelihood.....	57
3.3 Kolmogorov-Smirnov criterion .....	59
3.4 Generate correlated random variables .....	62
3.4.1 1 <sup>st</sup> step: Latin Hypercube Sampling.....	64
3.4.2 Correlate the uncorrelated variables – Cholesky's Transformation.....	66
3.4.3 Create Input for Ansys .....	68

3.5 Bootstrap Method.....	70
3.6 References .....	72
Chapter 4: Mechanics .....	75
4.1 Macromechanics of Laminae .....	75
4.2 Classical Lamination Theory .....	85
4.3 Failure Criteria .....	95
4.3.1 Maximum stress criterion .....	95
4.3.2 Puck failure criterion .....	96
4.3.3 Hashin failure criterion .....	99
4.4 Progressive damage modelling .....	100
4.5 References .....	103
Appendix A .....	105

## List of Figures

Figure 1-1: Zr. Ms. Schiedam, Alkmaar Class, in water since: 1986, old concept.....	3
Figure 1-2: Body plan of the new MCMV concept <sup>[20]</sup> .....	3
Figure 1-3: Transfer of stresses through the matrix <sup>[1]</sup> .....	6
Figure 1-4: Phases of composite material <sup>[14]</sup> .....	6
Figure 1-5: Building block Integration <sup>[16]</sup> .....	7
Figure 1-6: Building Block Approach <sup>[16]</sup> .....	8
Figure 2-1: Coupon for tensile test (0°) .....	14
Figure 2-2: Coupon for tensile test (90°) .....	15
Figure 2-3:h-refinement <sup>[11]</sup> .....	17
Figure 2-4: Tensile coupons geometry.....	18
Figure 2-5:Plane183 Geometry <sup>[5]</sup> .....	18
Figure 2-6: Boundary Conditions, Tensile test model.....	21
Figure 2-7: Displaced and undisplaced model, Tab-end, coupon connection .....	22
Figure 2-8: Shear stresses at the adhesive layer .....	22
Figure 2-9: characteristic shear response of Hysol EA 9394 paste adhesive with respect to the environment <sup>[12]</sup> .....	23
Figure 2-10: Shear stresses at the area of interest .....	23
Figure 2-11: Normal Stresses $\sigma_x$ at the area of interest .....	23
Figure 2-12: Coupon for compressive test (0°).....	25
Figure 2-13: Coupon for compressive test (90°).....	26
Figure 2-14: Geometry of compressive coupon, Top view .....	27
Figure 2-15: Element formulation of compressive coupon <sup>[5]</sup> .....	28
Figure 2-16: Definition of Lay-Up sequence, Ansys .....	28
Figure 2-17: Boundary Conditions, Compressive test model .....	30

Figure 2-18: Loading pattern of the compressive coupon .....	30
Figure 2-19: Elastic buckling, 1 <sup>st</sup> mode's vertical displacement field .....	31
Figure 2-20: Force-displacement diagram, Compressive test with various imperfections .....	32
Figure 2-21: V-Notched Rail Shear Test Specimen Schematic <sup>[10 §4.1]</sup> .....	33
Figure 2-22 Shear coupon test at 1-2 plane .....	34
Figure 2-23: Shear coupon test at 1-3 plane .....	35
Figure 2-24: Shear coupon test at 2-3 plane .....	36
Figure 2-25 Panel with fibers at 0°. Produced by KVE .....	38
Figure 2-26 Panel with fibers at 90°. Produced by KVE .....	39
Figure 2-27 Panel with fibers at 0°/90°. Produced by KVE .....	40
Figure 2-28 Thick panel with fibers at 0°. Produced by KVE .....	41
Figure 2-29 Panel with fibers at ±45°. Produced by KVE for the tabs used in tensile tests .....	42
Figure 2-30: Panel with fibers at 0°/90°. Produced by KVE for the tabs used in compressive tests .....	43
Figure 3-1: Empirical Rule for normal distribution <sup>[15]</sup> .....	48
Figure 3-2 Approximating the probability that X lies $\varepsilon$ -close to $\alpha$ <sup>[13 § 5.1]</sup> .....	56
Figure 3-3: Kolmogorov-Smirnov test statistic, $D$ .....	60
Figure 3-4: Sampling of two variables, 10 realizations .....	64
Figure 3-5: Sampling of two variables, 500 realizations .....	64
Figure 3-6: Sampling with LHS(left) and MCS(right) .....	65
Figure 3-7: Histogram, mean values from Bootstrap samples, example .....	71
Figure 4-1: A lamina with its material coordinate system <sup>[2]</sup> .....	75
Figure 4-2: Generally Orthotropic Lamina .....	76
Figure 4-3: Lamina with arbitrary fiber orientation, axially loaded .....	82
Figure 4-4: Kirchhoff's Hypothesis <sup>[7]</sup> .....	86
Figure 4-5: Kinematics of deformation as viewed in the " $x$ " – " $z$ " plane <sup>[7]</sup> .....	86
Figure 4-6: Variation of ply stresses and strains through the laminate thickness <sup>[8]</sup> .....	89
Figure 4-7: Element of single layer (lamina) with force and moment resultants <sup>[6]</sup> .....	90
Figure 4-8: Multidirectional laminate with coordinate notation of individual plies <sup>[6]</sup> .....	92
Figure 4-9: Three-dimensional stresses on a UD composite element <sup>[18]</sup> .....	97
Figure 4-10: ( $\sigma_2, \tau_{21}$ ) fracture curve for $\sigma_1 = 0$ , representing three different fracture modes A, B, C <sup>[18]</sup> . The curve is generated by two ellipses and one parabola .....	97

## List of Tables

Table 1-1: Mine warfare in two World Wars .....	2
Table 1-2: Main properties of the new MCMV concept .....	3

Table 1-3: Composition of commercial glass fibers ..... 4

Table 1-4: Physical Properties ..... 5

Table 1-5: Mechanical properties of commercial glass fibers ..... 5

Table 1-6: Typical Clear Casting properties at 23 °C, XX<sup>[20]</sup> ..... 6

Table 2-1: Modelled material properties in Ansys, tensile tests ..... 20

Table 2-2: Modelled material properties in Ansys, compressive tests ..... 29

Table 3-1: Expected results from Maximum likelihood method ..... 58

Table 3-2: Explanation of material properties' symbols ..... 59

Table 3-3: Results from Kolmogorov-Smirnov criterion, Distributions that best fit each material property ..... 63

Table 3-4: Results from LHS, *n* = 500 in our case ..... 66

Table 3-5: Uncorrelated variables that are normally distributed ..... 66

Table 3-6: Correlated variables that follow the standard normal distribution ..... 68

Table 3-7: Input for FEA model ..... 69

Table 3-8: Bootstrap Samples, example ..... 71

# Nomenclature

$A_{ij}$	Extensional stiffness matrix
ASM	American Society for Metals
ASTM	American Society for Testing and Materials
$B_{ij}$	Axial-Bending coupling stiffness matrix
cdf	cumulative density function
CLT	Classical Lamination Theory
$D_{ij}$	Bending stiffness matrix
DSNS	Damen Schelde Naval Shipbuilding
FAW	Fiber Arial weight
FEA	Finite Element Analysis
$G_{12}$	Shear Modulus in “1”, “2” plane
$G_{23}$	Shear Modulus in “2”, “3” plane
$G_{13}$	Shear Modulus in “1”, “3” plane
GRP	Glass reinforced polymers
icdf	Inverse cumulative function
IED	Improvised Explosive Device
LV	Last visited(references)
pdf	Probability density function
WWI	First World War (the Great War)
WWII	Second World War

## Greek Letters

$\gamma_{12}$	Engineering shear strain in the “1” , “2” plane
$\gamma_{23}$	Engineering shear strain in the “2” , “3” plane
$\gamma_{13}$	Engineering shear strain in the “1” , “3” plane
$\gamma_{xy}$	Engineering shear strain in the “x” , “y” plane
$\gamma_{yz}$	Engineering shear strain in the “y” , “z” plane
$\gamma_{xz}$	Engineering shear strain in the “x” , “z” plane
$\varepsilon_1$	Axial Strain at principal (“1”) direction
$\varepsilon_2$	Transverse Strain, lateral to principal (“2”) direction
$\varepsilon_3$	Strain at the vertical (“3”) direction
$\varepsilon_{12}$	Tensor shear strain in the “1” , “2” plane
$\varepsilon_{23}$	Tensor shear strain in the “2” , “3” plane
$\varepsilon_{13}$	Tensor shear strain in the “1” , “3” plane
$\varepsilon_{xy}$	Tensor shear strain in the “x” , “y” plane
$\varepsilon_{yz}$	Tensor shear strain in the “y” , “z” plane
$\varepsilon_{xz}$	Tensor shear strain in the “x” , “z” plane
$E_1$	Elastic modulus in the “1”-direction, (Axial)
$E_2$	Elastic modulus in the “2”-direction, (Transverse)
$E_3$	Elastic modulus in the “3”-direction, (Vertical)
$\nu_{12}$	Poisson’s ratio for transverse strain in “2” direction when stresses in the “1” direction
$\nu_{23}$	Poisson’s ratio for transverse strain in “3” direction when stresses in the “2” direction
$\nu_{13}$	Poisson’s ratio for transverse strain in “3” direction when stresses in the “1” direction
$\sigma_1$	Normal stress in the “1” direction

$\sigma_2$	Normal stress in the “2” direction
$\sigma_3$	Normal stress in the “3” direction
$\sigma_x$	Normal stress in the “x” direction, (Axial)
$\sigma_y$	Normal stress in the “y” direction, (Transverse)
$\sigma_z$	Normal stress in the “z” direction, (Vertical)
$\tau_{12}$	Shear stress in the “1” , “2” plane
$\tau_{23}$	Shear stress in the “2” , “3” plane
$\tau_{13}$	Shear stress in the “1” , “3” plane
$\tau_{xy}$	Shear stress in the “x” , “y” plane
$\tau_{yz}$	Shear stress in the “y” , “z” plane
$\tau_{xz}$	Shear stress in the “x” , “z” plane

# Abstract

In the main body of the thesis it is usual to encounter results based on specific theories/methods/techniques that are not explained. That was done on purpose in order to keep it simple and easily readable.

This document comes to cover this gap by explaining in detail the methods that were used. If a reader is not familiar with a specific theory that is presented in the main body of the thesis, he can easily refer to the respective (sub)chapter of this document and get the academic background of what was implemented. With such a combination, the main body answers the “what is done” question whereas this supporting document answers to “how it is done”.

At chapter 1(introduction), one can find briefly why this project is initiated at how it will be implement. Hence, at the start, a brief history of mine warfare is depicted in order to prove the necessity of having up to date MCMVs (Mine Counter Measure Vessels). Then, an explanation is given to why this specific combination of fibers and matrix is opted along with general information about these two parts of the laminated composite. Finally, the method at which the whole thesis is based upon, i.e. “*the building block approach*” is explained. This method shows how one can start a structural analysis by taking experimental results from small scale coupon tests and extrapolate them in order to design large scale components.

At chapter 2, the small scale coupons are analyzed. They are made of glass fibers ( $XX \text{ g/m}^2$ ) with XX resin and a fibre volume  $V_f = XX\%$ . The philosophy behind their design is presented along with two finite element models which are used to check if unwanted failure modes will be avoided. The experiments include the testing of 15 coupons in tension and compression in both  $0^\circ/90^\circ$  fibre direction as well as 15 in plane shear tests. Furthermore, 6 specimens were tested in out-of-plane shear for each of the 1 – 3 and 2 – 3 planes. The experimental results are shown at the main body of the thesis.

At chapter 3, the statistical analysis of the experimental results is being performed. Out of a family of chosen distributions, one is assigned to each one of the strength and stiffness properties, which best fits the experimental data. Further analysis shows the correlation (if any) of these properties and an algorithm is presented which generates correlated random variables which follow the same or different distributions.

At chapter 4, the academic background of the composites’ mechanics is explained. By starting in a lamina level, the mechanics of a structure made of fibers embedded in a matrix is depicted and then it is extrapolated to a composite laminate according to Classical Lamination Theory. Basically, this chapter presents the elementary theory of the composite laminates that has to be known prior to any structural analysis of a composite structure. Towards the end of the chapter, the failure criteria that were used in this thesis are presented along with their progressive damage model.

# Chapter 1: Introduction

Every structure around us, either natural or human-made, has materials as its basic constituents. Regardless the industry, any idea for a potential structure will be always bound to the available materials. New challenges appear endlessly which require high performance structures and these structures in turn, require the development of new materials or the improvement of the existing ones.

Approximately in mid-20<sup>th</sup> century, a new class of promising materials made its appearance which were (and still are) called composite materials. When two materials with distinct properties are combined in order to form a new one, the latter is called a composite material. In our case and throughout the whole thesis, the material that is analyzed, is a laminate composite which is made of XX fibers embedded in a XX resin. According to R. M. Jones<sup>[1, §4.1]</sup>, “a laminate is two or more laminae bonded together to act as an integral structural element” and from the same reference, “a lamina is a flat (sometimes curved as in a shell) arrangement of unidirectional fibers in a matrix”.

Since the mid-20<sup>th</sup> century laminated composite materials were used in several applications due to their attractive properties. Their advantages are plenty from which the most remarkably mentioned are the lower resultant total weight, the corrosion resistance, the high strength/stiffness to weight ratio and the lower life cycle cost when comparing with their steel counterparts<sup>[2]</sup>. Their wear resistance along with their thermal and acoustical insulation, qualified them as possible structural material to even more applications.

Regarding their usage for Mine Countermeasure Vessels(MCMVs), composite materials can additionally provide reduced electrical and infrared (thermal) signature, reduced radar cross section and when used for the propeller shafts, they can also provide noise suppression due to the inherent dampening properties of composite materials<sup>[3]</sup>. However, their most attractive characteristic, is their low magnetic signal which basically turns the MCMVs invisible to the magnetic mines. Before the constituents of the laminated composites are analyzed, a brief explanation about the MCMV project is being given below in order to prove its necessity and present the bigger picture behind this thesis.

## 1.1 Necessity of MCMVs to this date

Frequently, when engineers are assigned to a project, they tend to focus only on the technical details and they overlook what the ultimate aim is. The following two subchapters intend to present what was the main reason behind the initiation of this thesis and where this research will have an impact upon. Readers that are not interested in this part can continue [here](#).

### 1.1.1 Danger of sea mines to this day

According to Encyclopedia Britannica<sup>[4]</sup> “A submarine mine is an underwater weapon consisting of an explosive charge fitted with a device that causes it to explode when a ship or submarine enters into close proximity”. However, according to Robert C. Duncan<sup>[5]</sup>: “The sea mine is a weapon which lies in wait for its victim. Planted under the surface of the water, possibly hidden in the mud and sand on the bottom, it may remain there for weeks or months until a vessel comes to its lethal range” and according to Admiral Thad Allen (USCG Commandant, U.S. Coast Guard) in August 2007<sup>[6]</sup>: “What keeps me up at night? The threat of water-borne IEDs” further prove that sea mines are still assumed to be a real headache for the naval officers.

To quantify the above statements, we have to use some historical data. Since the invention of Bushnell's mine<sup>[7]</sup> (named after the inventor) in 1776, sea mines have been used to all major conflicts. In many cases the amount of ships that were sunk by mines was much greater than all the other means combined including torpedoes, bombs, submarines and surface ships<sup>[8],[9]</sup>. In table [1-1] their effectiveness is presented:

Table 1-1: Mine warfare in two World Wars

	Total Mines Laid	Offensive Mines Laid	Ships Lost	Offensive Mines Laid per Ship Lost
WW I	240000	45000 <sup>a</sup>	630 <sup>b</sup>	71
WW II	300000 <sup>c</sup>	100000 <sup>c</sup>	2665 <sup>d</sup>	37

- a. Central Powers Only
- b. Allied Losses
- c. U.S. and U.K. Only
- d. Japanese and Axis Powers Only

Even if we tend to think mines as something rusty and obsolete, it doesn't mean that they are not a threat today. On the contrary, even old mines can significantly harm a modern ship as was the case in 1980s where a 96 million \$ US ship was almost sunk by a 1,500 \$ mine based on a design of 1908<sup>[6]</sup>. If someone adds today's technology, mines are even more deadly and more undetectable. New counter-countermeasure techniques render mine hunting an even more difficult procedure and as a result we have a constant “battle” between mines and countermeasure technological progress.

### 1.1.2 MCMV Project

Up to this point, it should have been made clear that mines played and continue to play an important role at the naval strategic planning and their influence at the major fights since their invention can be assumed critical. Countries developed methods to counter this threat by creating minehunter and minesweeper vessels which use both passive and active countermeasures. One of the methods to avoid the explosion of the mines is to use composite materials for the hull of the MCMVs. This would make them invisible to magnetic mines because the magnetic field of the vessels will be almost eliminated. For that reason, research is being done for the development of vessels which can serve both as minehunters and minesweepers.

Currently, the capability of the Royal Netherlands Navy regarding minehunters relies mostly at the Tripartite Class (Alkmaar Class). According to Ref. [10], the name “Tripartite” was given to this class because it is the

product of collaboration between three countries, namely France, Belgium and the Netherlands. The first polyester minehunter vessel of this class was commissioned at the beginning of 1984 and the last one in 1989<sup>[11]</sup> resulting to a total force of 15 vessels at the end of the same year. However, today only 6 vessels are remaining. For that reason, DSNS is preparing for a potential request from the Royal Netherlands Navy for a new, modern class of mine countermeasure vessels that can serve as both minehunter and minesweeper vessel. At fig. [1-1] a vessel from the Alkmaar Class is depicted while at fig. [1-2] some concepts for the body plan of the new class are presented. Finally, at table [1-2], the main properties of the new class are shown.



Figure 1-1: Zr. Ms. Schiedam, Alkmaar Class, in water since: 1986, old concept

Table 1-2: Main properties of the new MCMV concept

Property	Symbol	Value
Length over all	$L_{oa}$	$XX\ m$
Length between perpendiculars	$L_{pp}$	$XX\ m$
Breadth	$B$	$XX\ m$
Depth	$D$	$XX\ m$
Summer Draft	$T$	$XX\ m$
Block coefficient	$C_b$	$XX$
Design Speed	$V_{max}$	$XX\ kn$

Confidential. Contact: [J.Broekhuijsen@damennaval.com](mailto:J.Broekhuijsen@damennaval.com)

Figure 1-2: Body plan of the new MCMV concept

## 1.2 Glass-based fibres

Throughout the whole thesis, a specific combination of fibres and resin was used to form the laminated composites under consideration. For this reason, this subchapter provides some basic information about the XX-fibres which are the load-carrying constituents of the structures being analysed.

Polymer matrix composites are being made from XX fibres in most of the cases. The main reason is that they are relatively cheap when comparing to their counterparts but they can still provide high strength. They also exhibit additional useful properties such as hardness, transparency and resistance to chemical attack among others. Generally, even if they are expected to be lower performing than their graphite counterparts, their low cost has led to their existence in playground equipment, recreational items, piping for corrosive materials and countless other everyday applications.

Silica,  $\text{SiO}_2$ , forms the basis of nearly all commercial glasses and it is appropriate for various industrial applications. Regarding its thermal properties, it decomposes at  $2000\text{ }^\circ\text{C}$  and until this temperature it just softens but it doesn't melt. Its major drawback has to do with the high processing temperatures under which it has to be formed but new types of glass render this procedure easier. Specifically, there are 4 predominant glass compositions; namely, the Type A, a soda lime glass, the type E, a borosilicate glass, the Type C which shows improved durability when exposed to acids and alkalis and Type S which shows increased strength and stiffness (Type S can be 10 times more expensive than E-Glass). This thesis analyses composites made of XX glass fibres and thus, we overlook the rest of the types.

XX-glass fibres come in two types regarding their concentration in boron. The incumbent one comes with 5 – 6 wt% of boron oxide and the second one is boron free. Environmental regulations require the control of off-gases produced by boron containing melts and thus either expensive systems which control the emissions should be used or a boron free XX glass product. The properties of these two types are shown at the tables below:

Table 1-3: Composition of commercial glass fibers

	Composition, wt%												
	$\text{SiO}_2$	$\text{B}_2\text{O}_3$	$\text{Al}_2\text{O}_3$	CaO	MgO	ZnO	$\text{TiO}_2$	$\text{Zr}_2\text{O}_3$	$\text{Na}_2\text{O}$	$\text{K}_2\text{O}$	$\text{Li}_2\text{O}$	$\text{Fe}_2\text{O}_3$	$\text{F}_2$
Boron containing E-glass	52 – 56	4 – 6	12 – 15	21 – 23	0.4 – 4	...	0.2 – 0.5	...	0 – 1	Trace	...	0.2 – 0.4	0.2 – 0.7
Boron free E-glass	60.1	...	13.2	22.1	3.1	...	0.5	...	0.6	0.2	...	0.2	0.1

Table 1-4: Physical Properties

	Log 3 forming temperature, °C	Liquidus temperature, °C	Softening temperature, °C	Annealing temperature, °C	Straining temperature, °C	Bulk density annealed glass, $g/cm^3$
Boron containing E-glass	1160 – 1196	1065 – 1077	830 – 860	657	616	2.54 – 2.55
Boron free E-glass	1260	1200	916	736	691	2.62

Log 3 forming temperature of a melt at a reference viscosity of  $100 Pa \cdot s$

Table 1-5: Mechanical properties of commercial glass fibers

	Coefficient of linear expansion, $10^{-6}/^{\circ}C$	Specific heat, $cal/g/cm$	Dielectric constant at room temperature	Dielectric strength, $kV/cm$	Volume resistivity at room temperature, $\log_{10}(\Omega cm)$	Refractive index, (bulk)	Weight loss in 24 h in 10% $H_2SO_4$	Tensile strength at 23 °C	Young's Modulus, $GPa$	Filament elongation at break, %
Boron containing E-glass	4.9	0.192	5.86 – 6.6	103	22.7 – 28.6	1.547	~ 41	3100 – 3800	76 – 78	4.5 – 4.9
Boron free E-glass	6.0	...	7.0	102	28.1	1.56	~ 6	3100 – 3800	80 – 81	4.6

## 1.3 Matrix

The aforementioned attractive properties of the fibres cannot be fully attained without the use of a binding material, i.e. a matrix. The fibres are bound with a matrix material whose main purpose is to keep the fibres in place, protect them from environmental conditions and give the final shape to the structure. The stiffness of the matrix should correspond to the stiffness of the fibres in order to provide uniform loading to the latter. Generally, fibres show a large scatter in their strength and if someone adds the damage imposed to them by the manufacturing process, it is safe to claim that weak spots at the fibres will be present. However, the fracture of these weak links should not result in a material failure. The matrix which surrounds the fracture spots should redistribute the loads to the neighbouring fibres. Also, the broken fibre will again be loaded after some distance which is depended on the matrix's stiffness. The higher the matrix's stiffness, the smaller the required length to achieve the loading of the neighbouring fibres. For better understating of the mechanism, the following figures 1-3,1-4 are presented. Another important factor to be taken into account is the adhesion between fibres and the matrix. The desired material properties of a laminated composite material can only be achieved if the interface between the fibres and the matrix is made properly. In order to achieve that, the matrix should have such a low viscosity that enables the matrix to flow uniformly between the fibres. but high

enough to retain the liquid matrix in the process of fabrication. Moreover, the fibre surface should have good wettability with the matrix. These are the general aspects applying to every composite material that is made of fibres and resin(matrix). The matrix that was used throughout this thesis is a XX resin and is discussed below.

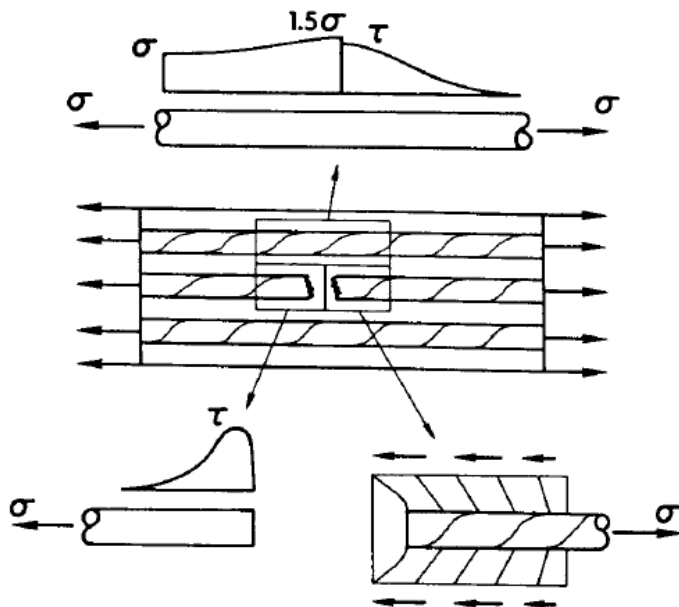


Figure 1-3: Transfer of stresses through the matrix<sup>[1]</sup>

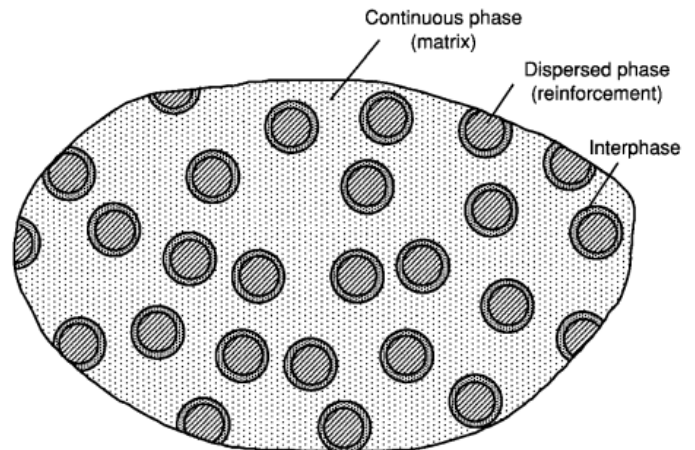


Figure 1-4: Phases of composite material<sup>[14]</sup>

This resin is a thermoset plastic. It has a cross-linked or network structure with covalent bonds between all molecules. When it takes its final form, i.e. by the time that it is solidified, it cannot be reshaped as it does not melt under high temperatures but it just decomposes. For that reason, like the rest of the thermoset resins, it is extremely difficult to recycle; though, there are new companies that extract the fibres through pyrolyzation. The benefits of thermoset resins include: excellent resistance to solvents and corrosives, resistance to heat and high temperature, tailored elasticity and excellent adhesion among others<sup>[15]</sup>. XX combine good mechanical and thermal properties with simple curing and along with their resistance to corrosive environments, they are used extensively to marine applications<sup>[14]</sup>. The typical properties of XX are:

Table 1-6: Typical Clear Casting properties at 23 °C, XX<sup>[20]</sup>

Properties	Unit	Value	Test method
Tensile Strength	MPa	XX	ISO 527-2:2012
Tensile modulus	MPa	XX	ISO 527-2:2012
Tensile elongation	%	XX	ISO 527-2:2012
Flexural Strength	MPa	XX	ISO 78-2010
Flexural modulus	MPa	XX	ISO 78-2010
Heat distortion temperature	°C	XX	ISO 78-2010
Hardness, Barcol 934-1	-	XX	ASTM D 2583-13a
Water Absorption (28 days)	%	XX	ISO 62-1999

## 1.4 Building Block Approach

Engineers opt for composite materials for various applications due to their numerous advantages. But these advantages come with a cost. The presence of at least two distinct materials in a composite structure gives the opportunity to the designer to tailor his designs according to the exact needs of the desired, finished structure. Simultaneously though, the presence of these materials complicate significantly the analysis required before the final design, as many new aspects have to be examined. These aspects can be the behaviour of the composite into the operating environmental conditions, the effect of the geometrical configurations, the different failure modes as well as the deep understanding of the fibres' and resin's behaviour both separately and in contact. The building block approach is a method which aims to fully comprehend the behaviour of a structure made by composites and it is based on the philosophy that if the structural response cannot be accurately predicted, it is not really understood.

The building block approach suggests to build this knowledge step by step; it starts by analysing some simple, basic structural elements and the knowledge derived from them is used for the next step which refers to a detail or a sub-component. According to the complexity of the final structure, the amount of steps is determined and at the end, the full-scale structure is analysed, if it is economically feasible, or large components of it. Each one of these steps, which will be called building blocks from now and onwards, are integrated with supporting technologies and design considerations as it is shown in figure 1-5.

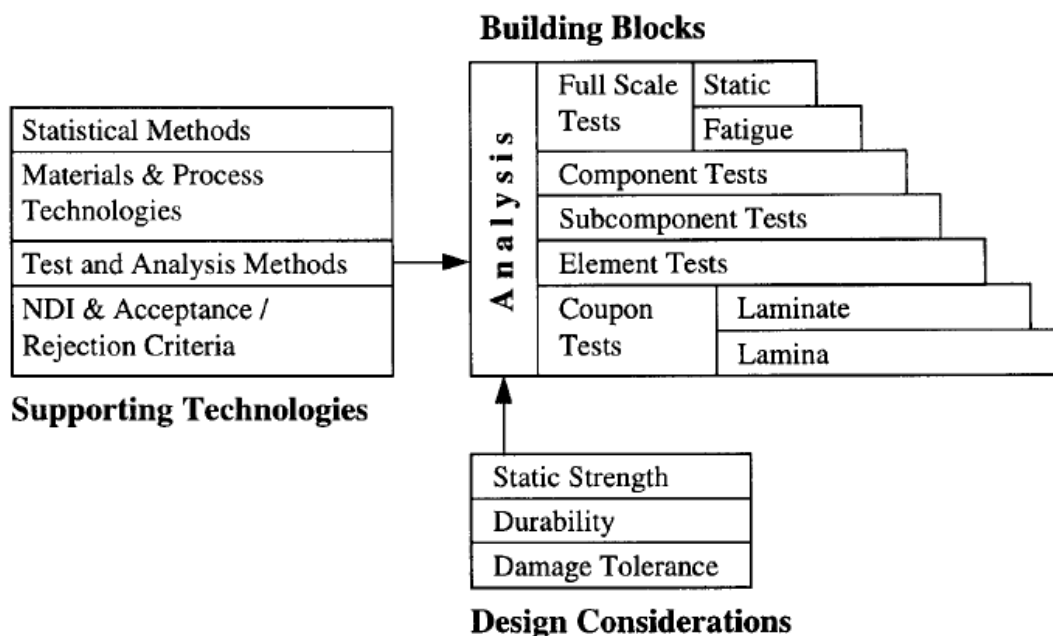


Figure 1-5: Building block Integration<sup>[16]</sup>

*Note:* The implementation of an analysis for the whole building block approach that is presented above, refers to much bigger projects than a master thesis and as result certain parts are analysed here and not the full testing plan.

Another way to present the building block approach is shown below in figure 1-6.

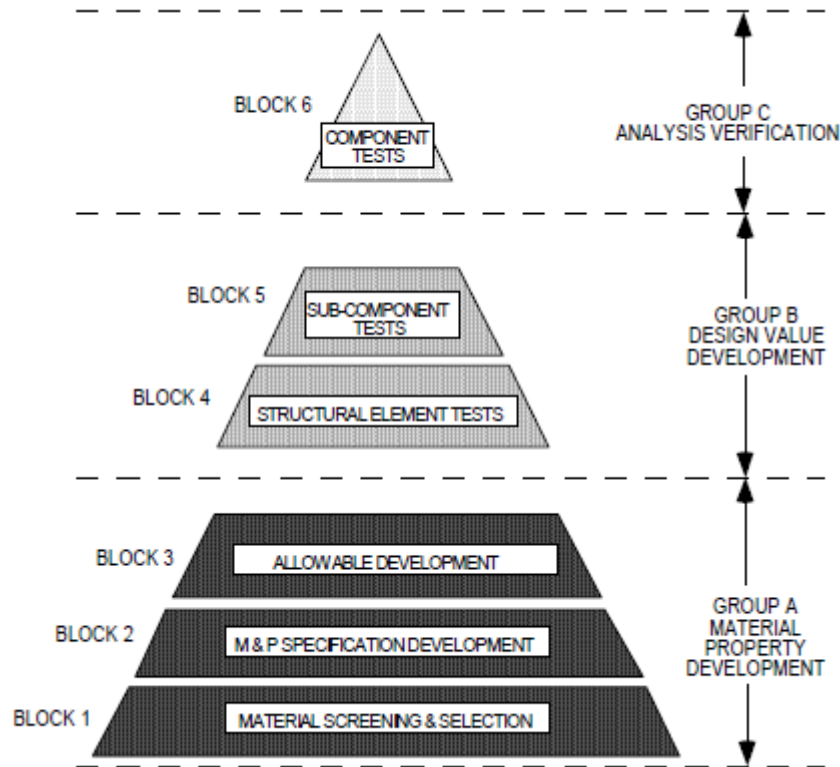


Figure 1-6: Building Block Approach<sup>[16]</sup>

Figure 1-6 is more representative of what this thesis includes and more specifically, the focus is given on Group A and B as shown above.

### 1.4.1 Group A: Material property development

#### 1.4.1.1 Block 1 - Material screening and selection

Block 1 aims to collect information about all the potential materials that can be used for the specific application. Materials such as steel, aluminium, wood, glass/carbon/aramid fibres and resins are being investigated and a decision is made regarding the materials that will be used for the given project. This block can contain some typical tests on basic specimens but without the imposition of any specifications which means that the resultant allowables are expected to change as the understating of the material system matures. However, more complex tests can be necessary to check if all the materials can satisfy specific configurations that will be used at the final application. For the given project, it was decided to use XX fibres in combination with a XX resin for the formation of the composite material. The main reasons are explained above(1.2 , 1.3) and a detailed analysis of all the alternatives would require a thesis itself.

### 1.4.1.2 Block 2 – Material and process specification development

Block 2 assumes that the material has already been defined and the processing specifications have been prepared for the material system. At this block, the specifications of the material must be validated and its behaviour should be understood as a function of the different process variables. For the case of a composite material, these different process variables can relate to several resin infusion techniques, cutting methods as well as curing and post curing procedures. The validation of the specifications can lead to the qualification of the material as long as its properties can support the design and as a result, a financial study can be implemented on a number of batches. This block enhances the understanding of the material behaviour and preliminary allowables can be derived from tests in this block, but with caution, because potential specification changes after the fabrication of the test specimens may invalidate the test results. In this thesis, no tests were performed as part of this block. For this thesis, the exact material's characteristics were decided straightforwardly, which included XX glass fibres embedded in XX, in a volume concentration of  $V_f = XX\%$ , produced by vacuum assisted resin transfer molding (VARTM) and cut by a water-cooled diamond plate cutter.

### 1.4.1.3 Block 3 – Allowables development

At this block the material is fully specified and its exact description is given above. The majority of the tests took place at this block and they resulted to an allowables database. The specimens that were tested will be called small scale coupons for the rest of this thesis. The tests aimed to the determination of a database with all the strength and stiffness properties of the aforementioned composite material. This database will be used for the prediction of the sub-components behaviour presented at block 4. Generally, the purpose of the tests at this block is:

- To develop statistically significant data. For the aerospace industry, these tests define the A-basis and B-basis allowables. For the marine industry, no such specifications are given and as a result the required amount of tests was chosen in order to allow for the statistical analysis of the results but keep the total cost relatively low
- To determine the effects of the environment. The testing plan of this thesis was at room temperature; ergo, this factor is not included in this thesis.
- To determine of notch effects. No notches were included in the testing plan of this thesis
- To define changes in properties due to lamination effects. The laminate configuration was unaltered for each test which means that no examination was implemented regarding different stacking sequence, laminate thicknesses, ply orientations etc.
- To understand manufacturing imperfections and the effect of these defects. The imperfections are related to the production methods and it can be evaluated if they are in the tolerance that is required.
- Understand the sensitivity of the structure on the fabrication process.

As part of this thesis, the testing plan at this block included 15 specimens tested in: tension at each direction ( $0^\circ, 90^\circ$ ), compression at each direction and in-plane shear. Moreover, 6 specimens were tested in

out-of-plane shear for each of the 1 – 3 and 2 – 3 planes. Hence, the total amount of coupons tested in this block is:  $n_{coupons} = 15 \cdot 5 + 2 \cdot 6 = 87 \text{ tests}$ . The advantage of performing tests at this block is that they can be used as the base of building block approaches for other projects too. To further elaborate on this, let's assume that DSNS is interested in another project where the material composition is exactly the same. Instead of implementing the aforementioned tests again, the experimental results from this testing plan can be used. However, as we go upwards to the pyramid shown in figure 1-6, the tests become more and more application-driven and they are different for distinct projects.

### 1.4.2 Group B: design-value development

Group B aims to develop design values which actually describe the real structure. In contrast with the tests at [block 3](#) where allowables were extracted, this block requires a preliminary configuration with general sizing and as a result the design values can be defined. The difference between allowables and design values is given clearly at Ref. [16, §4.4.3.2.2]:

- *Allowable* - A material property value (e.g., modulus, maximum stress level, maximum strain level) that is statistically derived from test data.
- *Design Value* - A material property or load value that takes into consideration program requirements (e.g., fitting and scaling factors, cutoff levels) and that has been approved for use in the design and analysis of structure.

#### 1.4.2.1 Block 4 – Structural Element tests

This block consists of local structural details that are repeated in the final design. From this step and onwards the tests are more project oriented. For example, at this block, 2 tests have been implemented; they were 3-point bending tests on a monolithic panel with dimensions:  $Length = XX \text{ m}, Width = XX \text{ m}, Thickness \approx XX \text{ mm}$ . These dimensions are not random, but they represent a typical panel of the MCMV's hull. The main objectives of the tests at this building block are:

- To develop design values that are structural configuration related.
- To understand manufacturing imperfections and the effect of these defects. The imperfections are related to the production methods and it can be evaluated if they are in the tolerance that is required taking into consideration the new scale of the samples.
- Understand the sensitivity of the structure on the fabrication process.

Example: Let's assume that DSNS is interested to make helipads out of composites with the same material composition. The tests at [block 3](#) can be used for this project too because everything that includes the material stays unaltered. However, the test results from [block 4](#) cannot be used because monolithic panels with that dimensions are not applicable to helipads.

Building block 5 includes configurations that are even more complex. Usually, there is load redistribution due to local damage at the tests which are part of this block (ex. multi-stiffened panels). Finally, building block 6 which is the final step of this method, includes test at full scale structures or parts of them (ex. whole midship

section). These block are not presented here as this would be out of the scope of this thesis. If the reader is interested in the next steps of this method, he can find useful information at Ref [16-19].

## 1.5 References

- [1.1] Robert M. Jones, *Mechanics of Composite Materials*, 1<sup>st</sup> edition, 1975, ISBN: 0-07-0.3790-4
- [1.2] Jasper Graham-Jones John Summerscale, *Marine Applications of Advanced Fibre-reinforced Composites*, 1<sup>st</sup> Edition, 2015, ISBN: 9781782422501
- [1.3] Jack R. Vinson, Robert L. Sierakowski, *The Behavior of Structures Composed of Composite Materials*, 2nd Edition, 2008, ISBN-10: 1402009046
- [1.4] Encyclopedia Britannica, source <https://www.britannica.com/technology/mine-weapon> (LV: 10/ 11/ 2017)
- [1.5] Robert C. Duncan, *America.s Use of Sea Mines (United States Naval Ordnance Laboratory) White Oak*, United States Government Printing Office, 1962)
- [1.6] Major General Thomas A. Benes, E. Anne Sandel, Navy's 2009 report, "21st Century U.S. Navy Mine Warfare; Ensuring Global Access and Commerce, source: [http://www.wolaa.org/files/The\\_History\\_of\\_the\\_Sea\\_Mine.pdf](http://www.wolaa.org/files/The_History_of_the_Sea_Mine.pdf) (LV: 10/ 11/ 2017)
- [1.7] Association of minemen, official web site, source: <http://minemen.org/BushnellMine.htm> (LV: 10/ 11/ 2017)
- [1.8] Navweaps, Naval Weapons, Naval Technology and Naval Reunions, Germany Mines, Article from the Web: [http://www.navweaps.com/Weapons/WAMGER\\_Mines.php](http://www.navweaps.com/Weapons/WAMGER_Mines.php) (LV: 10/ 11/ 2017)
- [1.9] *Naval Mine Warfare: Operational and Technical Challenges for Naval Forces*, National Research Council, Division on Engineering and Physical Sciences, Mathematics, Applications Commission on Physical Sciences, Naval Studies Board, Committee for Mine Warfare Assessment, 2001, ISBN-10: 0309076854
- [1.10] Ministry of Defense, Mijnenjagers, source: <https://www.defensie.nl/onderwerpen/materieel/inhoud/schepen/mijnenjagers> (LV: 10/ 11/ 2017)
- [1.11] Nederlands Instituut voor Militaire Historie, *Minehunting in the red Sea and the Gulf of Suez*, 1984, Updated in 2009, source: <https://www.google.nl/url?sa=t&rct=j&q=&esrc=s&source=web&cd=7&ved=0ahUKEwjYg7jZirPTAhURZIAKH7jB6oQFghQMAY&url=https%3A%2F%2Fwww.defensie.nl%2Fbinaries%2Fdefence%2Fdocuments%2Fleaflets%2F2009%2F05%2F01%2Fminehunting-in-the-red-sea-and-the-gulf-of-suez%2Fminehunting-in-the-red-sea-and-the-gulf-of-suez.pdf&usq=AFQjCNHBF8MoGEamsD2WcFE9EdQLwYlxQ&cad=rja> (LV: 10/ 11/ 2017)
- [1.12] Bhagwan. D. Agarwal, Lawrence J. Broutman, K. Chandrashekhara, *Analysis and performance of fiber composites*, 3<sup>rd</sup> edition, 2006, ISBN: 978-81-265-3636-8
- [1.13] *ASM Handbook*, Volume 21, *Composites*, ASM International
- [1.14] Isaac M. Daniel, Ori Ishai, *Engineering mechanics of Composite materials*, 2nd edition, 2006, ISBN: 978-0-19-515097-1
- [1.15] Todd Johnson, *Thermoplastic vs Thermoset Resins, the difference in two resins used in frp composites*, March 2017, source: <https://www.thoughtco.com/thermoplastic-vs-thermoset-resins-820405> (LV: 10/ 11/ 2017)

- [1.16] Composite materials handbook, Volume 3. Polymer matrix composites materials usage, design, and analysis, Department of Defense Handbook, MIL-HDBK-17-3E, 23 January 1997
- [1.17] Composite materials handbook, Volume 1. Polymer matrix composites guidelines for characterization of structural materials Department of Defense Handbook, MIL-HDBK-17-3E, 23 January 1997
- [1.18] Ivatury S. Raju et al., Comparison of Requirements for Composite structures for aircraft and Space Applications, International Conference on Composites for 21<sup>st</sup> Century: Current & Future Trends, January 2011, Bangalore, India
- [1.19] Marshall Rouse et al., Utilization of the building-block approach in structural mechanics research, report from NASA, source: <https://ntrs.nasa.gov/archive/nasa/casi.ntrs.nasa.gov/20050199405.pdf> (LV: 10/ 11/ 2017)
- [1.20] Confidential: Matrix reference

# Chapter 2: Small Scale Coupons

During the previous chapter, the rationale behind the implementation of tests was given. At this chapter, focus will be given on the small scale coupon tests which resulted in the determination of the allowable values. The preparation of these tests is explained, which resulted in the design of the coupon specimens (drawings are included). At the end of the chapter, the results from these tests are shown and they will be used as the basis for the prediction of the large scale coupons' structural response (tests at [block 4](#)).

## 2.1 Tensile Tests

At this subchapter, the preparation of the tensile tests is shown. The testing plan includes tensile tests of coupons with fibers at  $0^\circ$  direction as well as at  $90^\circ$ . The change in the fiber alignment doesn't influence the design of the coupons (but of course it affects the results) and for that reason coupons with fibers at  $0^\circ$  and  $90^\circ$  will be examined together.

The purpose of these tests is to define the following (for each fiber direction):

- Ultimate tensile strength,
- Ultimate tensile strain,
- Tensile chord modulus of elasticity,
- Poisson's ratio, and
- Transition strain.

As a first step, the norm ASTM D 3039<sup>[1]</sup> was studied extensively and the coupons were designed in such a way that the norm's specifications are satisfied. The geometry of the coupons is not strictly defined in the norm but some suggestions are made. For the experiments involved in this thesis, a literature review showed various initial geometries from which one was chosen for the tests. Except from the composite coupons that have to be defined for the tensile tests, the tabs on which the grips will transfer the load have to be designed. For the tabs, the specifications from the norm were followed which resulted to the use of composite tabs with fiber orientation at  $[\pm 45^\circ]_s$  with respect to the load direction with the same material composition as the coupons. Furthermore, the adhesive that was used to bond the tabs on the coupon was the result of literature review and it was decided to use Hysol EA 9394 two-part structural paste adhesive<sup>[2]</sup> with a nominal thickness of 0.2 mm. Finally, the end of tab was decided to be machined with an inclination of 1:4 in order to lead to a soft introduction of the load from the grips to the coupon specimen. The resultant designs are shown below:

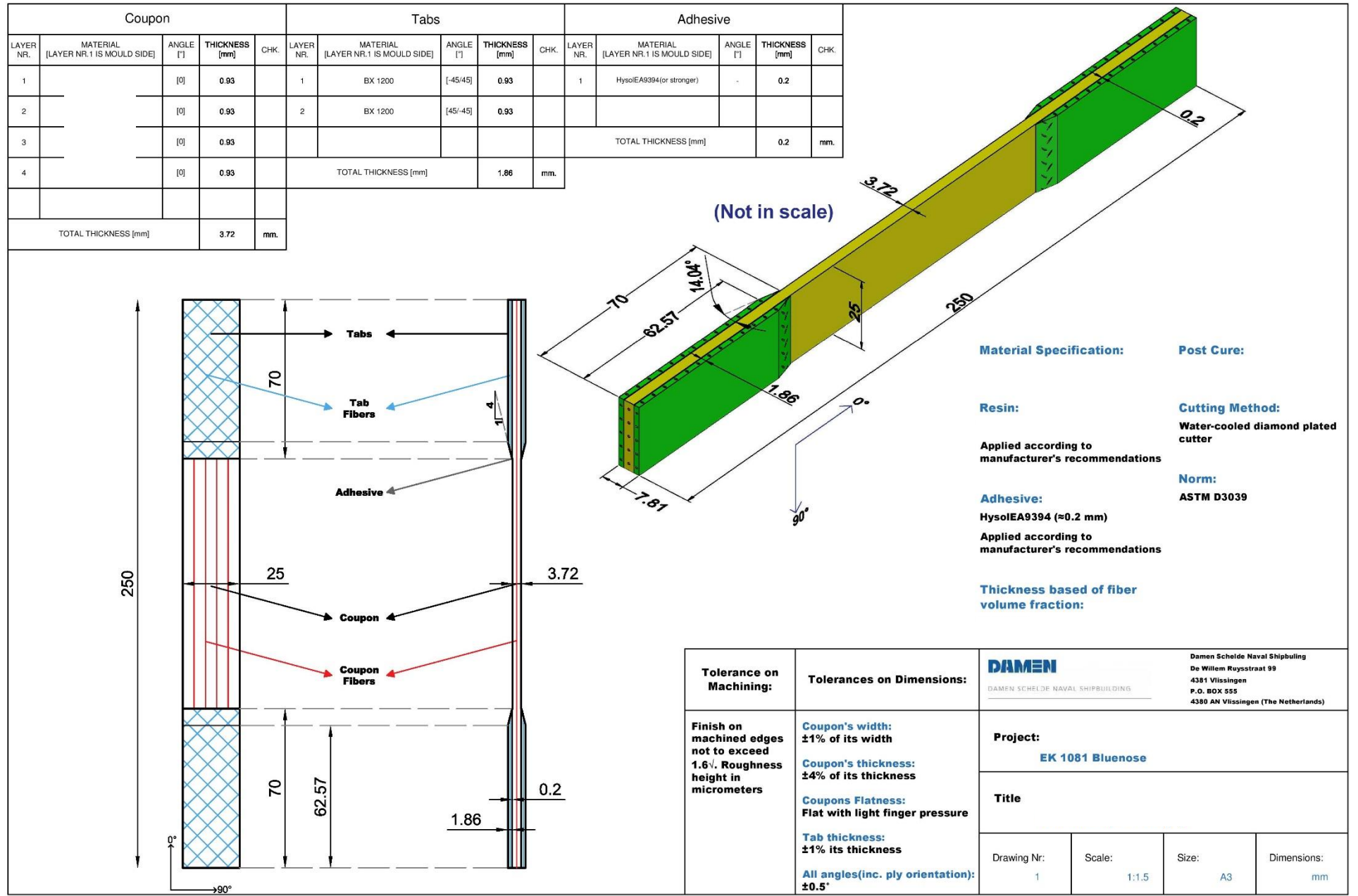


Figure 2-1: Coupon for tensile test (0°)

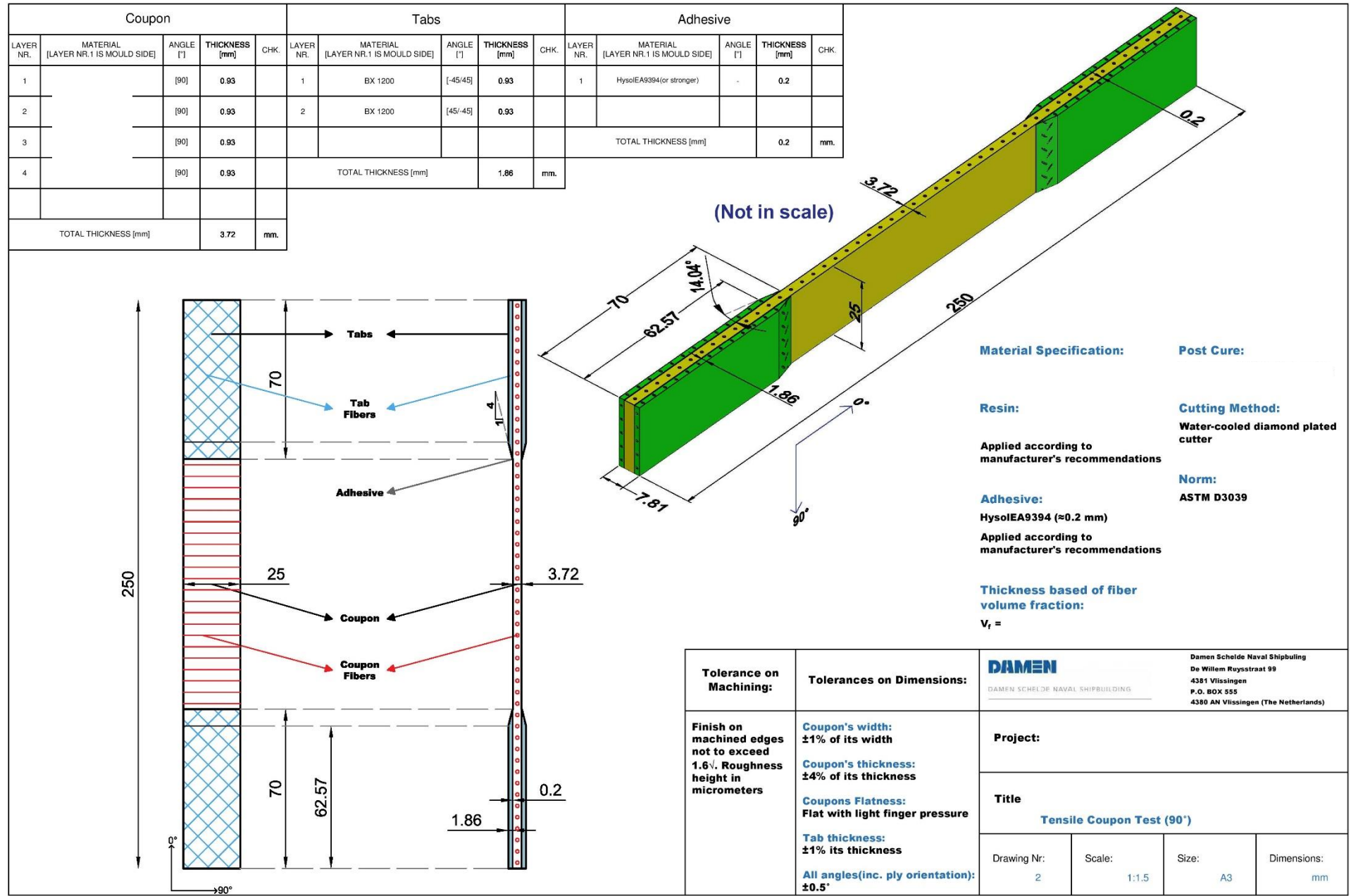


Figure 2-2: Coupon for tensile test (90°)

At figures 2-1 & 2-2, the final drawings for the tensile tests are shown. However, one should firstly be sure that this geometrical configuration does not lead to unwanted failure modes. For example, a failure mode that should be avoided, is the failure of the adhesive. If the adhesive fails to transfer the load from the tabs to the coupon specimen, it will not be possible to measure the ultimate tensile strength/strain of the coupon. For that reason, the norm specifies that the minimum length of the tabs should be:

$$L_{min} = \frac{F^{tu} \cdot h}{2 \cdot F^{su}} \quad (2.1.1)$$

where:

$L_{min}$  = minimum required bonded tab length, mm

$F^{tu}$  = ultimate tensile strength of coupon material, MPa

$h$  = coupon thickness, mm

$F^{su}$  = ultimate shear strength of adhesive, coupon material, or tab material (the lowest), MPa

For the calculation of  $L_{min}$ , the ultimate tensile strength of the coupon,  $F^{tu}$  is necessary. However, this value is the one that has to be extracted from the experiments. Thus, by searching in the inner reports of DSNS, it was found that similar experiments have been implemented, where XX fibers were embedded in a XX resin with a fiber volume  $V_f = XX\%$ . These experiments resulted in  $F^{tu} = XX \text{ MPa}$ . The thickness  $h$ , is equal to the number of plies used to form the coupon times the thickness of each ply. It was decided to use 4 plies at each coupon and the thickness of each ply can be calculated by<sup>[3 Spage 1706]</sup>:

$$h_f = \frac{FAW}{\rho_f} = XX \text{ mm} \quad (2.1.2)$$

where:

$h_f$  = equivalent thickness of solid fiber material in one ply

$FAW = XX \text{ gr/m}^2$

$\rho_f = XX \cdot 10^4 \text{ gr/m}^2$

Hence, the total thickness of each coupon is:

$$h = h_{ply} \cdot n_{plies} = \frac{h_f}{V_f} \cdot n_{plies} = 3.72 \text{ mm}, \quad \text{where } V_f = \text{fibre volume } [\%] \quad (2.1.3)$$

$F^{su}$  corresponds to the lowest value between the shear strengths of the adhesive, the coupon material and the tab material. The adhesive was found to be the weakest link with a shear strength of  $S = XX \text{ MPa}^{[2]}$ . Thus, the equation 2.1.1 results:

$$L_{min} = \frac{F^{tu} \cdot h}{2 \cdot F^{su}} = 48.95 \text{ mm} \leq 70 \text{ mm} \quad (2.1.4)^{[1]}$$

The choice of a tab length equal to  $L_{tab} = 70 \text{ mm}$  satisfies the above equation and gives a substantial safety margin to the values that were used. By looking at the literature, this is approximately the upper value of  $L_{min}$  which is used for the tensile tests. Furthermore, by coming into contact with the laboratory where the experiments were performed, this length tab was suggested which best fits with at their grips.

As a final step, a FEA model was built to check the development of stresses on the adhesive and the structural stress concentration on the tab end. The main reason behind the preparation of this FEA model is to build a tool with which different tensile experiments can be investigated and check the sensitivity of the stresses on different parameters such as different stiffness properties, different geometries etc.

## 2.1.1 FEA Model for tensile tests

### 2.1.1.1 Finite element method, general information

The presentation of the academic background of the finite element methods will require a thesis on its own and a presentation here will be out of the scope of the thesis. Readers that are interested to become familiar with the origins of these methods as well as with applications concerning modern problems, are suggested to read Ref. [14-18].

In order to avoid any potential confusion, a difference in the refinement of the mesh is depicted below between the academic version of Ansys v.17.1 that was used for this thesis and the respective commercial Ansys version.

The academic version of Ansys v.17.1 allows the usage only of the h-method (p-method is not included) for the refinement of the mesh under the choice of discipline options. This method is a way to add degrees of freedom in order to get improved results and the way that this is implemented is shown in figure 2-3. Basically, h-method keeps the type of each element but decreases its characteristic length by dividing it into two or more elements. Hence, improved results are obtained by making the mesh finer as the option to increase the order of the elements is available only to p-method which is available at the commercial Ansys version and can potentially lead to faster convergence<sup>[11]</sup>.

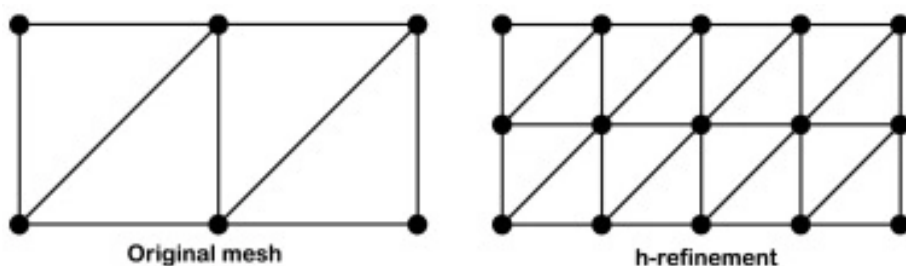


Figure 2-3:h-refinement<sup>[11]</sup>

Hence, improved results are obtained by making the mesh finer as the option to increase the order of the elements is available only to p-method which is available at the commercial Ansys version and can potentially lead to faster convergence<sup>[11]</sup>.

2.1.1.2 FEM model of the tensile coupon

Now let's focus on the specific application, i.e. the modeling of the tensile coupon. The model was composed of 1/4 of the tensile coupon( due to the symmetry both horizontally and vertically) with fibers at 0° which will lead to the development of the highest potential stresses at the adhesive comparing with fibers at different orientations. A representative figure of the geometry is shown in fig.2-4. The input data that were used are shown below:

Geometry (Dimensions shown in fig 2-1):

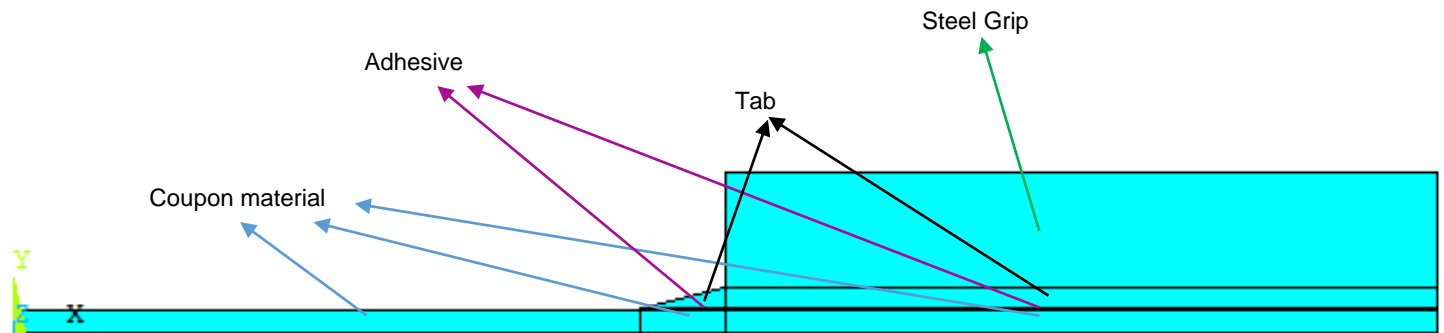


Figure 2-4: Tensile coupons geometry

Element Type: Plane183

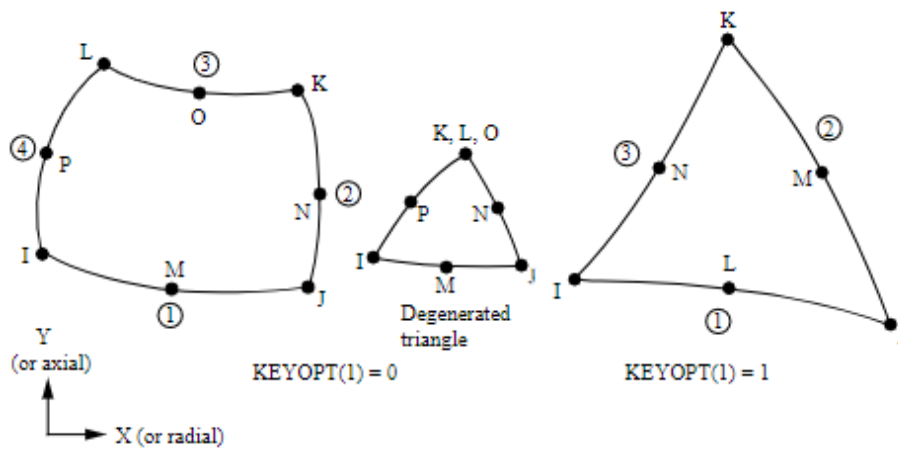


Figure 2-5:Plane183 Geometry<sup>[5]</sup>

Plane183 is a higher order 2 – D, 8-node or 6-node element and has a quadratic displacement behavior(shape functions are shown below). It has 2 degrees of freedom at each node, i.e. translation in the nodal x and y directions. At this model only 8-node elements were used with the exception of the elements at the machined edge of the tab where triangular, 6-node elements, can be found. Moreover, the test was modelled in 2 dimensions (2 – D model) which enabled to apply plane strain conditions. This assumption (plane strain conditions) is valid because the section that is analyzed is repeated in the out of plane direction (z direction in the Ansys model).

$$\begin{aligned}
u = \frac{1}{4} & \left( u_I(1-s)(1-t)(-s-t-1) + u_J(1+s)(1-t)(s-t-1) \right. \\
& \left. + u_K(1+s)(1+t)(s+t-1) + u_L(1-s)(1+t)(-s+t-1) \right) \\
& + \frac{1}{2} \left( u_M(1-s^2)(1-t) + u_N(1+s)(1-t^2) + u_O(1-s^2)(1+t) \right. \\
& \left. + u_P(1-s)(1-t^2) \right)
\end{aligned} \tag{2.1.5}$$

At eq. 2.1.5 the quadratic displacement behavior(shape function<sup>[5]</sup>) is shown for the horizontal displacement. Analogous to that the vertical displacement can be derived as  $v = 1/4 (v_I(1-s) \dots$ . As mentioned above, the only key option that was activated was keyopt,1,3,2 which activated the plain strain conditions.

### Material Properties

Four different material models were input in the analysis. The first one, was an orthotropic material model and was assigned to the coupon material. The fact that the fibers were only at  $0^\circ$  direction( $x$  direction in Ansys) meant that no changes had to be made in order to adjust for the fiber alignment. The input values were taken from the same inner report of DSNS which was used for the calculation of the minimum tab length at eq. 2.1.1. As far as the adhesive is concerned, it was modelled as an isotropic material and its properties were extracted from Ref.[2]. Finally, the tab's material properties have to be modified due to the fiber orientation ( $\pm 45^\circ$ ) according to the following formulas<sup>[6 §2.6]</sup>:

$$\begin{aligned}
\frac{1}{E_x} &= \frac{1}{E_1} \cos^4 \theta + \left( \frac{1}{G_{12}} - \frac{2\nu_{12}}{E_1} \right) \sin^2 \theta \cos^2 \theta + \frac{1}{E_2} \sin^4 \theta \\
\nu_{xy} &= E_x \left[ \frac{\nu_{12}}{E_1} (\sin^4 \theta + \cos^4 \theta) - \left( \frac{1}{E_1} + \frac{1}{E_2} - \frac{1}{G_{12}} \right) \sin^2 \theta \cos^2 \theta \right] \\
\frac{1}{G_{xy}} &= 2 \left( \frac{2}{E_1} + \frac{2}{E_2} + \frac{4\nu_{12}}{E_1} - \frac{1}{G_{12}} \right) \sin^2 \theta \cos^2 \theta + 1/G_{12} (\sin^4 \theta + \cos^4 \theta)
\end{aligned} \tag{2.1.6}$$

The modelled properties are:

Orthotropic Material			Isotropic Material	
	Coupon Material	Tabs (eq. 2.1.6)		Adhesive
$E_x$ [MPa]	XX	XX	$E$ [MPa]	$4.237 \cdot 10^3$
$E_y$ [MPa]	XX	XX	$\nu$ [-]	0.45
$E_z$ [MPa]	XX	XX		
$\nu_{xy}$ [-]	XX	XX		
$\nu_{yz}$ [-]	XX	XX		
$\nu_{xz}$ [-]	XX	XX		
$G_{xy}$ [MPa]	XX	XX		
$G_{yz}$ [MPa]	XX	XX		
$G_{xz}$ [MPa]	XX	XX		

		Isotropic Material	
		Steel Grip	
		$E$ [MPa]	$200 \cdot 10^6$
		$\nu$ [-]	0.3

Table 2-1: Modelled material properties in Ansys, tensile tests

#### Assumptions on material properties:

- Coupon material: The elastic modulus at the  $y$ -direction as modelled in Ansys is assumed to be equal to the “weak” elastic modulus, i.e. the modulus transverse to the direction of the fibres
- Coupon material: The out of plane Poisson ratios and Shear modulus are assumed to be equal to the respective in plane properties
- Tabs: The material properties are adjusted according to eq. 2.1.6. However, the elastic modulus at the  $y$ -direction is assumed unaltered by the change of the fibre alignment in the  $xz$  plane as modelled in Ansys
- Tabs: The Poisson ratios in  $xy$  and  $yz$  planes are assumed unaltered by the change of the fibre alignment in the  $xz$  plane. The same stands for the Shear modulus at the same planes.
- Steel Grip: The elastic modulus of the steel grips was assumed to be extremely high. The reason of the grip’s presence is to introduce the load to the tab.

*Note: The equations 2.1.6 take into account that the fibres are in the  $xy$  plane. However, the  $xy$  plane in the 2 – D Ansys model shows a vertical cut of the tensile coupon. Hence, according to the model, the fibres of*

the tabs lie in its  $xz$  plane. The material properties shown at the table 2-1 are the adjusted properties that were introduced in the Ansys script.

Boundary conditions:



Figure 2-6: Boundary Conditions, Tensile test model

- At  $y = 0$ ,  $U_y = 0$
- At  $x = 0$ ,  $U_x = 0$
- At  $y = t_{coupon} + t_{adh} + t_{tab}$ , the vertical displacements are coupled

Symmetric boundary conditions have been implemented at  $x = 0$  &  $y = 0$  due to the symmetric structure and loading. The vertical displacement of the nodes at the outer surface of the tabs are coupled because it is assumed that the grips are rigid and they always apply uniform vertical pressure on the tabs.

Loading:

The loading has been applied at the top of the steel grip. It consists of a uniform, vertical pressure load and a uniform horizontal pressure. The horizontal pressure was introduced as concentrated forces at nodes and their values were dependent on the elements' area that surrounded the nodes. To clarify this, the nodes that lie at  $x = L_{coup} - L_{tab}$  (tab end) have finer mesh and as a result the horizontal forces at the nodes had smaller values than the ones close to the end of the model ( $x = L_{coup}$ ) where the mesh is coarser due to the lack of interest in this area. Generally, the forces have been adjusted in order to represent a uniform horizontal pressure at the top of the grip.

Regarding the vertical pressure, the calculation of its value was based in simple mechanics. The procedure that was followed was the following

$$\text{Total Tensile force, } F_{tot} = T_{11} \cdot w_{coup} \cdot h_{tot} = XX \text{ kN}$$

$$\text{Force at grip, } F_{grip} = \frac{F_{tot}}{2} = XX \text{ kN} \quad (2.1.7)$$

$$\text{Vertical pressure on line, } p_{vert} = \frac{F_{grip}}{\mu_{static} \cdot A_{tab} \cdot L_{tab}} = XX \text{ MPa/mm}$$

The value of  $\mu_{static} = 0.3$  was taken from Ref. [8].

Results:

By implementing the post-processing of this model, the focus was concentrated at the adhesive layer. The shear stress-strain curve is known<sup>[12]</sup> and is shown in figure 2-9. The displaced (dark blue) and undisplaced (dashed) models are shown below along with the area that is of interest:

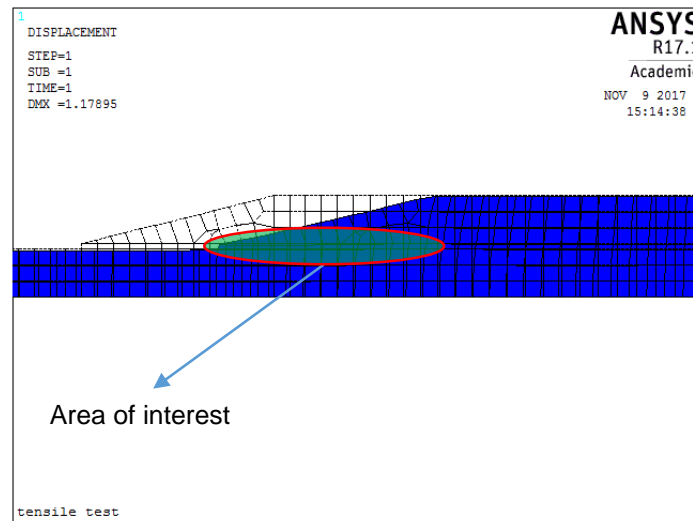


Figure 2-7: Displaced and undisplaced model, Tab-end, coupon connection

At the area of interest, the highest shear stresses of the adhesive are developed. However, due to its non-linear, plastic behavior, it is expected to withstand the stresses and not to fail. The expected mechanism is to have a part close to the tab end which is in the non-linear region of figure 2-9 and then, the load to be spread at the part of the adhesive which lies further to the tab end, i.e. to get bigger and bigger plastic zones. The length that at least will be plastified is shown in figure 2-8. This length,  $d = 18.68 \text{ mm}$  is small compared to the total length of the adhesive layer which is  $70 \text{ mm}$  and as a result, the adhesive is not expected to fail.

At this point, it should be mentioned that the values at figure 2-9 are slightly higher than the ones that are provided at the technical datasheet at Ref. [4]. Generally, the technical datasheet is provided from the manufacturer and can be trusted more than the experiments shown in Ref[12]. Nonetheless, the experiments show even higher ultimate shear strength which means that that we are on the safe side and apart from that the main reason of including figure 2-9 is to show the capability of Hysol 9394 to deform plastically

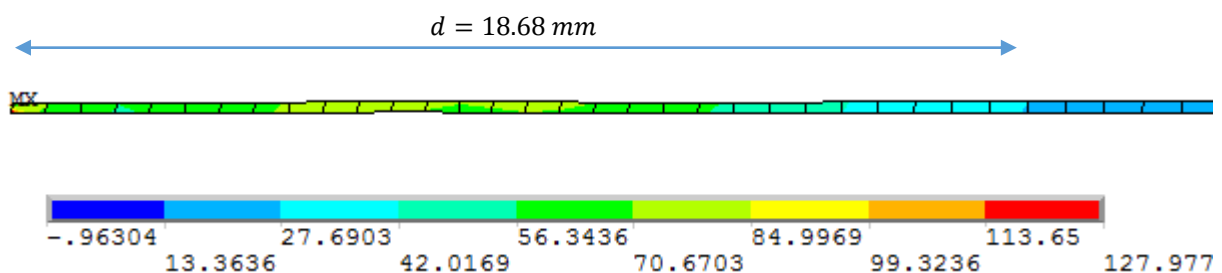


Figure 2-8: Shear stresses at the adhesive layer

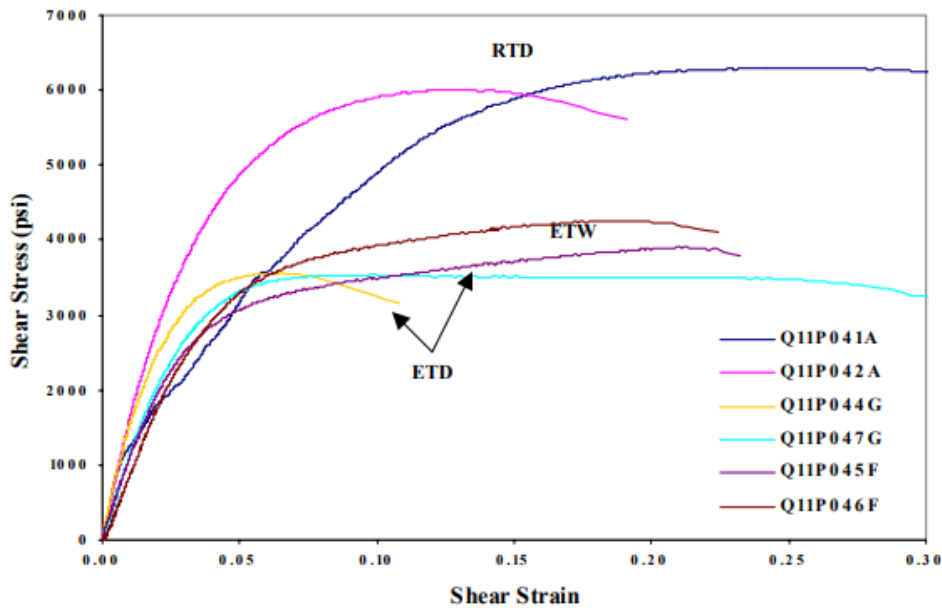


Figure 2-9: characteristic shear response of Hysol EA 9394 paste adhesive with respect to the environment [12]

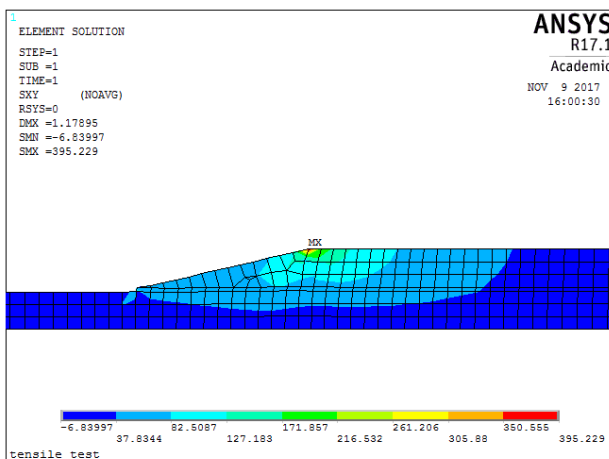


Figure 2-10: Shear stresses at the area of interest

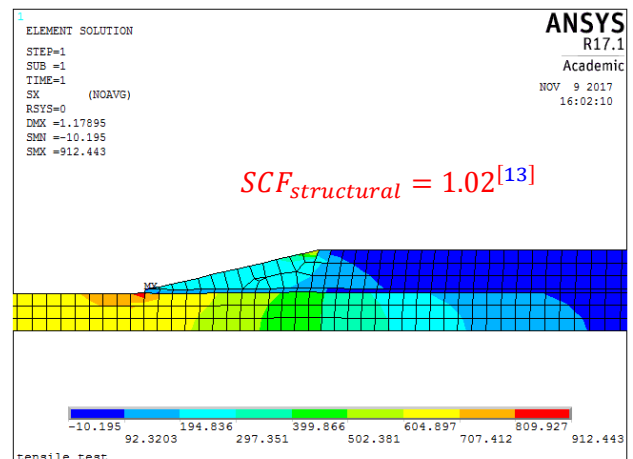


Figure 2-11: Normal Stresses  $\sigma_x$  at the area of interest

## 2.2 Compressive tests

At this subchapter, the preparation of the compressive tests is shown. The testing plan includes compressive tests of coupons with fibers at  $0^\circ$  direction as well as at  $90^\circ$ . Similarly to the tensile tests, the change in the fiber alignment doesn't influence the design of the coupons and for that reason coupons with fibers at  $0^\circ$  and  $90^\circ$  will be examined together.

The purpose of these tests is to define the following (for each fiber direction):

- Ultimate compressive strength,
- Ultimate compressive strain,
- Compressive (linear or chord) modulus of elasticity,
- Poisson's ratio in compression, and
- Transition strain.

As a first step, the norm ASTM D 3410<sup>[9]</sup> was studied extensively and the coupons were designed in such a way that the norm's specifications are satisfied. Similarly, the geometry was the result of literature review and critical thinking of the writer as the norm doesn't specify the dimensions but again stays to some suggestions. The coupon designs are shown in figures 2-12, 2-13 for the coupon with fibers at 0° and 90° respectively. The same material composition is used for the tabs as the one for coupon, but for these tests, the norm doesn't specify that the fiber alignment should be changed. Hence, the tabs have a [0°/90°]<sub>s</sub> stack up sequence. The adhesive that is used is the same one with tensile tests, i.e. Hysol EA 9394 two-part structural paste adhesive, and there is no machined edge for the soft introduction of the load.

Previously, the focus was given at the failure of the adhesive. In the case of the compressive tests, the adhesive will not be examined as it will be the same as the one in tensile tests and its stress state will be less intense. However, a different unwanted failure should be avoided at these tests which is related to buckling. Generally, it is desired to design the coupon in such a way that it will fail by crushing before it buckles and starts losing its stiffness at the longitudinal axis. In order to prevent that failure, the norm defines:

$$h_{coup} \geq \frac{l_g}{0.9069 \cdot \sqrt{\left(1 - \frac{1.2F^{cu}}{G_{xz}}\right) \left(\frac{E^c}{F^{cu}}\right)}} \quad (2.2.1)$$

Where:

$h_{coup}$  = specimen thickness, [mm]

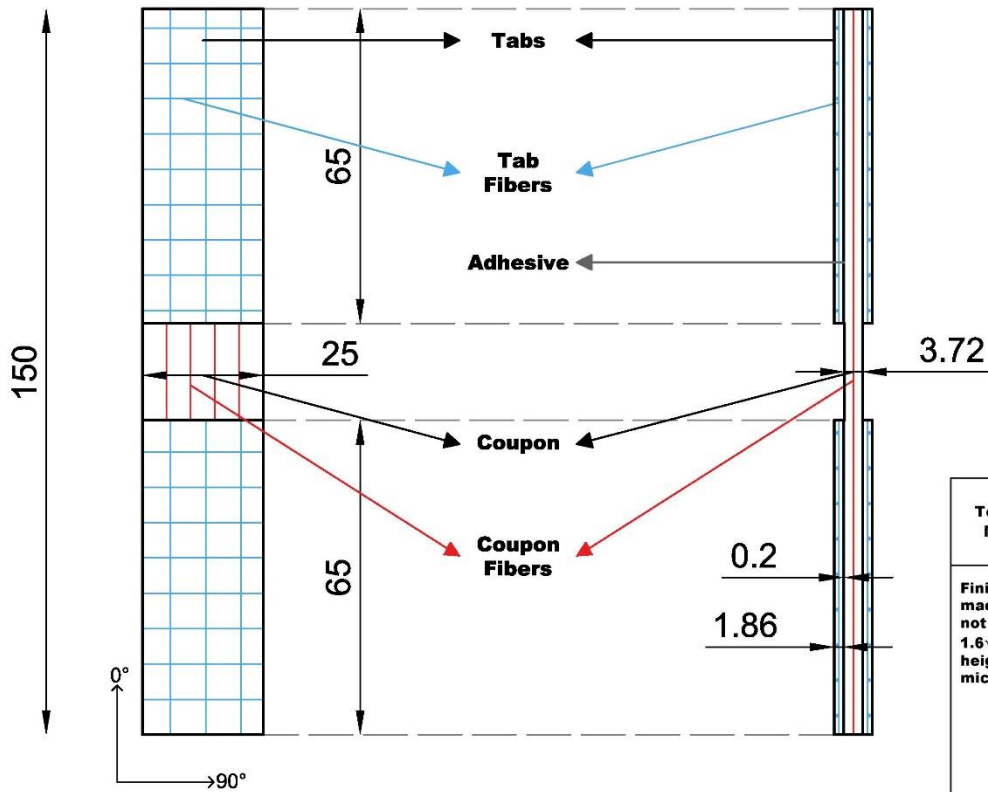
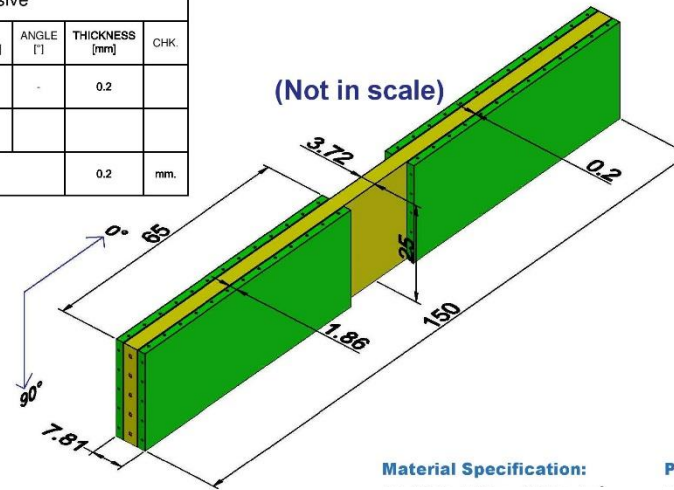
$l_g$  = length of gage section, [mm]

$G_{xz}$  = through the thickness shear modulus, [MPa]

$F^{cu}$  = ultimate compressive Strength, [MPa]

$E^c$  = longitudinal modulus of elasticity, [MPa]

Coupon					Tabs					Adhesive				
LAYER NR.	MATERIAL [LAYER NR.1 IS MOULD SIDE]	ANGLE [°]	THICKNESS [mm]	CHK.	LAYER NR.	MATERIAL [LAYER NR.1 IS MOULD SIDE]	ANGLE [°]	THICKNESS [mm]	CHK.	LAYER NR.	MATERIAL [LAYER NR.1 IS MOULD SIDE]	ANGLE [°]	THICKNESS [mm]	CHK.
1		[0]	0.93		1	BX 1200	[90/0]	0.93		1	HysolEA9394(or stronger)	-	0.2	
2		[0]	0.93		2	BX 1200	[0/90]	0.93						
3		[0]	0.93							TOTAL THICKNESS [mm]			0.2	mm.
4		[0]	0.93		TOTAL THICKNESS [mm]			1.86	mm.					
TOTAL THICKNESS [mm]			3.72	mm.										



**Material Specification:**

**Post Cure:**

**Resin:**

**Cutting Method:**

Applied according to manufacturer's recommendations

Water-cooled diamond plated cutter

**Adhesive:**

**Norm:**

HysolEA9394 (≈0.2 mm)

ASTM D3410

Applied according to manufacturer's recommendations

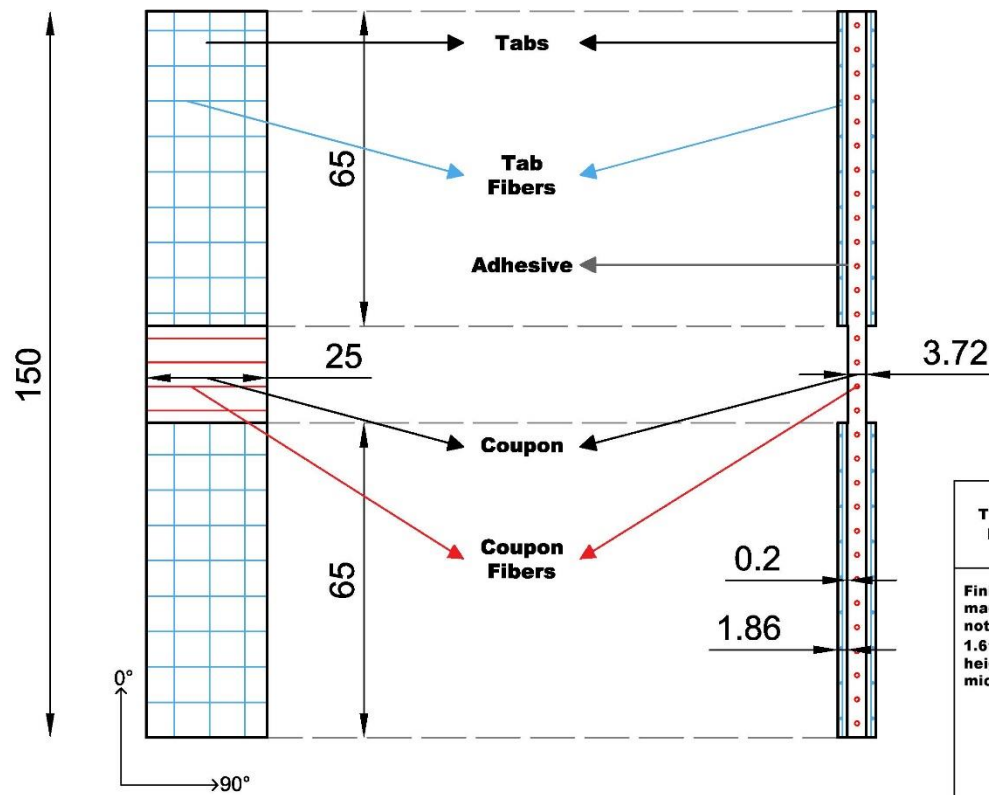
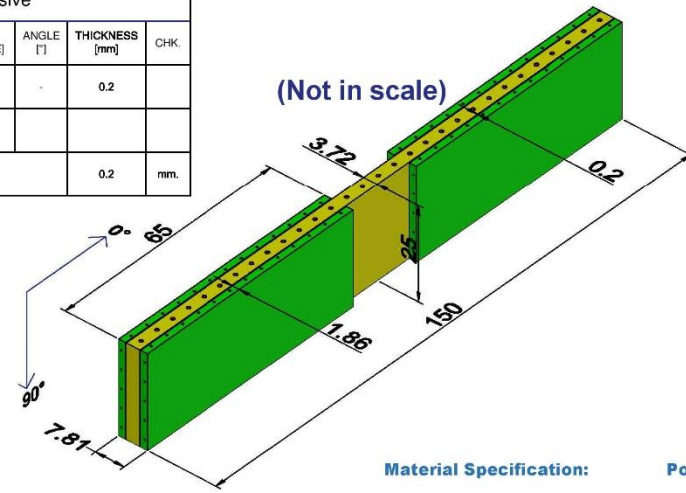
**Thickness based of fiber volume fraction:**

$V_f =$

<b>Tolerance on Machining:</b>	<b>Tolerances on Dimensions:</b>	<b>DAMEN</b> <small>DAMEN SCHELDE NAVAL SHIPBUILDING</small> <small>Damen Schelde Naval Shipbuilding          De Willem Ruysstraat 99          4381 Vlissingen          P.O. BOX 555          4380 AN Vlissingen (The Netherlands)</small>	
		<b>Project:</b>	
<b>Finish on machined edges not to exceed 1.6√. Roughness height in micrometers</b>	<b>Coupon's width:</b> $\pm 1\%$ of its width  <b>Coupon's thickness:</b> $\pm 2\%$ of its thickness  <b>Coupons Flatness:</b> Flat with light finger pressure  <b>Tab thickness:</b> $\pm 1\%$ its thickness  <b>All angles(inc. ply orientation):</b> $\pm 0.5^\circ$	<b>Title</b>	
	<b>Compressive Coupon Test (0°)</b>		
	Drawing Nr: 3	Scale: 1:1	Size: A3
			Dimensions: mm

Figure 2-12: Coupon for compressive test (0°)

Coupon					Tabs					Adhesive					
LAYER NR.	MATERIAL [LAYER NR.1 IS MOULD SIDE]	ANGLE [°]	THICKNESS [mm]	CHK.	LAYER NR.	MATERIAL [LAYER NR.1 IS MOULD SIDE]	ANGLE [°]	THICKNESS [mm]	CHK.	LAYER NR.	MATERIAL [LAYER NR.1 IS MOULD SIDE]	ANGLE [°]	THICKNESS [mm]	CHK.	
1		[90]	0.93		1	BX 1200	[90/0]	0.93		1	HysolEA9394 (or stronger)	-	0.2		
2		[90]	0.93		2	BX 1200	[0/90]	0.93							
3		[90]	0.93								TOTAL THICKNESS [mm]			0.2	mm.
4		[90]	0.93		TOTAL THICKNESS [mm]			1.86	mm.						
TOTAL THICKNESS [mm]			3.72	mm.											



**Material Specification:**

**Resin:**  
Applied according to manufacturer's recommendations

**Adhesive:**  
HysolEA9394 (≈0.2 mm)  
Applied according to manufacturer's recommendations

**Thickness based of fiber volume fraction:**  
 $V_f =$

**Post Cure:**

**Cutting Method:**  
Water-cooled diamond plated cutter

**Norm:**  
ASTM D3410

<b>Tolerance on Machining:</b>	<b>Tolerances on Dimensions:</b>	<b>DAMEN</b> DAMEN SCHELDIJE NAVAL SHIPBUILDING			
		Damen Schelde Naval Shipbuilding De Willem Ruysstraat 99 4381 Vlissingen P.O. BOX 555 4380 AN Vlissingen (The Netherlands)			
<b>Finish on machined edges not to exceed 1.6<math>\mu</math>. Roughness height in micrometers</b>	<b>Coupon's width:</b> $\pm 1\%$ of its width  <b>Coupon's thickness:</b> $\pm 2\%$ of its thickness  <b>Coupons Flatness:</b> Flat with light finger pressure  <b>Tab thickness:</b> $\pm 1\%$ its thickness  <b>All angles (inc. ply orientation):</b> $\pm 0.5^\circ$	<b>Project:</b>			
		<b>Title</b> Compressive Coupon Test (90°)			
		Drawing Nr: 4	Scale: 1:1	Size: A3	Dimensions: mm

Figure 2-13: Coupon for compressive test (90°)

$$h_{coup} \geq \frac{l_g}{0.9069 \cdot \sqrt{\left(1 - \frac{1.2F^{cu}}{G_{xz}}\right) \left(\frac{E^c}{F^{cu}}\right)}} = XX \checkmark, \text{ for fibers at } 0^\circ$$

$$h_{coup} \geq \frac{l_g}{0.9069 \cdot \sqrt{\left(1 - \frac{1.2F^{cu}}{G_{xz}}\right) \left(\frac{E^c}{F^{cu}}\right)}} = XX \checkmark, \text{ for fibers at } 90^\circ$$

Assumptions:

- The above formula assumes that the boundary conditions are pinned and the column buckling is based on linear elastic material response.
- The through-the-thickness shear modulus was assumed equal to the in-plane one, i.e.  $G_{xz} = G_{xy}$

Even if the formulas are satisfied for both fibre directions, it was decided that further investigation of the compressive coupons' response should be made. For that reason, the following Ansys models were made:

## 2.2.1 FEA models for compressive tests

### 2.2.1.1 Elastic buckling analysis

As the first step, an Ansys script was made which aimed to define the linear elastic buckling load. This script will result in a predefined number of mode shapes along with the required load that leads to the elastic buckling of the coupon for each mode. The resultant displacement field was used in order to define the imperfections that are introduced to the next script, where a static analysis was implemented. This subchapter (2.2.1.1) focuses only at the linear elastic buckling analysis for the compressive coupon with fibres at  $0^\circ$ . For conservatism, the imperfections were taken only from the 1<sup>st</sup> buckling mode which resulted to the lowest stiffness for realistic, relative vertical displacements of the nodes. The procedure that was followed is described below:

Geometry (Dimensions shown in fig 2-12):

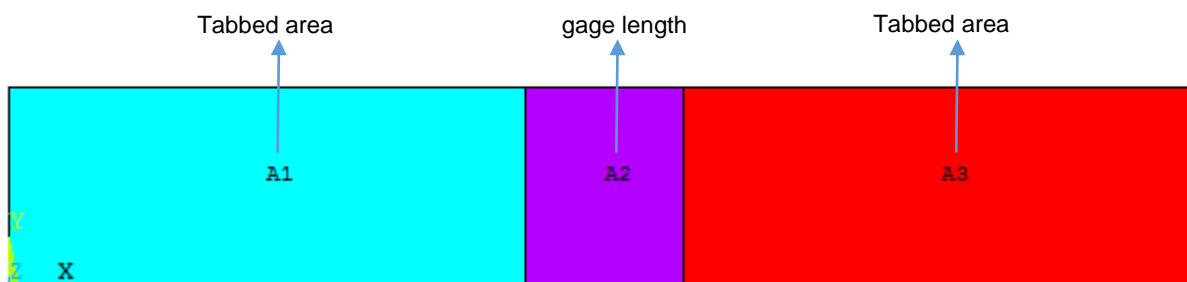
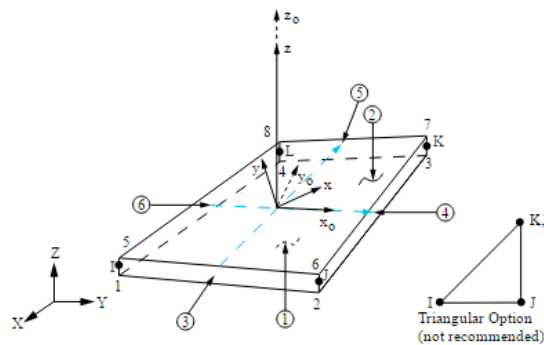


Figure 2-14: Geometry of compressive coupon, Top view

Element Type: Shell181



$x_0$  = Element x-axis if ESYS is not provided.  
 $x$  = Element x-axis if ESYS is provided.

Figure 2-15: Element formulation of compressive coupon<sup>[5]</sup>

For the modelling of the compressive coupon, the element type shell181 was used. This is a four node element as shown in figure 2-15 with six degrees of freedom at each node. The shape function of this element can be given from the following equation for the horizontal displacements.

$$u = \frac{1}{4} [u_I(1 - s)(1 - t) + u_J(1 + s)(1 - t) + u_K(1 + s)(1 + t) + u_L(1 - s)(1 + t)]$$

Analogous to the horizontal displacement, one can derive the vertical and the out of plane displacements  $v, z$  respectively, as well as the three rotations  $\theta_x, \theta_y, \theta_z$ .

Apart from that, by inserting the command `keyopt,1,1,0` both the membrane and the bending stiffness are taken into account. The command `keyopt,1,3,2` allows the element to have 4(2x2) in plane integration points and the command `keyopt,1,8,1` allows the storage of the results for both top and bottom layers.

Lay-Up sequence

The lay-up sequence of the coupon was given through Preprocessor->Sections->Shell->Lay-Up->Add/Edit. There, the thickness of each ply was defined along with the fiber direction and the through-the - thickness integration points. The figure below shows how the lay-up was defined:

	Thickness	Material ID	Orientation	Integration Pts	Pictorial View
4	0.9292	1	0	3	
3	0.9292	1	0	3	
2	0.9292	1	0	3	

Add Layer      Delete Layer

Figure 2-16: Definition of Lay-Up sequence, Ansys

### Material Properties

Similar to the tensile tests, the material properties were extracted from the same inner report of DSNS. Hence, the material properties for the compressive coupon are the same as the ones for the tensile coupon, i.e.

Orthotropic Material	
	Coupon Material
$E_x$ [MPa]	XX
$E_y$ [MPa]	XX
$E_z$ [MPa]	XX
$\nu_{xy}$ [-]	XX
$\nu_{yz}$ [-]	XX
$\nu_{xz}$ [-]	XX
$G_{xy}$ [MPa]	XX
$G_{yz}$ [MPa]	XX
$G_{xz}$ [MPa]	XX

Table 2-2: Modelled material properties in Ansys, compressive tests

#### Assumptions on material properties:

- Coupon material: The elastic modulus at the z-direction as modelled in Ansys is assumed to be equal to the “weak” elastic modulus, i.e. the modulus transverse to the direction of the fibres
- Coupon material: The out of plane Poisson ratios and Shear modulus are assumed to be equal to the respective in plane properties

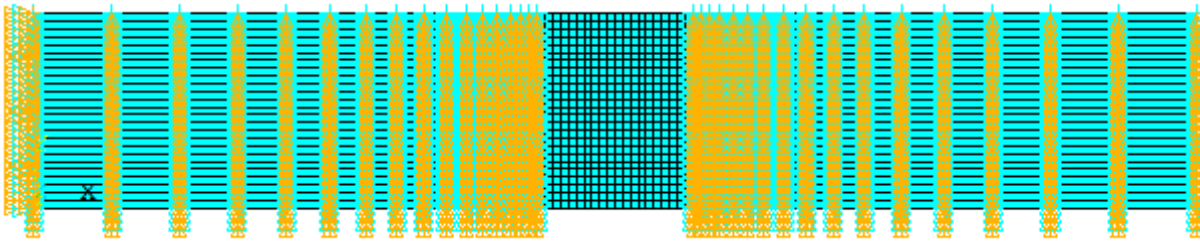
Boundary conditions:

Figure 2-17: Boundary Conditions, Compressive test model

- At  $0 < x \leq l_{tab}$ ,  $U_y = U_z = Rot_y = 0$
- At  $x = 0$ ,  $U_x = U_y = U_z = Rot_y = 0$
- At  $l_{coup} - l_{tab} \leq x \leq l_{coup}$ ,  $U_y = U_z = Rot_y = 0$

Assumption:

- It is assumed that the grips are rigid; ergo, the rotations,  $Rot_y$ , are restricted

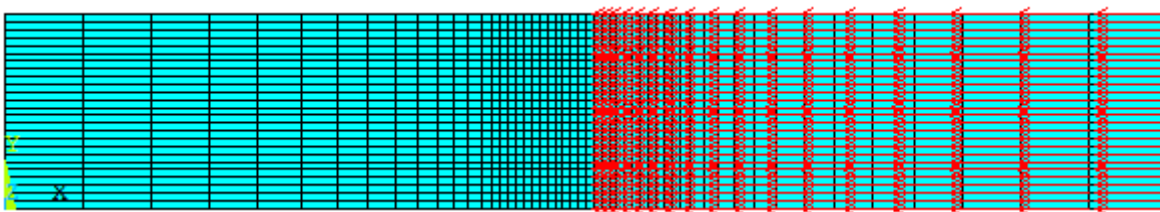
Loading:

Figure 2-18: Loading pattern of the compressive coupon

The loading has been applied at the part of the structure that lies below the right tab. Similar to the horizontal pressure at the tensile coupons, the values of the loads at the nodes have been adjusted properly in order to form a uniform field with horizontal pressure. More specifically, as it can be seen in figure 2-18, the mesh is finer at the free length and coarser towards both ends of the coupon. Hence, an algorithm has been developed in Ansys which applies a concentrated force at each node according to the area of the elements that surround the node. The total force introduced in the coupon was equal to the compressive force under which the coupon is expected to fail, i.e.:

$$F_{tot} = 25 \cdot 3.72 \cdot XX = XX \text{ kN}$$

This force was spread to all the nodes shown at figure 2-18 according to the aforementioned algorithm.

Results:

By performing a buckling analysis(`antype,1`), one can extract the critical elastic buckling load. In figure 2-19 the 1<sup>st</sup> mode shape is shown and in the red box the resultant factor is given. This factor represents the value with which the loading pattern should be multiplied in order to reach the load under which the structure buckles elastically.

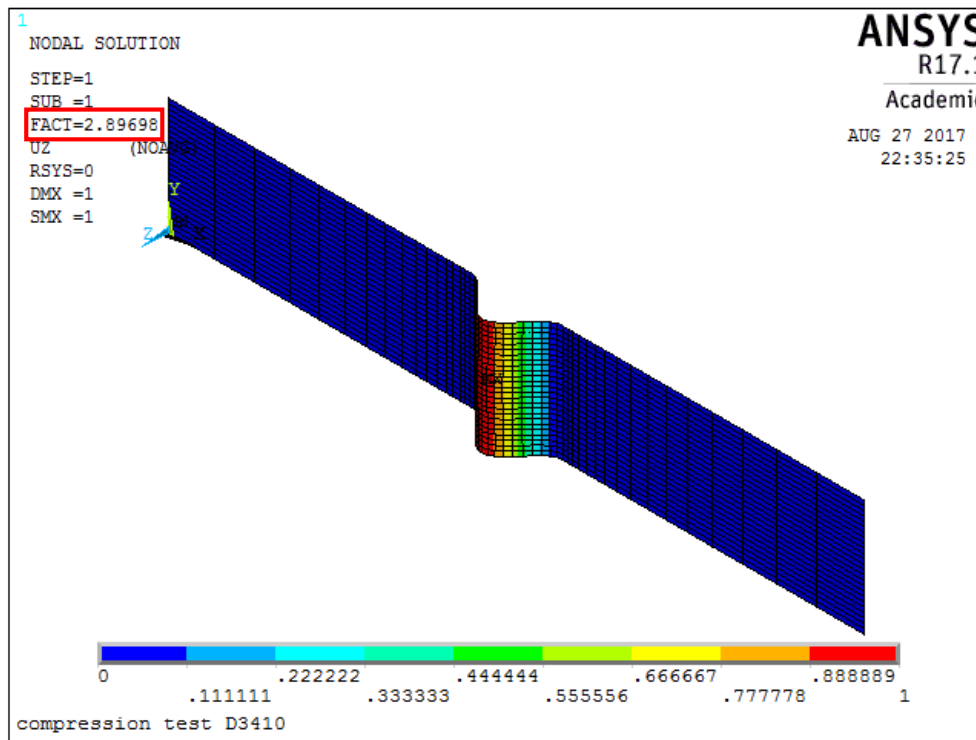


Figure 2-19: Elastic buckling, 1<sup>st</sup> mode's vertical displacement field

$$P_{crit} = XX \text{ kN}$$

Note: No focus should be given to the actual values of the vertical displacements shown in figure 2-19. Only the relative displacement of the nodes has to be taken into account. The largest displacement in this plot has been normalized to a value of 1.0. If the reader is interested for the rest of the modes, he can run the Ansys script with all the details mentioned above.

### 2.2.1.2 Non-linear static analysis

With the elastic analysis being implemented, the next step is to perform a non-linear static analysis where the large deformation theory is activated. Furthermore, various imperfections were introduced in the coupon which are derived from the 1<sup>st</sup> mode shape (most conservative approach). The static analysis was implemented with the command `antype,0`, the large deformation theory with `nlgeom,on` and the imperfections with `upgeom,"imperfection",1,1,compression test,rst`. At "imperfection" the user can give various values in order to check the effect of the imperfections' magnitude. The value that will be assigned

will represent a factor with which all the displacements/rotations will be multiplied with. Moreover, special attention should be given to this value in order to keep the units correct (*mm* in this case)

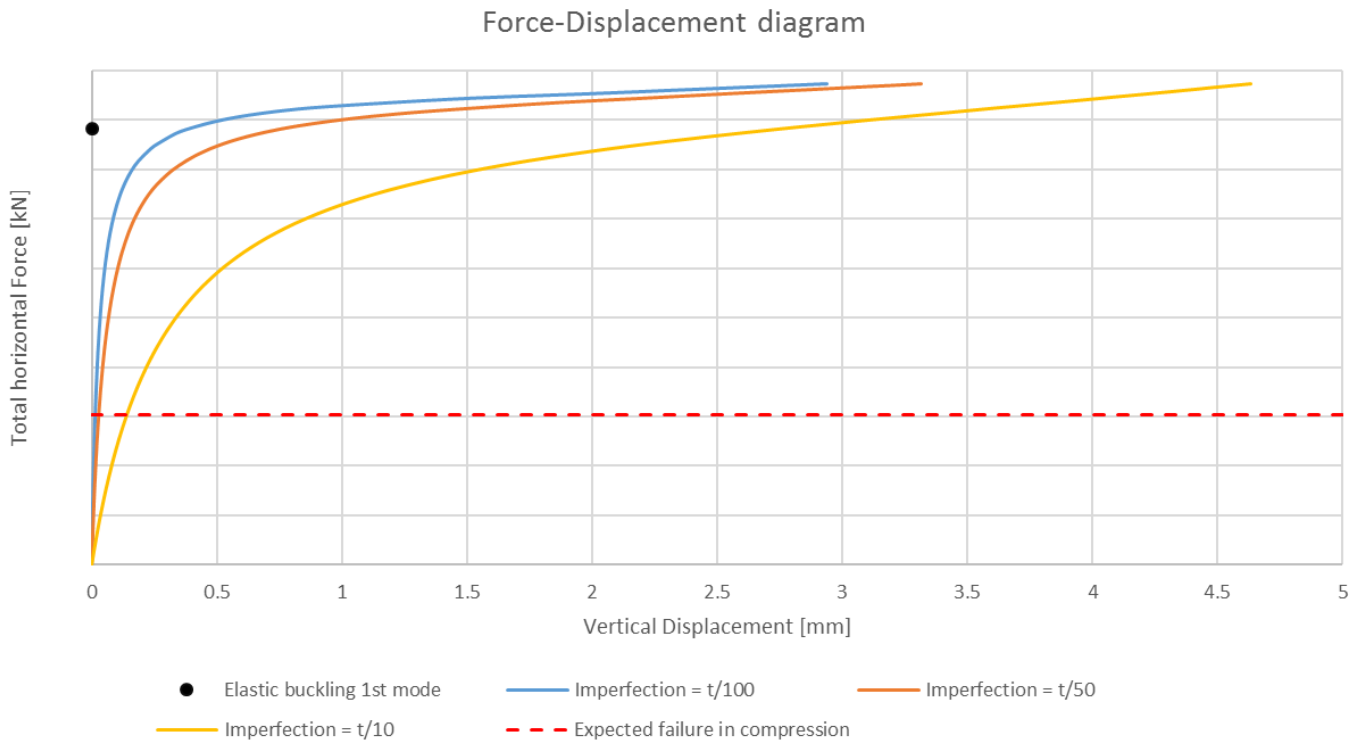


Figure 2-20: Force-displacement diagram, Compressive test with various imperfections

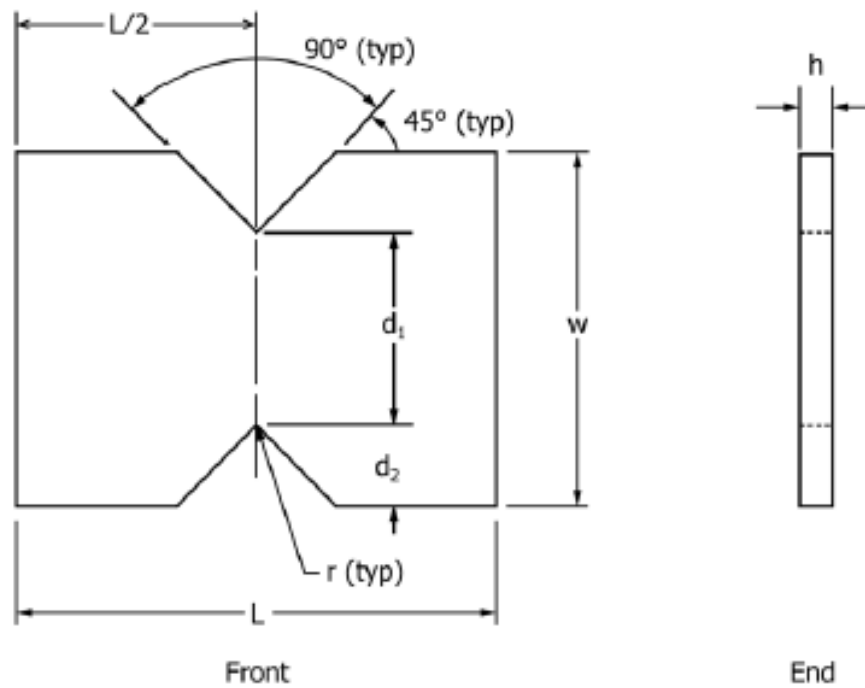
The results show that the coupon will crush before it starts losing its stiffness due to buckling which leads to the conclusion that the design is accepted.

## 2.3 Shear tests

On contrary to the tensile and compressive tests, shear tests are pretty much defined by the respective norm. This norm is the ASTM D7078<sup>[10]</sup> and aims to the determination of the shear properties of high-modulus fibre-reinforced composite materials. The drawings shown in figures 2-19, 2-20, 2-21 follow the exact geometry proposed by the norm. The coupons' thickness is in the range that the norm specifies<sup>[10 §8.2.2.1]</sup> ( $2 \text{ mm} \leq t_{\text{coup}} \leq 5 \text{ mm}$ ) and the fibre alignment was determined according to the norm's suggestions.

The purpose of these tests is to define the following (for each plane):

- Shear stress versus shear engineering strain response,
- Ultimate shear strength,
- Ultimate engineering shear strain,
- Shear chord modulus of elasticity

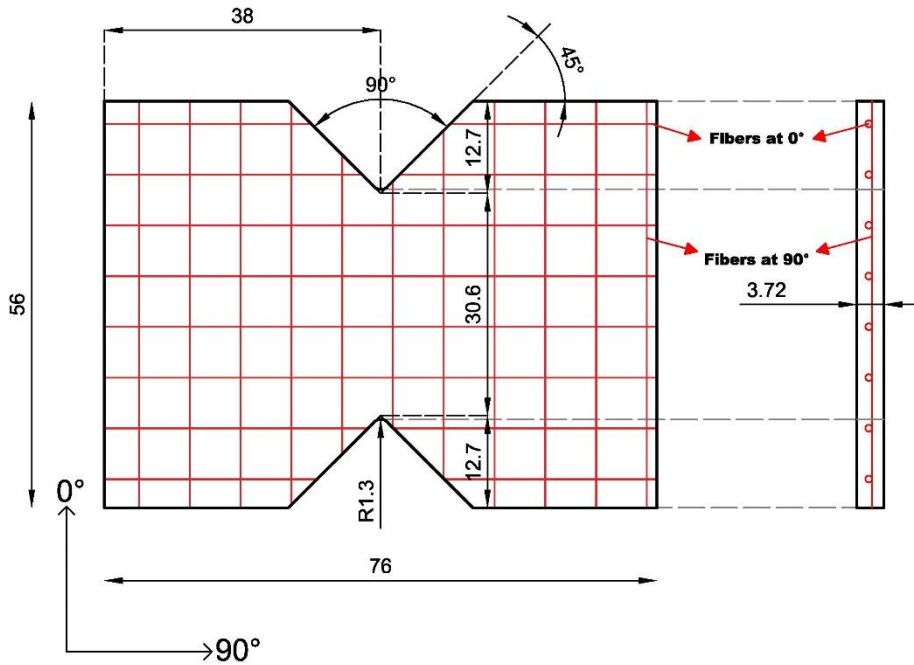
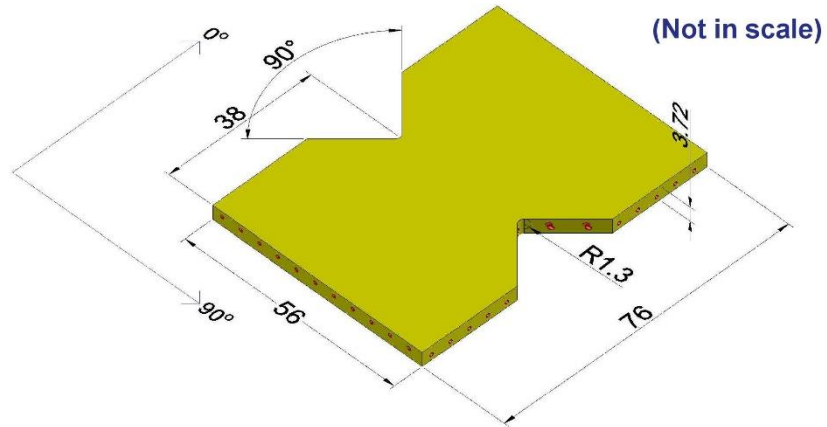


Nominal Specimen Dimensions

- $d_1 = 31.0 \text{ mm [1.20 in.]}$
- $d_2 = 12.7 \text{ mm [0.50 in.]}$
- $h = \text{as required}$
- $L = 76.0 \text{ mm [3.0 in.]}$
- $r = 1.3 \text{ mm [0.05 in.]}$
- $w = 56.0 \text{ mm [2.20 in.]}$

Figure 2-21: V-Notched Rail Shear Test Specimen Schematic<sup>[10 §4.1]</sup>

Coupon				
LAYER NR.	MATERIAL [LAYER NR. 1 IS MOULD SIDE]	ANGLE [°]	THICKNESS [mm]	CHK.
1		[90/0]	0.93	
2		[90/0]	0.93	
3		[0/90]	0.93	
4		[0/90]	0.93	
TOTAL THICKNESS [mm]			3.72	mm.



**Production Method:**  
Vacuum Infusion

**Material Specification:**

**Resin:**

Applied according to manufacturer's recommendations

**Thickness based of fiber volume fraction:**

$V_f =$

**Post Cure:**

**Cutting Method:**

Water-cooled diamond plated cutter

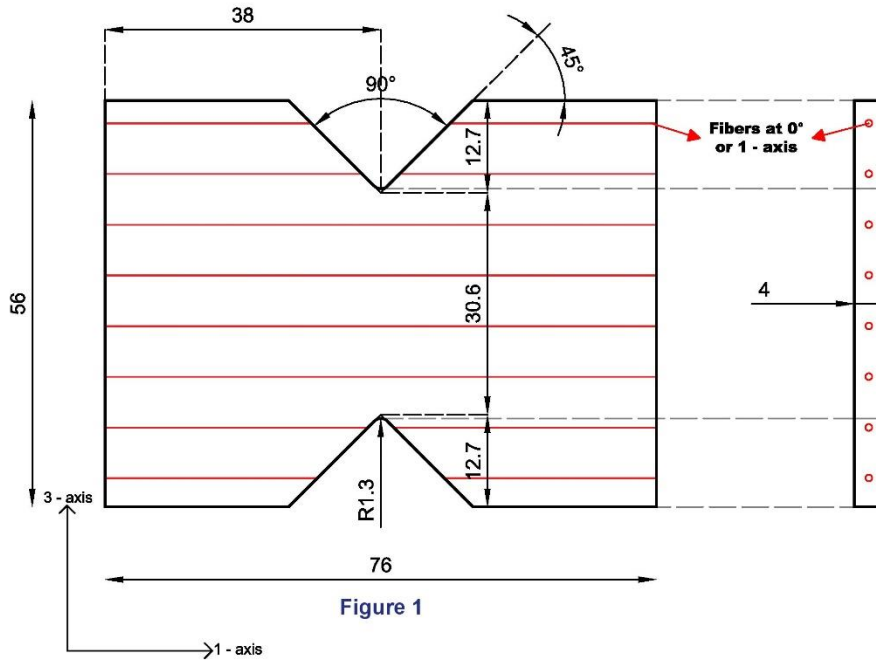
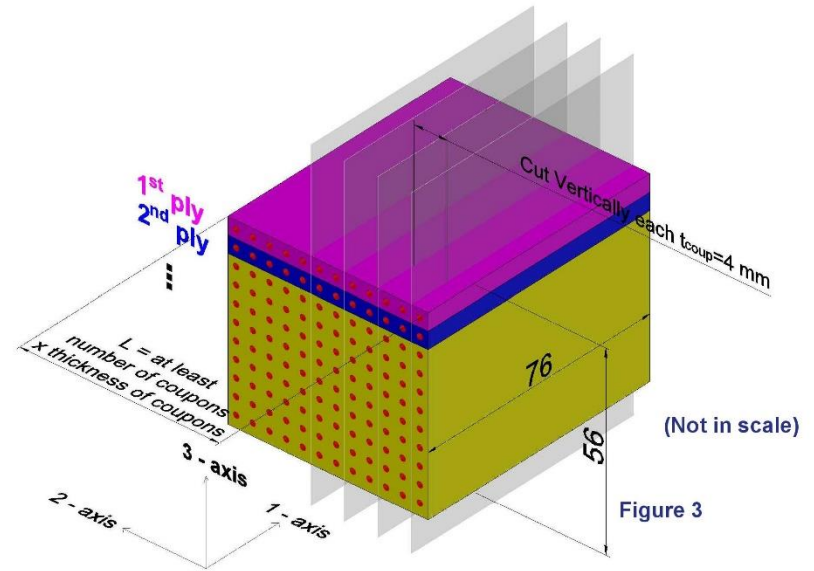
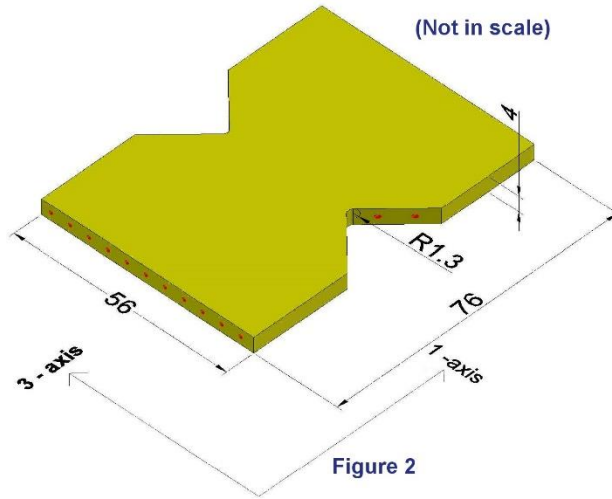
**Norm:**

ASTM D7078

<b>Tolerance on Machining:</b>	<b>Tolerances on Dimensions:</b>	<b>DAMEN</b> DAMEN SCHELDE NAVAL SHIPBUILDING		Damen Schelde Naval Shipbuilding De Willem Ruysstraat 99 4381 Vlissingen P.O. BOX 555 4380 AN Vlissingen (The Netherlands)	
		<b>Project:</b> EK 1081		<b>Title:</b> Shear Coupon Test at 1-2 plane [0°/90°] <sub>2s</sub>	
<b>Finish on machined edges not to exceed 1.6√. Finish on V-notch not to exceed 0.8√. Roughness height in micrometers</b>	<b>No decimal</b> ±2.5 mm <b>One decimal, 0.X</b> ±0.75 mm <b>Two decimals, 0.XX</b> ±0.25 mm <b>All angles(inc. ply orientation):</b> ±0.5°	<b>Drawing Nr:</b> 5	<b>Scale:</b> 1.5:1	<b>Size:</b> A3	<b>Dimensions:</b> mm

Figure 2-22: Shear coupon test at 1-2 plane

Coupon				
LAYER NR.	MATERIAL [LAYER NR.1 IS MOULD SIDE]	ANGLE [°]	THICKNESS [mm]	CHK.
1		[0]	0.93	
2		[0]	0.93	
⋮		⋮	⋮	
n (roughly on layers)		[0]	0.93	
TOTAL THICKNESS [mm]			56	mm.



**Production Method:**  
Vacuum Infusion

**Material Specification:**

**Resin:**

Applied according to manufacturer's recommendations

**Thickness based of fiber volume fraction:**  
 $V_f =$

**Post Cure:**

**Cutting Method:**

Water-cooled diamond plated cutter

**Procedure:**

1. Manufacture thick block as shown in fig. 3 with only UD at 1 - axis
2. Cut vertically as shown in the gray planes at the same figure
3. Give "butterfly" shape

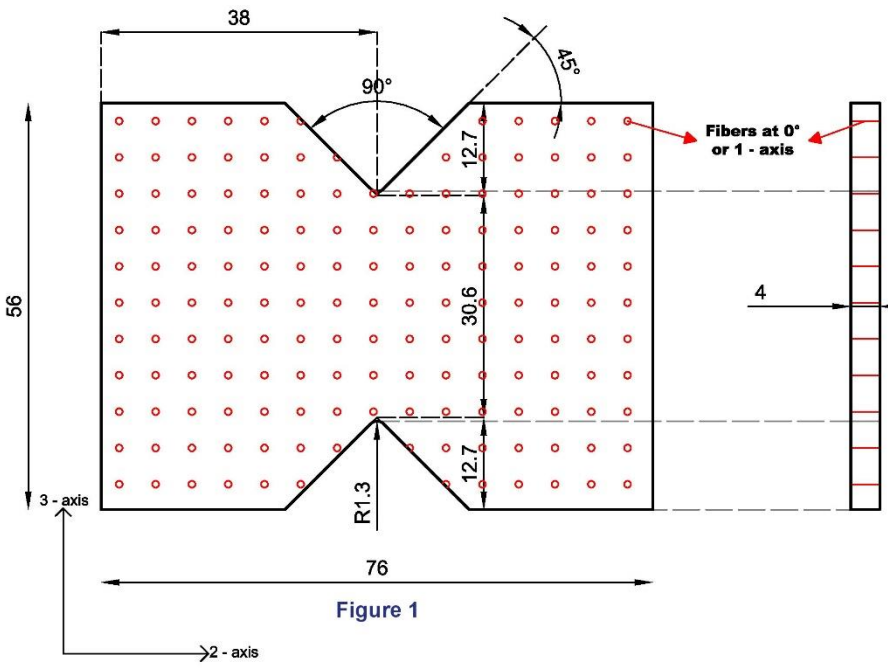
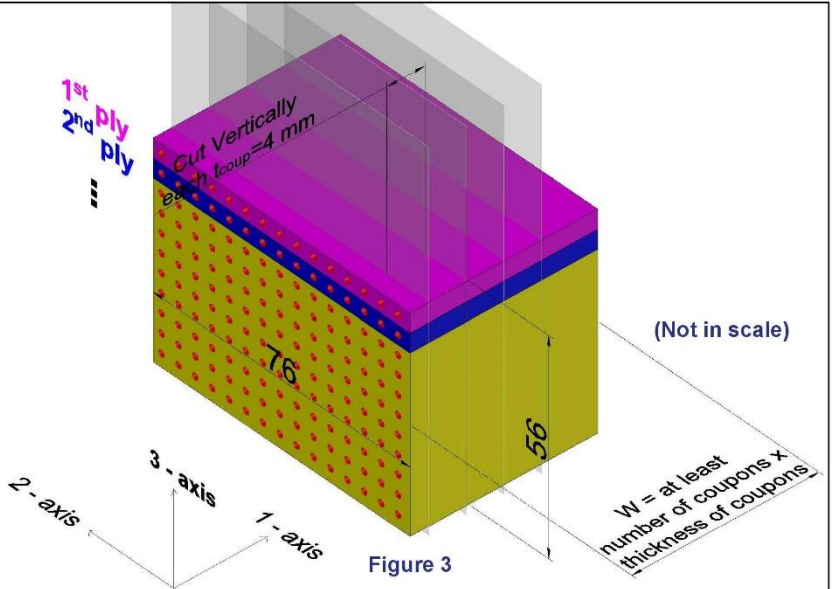
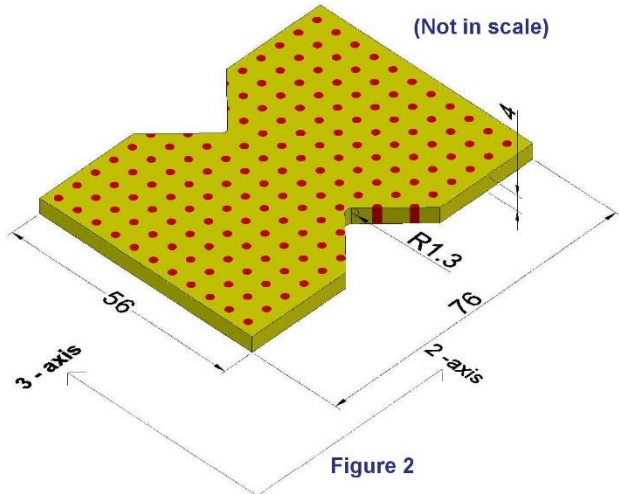
**Norm:**

ASTM D7078

<b>Tolerance on Machining:</b>	<b>Tolerances on Dimensions:</b>	<b>DAMEN</b> DAMEN SCHELDE NAVAL SHIPBUILDING	
		Damen Schelde Naval Shipbuilding De Willem Ruysstraat 99 4381 Vlissingen P.O. BOX 535 4380 AN Vlissingen (The Netherlands)	
<b>Finish on machined edges not to exceed 1.6<math>\mu</math>. Finish on V-notch not to exceed 0.8<math>\mu</math>. Roughness height in micrometers</b>	No decimal $\pm 2.5$ mm One decimal, 0.X $\pm 0.75$ mm Two decimals, 0.XX $\pm 0.25$ mm All angles (inc. ply orientation): $\pm 0.5^\circ$	<b>Project:</b>	
		<b>Title</b> (Interlaminar) Shear Coupon Test at 1-3 plane [0°]	
Drawing Nr: 6	Scale: 1.5:1	Size: A3	Dimensions: mm

Figure 2-23: Shear coupon test at 1-3 plane

Coupon				
LAYER NR.	MATERIAL [LAYER NR.1 IS MOULD SIDE]	ANGLE [°]	THICKNESS [mm]	CHK.
1		[0]	0.93	
2		[0]	0.93	
⋮		⋮	⋮	
n (roughly 60 layers)		[0]	0.93	
TOTAL THICKNESS [mm]			86	mm.



**Production Method:**  
Vacuum Infusion

**Material Specification:**  
|

**Resin:**

Applied according to manufacturer's recommendations

**Thickness based of fiber volume fraction:**  
 $V_f =$

**Post Cure:**

**Cutting Method:**  
Water-cooled diamond plated cutter

**Procedure:**

1. Manufacture thick block as shown in fig. 3 with only UD at 1 - axis
2. Cut vertically as shown in the gray planes at the same figure
3. Give "butterfly" shape

**Norm:**  
ASTM D7078

<b>Tolerance on Machining:</b>	<b>Tolerances on Dimensions:</b>	<b>DAMEN</b> DAMEN SCHELDE NAVAL SHIPBUILDING		Damen Scheide Naval Shipbuilding De Willem Ruysstraat 99 4381 Vlissingen P.O. BOX 555 4380 AN Vlissingen (The Netherlands)	
		<b>Project:</b>		<b>Title</b> (Interlaminar) Shear Coupon Test at 2-3 plane [0°]	
<b>Finish on machined edges not to exceed 1.6√. Finish on V-notch not to exceed 0.8√. Roughness height in micrometers</b>	<b>No decimal ±2.5 mm</b> <b>One decimal, 0.X ±0.75 mm</b> <b>Two decimals, 0.XX ±0.25 mm</b> <b>All angles(inc. ply orientation): ±0.5°</b>	Drawing Nr: 7	Scale: 1.5:1	Size: A3	Dimensions: mm

Figure 2-24: Shear coupon test at 2-3 plane

## 2.4 Fibre volume and density tests

Specialists in the area know that the production methods cannot be perfect and as a result, deviations between the real structures and the designs can be expected. One of these deviations is the fibre volume which was specified as  $V_f = XX\%$  during the design phase. Hence, the panels produced from KVE which are shown at fig. (2-25 till 2-30), had to be checked in order to verify their quality. That was done by burning certain pieces (at various positions) of the panels from which the coupons were extracted by cutting at the specified locations. By ignition, one can remove the matrix from the structure, leaving the reinforcement essentially unaffected. Then, the reinforcement can be calculated by measuring the weight or the volume before and after the ignition. The results for the various panels are shown in the main body of the thesis. For the calculation of the fibre volume, the norm ASTM D3171-15<sup>[20]</sup> was followed

Apart from the fibre volume, the density of the composite,  $\rho$ , had to be measured in order to have the material's library complete. That was done by following the norm ASTM D792-13<sup>[21]</sup>.

Further explanation of these tests is not presented here because it will be a presentation of what the norms suggest. Hence, readers that are interested in how these tests are being performed are suggested to visit Ref. [20-21].

## 2.5 Out-of-plane Poisson's ratios

No tests were implemented for the determination of the out-of-plane Poisson's ratios. It was assumed that  $\nu_{12} = \nu_{13}$  and that  $\nu_{23}$  was calculated according to Ref. [22] as shown below:

$$\begin{aligned}
 K_p &= \frac{E_{p1}}{3 - 6 \cdot \nu_{p12}} \\
 G_{p12} &= \frac{E_{p1}}{2 \cdot (1 + \nu_{p12})} \\
 \zeta &= \frac{[K_p/G_{p12}]}{[K_p/G_{p12}] + 2} \\
 \nu_{23} &= \frac{\zeta \cdot (3 - 4 \cdot \nu_{12}^2) - 1}{\zeta + 1}
 \end{aligned}
 \tag{2.5.1}$$

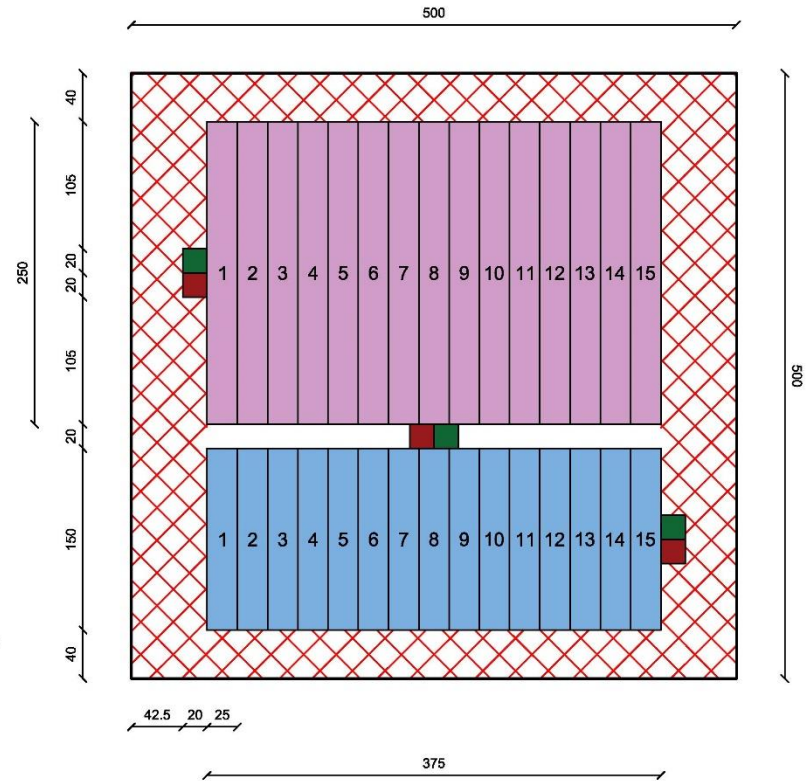
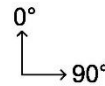
$K_p$  = Bulk modulus of polymer

$E_{p1}$  = longitudinal modulus of polymer (table 1 – 6)

$\nu_{p12}$  = Poisson's ratio of Polymer<sup>[23]</sup>

Coupon				
LAYER NR.	MATERIAL [LAYER NR.1 IS MOULD SIDE]	ANGLE [°]	THICKNESS [mm]	CHK.
1		[0]	0.93	
2		[0]	0.93	
3		[0]	0.93	
4		[0]	0.93	
TOTAL THICKNESS [mm]			3.72	mm.

-  Tensile Test 0°
-  Compressive Test 0°
-  Margin for cuts
-  Density Test
-  Fibre Volume test



Fiber direction: 0°

**Production Method:**  
Vacuum Infusion

**Material Specification:**

**Resin:**

Applied according to manufacturer's recommendations

**Cutting Method:**  
Water-cooled diamond plated cutter

**Thickness based on fiber volume fraction:**  
 $V_f =$

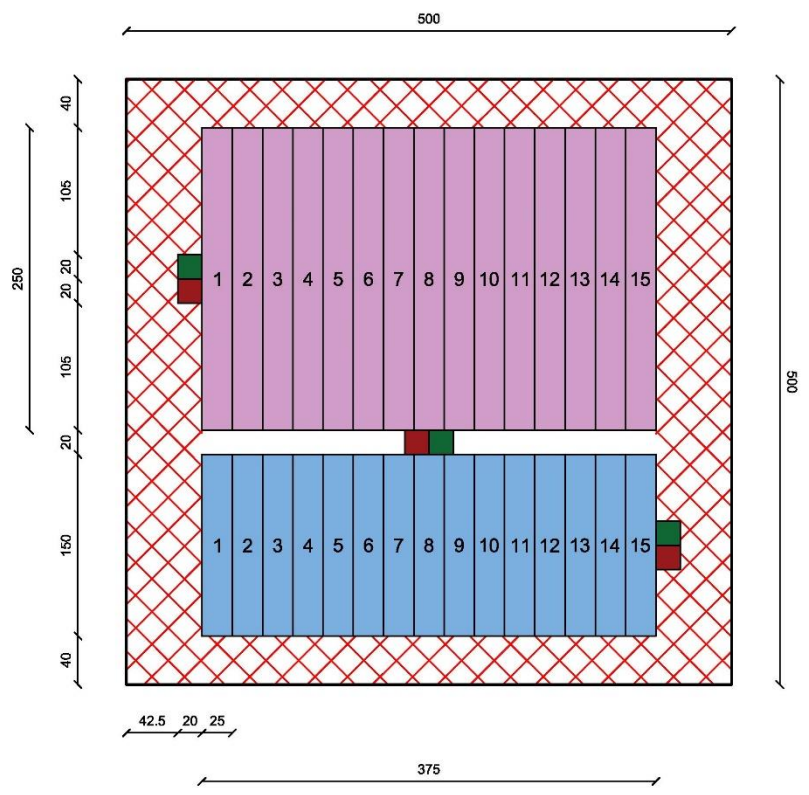
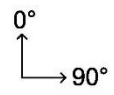
**Post Cure:**

<b>Tolerance on Machining:</b>	<b>Tolerances on Coupons:</b>	<b>DAMEN</b> DAMEN SCHELDE NAVAL SHIPBUILDING		Damen Schelde Naval Shipbuilding De Willem Ruysstraat 99 4381 Vlissingen P.O. BOX 555 4380 AN Vlissingen (The Netherlands)	
		<b>Project:</b>		<b>Title</b>	
<b>Finish on machined edges not to exceed 1.6√. Roughness height in micrometers</b>	<b>Length's tolerance (tensile tests) ±2.5 mm</b> <b>Length's tolerance (compressive tests) ±0.25 mm</b> <b>Width's tolerance ±0.25 mm</b>	<b>Tensile and compressive coupons (0°)</b>			
		Drawing Nr: i	Scale: 1:4	Size: A3	Dimensions: mm

Figure 2-25 Panel with fibers at 0°. Produced by KVE

Coupon				
LAYER NR.	MATERIAL [LAYER NR.1 IS MOULD SIDE]	ANGLE [°]	THICKNESS [mm]	CHK.
1		[90]	0.93	
2		[90]	0.93	
3		[90]	0.93	
4		[90]	0.93	
TOTAL THICKNESS [mm]			3.72	mm.

-  Tensile Test 90°
-  Compressive Test 90°
-  Margin for cuts
-  Density Test
-  Fibre Volume test



Fiber direction: 90°

**Production Method:**  
Vacuum Infusion

**Material Specification:**

**Resin:**

Applied according to manufacturer's recommendations

**Cutting Method:**  
Water-cooled diamond plated cutter

**Thickness based on fiber volume fraction:**  
 $V_f =$

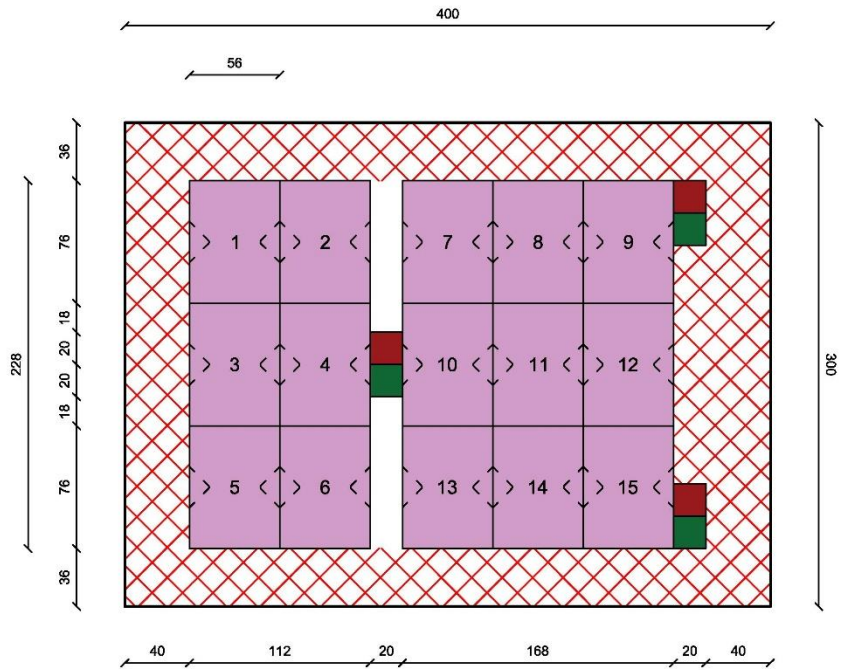
**Post Cure:**

<b>Tolerance on Machining:</b>	<b>Tolerances on Coupons:</b>				
		Damen Schelde Naval Shipbuilding De Willem Ruysstraat 99 4381 Vlissingen P.O. BOX 555 4380 AN Vlissingen (The Netherlands)			
<b>Finish on machined edges not to exceed 1.6√. Roughness height in micrometers</b>	<b>Length's tolerance (tensile tests) ±2.5 mm</b>  <b>Length's tolerance (compressive tests) ±0.25 mm</b>  <b>Width's tolerance ±0.25 mm</b>	<b>Project:</b>			
		<b>Title</b>			
		Drawing Nr:	Scale:	Size:	Dimensions:
		ii	1:4	A3	mm

Figure 2-26 Panel with fibers at 90°. Produced by KVE

Coupon				
LAYER NR.	MATERIAL [LAYER NR.1 IS MOULD SIDE]	ANGLE [°]	THICKNESS [mm]	CHK.
1		[90/0]	0.93	
2		[90/0]	0.93	
3		[0/90]	0.93	
4		[0/90]	0.93	
TOTAL THICKNESS [mm]			3.72	mm.

-  Shear Test xy
-  Margin for cuts
-  Density Test
-  Fibre Volume test



Fiber direction:  $[0^\circ/90^\circ]_{2s}$

Production Method:

Cutting Method:

Water-cooled diamond plated cutter

Note: The outer fibers should be at  $0^\circ$  direction

Material Specification:

Thickness based on fiber volume fraction:

$V_f =$

Resin:

Applied according to manufacturer's recommendations

Post Cure:

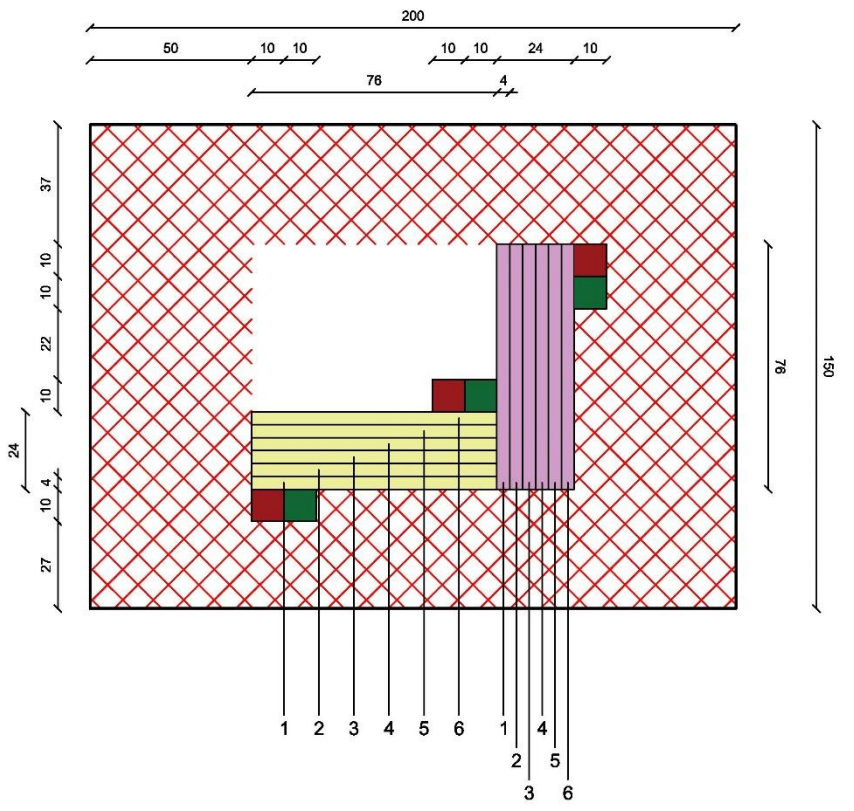
Post cure at  $50^\circ\text{C}$  during 24h

Tolerance on Machining:	Tolerances on Coupons:	 <small>DAMEN SCHELDE NAVAL SHIPBUILDING</small>				<small>Damen Schelde Naval Shipbuilding De Willem Ruysstraat 99 4381 Vlissingen P.O. BOX 555 4380 AN Vlissingen (The Netherlands)</small>			
		Project: _____							
Finish on machined edges not to exceed 1.6√. Finish on V-notch not to exceed 0.8√. Roughness height in micrometers	No decimal $\pm 2.5$ mm  One decimal, 0.X $\pm 0.75$ mm  Two decimals, 0.XX $\pm 0.25$ mm  All angles(inc. ply orientation): $\pm 0.5^\circ$	Title <p style="text-align: center;"><b>Shear coupons xy</b></p>							
		Drawing Nr:	Scale:	Size:	Dimensions:				
		iii	1:3	A3	mm				

Figure 2-27 Panel with fibers at  $0^\circ/90^\circ$ . Produced by KVE

Coupon				
LAYER NR.	MATERIAL [LAYER NR.1 IS MOULD SIDE]	ANGLE [°]	THICKNESS [mm]	CHK.
1		[0]	0.93	
2		[0]	0.93	
⋮		⋮	⋮	
n (roughly 60 layers)		[0]	0.93	
TOTAL THICKNESS [mm]			56	mm.

-  Shear Test xz
-  Shear Test yz
-  Margin for cuts
-  Density Test
-  Fibre Volume test



Fiber direction: [0°]<sub>n</sub>

**Production Method:**  
Vacuum Infusion

**Material Specification:**  
|

**Resin:**  
|  
Applied according to manufacturer's recommendations

**Cutting Method:**  
Water-cooled diamond plated cutter

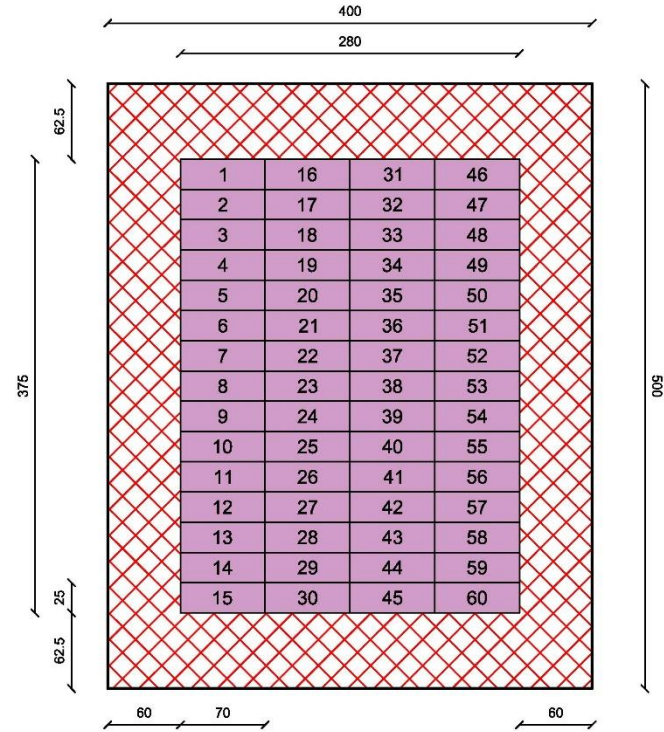
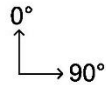
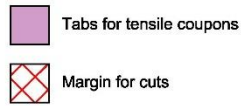
**Thickness based on fiber volume fraction:**  
 $V_f =$

**Post Cure:**

<b>Tolerance on Machining:</b>  Finish on machined edges not to exceed 1.6√. Finish on V-notch not to exceed 0.8√. Roughness height in micrometers	<b>Tolerances on Coupons:</b>  No decimal ±2.5 mm One decimal, 0.X ±0.75 mm Two decimals, 0.XX ±0.25 mm All angles(inc. ply orientation): ±0.5°	<b>DAMEN</b> DAMEN SCHELDE NAVAL SHIPBUILDING			
		Damen Scheide Naval Shipbuilding De Willem Ruysstraat 99 4381 Vlissingen P.O. BOX 555 4380 AN Vlissingen (The Netherlands)			
<b>Project:</b>		<b>Title</b> Shear coupons xz & yz			
Drawing Nr: iv	Scale: 1:1.5	Size: A3	Dimensions: mm		

Figure 2-28 Thick panel with fibers at 0°. Produced by KVE

Tabs for compressive coupons				
LAYER NR.	MATERIAL [LAYER NR.1 IS MOULD SIDE]	ANGLE [°]	THICKNESS [mm]	CHK.
1		[-45/45]	0.93	
2		[45/-45]	0.93	
TOTAL THICKNESS [mm]			1.86	mm.



**Fiber direction:** [45°/-45]s

**Production Method:**  
Vacuum Infusion

**Cutting Method:**  
Water-cooled diamond plated cutter

**Note:** The outer fibers should be at 45° direction

**Material Specification:**

**Thickness based on fiber volume fraction:**  
 $V_f =$

**Procedure:**

**Resin:**

**Post Cure:**

1. Cut each of the four column of tabs (first column numbered from 1 to 15).

Applied according to manufacturer's recommendations

2. Bond these columns to 15 tensile coupons which are not yet separated.

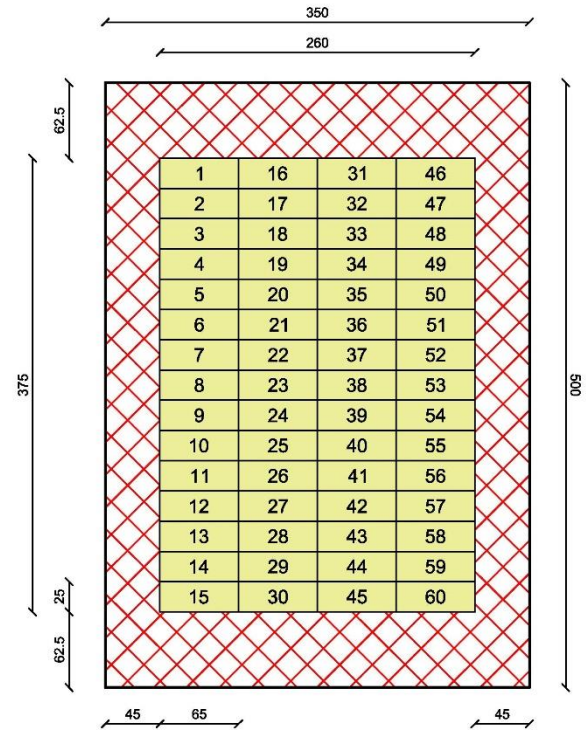
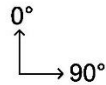
3. Cut to individual coupons ready to be tested

<b>Tolerance on Machining:</b>	<b>Tolerances on Tabs:</b>	<b>DAMEN</b> DAMEN SCHELDE NAVAL SHIPBUILDING		Damen Scheide Naval Shipbuilding De Willem Ruysstraat 99 4381 Vlissingen P.O. BOX 555 4380 AN Vlissingen (The Netherlands)	
		<b>Project:</b>		<b>Title</b> Tabs to be used for tensile tests	
<b>Finish on machined edges not to exceed 1.6√. Roughness height in micrometers</b>	<b>Length's tolerance ±2.5 mm</b> <b>Width's tolerance ±0.25 mm</b>	Drawing Nr: v	Scale: 1:4	Size: A3	Dimensions: mm

Figure 2-29 Panel with fibers at ±45°. Produced by KVE for the tabs used in tensile tests

Tabs for compressive coupons				
LAYER NR.	MATERIAL [LAYER NR.1 IS MOULD SIDE]	ANGLE [°]	THICKNESS [mm]	CHK.
1		[90/0]	0.93	
2		[0/90]	0.93	
TOTAL THICKNESS [mm]			1.86	mm.

 Tabs for compressive coupons  
 Margin for cuts



**Fiber direction:** [0°/90°]<sub>s</sub>

**Production Method:**  
Vacuum Infusion

**Cutting Method:**  
Water-cooled diamond plated cutter

**Note:** The outer fibers should be at 0° direction

**Material Specification:**

**Thickness based on fiber volume fraction:**  
 $V_f =$

**Procedure:**

Follow the same procedure used at tensile tests. (design # v)

**Resin:**

Applied according to manufacturer's recommendations

**Post Cure:**  
Post cure at 50°C during 24h

<b>Tolerance on Machining:</b>  Finish on machined edges not to exceed 1.6√. Roughness height in micrometers	<b>Tolerances on Tabs:</b>  Length's tolerance ±0.25 mm Width's tolerance ±0.25 mm	<b>DAMEN</b> DAMEN SCHELDE NAVAL SHIPBUILDING		Damen Schelde Naval Shipbuilding De Willem Ruysstraat 99 4381 Vlissingen P.O. BOX 555 4380 AN Vlissingen (The Netherlands)	
		<b>Project:</b>		<b>Title</b> <b>Tabs to be used for compressive tests</b>	
Drawing Nr: vi	Scale: 1:4	Size: A3	Dimensions: mm		

Figure 2-30: Panel with fibers at 0°/90°. Produced by KVE for the tabs used in compressive tests

---

## 2.6 References

- [2.1] ASTM International, Standard Test Method for Tensile Properties of Polymer Matrix Composite Materials, D3039/D3039M-14, Approved: 15 May 2014, DOI: 10.1520/D3039\_D3039M-14
- [2.2] Technical Datasheet, Hysol EA 9394, Epoxy Paste adhesive. Structural paste Adhesive, source: [http://www.northerncomposites.com/docs/default-source/data-sheets/hysol\\_ea\\_9394-en15a40c281cc2688d932fff000006e6f6.pdf?sfvrsn=2](http://www.northerncomposites.com/docs/default-source/data-sheets/hysol_ea_9394-en15a40c281cc2688d932fff000006e6f6.pdf?sfvrsn=2) (LV: 10/ 11/ 2017)
- [2.3] ASM Handbook, Volume 21, Composites, ASM International
- [2.4] US Department of Transportation, Federal Aviation administration, Tabbing Guide for Composite test specimens, October 2002, final report, source: <http://www.tc.faa.gov/its/worldpac/techrpt/ar02-106.pdf> (LV: 10/ 11/ 2017)
- [2.5] Ansys Mechanical User's Guide, help manual v.17.1
- [2.6] Robert M. Jones, Mechanics of Composite Materials, 1<sup>st</sup> edition, 1975, ISBN: 0-07-03790-4
- [2.7] D.J. Lekou, PhD thesis, Reliability determination for the design of structures made by composite materials", 2010, [Greek]
- [2.8] G. Odegard, M. Kumosa, Determination of shear strength of unidirectional composite materials with the Iosipescu and 10° axis shear tests, Composites Science and Technology 60 (2000) 2917
- [2.9] ASTM International, Standard Test Method for Compressive Properties of Polymer Matrix Composite Materials, with Unsupported Gage Section by shear Loading, D3410/D410M-03, Approved: 1 Sept 2008,, DOI: 10.1520/D3410\_D3410M-03R08.
- [2.10] ASTM Standard Test Method for Shear Properties of Composite materials by V-notched Rail Shear Method, D7078/D7078M-12, Approved: 15 June 2012,, DOI: 10.1520/D7078\_D7078M-12
- [2.11] h-Method and p-Method, Anonymous, 2014, source: <https://deust.wordpress.com/2014/11/30/h-method-p-method/> ((LV: 10/ 11/ 2017)
- [2.12] US Department of Transportation, Federal Aviation administration, Shear Stress-Strain Data for Structural Adhesives, November 2002, source: <http://www.tc.faa.gov/its/worldpac/techrpt/ar02-97.pdf> (LV: 10/ 11/ 2017)
- [2.13] Henk den Besten, Fatigue and Fracture in Marine Structures, Lecture Notes, OE4631#03
- [2.14] Robert D. Cook, David S. Malkus, Michael E. Plesha, Robert J. Witt, Concepts and Applications of Finite Element Analysis, 4th Edition,(2002), ISBN-13: 978-0471356059
- [2.15] Klaus-Jurgen Bathe, Finite Element Procedures,(1996), ISBN: 0-13-301458-4
- [2.16] Edmund Wittbrodt, Marek Szczotka, Andrzej Maczyński, Rigid Finite Element Method in Analysis of Dynamics of Offshore Structures,(2012), ISBN-13: 978-3642298851
- [2.17] Ever J. Barbero, finite element analysis of composite materials using Ansys®, 2nd Edition, (2014), ISBN-13: 978-1-4665-1690-8
- [2.18] Hughes, Owen F.; Paik, Jeom Kee, Ship Structural Analysis and Design, (2010), ISBN: 978-0-939773-78-3
- [2.19] KVE Composites Group, source: <https://www.kve.nl> (LV: 10/ 11/ 2017)
- [2.20] ASTM International, Standard Test Method for Constituent Content of Composite materials, D3171/15, Approved: 1 April 2015, DOI: 10.1520/D3171-15

---

[2.21] ASTM International, Standard Test Method for Density and Specific Gravity (Relative Density) of Plastics by displacement, D792-13, Approved: 1 November 2013, DOI: 10.1520/D0792-13.

[2.22] Prediction of composite mechanical properties (Theory), source:

<https://knowledge.autodesk.com/support/moldflow-insight/learn-explore/caas/CloudHelp/cloudhelp/2018/ENU/MoldflowInsight/files/GUID-CAEAE1AD-36FA-4BF1-8A09-0F1B91C9FE41-htm.html> (LV: 3-1-2018)

[2.23] H. Ku, V. Kota; M. Trada, Optimum Percentage of Fly Ash Reinforcement in XX Composites, Technical Notes, journal of materials in civil engineering © ASCE / January 2010, DOI: 10.1061/(ASCE)0899-1561(2010)22:1(104)



# Chapter 3: Statistics

The results shown at the [last sub-chapter](#) of [chapter 2](#) will be used to perform a statistical analysis at this chapter. Generally, according to the norms that were used for the coupon testing, i.e. ASTM D3039<sup>[1]</sup>, D3410<sup>[2]</sup>, D7078<sup>[3]</sup>, for the tensile, compressive and shear tests respectively, only the samples' mean and standard deviation should be calculated. However, at this thesis, the statistical analysis goes one step further by assigning distributions to the material's strength and stiffness properties. Only for the out of plane shear tests, the analysis will be restricted to the samples' mean and standard deviation due to their increased production and testing costs (only 6 coupons will be tested per plane).

The reader can find here all the statistical tools that were used for the statistical analysis. Briefly, for each material property, the maximum likelihood estimate is used to define the parameters of all the distributions that have been chosen as being the most probable ones to describe the material properties. Then, for each of these distributions the Kolmogorov-Smirnov criterion is applied to check if they can describe the material property at which they are assigned. The next step is to choose the best fit from all the distributions that qualified through the Kolmogorov-Smirnov criterion. Then, the correlation between properties is being investigated for properties that are derived from the same test. For academic reasons, a histogram of these correlations is given in the appendix through the bootstrap method, for readers that want to cross check the correlation of the properties that are part of this thesis' testing plan with their own. Finally, a latin hypercube Monte Carlo simulation is performed which uses as input the distribution that best fits the results for each material property. This last step, will define the spatial variability of the GFRP panels' material properties that are analysed in chapter 5.

## 3.1 Chosen distributions

### 3.1.1 Normal Distribution

The normal distribution is probably the most famous and common used distribution which is also known as the Gaussian distribution. Its probability density function(pdf) is given as:

$$f(x; \mu, \sigma) = \frac{1}{\sigma\sqrt{2\pi}} \exp\left[-\frac{1}{2}\left(\frac{x-\mu}{\sigma}\right)^2\right], \quad \begin{array}{l} -\infty < \mu < \infty \\ \sigma > 0 \\ -\infty < x < \infty \end{array} \quad (3.1.1)$$

The normal distribution was introduced by the French mathematician Abraham de Moivre in 1733<sup>[12]</sup> and one of its first application was due to C.F.Gauss, who used it in 1809 to model observational errors in astronomy<sup>[13]</sup>. Nowadays, it is used to describe several groups of data such as heights of people, measurement errors, blood pressure, points on a test, IQ scores, salaries<sup>[14]</sup> and many more.

The normal distribution is being described by two parameters, namely the mean value “ $\mu$ ” (location parameter) and the standard deviation “ $\sigma$ ” (shape parameter). It is symmetric around the mean which means that half of the data will fall left to the mean and half at the right part. A typical pdf of a normal distribution is shown below:

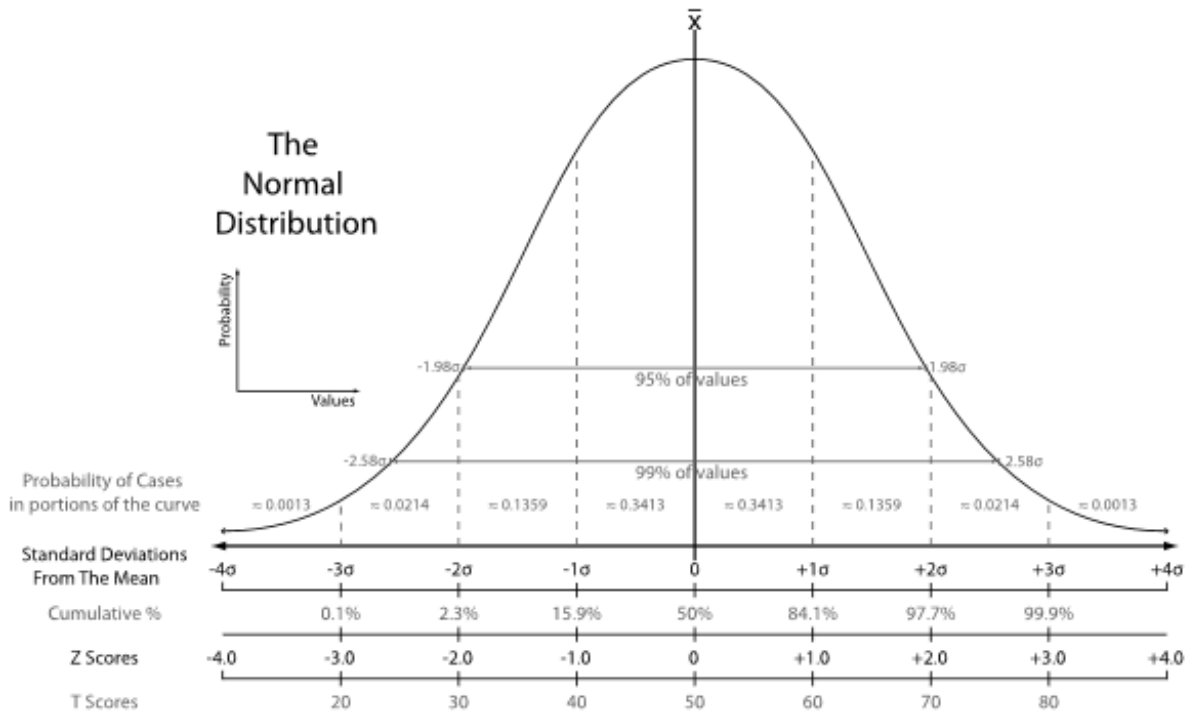


Figure 3-1: Empirical Rule for normal distribution<sup>[15]</sup>

A special case of the normal distribution is the standard normal distribution which is described by  $N(0,1)$ . Its pdf can be written as:

$$\phi(x) = \frac{1}{\sqrt{2\pi}} \exp\left(-\frac{1}{2}x^2\right), \quad -\infty < x < \infty \tag{3.1.2}$$

This form of normal distribution is of great interest because it can compose the intermediate tool towards the estimation of the probability of an event’s occurrence. The procedure is shown below.

Let’s assume that a group of data follows a normal distribution  $N(\mu, \sigma)$  and the probability that a random variable is between two values has to be calculated. In a mathematical form, the following probability has to be calculated:

$$P(a < X \leq b) = \int_a^b \frac{1}{\sigma\sqrt{2\pi}} \exp\left[-\frac{1}{2}\left(\frac{X-\mu}{\sigma}\right)^2\right] dx \quad (3.1.3)$$

One way to estimate the probability is to directly calculate the integral. However, it would be much easier if the following transformation takes place first:

$$s = \frac{X - \mu}{\sigma} \quad \text{and} \quad dx = \sigma ds \quad (3.1.4)$$

Then the probability shown in eq.(3.1.3) becomes:

$$P(a < X \leq b) = \frac{1}{\sigma\sqrt{2\pi}} \int_{(a-\mu)/\sigma}^{(b-\mu)/\sigma} \exp\left(-\frac{1}{2}s^2\right) \sigma ds = \frac{1}{\sqrt{2\pi}} \int_{(a-\mu)/\sigma}^{(b-\mu)/\sigma} \exp\left(-\frac{1}{2}s^2\right) ds \quad (3.1.5)$$

It is easily observed that now the values of the standard normal cumulative distribution function have to be estimated. These values are shown in Appendix A and as a result the aforementioned probability is equal to:

$$P(a < X \leq b) = \Phi\left(\frac{b-\mu}{\sigma}\right) - \Phi\left(\frac{a-\mu}{\sigma}\right) \quad (3.1.6)$$

Hence, with the help of the table at [Appendix A](#), the probability of an event that follows any normal distribution  $N(\mu, \sigma)$  can be calculated if the mean and the standard deviation are known.

### 3.1.2 Gamma ( $\Gamma$ ) distribution

Before one describes the gamma distribution, he should first introduce the Poisson distribution.

There are plenty physical problems where an event can happen at any time(or spatial) spot. These events can sometimes be described as a Poisson process. The necessary characteristics that have to be valid in order to define a process as Poisson, are:

- An event can happen randomly at any time (or spatial) spot.
- The realization of an event in a time (or spatial) interval is independent of the event's realization in any other interval(as long as there is no overlapping of intervals)
- The probability of an event's realization in an interval  $\Delta t$  is proportional to the interval  $\Delta t$  and equal to  $\nu \Delta t$ , where  $\nu$  is the mean of events' realizations in time. The probability of two or more events in the interval  $\Delta t$  is equal to zero.

According to the above, the number of events in  $t$  units of time or space can be modelled with the poisson distribution and more specifically, if  $X_t =$  the number of successes in an interval of  $t$  units of time or space:

$$P(X_t = x) = \frac{(vt)^x}{x!} \exp(-vt), \quad x = 0, 1, \dots \quad (3.1.7)$$

where:

$v = \text{mean number of successes in a unit of time(or space)}$

Regarding the gamma distribution, if the realization of an event follows a Poisson distribution, then the time until the  $k^{\text{th}}$  realization of this event follows a gamma distribution. To further elaborate on that, the cumulative distribution function of an event  $T_k$ , which represents that the event is realized at least  $k$  times ( $T_k < t$ ) in time  $t$ , is:

$$F_{T_k}(t) = \sum_{x=k}^{\infty} P(X_t = x) = 1 - \sum_{x=0}^{k-1} \frac{(vt)^x}{x!} \exp(-vt) \quad (3.1.8)$$

The respective pdf of a gamma function can be found by differentiating the eq.(3.1.8) with respect to  $t$ :<sup>[33]</sup>

$$f_{T_k}(t) = \frac{v(vt)^{k-1}}{(k-1)!} \exp(-vt), \quad t \geq 0 \quad (3.1.9)$$

A different and more usual way to present the pdf of a gamma distribution is:

$$f(x; \lambda, \eta) = \frac{\lambda^\eta}{\Gamma(\eta)} x^{\eta-1} \exp(-\lambda x), \quad \begin{matrix} x \geq 0 \\ \lambda, \eta > 0 \end{matrix} \quad (3.1.10)$$

The eq.(3.1.9) is equivalent to eq.(3.1.10) under the following changes:

- $\lambda = v$
- $k - 1 = \eta$
- The gamma function is:  $\Gamma(\eta) = \int_0^{\infty} x^{\eta-1} \exp(-x) dx$ . One of its properties is:  $\Gamma(\eta) = (\eta - 1)!$ <sup>[6]</sup>

### 3.1.3 Log-normal distribution

A random variable  $X$  has logarithmic probability distribution if the natural logarithm of  $X$ ,  $\ln X$ , is a normal variable. In that case, the pdf of  $X$  will be:

$$f(x; \mu, \sigma) = \frac{1}{\sigma x \sqrt{2\pi}} \exp \left[ -\frac{1}{2} \left( \frac{\ln x - \mu}{\sigma} \right)^2 \right], \quad \begin{array}{l} \mu > 0 \\ \sigma > 0 \\ x > 0 \end{array} \quad (3.1.11)$$

where:

$\mu = E(\ln X)$ , mean value of random variable  $\ln X$

$\sigma = \sqrt{\text{Var}(\ln X)}$ , standard deviation of random variable  $\ln X$

By assuming that:

$$s = \frac{\ln X - \mu}{\sigma} \quad \text{and} \quad dx = x \sigma ds \quad (3.1.12)$$

the probability:

$$P(a < X \leq b) = \int_a^b \frac{1}{\sigma x \sqrt{2\pi}} \exp \left[ -\frac{1}{2} \left( \frac{\ln x - \mu}{\sigma} \right)^2 \right] \quad (3.1.13)$$

becomes:

$$P(a < X \leq b) = \frac{1}{\sqrt{2\pi}} \int_{(\ln a - \mu)/\sigma}^{(\ln b - \mu)/\sigma} \exp \left( -\frac{1}{2} s^2 \right) = \Phi \left( \frac{\ln b - \mu}{\sigma} \right) - \Phi \left( \frac{\ln a - \mu}{\sigma} \right) \quad (3.1.14)$$

The table of the Standard Normal Cumulative Distribution function is given in [appendix A](#).

### 3.1.4 Weibull Distribution

The fact that the exponential distribution assumes a constant rate of failure (or success) restricts it from defining many events. In many cases, it is more realistic to assume that the rate of failure changes with time and for that reason the Weibull distribution was opted to be included in the family of distributions that are checked in this thesis. The Weibull distribution is a more generic distribution which can transform to an exponential one or a Rayleigh one with proper adjustment of its parameters. The pdf of the Weibull distribution is:

$$f(x; k, \lambda) = \frac{k}{\lambda} \left( \frac{x}{\lambda} \right)^{k-1} \exp \left[ -\left( \frac{x}{\lambda} \right)^k \right], \quad \begin{array}{l} x \geq 0 \\ k, \lambda > 0 \end{array} \quad (3.1.15)$$

where:

$\lambda = \text{scale parameter}$

$k = \text{shape parameter}$

For the special case where  $k = 1$  the Weibull distribution is equivalent to the exponential distribution. Moreover, when  $k = 2$  and  $\lambda = \sqrt{2}\sigma$  the Weibull distribution is equivalent to the Rayleigh one.

Waloddi Weibull; developed this distribution in 1939 and his main area of interest was the strength of materials and fatigue analysis. Generally, it is assumed that the strength of composite materials follows a Weibull distribution as shown in Ref. [22],[23],[24]. Above, the two-parameter version of his distribution is shown which was used for the statistical analysis in this thesis. The three-parameter version is shown below for educational reasons:

$$f(x; k, l, \gamma) = \frac{k}{\lambda} \left( \frac{x - \gamma}{\lambda} \right)^{k-1} \exp \left[ - \left( \frac{x - \gamma}{\lambda} \right)^k \right], \quad \begin{array}{l} x \geq \gamma \\ k, \lambda > 0 \\ -\infty < \gamma < \infty \end{array} \quad (3.1.16)$$

where:

$\gamma = \text{location parameter}$

### 3.1.5 Nakagami distribution

In communications theory, the Nakagami distribution along with the Rician distribution are often used for modelling the transmission in a fading radio-communication channel. Depending on the density of the scatter, the signal will display different fading characteristics. It is fairly a new distribution as it developed in 1960 and it is related to the gamma distribution<sup>[7,8,9]</sup>. Its pdf is:

$$f(x; \mu, \omega) = 2 \cdot \left( \frac{\mu}{\omega} \right)^\mu \frac{1}{\Gamma(\mu)} x^{2\mu-1} \exp \left( - \frac{\mu}{\omega} x^2 \right), \quad \begin{array}{l} \mu \geq 0.5 \\ \omega > 0 \\ x > 0 \end{array} \quad (3.1.17)$$

where:

$\mu = \text{shape parameter}$

$\omega = \text{scale parameter}$

If a random variable  $X$  follows a Nakagami distribution with shape parameter  $\mu$  and scale parameter  $\omega$ , then  $X^2$  follows a gamma distribution with shape parameter  $\mu$  and scale parameter  $\omega/\mu$ . To further elaborate on that, when the gamma pdf is defined as:

$$f(x; k, \theta) = \frac{1}{\Gamma(k)\theta^k} x^{k-1} \exp\left(-\frac{x}{\theta}\right), \quad \begin{array}{l} k > 0 \\ \theta > 0 \\ x > 0 \end{array} \quad (3.1.18)$$

then, the Nakagami distribution is equivalent to gamma function for  $k = \mu$  and  $\theta = \omega/\mu$  for a random variable  $X^2$ .

- *Proof of Connection between Nakagami and Gamma distribution:*

Suppose that  $X$  is *Nakagami* $[\mu, \omega]$ . Then,  $Y = X^2$  where  $Y$  is *Gamma* $[k = \mu, \theta = \omega/\mu]$ .

$$\text{Prob}(X < k) = \text{Prob}(\sqrt{Y} < k) = \text{Prob}(Y < k^2) =$$

$$\left. \int_0^{k^2} \frac{1}{\Gamma(\mu)(\omega/\mu)^\mu} y^{\mu-1} \exp\left(-\frac{y}{\omega/\mu}\right) dy \right\} = \int_0^k \frac{1}{\Gamma(\mu)(\omega/\mu)^\mu} (x^2)^{\mu-1} \exp\left(-\frac{\mu}{\omega} x^2\right) 2x dx =$$

$$y = x^2, dy = 2x dx$$

$$\int_0^k 2 \cdot \left(\frac{\mu}{\omega}\right)^\mu \frac{1}{\Gamma(\mu)} x^{2\mu-1} \exp\left(-\frac{\mu}{\omega} x^2\right) dx, \quad \text{which corresponds to a Nakagami}[\mu, \omega], \text{ eq. (3.1.17)}$$

### 3.1.6 Logistic

The logistic distribution is used for modelling growth and in logistic regression. Its shape is pretty close to the normal distribution but it has fatter tails (higher kurtosis). For this characteristic, it was chosen to be included in the statistical analysis. Its pdf is:

$$f(x; \mu, \sigma) = \frac{\exp\left(\frac{x - \mu}{\sigma}\right)}{\sigma \left[1 + \exp\left(\frac{x - \mu}{\sigma}\right)\right]^2}, \quad \begin{array}{l} -\infty < \mu < \infty \\ \sigma > 0 \\ -\infty < x < \infty \end{array} \quad (3.1.19)$$

### 3.1.7 Rician:

Similar to Nakagami distribution, Rician is being used in communications theory. Both are used to model scattered signals that reach a receiver by multiple paths<sup>[8]</sup>. Its probability distribution function is:

$$f(x; s, \sigma) = I_0\left(\frac{x s}{\sigma^2}\right) \frac{x}{\sigma^2} \exp\left[-\left(\frac{x^2 + s^2}{2\sigma^2}\right)\right], \quad \begin{array}{l} s \geq 0 \\ \sigma > 0 \\ x > 0 \end{array} \quad (3.1.20)$$

where:

$s$  = noncentrality parameter

$\sigma$  = scale parameter

$I_0$  = the zero – order modified Bessel function of the first kind

$$I_0(z) = \sum_{k=0}^{\infty} (-1)^k \frac{\left(\frac{1}{4}z^2\right)^k}{(k!)^2}, \quad \text{series form} \quad (3.1.21)^{[16]}$$

$$I_0(z) = \frac{1}{\pi} \int_0^{\pi} e^{iz \cos \theta} d\theta, \quad \text{integral form}$$

The derivation of the Rician distribution is a complex procedure and out of the scope of this thesis. Nonetheless, readers that are interested into finding the origins of this distribution can check the Ref. [16,17,18].

To conclude, it is worth-mentioning (for the academic knowledge) that if a random variable  $X$  follows a Rician distribution, then the random variable  $(X/\sigma)^2$  has a noncentral chi-squared distribution with two degrees of freedom,  $n = 2$  and noncentrality parameter  $\lambda = (s/\sigma)^2$ . The pdf of a noncentral chi-squared distribution is:

$$f(x; n, \lambda) = \frac{1}{2} e^{-\frac{(x+\lambda)}{2}} \left(\frac{x}{\lambda}\right)^{n/4-1/2} I_{\frac{n}{2}-1}(\sqrt{\lambda x}) \quad \begin{array}{l} k > 0 \\ \lambda > 0 \\ x \geq 0 \end{array} \quad (3.1.22)^{[20]}$$

where:

$n$  = degrees of freedom

$\lambda$  = noncentrality parameter

The proof follows the same rationale shown above for the relation between *Gamma* and *Nakagami* distributions.

### 3.1.8 Extreme value distributions

It is quite often that one is interested at the distribution of the extreme values of a data group. For example, let's assume that there is a database with wave heights. One can be interested only at the values of the highest wave heights because these are the determining factor for the structural design of an element or the height of a structure in order to avoid flooding. The same rationale can be applied to maximum wind speeds or the minimum values of a material's strength properties. For that reason, this distribution was included in the chosen distributions for this analysis and its pdf is:

$$f(x; \mu, \sigma) = \frac{1}{\sigma} \exp \left\{ \mp \frac{x - \mu}{\sigma} - e^{\mp \frac{x - \mu}{\sigma}} \right\} \quad \begin{array}{l} \sigma > 0 \\ -\infty < x < \infty \end{array} \quad (3.1.23)$$

where:

$\mu$  = location parameter

$\sigma$  = scale parameter

The " - " sign corresponds to the extreme value distribution for maxima whereas the " + " sign corresponds to the distribution for minima. This distribution is known as Fischer-Tippet distribution (type I), the log-Weibull distribution or the Gumbel distribution<sup>[21]</sup>. It is an asymptotic distribution and has been developed for the analysis of either minimum or maximum values which are extracted from different distributions of exponential type such as normal, gamma, exponential and others.

## 3.2 Maximum likelihood estimates

At subchapter 3.1 the distributions that will be used in the statistical analysis of this thesis were presented in detail. The next step is to find a method in order to estimate the parameters of each one distribution according to the experimental results. To keep it simple, let's focus on the tensile strength of the material under investigation when it is loaded in the direction which is parallel to the orientation of the fibres, i.e. at  $0^\circ$ , which is called  $S_{11T}$ . The experimental results are shown at table 2-3 but to keep it general the dataset will be shown in a generic form as  $x_1, x_2, \dots, x_n$  ( $n = 15$  for the case of in plane tests). Basically, through this method, one can estimate which are the most probable values of each distribution's parameters that can describe best the given dataset  $x_i$ . One basic assumption that is used is that the experimental results are independent, i.e. that there is no influence of a specimen's results on another specimen's results. This assumption is valid because the results of  $i^{\text{th}}$  test do not alternate the results of any other test. Factors such as the wear of the testing device are assumed negligible because the apparatus is certified according to the respective norms.

The first step towards the understanding of this method is to define a likelihood function,  $L(\theta)$ . Here,  $\theta$  is a parameter which (in this analysis) has a vector form:  $\theta = [1^{\text{st}} \text{ parameter}; 2^{\text{nd}} \text{ parameter}]$ . This is the case because all the chosen distributions can be fully described by two parameters. For example,  $\theta = [\mu, \sigma]$  in case of the normal distribution. In case that one parameter was enough for the description of the distribution such as the exponential one, then there would be no reason to give  $\theta$  a vector form. Similarly, if there were

3-parameter distributions in the analysis such as the generalized extreme value distribution, then  $\theta$  would be a vector:  $\theta = [1^{st} \text{ parameter} ; 2^{nd} \text{ parameter} ; 3^{rd} \text{ parameter}]$ .

The next step is to define a probability that takes into account the experimental results, i.e. to define a probability to extract these results under the assumption that the results follow one of the chosen distributions. In the analysis, only continuous distributions are included (no discrete ones), hence the probability can be defined as:

$$P(x_1 - \varepsilon, X_1, x_1 + \varepsilon, \dots, x_n - \varepsilon, X_n, x_n + \varepsilon) \Bigg\{ \begin{array}{l} \\ \text{Assumption that } X_i \text{ are independent} \end{array} \right\} = P(x_1 - \varepsilon, X_1, x_1 + \varepsilon) \cdot \dots \cdot P(x_n - \varepsilon, X_n, x_n + \varepsilon) \quad (3.2.1)$$

where:

$\varepsilon = a \text{ small positive value}$

However, it is known that (figure 3-2):

$$P(a - \varepsilon, X_1, a + \varepsilon) = \int_{a-\varepsilon}^{a+\varepsilon} f_{\theta} dx \approx 2\varepsilon f_{\theta}(a) \quad (3.2.2)$$

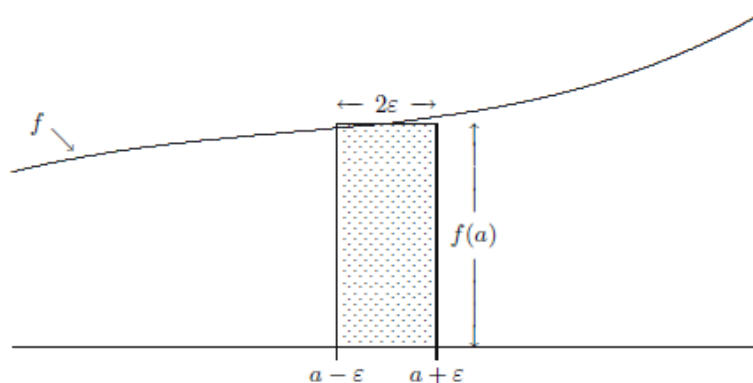


Figure 3-2 Approximating the probability that X lies ε-close to  $a$  [13 § 5.1]

By combining eq.(3.2.1) and eq.(3.2.2)

$$P(x_1 - \varepsilon, X_1, x_1 + \varepsilon, \dots, x_n - \varepsilon, X_n, x_n + \varepsilon) \approx f_{\theta}(x_1) \cdot f_{\theta}(x_2) \cdot \dots \cdot f_{\theta}(x_n) \cdot (2\varepsilon)^n \quad (3.2.3)$$

As it was stated before, the aim of this method is to find the values of  $\theta$  for which the likelihood of getting the experimental results is maximum. Hence, it is sufficient to maximize the probability shown in eq. (3.2.3) and for that reason the likelihood function is defined as:

$$L(\theta) = f_{\theta}(x_1) \cdot f_{\theta}(x_2) \cdot \dots \cdot f_{\theta}(x_n) \quad (3.2.4)$$

By taking the partial derivatives of the likelihood function and equating them to zero, one can find the values of the vector  $\theta$ . For the case of the normal distribution, the following  $2 \times 2$  system has to be solved.

$$\begin{aligned} \frac{\partial L(\mu, \sigma)}{\partial \mu} &= 0 \\ \frac{\partial L(\mu, \sigma)}{\partial \sigma} &= 0 \end{aligned} \quad (3.2.5)$$

The resultant values of  $\mu, \sigma$  will correspond to the mean and the standard deviation of a normal distribution which is the most probable to produce the experimental results of  $S_{11T}$ . This procedure is followed for all the distributions in order to define their parameters for each one of the material properties for which a stochastic analysis is to be performed.

### 3.2.1 Loglikelihood

It can be easily shown at eq.(3.2.5) that the derivations and the solution of the  $2 \times 2$  system can be cumbersome due to the product rule from calculus. Hence, the calculations can become much easier by taking the natural logarithm of the likelihood function because its derivative will result into a sum of logarithms as shown below. In this way, the calculations can become much faster without losing any accuracy at the results. The loglikelihood function is defined as:

$$\ell(\theta) = \ln(L(\theta)) \quad (3.2.6)$$

Let's take again the example with the normal distribution. Its likelihood function as shown in eq. (3.2.4) is:

$$L(\mu, \sigma) = f_{\mu, \sigma}(x_1) \cdot f_{\mu, \sigma}(x_2) \cdot \dots \cdot f_{\mu, \sigma}(x_n) \quad (3.2.7)$$

and its pdf is given at equation (3.1.1):

$$f(x; \mu, \sigma) = \frac{1}{\sigma\sqrt{2\pi}} \exp\left[-\frac{1}{2}\left(\frac{x-\mu}{\sigma}\right)^2\right], \quad \begin{array}{l} -\infty < \mu < \infty \\ \sigma > 0 \\ -\infty < x < \infty \end{array}$$

By combining eq. (3.1.1), (3.2.6) and (3.2.7):

$$\left. \begin{aligned} \ell(\mu, \sigma) = \ln(L(\mu, \sigma)) &= \ln(f_{\mu, \sigma}(x_1) \cdot \dots \cdot f_{\mu, \sigma}(x_n)) = \ln(f_{\mu, \sigma}(x_1)) + \dots + \ln(f_{\mu, \sigma}(x_n)) \\ \ln(f_{\mu, \sigma}(x)) &= -\ln(\sigma) - \ln(\sqrt{2\pi}) - \frac{1}{2} \left( \frac{(x - \mu)^2}{\sigma^2} \right) \end{aligned} \right\} \Rightarrow \quad (3.2.8)$$

$$\Rightarrow \ell(\mu, \sigma) = -n \ln(\sigma) - n \ln(\sqrt{2\pi}) - \frac{1}{2\sigma^2} [(x_1 - \mu)^2 + \dots + (x_n - \mu)^2]$$

The next step is to take the partial derivatives of the loglikelihood function with respect to the mean value  $\mu$  and with respect to the standard deviation  $\sigma$  and then equal them to zero:

$$\frac{\partial \ell(\mu, \sigma)}{\partial \mu} = \frac{1}{\sigma^2} [(x_1 - \mu) + \dots + (x_n - \mu)] = \frac{n}{\sigma^2} (\bar{x}_n - \mu) = 0 \quad (3.2.9)$$

$$\frac{\partial \ell(\mu, \sigma)}{\partial \sigma} = -\frac{n}{\sigma} + \frac{1}{\sigma^3} [(x_1 - \mu)^2 + \dots + (x_n - \mu)^2] = -\frac{n}{\sigma^3} \left( \sigma^2 - \frac{1}{n} \sum_{i=1}^n (x_i - \mu)^2 \right) = 0$$

It can be shown easily from eq. (3.2.9) that the values are the expected ones:

$$\mu = \bar{x}_n$$

$$\sigma = \sqrt{\frac{1}{n} \sum_{i=1}^n (x_i - \mu)^2} \quad (3.2.10)$$

The same procedure is followed for the rest of the distributions with the only alternation to be at the introduction of the respective pdf. At the subchapter 3.1, 9 distributions were depicted and as a result the aforementioned method will be used 9 times for the results of  $S_{11T}$ . Then, the same procedure will be followed for the next material property which is the elastic modulus at the direction which is parallel to the fibers, i.e.  $E_1$ . At the end of this analysis the following results are expected:

	<i>Normal</i> ( $\mu, \sigma$ )	<i>Gamma</i> ( $\lambda, \eta$ )	<i>Lognorma</i> ( $\mu, \sigma$ )	<i>Weibull</i> ( $k, \lambda$ )	<i>Nakagam</i> ( $\mu, \omega$ )	<i>Logistic</i> ( $\mu, \sigma$ )	<i>Rician</i> ( $s, \sigma$ )	<i>Min Extr</i> ( $\mu, \sigma$ )	<i>Max Extr</i> ( $\mu, \sigma$ )
<b>S<sub>11T</sub></b>	$\mu_{n,1}, \sigma_{n,1}$	$\lambda_{g,1}, \eta_{g,1}$	$\mu_{ln,1}, \sigma_{ln,1}$	$k_{w,1}, \lambda_{w,1}$	$\mu_{nak,1}, \omega_{nak,1}$	$\mu_{log,1}, \sigma_{log,1}$	$S_{r,1}, \sigma_{r,1}$	$\mu_{min\ ex,1}, \sigma_{min\ ex,1}$	$\mu_{max\ ex,1}, \sigma_{max\ ex,1}$
<b>E<sub>1</sub></b>	$\mu_{n,2}, \sigma_{n,2}$	$\lambda_{g,2}, \eta_{g,2}$	$\mu_{ln,2}, \sigma_{ln,2}$	$k_{w,2}, \lambda_{w,2}$	$\mu_{nak,2}, \omega_{nak,2}$	$\mu_{log,2}, \sigma_{log,2}$	$S_{r,2}, \sigma_{r,2}$	$\mu_{min\ ex,2}, \sigma_{min\ ex,2}$	$\mu_{max\ ex,2}, \sigma_{max\ ex,2}$
<b>S<sub>11C</sub></b>	$\mu_{n,3}, \sigma_{n,3}$	$\lambda_{g,3}, \eta_{g,3}$	$\mu_{ln,3}, \sigma_{ln,3}$	$k_{w,3}, \lambda_{w,3}$	$\mu_{nak,3}, \omega_{nak,3}$	$\mu_{log,3}, \sigma_{log,3}$	$S_{r,3}, \sigma_{r,3}$	$\mu_{min\ ex,3}, \sigma_{min\ ex,3}$	$\mu_{max\ ex,3}, \sigma_{max\ ex,3}$
<b>v<sub>12</sub></b>	$\mu_{n,4}, \sigma_{n,4}$	$\lambda_{g,4}, \eta_{g,4}$	$\mu_{ln,4}, \sigma_{ln,4}$	$k_{w,4}, \lambda_{w,4}$	$\mu_{nak,4}, \omega_{nak,4}$	$\mu_{log,4}, \sigma_{log,4}$	$S_{r,4}, \sigma_{r,4}$	$\mu_{min\ ex,4}, \sigma_{min\ ex,4}$	$\mu_{max\ ex,4}, \sigma_{max\ ex,4}$
<b>S<sub>22T</sub></b>	$\mu_{n,5}, \sigma_{n,5}$	$\lambda_{g,5}, \eta_{g,5}$	$\mu_{ln,5}, \sigma_{ln,5}$	$k_{w,5}, \lambda_{w,5}$	$\mu_{nak,5}, \omega_{nak,5}$	$\mu_{log,5}, \sigma_{log,5}$	$S_{r,5}, \sigma_{r,5}$	$\mu_{min\ ex,5}, \sigma_{min\ ex,5}$	$\mu_{max\ ex,5}, \sigma_{max\ ex,5}$
<b>E<sub>2</sub></b>	$\mu_{n,6}, \sigma_{n,6}$	$\lambda_{g,6}, \eta_{g,6}$	$\mu_{ln,6}, \sigma_{ln,6}$	$k_{w,6}, \lambda_{w,6}$	$\mu_{nak,6}, \omega_{nak,6}$	$\mu_{log,6}, \sigma_{log,6}$	$S_{r,6}, \sigma_{r,6}$	$\mu_{min\ ex,6}, \sigma_{min\ ex,6}$	$\mu_{max\ ex,6}, \sigma_{max\ ex,6}$
<b>S<sub>22C</sub></b>	$\mu_{n,7}, \sigma_{n,7}$	$\lambda_{g,7}, \eta_{g,7}$	$\mu_{ln,7}, \sigma_{ln,7}$	$k_{w,7}, \lambda_{w,7}$	$\mu_{nak,7}, \omega_{nak,7}$	$\mu_{log,7}, \sigma_{log,7}$	$S_{r,7}, \sigma_{r,7}$	$\mu_{min\ ex,7}, \sigma_{min\ ex,7}$	$\mu_{max\ ex,7}, \sigma_{max\ ex,7}$
<b>S<sub>12</sub></b>	$\mu_{n,8}, \sigma_{n,8}$	$\lambda_{g,8}, \eta_{g,8}$	$\mu_{ln,8}, \sigma_{ln,8}$	$k_{w,8}, \lambda_{w,8}$	$\mu_{nak,8}, \omega_{nak,8}$	$\mu_{log,8}, \sigma_{log,8}$	$S_{r,8}, \sigma_{r,8}$	$\mu_{min\ ex,8}, \sigma_{min\ ex,8}$	$\mu_{max\ ex,8}, \sigma_{max\ ex,8}$
<b>G<sub>12</sub></b>	$\mu_{n,9}, \sigma_{n,9}$	$\lambda_{g,9}, \eta_{g,9}$	$\mu_{ln,9}, \sigma_{ln,9}$	$k_{w,9}, \lambda_{w,9}$	$\mu_{nak,9}, \omega_{nak,9}$	$\mu_{log,9}, \sigma_{log,9}$	$S_{r,9}, \sigma_{r,9}$	$\mu_{min\ ex,9}, \sigma_{min\ ex,9}$	$\mu_{max\ ex,9}, \sigma_{max\ ex,9}$

Table 3-1: Expected results from Maximum likelihood method

Let's choose randomly an element from table 3.1, for example  $s_{r,6}, \sigma_{r,6}$ . This element will contain the non-centrality parameter “ $s$ ” and the scale parameter “ $\sigma$ ” of a Rician distribution that is the most probable to describe the experimental data which were extracted for the elastic modulus at the perpendicular direction with respect to the fiber's orientation. Similarly,  $\mu_{n,6}, \sigma_{n,6}$  includes the mean and standard deviation values of a normal distribution that is the most probable to describe the same material property. The material properties shown in table 3.1 are described below:

Stiffness Properties		Explanation		Strength Properties		Explanation	
$E_1$	Elastic modulus, loading direction parallel to fibers			$S_{11T}$	Tensile strength, loading direction parallel to fibers		
$E_2$	Elastic modulus, loading direction perpendicular to fibers			$S_{11c}$	Compressive strength, loading direction parallel to fibers		
$\nu_{12}$	In-plane Poisson's ratio			$S_{22T}$	Tensile strength, loading direction perpendicular to fibers		
$G_{12}$	In-plane shear Modulus			$S_{22c}$	Compressive strength, loading direction perpendicular to fibers		
				$S_{12}$	In-Plane shear strength		

Table 3-2: Explanation of material properties' symbols

The out of plane strength properties  $S_{13}, S_{23}$  and stiffness properties  $G_{13}, G_{23}$  are not be included in the statistical analysis because only 6 tests were performed for their determination. Hence, the mean value of each of these properties will be included in the finite element model which is presented in Chapter 5.

### 3.3 Kolmogorov-Smirnov criterion

Up to this point, by applying the maximum likelihood method, the parameters of every chosen distribution have been defined. Nonetheless, that doesn't mean that all the distributions are capable of describing the data with accuracy. For example, let's take into consideration again the material property,  $S_{11T}$ . The maximum likelihood method answers to the question: “If we assume that the tensile strength  $S_{11T}$  follows for example the normal distribution, what are the most probable values of the mean and standard deviation that can describe the dataset of  $S_{11T}$ ?”. The answer gives the values  $\mu_{n,1}, \sigma_{n,1}$  but there will be no indication if the normal distribution  $N(\mu_{n,1}, \sigma_{n,1})$  can describe adequately this dataset. Hence, a criterion for the goodness-of-fit should be applied and for this thesis, the Kolmogorov-Smirnov criterion was chosen which is explained below.

The first step for the application of the Kolmogorov-Smirnov criterion is to create the empirical distribution for every dataset of the material properties which was extracted from the experiments. Let's assume that  $x_1, x_2, \dots, x_n$  is the dataset for the tensile strength  $S_{11T}$ . The dataset is sorted in an ascending order which means that  $x_1^* = \min(x_1, x_2, \dots, x_n)$  and  $x_n^* = \max(x_1, x_2, \dots, x_n)$  with  $x_2^*$  being the second smallest value and so on for the rest of the values. Its empirical distribution function is given as:

$$F_N(x) = \begin{cases} 0, & \text{if } x < x_1^* \\ \frac{1}{n}, & \text{if } x_1^* \leq x < x_2^* \\ \vdots & \\ \frac{i}{n} & \text{if } x_i^* \leq x < x_{i+1}^* \\ \vdots & \\ 1, & \text{if } x_n^* < x \end{cases} \quad (3.3.1)$$

Then, it is assumed that there is an unknown distribution with cumulative distribution function,  $F_X(x)$ . The random quantity

$$D = \max_{-\infty < x < \infty} |F_N(x) - F_X(x)| \quad (3.3.2)$$

is called the Kolmogorov-Smirnov test statistic and it measures how much the empirical distribution function deviates from the unknown distribution  $F_X(x)$ . A figure is shown below where this distance is depicted for a randomly chosen sample (tensile experimental results with fibres at  $0^\circ$ ) and for the maximum extreme distribution that best fits according to the maximum likelihood estimates and the Kolmogorov-Smirnov criterion.

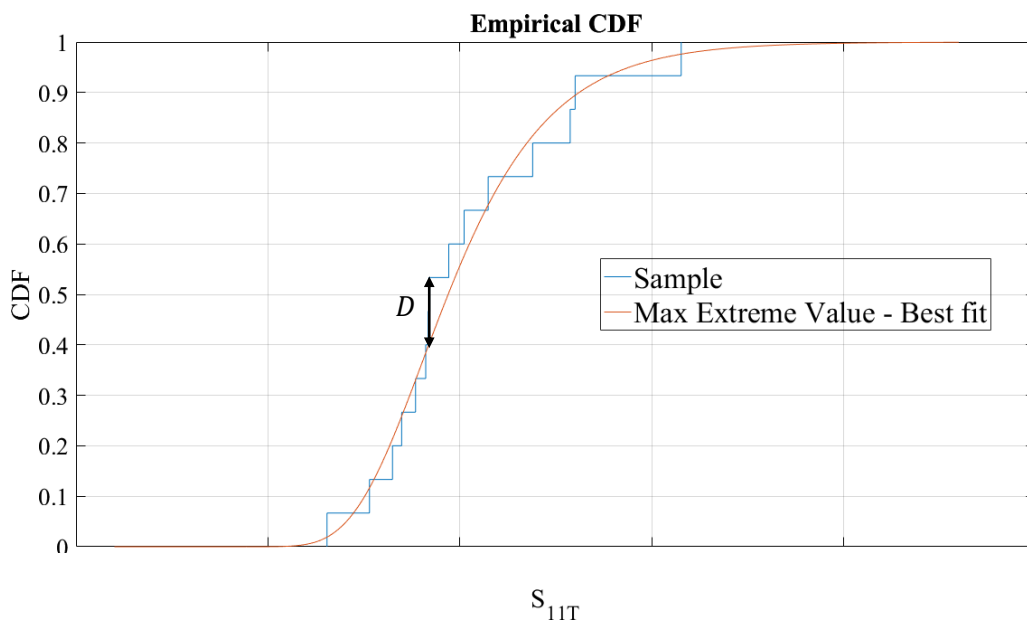


Figure 3-3: Kolmogorov-Smirnov test statistic,  $D$

It can be shown that for every continuous distribution, the Kolmogorov distribution for the Kolmogorov-Smirnov test statistic is given as<sup>[4,25]</sup>

$$H(x) = 1 - 2 \sum_{j=1}^{\infty} (-1)^{-j} \exp(-2j^2 x^2) \quad (3.3.3)$$

The cumulative distribution  $H(x)$  does not depend on the distribution from which the data were extracted and as a result the use of  $D$  is allowed to be used as a way to define the goodness of the distribution's fit on the experimental data. It can also be shown that<sup>[4,26]</sup>:

$$\lim_{n \rightarrow \infty} P(\sqrt{n}D \leq x) \approx 1 - 2 \sum_{j=1}^{\infty} (-1)^{-j} \exp(-2j^2 x^2) = H(x) \quad (3.3.4)$$

Hence, the next step is to make a null hypothesis  $H_0$ . This hypothesis states that the dataset  $x_1, x_2, \dots, x_n$  follows a purely defined distribution, for example the normal distribution with  $\mu_{n,1}$  and  $\sigma_{n,1}$ . Hence, keeping the consistency shown in equation (3.3.2) the null hypothesis that it is made is  $H_0: F_X(x) = F_0(x)$  where  $F_0 = N(\mu_{n,1}, \sigma_{n,1})$  according to the given example. If  $H_0$  is true, the quantity  $\sqrt{n}D$  at eq. (3.3.4) will be equal to:

$$\sqrt{n}D = \sqrt{n} \cdot \max_{-\infty < x < \infty} |F_N(x) - F_0(x)| \quad (3.3.5)$$

By combining eq.(3.3.4) and eq.(3.3.5) and under the assumption that  $H_0$  is true, it is concluded that:

$$\lim_{n \rightarrow \infty} P\left(\sqrt{n} \cdot \max_{-\infty < x < \infty} |F_N(x) - F_0(x)| \leq x\right) \approx 1 - 2 \sum_{j=1}^{\infty} (-1)^{-j} \exp(-2j^2 x^2) = H(x) \quad (3.3.6)$$

If later it is proved that  $H_0$  was wrong, that would mean that  $F_0(x) \neq F_X(x)$  and as a result the normal distribution  $N(\mu_{n,1}, \sigma_{n,1})$  cannot describe adequately the tensile strength  $S_{11T}$  according to the experimental results  $x_1, x_2, \dots, x_n$ . It is intuitive that as the quantity  $\max_{-\infty < x < \infty} |F_N(x) - F_0(x)|$  gets bigger and bigger, it becomes more difficult to get the aforementioned null hypothesis true.

The last step is to define a criterion which will determine if the null hypothesis is true or not. For that reason, a predefined level of significance  $\alpha_0$  should be introduced which for this thesis is equal to  $\alpha_0 = 5\%$ . Generally, the null hypothesis is rejected if and only if  $\sqrt{n}D > x_{1-\alpha}$  where in most of the cases  $x_{1-\alpha}$  is defined from tables for certain values of  $\alpha_0$ .

However, the quantity  $D^*$  has to be considered if the use of tables is to be avoided:

$$D^* = \left(\sqrt{n} + 0.12 + \frac{0.11}{\sqrt{n}}\right) D \quad (3.3.7)$$

Then, the level of significance is given as:

$$\alpha = 2 \sum_{j=1}^{\infty} (-1)^{-j} \exp(-2j^2 D^{*2}) \quad (3.3.8)$$

If  $\alpha > \alpha_0$ , then the null hypothesis  $H_0$  is accepted and it is assumed that the predefined distribution  $F_0(x)$  can describe adequately the dataset  $x_1, x_2, \dots, x_n$ . To put it simply, the level of significance  $\alpha$  gives an indication of how much one should be surprised when he sees the dataset  $x_1, x_2, \dots, x_n$  being randomly drawn from the assumed distribution at the null hypothesis. The smaller the value of  $\alpha$ , the bigger the surprise. For further information about the null hypothesis, significance levels, Type I and Type II errors, the reader can refer to Ref. [4,12,13]. Finally, 5% is common value used in the literature for the predefined significance level as shown in Ref.[4,28,29,30].

The results from the analysis at this step will give a significance level for all the distributions for each material table. To further elaborate, similar to the table 3.1, a new table will be made where all the elements will contain the significance levels of the corresponding distributions for the respective material property. For example,  $\alpha_{n,1}$  is the significance level for the normal distribution according to the dataset of  $S_{11T}$ . All the significance levels that are higher than 5% will indicate that the corresponding distribution can describe adequately the respective material property and if two or more distributions have significance levels higher than 5%, the distribution with the highest  $\alpha$  (largest value of type I error) will qualify as the distribution that describes best the respective material property.

Note: The method that is followed in order to evaluate the goodness-of-fit is described above in detail. The advantages of the Kolmogorov-Smirnov method are<sup>[31]</sup>:

- The test is distribution free.
- The D statistic is easy to calculate.
- It can be used as a goodness of fit test following regression analysis.
- There aren't any restrictions on sample size but  $n \geq 8$ <sup>[32]</sup>
- Tables are readily available (one has just to calculate  $D$  as shown in fig.3-3)

However, it should be mentioned that a disadvantage of this method is that the sensitivity is higher at the centre than the tails as shown in figure 3-3.

## 3.4 Generate correlated random variables

The analysis presented in subchapter 3.3 resulted in the table below:

Material Property	Best Fit
$S_{11T}$	<i>Distribution<sub>1</sub>(1st parameter, 2nd parameter)</i>
$E_1$	<i>Distribution<sub>2</sub>(1st parameter, 2nd parameter)</i>
$S_{11C}$	<i>Distribution<sub>3</sub>(1st parameter, 2nd parameter)</i>
$\nu_{12}$	<i>Distribution<sub>4</sub>(1st parameter, 2nd parameter)</i>
$S_{22T}$	<i>Distribution<sub>5</sub>(1st parameter, 2nd parameter)</i>
$E_2$	<i>Distribution<sub>6</sub>(1st parameter, 2nd parameter)</i>
$S_{22C}$	<i>Distribution<sub>7</sub>(1st parameter, 2nd parameter)</i>
$S_{12}$	<i>Distribution<sub>8</sub>(1st parameter, 2nd parameter)</i>
$G_{12}$	<i>Distribution<sub>9</sub>(1st parameter, 2nd parameter)</i>

Table 3-3: Results from Kolmogorov-Smirnov criterion, Distributions that best fit each material property

The statistical analysis applied up to this point, was made in order to introduce the stochastic nature of the material properties into the FEA model(Ansys). The details of the FEA model are shown in chapter 5 and it was decided that each element in the model will have its unique material properties that are based on the results shown in table 3-3. For more information about how these material properties are assigned to each element, the reader is directed to the main body of the thesis, here. Generally, in total there are 500 shell elements in the model and an element with a number “ $i$ ” will have the following material properties:  $S_{11T,i}, E_{1,i}, S_{11C,i}, \nu_{12,i}, S_{22T,i}, E_{2,i}, S_{22C,i}, S_{12,i}, G_{12,i}$ . One way to define the material properties for all the elements is to take a random number between 0 and 1 and then find the corresponding value of a material property by calculating the inverse cumulative function of the respective distribution at this number. This would be acceptable if there were no correlations between the material properties.

However, the experimental results showed correlations between certain material properties which were derived from the same experiments. For example, correlation was detected between the tensile strength  $S_{11T}$  and the elastic modulus  $E_1$  as both these material properties are extracted from tensile tests according to ASTM D 3039. It was decided that this correlation will be taken into account at the introduction of the material properties in the Ansys model and as a result the correlation coefficients  $\rho(S_{11T}, E_1)$ ,  $\rho(S_{22T}, E_2)$  and  $\rho(S_{12}, G_{12})$  were calculated as:

$$\rho(X, Y) = \frac{1}{n-1} \sum_{i=1}^n \left( \frac{X_i - \mu_X}{\sigma_X} \right) \left( \frac{Y_i - \mu_Y}{\sigma_Y} \right) \quad (3.4.1)$$

These coefficients were used for the Cholesky decomposition that is shown below. Generally, the aim of this subchapter is to show how one can produce different realizations of dependent random variables for two datasets (let's say  $S_{11T}$  and  $E_1$ ) which follow the same or different distributions. To put it in a more scientific way, the aim is to produce a Spearman rank correlation matrix  $\tilde{M}$ , for the correlated properties that will be introduced in Ansys, which is close to the rank correlation matrix which was extracted from the experiments

and is of the form  $\begin{bmatrix} 1 & \rho \\ \rho & 1 \end{bmatrix}$ . Simultaneously, the initial properties of the marginal distributions should be preserved as well as the sampling scheme (Latin Hypercube Sampling in this case). The procedure is presented in steps.

### 3.4.1 1<sup>st</sup> step: Latin Hypercube Sampling

As it was mentioned above, the aim is to produce dependent realizations for 2 material properties, let's say  $S_{11T}$  and  $E_1$ . The first step is to create a Latin Square which will be the base for the sampling technique. If only 10 elements had to be created for each material property, the Latin Square would look like fig. 3-4 and if 500 elements are to be used, the Latin Square would look like fig.3-5 (grid is off for the resolution):

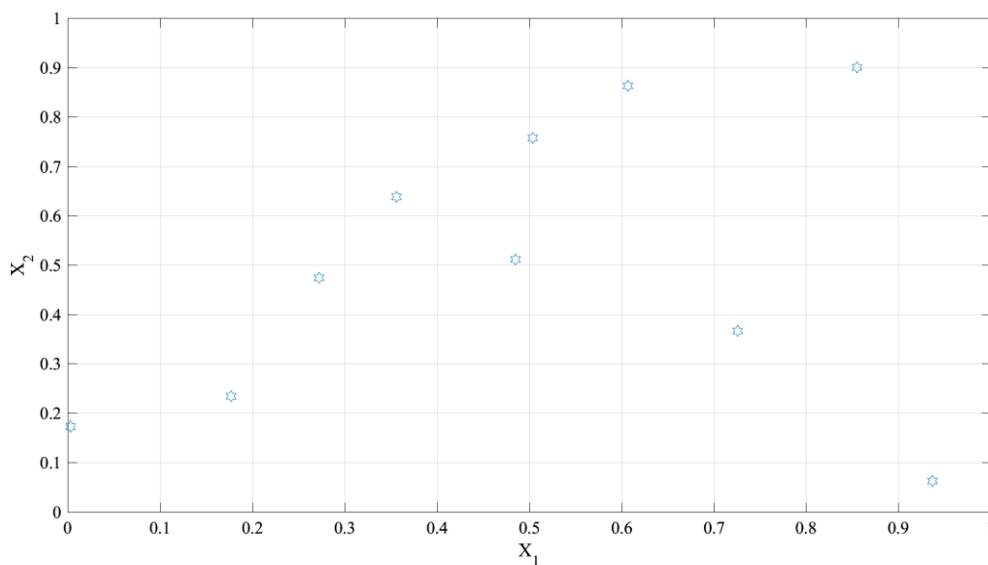


Figure 3-4: Sampling of two variables, 10 realizations

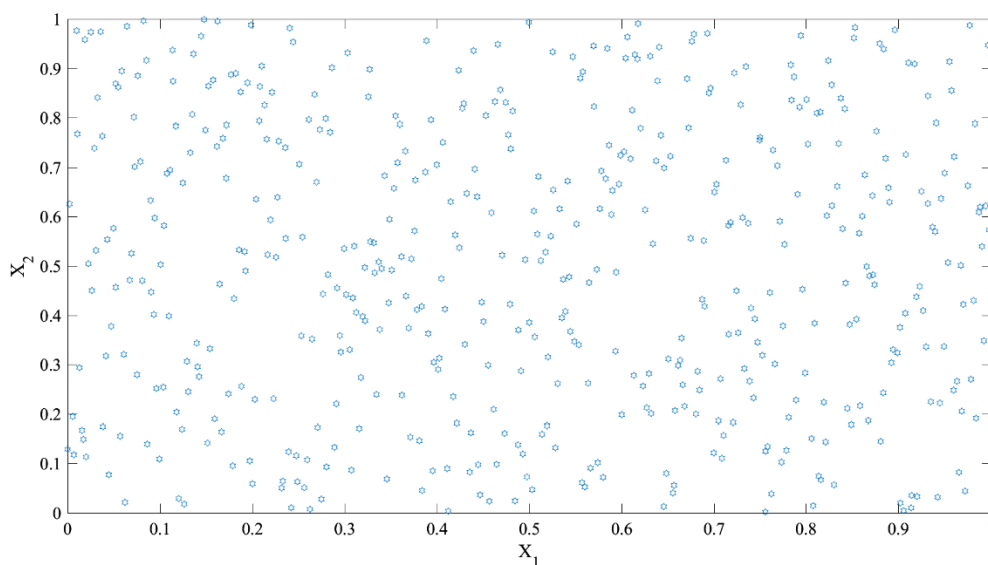


Figure 3-5: Sampling of two variables, 500 realizations

This sampling method was opted instead of the usual Monte Carlo sampling because it is more efficient<sup>[34,35,36]</sup>. A simple way to explain this can be seen at figure 3-4. Each row and each column has only one element which allows the user to take into account the whole distribution equally. The reason that leads to enhanced efficiency comes from the fact that these values are generated in order to be used for the calculation of the inverse cumulative functions which best fit to each of the material properties (table 3-3).

To keep it simple, let's assume a univariate distribution. In figure 3-6, the difference of choosing 10 elements from the usual Monte Carlo Sampling (MCS) method is compared to the Latin Hypercube sampling (LHS). With both methods, random numbers between 0 and 1 were generated which were used for the calculation of the inverse cumulative function of a chosen distribution. Let's assume that a random variable  $X_1$  is following the standard normal distribution,  $N(0,1)$ .

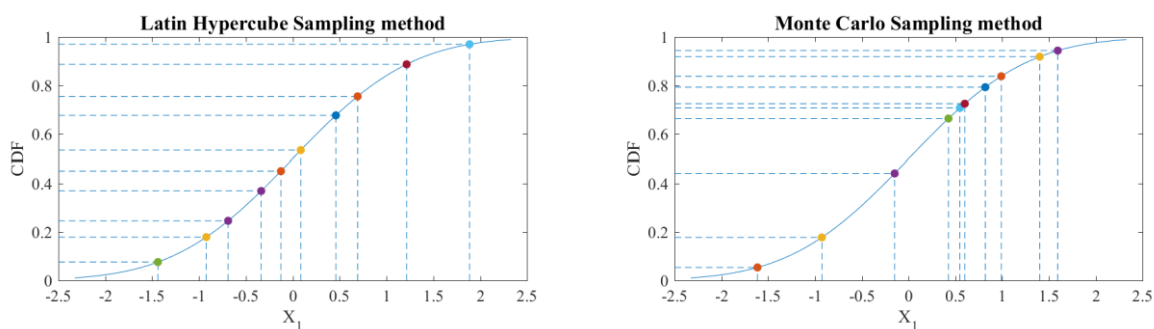


Figure 3-6: Sampling with LHS(left) and MCS(right)

It is obvious that the results from the Latin Hypercube Sampling method are more representative and describe better the standard normal cumulative distribution rather than the Monte Carlo Sampling. When the latter was used, 10 random values were generated in Matlab from a uniform distribution  $U(0,1)$ . No restrictions were introduced during this procedure and as a result a cluster between 0.65 and 0.95 is obvious in figure 3-6 (right). Furthermore, big gaps are observed between 0.19 and 0.45 as well as between 0.45 and 0.65 as the algorithm didn't generate any values between these two sets of numbers. Hence, the high values of  $X_1$  are over-represented whereas the low values are under-represented. The opposite could happen in a following run which makes it clear that this method is inefficient especially for small amount of elements such as 10 in that case.

On the other hand, the Latin Hypercube Sampling generated values between 0 and 1 in a totally different manner. The first step of the algorithm is to divide the interval,  $Int(0,1)$ , into  $n$  divisions, where  $n$  is the amount of elements that have to be generated (10 in that case). Then, for each division, it chooses randomly a number which follows a uniform distribution with parameters equal to the edges of the interval. Hence,  $x_1 = U(0, 1/n)$ ,  $x_2 = U(1/n, 2/n), \dots, x_n = U(1 - 1/n, 1)$ . As a result, the distribution is divided in  $n$  segments and a realization is made for each segment separately which leads to a better representation of the given distribution.

Following the same rationale, a multivariate sample can be generated that guarantees non-overlapping values. Of course the algorithm becomes slightly more complex because each row and each column should include only one element. The results of the LHS for a bivariate distribution is shown in figures 3-4 and 3-5 for 10 and 500 elements respectively.

Notes:

- For big amount of elements, the two sampling methods become equivalent. However, this statistical analysis was built to apply to many models and it is not restricted to the case under investigation where 500 elements were used.
- The Latin Hypercube Sampling has been developed a lot since it was first introduced by McKay et al. in 1979<sup>[35]</sup>. An enhanced algorithm is used in matlab which follows everything that was stated above but it also includes a procedure through which the resultant numbers from the sampling method have the least possible correlation. The explanation of this algorithm is far out of this thesis' scope. The main reason for the inclusion of this algorithm is shown in subchapter 3.4.2 where the Cholesky's decomposition is explained
- If the LHS has to be implemented for 3 variables instead of 2 then the Latin Square becomes a Latin cube. The term "Hypercube" extends this concept into higher dimensions where several design variables are included
- The LHS method is also known as the "Stratified Sampling Technique"<sup>[37]</sup>
- If the reader is interested more in the LHS method, he can find useful information in Ref. [34,35,36,37].

### 3.4.2 Correlate the uncorrelated variables – Cholesky's Transformation

The LHS resulted in the following table with samples (fig. 3-5):

$X_1$	$X_2$
$x_{1,1}$	$x_{2,1}$
$x_{1,2}$	$x_{2,2}$
$x_{1,3}$	$x_{2,3}$
$\vdots$	$\vdots$
$x_{1,n}$	$x_{2,n}$

Table 3-4: Results from LHS,  $n = 500$  in our case

The next step was to make each one of the two variables normally distributed with a zero mean and a unit standard deviation. For that reason, each sample was transformed from its original value (result from LHS) to a new one based on the inverse standard cumulative function. The results from this step were:

$X_1$	$X_2$
$x_{1,1}^* = icdf(normal, x_{1,1}, \mu = 0, \sigma = 1)$	$x_{2,1}^* = icdf(normal, x_{2,1}, \mu = 0, \sigma = 1)$
$x_{1,2}^* = icdf(normal, x_{1,2}, \mu = 0, \sigma = 1)$	$x_{2,2}^* = icdf(normal, x_{2,2}, \mu = 0, \sigma = 1)$
$x_{1,3}^* = icdf(normal, x_{1,3}, \mu = 0, \sigma = 1)$	$x_{2,3}^* = icdf(normal, x_{2,3}, \mu = 0, \sigma = 1)$
$\vdots$	$\vdots$
$x_{1,n}^* = icdf(normal, x_{1,n}, \mu = 0, \sigma = 1)$	$x_{2,n}^* = icdf(normal, x_{2,n}, \mu = 0, \sigma = 1)$

Table 3-5: Uncorrelated variables that are normally distributed

In table 3-5 this transformation is observed which is made by taking the inverse cumulative function of the standard normal distribution at  $x_{i,j}^*$ . Now both  $X_1 = [x_{1,1}^*, x_{1,2}^*, x_{1,3}^*, \dots, x_{1,n}^*]$  and  $X_2 = [x_{2,1}^*, x_{2,2}^*, x_{2,3}^*, \dots, x_{2,n}^*]$  are normally distributed but their values are still uncorrelated. Hence,  $\rho(X_1, X_2) \approx \begin{bmatrix} 1 & \approx 0 \\ \approx 0 & 1 \end{bmatrix} \approx I$  where “ $\rho$ ” is the correlation matrix and the approximation symbol “ $\approx$ ” corresponds to the fact that unwittingly some correlations will be detected during the sampling (the algorithm referred at the notes of the previous subchapter, aims to reduce this correlation).

The next step is to correlate the random variables  $X_1, X_2$ . This can happen through Cholesky’s decomposition as it is explained below from Ref. [39]:

*Quote: [...] take a random vector,  $X$ , consisting of uncorrelated random variables with each random variable,  $X_i$ , having zero mean and unit variance 1. Since  $X_i$ ’s are uncorrelated random variables with zero mean and unit variance, we have  $\mathbb{E}(X_i X_j) = \delta_{ij}$ . Hence,*

$$\mathbb{E}(XX^T) = I \quad (3.4.2)$$

*To generate a random vector with a given covariance matrix  $Q$ , look at the Cholesky decomposition of  $Q$  i.e.  $Q = LL^T$ . Note that it is possible to obtain a Cholesky decomposition of  $Q$  since by definition the co-variance matrix  $Q$  is symmetric and positive definite.*

*Now look at the random vector  $Z = LX$ . We have*

$$\mathbb{E}(ZZ^T) = \mathbb{E}((LX)(LX)^T) = \underbrace{\mathbb{E}(LXX^T L^T)}_{\text{since expectation is linear operator}} = L\mathbb{E}(XX^T)L^T = LIL^T = LL^T = Q \quad (3.4.3)$$

*Hence, the random vector  $Z$  has the desired co-variance matrix,  $Q$*

*End of Quote*

The Cholesky factorization scheme is used to obtain the lower triangular matrix  $L$  such that  $LL^T = Q$ <sup>[40]</sup>. The new random vector  $Z = [X_1, X_2]$  will have correlated samples where both  $X_1$  and  $X_2$  follow the standard normal distribution. However, as it was mentioned above, the effect of having correlations (unwittingly) after the sampling method will lead to slightly distorted results as  $\rho(X_1, X_2) \approx I$ . Ergo, a correction has to be made as it is explained in Ref. [41]; this correction is presented below:

Let’s assume that  $T$  is the correlation matrix of  $Z$  and that is positive definite and symmetric. A matrix  $S$  (lower triangular) can be defined such that  $STS^T = Q$  where  $Q = \begin{bmatrix} 1 & \rho(S_{11T}, E_1) \\ \rho(S_{11T}, E_1) & 1 \end{bmatrix}$  for the case where the  $S_{11T}$  and  $E_1$  have to be correlated. Again, the Cholesky factorization can be used in order to find the lower triangular matrix  $M$  such that  $T = MM^T$ . By considering that  $Q = LL^T$  as shown at the quote above, the following relationship can be defined:

$$SMM^T S^T = LL^T \Rightarrow SM = L \Rightarrow S = LM^{-1} \quad (3.4.4)$$

This last transformation is necessary for the extraction of correlated samples  $\tilde{X}$ . By multiplying  $X = [X_1 \ X_2]$  where  $X_1 = [x_{1,1}^*, x_{1,2}^*, x_{1,3}^*, \dots, x_{1,n}^*]$  and  $X_2 = [x_{2,1}^*, x_{2,2}^*, x_{2,3}^*, \dots, x_{2,n}^*]$  with  $S^T$ , i.e.  $\tilde{X} = XS^T$ , the resultant realizations will have exactly the same correlation with the given one, i.e.  $\text{corr}(\tilde{X}) = Q = \begin{bmatrix} 1 & \rho(S_{11T}, E_1) \\ \rho(S_{11T}, E_1) & 1 \end{bmatrix}$ , while  $\tilde{X}_1$  and  $\tilde{X}_2$  will follow the standard normal distribution.

### 3.4.3 Create Input for Ansys

The results from the previous step will give a matrix with  $\tilde{X}_1$  and  $\tilde{X}_2$  which are correlated and they follow the standard normal distribution  $N(0,1)$ :

$\tilde{X}_1$	$\tilde{X}_2$
$\tilde{x}_{1,1}$	$\tilde{x}_{2,1}$
$\tilde{x}_{1,2}$	$\tilde{x}_{2,2}$
$\tilde{x}_{1,3}$	$\tilde{x}_{2,3}$
$\vdots$	$\vdots$
$\tilde{x}_{1,n}$	$\tilde{x}_{2,n}$

Table 3-6: Correlated variables that follow the standard normal distribution

The next step is to find the value that corresponds to the cumulative function of the standard normal distribution. It is known that the cumulative distribution of any distribution follows the Uniform distribution  $U[0,1]$ . The proof is shown below:

Proof: Let's assume that  $F_X$  is the cumulative distribution and is continuous, one-to-one and increasing (all assumption are valid for the standard cumulative function). Then, "Y" is defined as  $Y = F_X$  while it is known that Y takes values between 0 and 1 as the probability of an event should satisfy the relation  $0 \leq P(X) \leq 1$ . Then:

$$F_Y(x) = P(F_X(X) \leq x) = P(X \leq F_X^{-1}(x)) = F_X(F_X^{-1}(x)) = x \quad (3.4.5)$$

Now, if we assume a uniform distribution  $U[0,1]$  it is known that its cumulative distribution is:

$$F_U(x) = \int_R f_U(u) du = \int_0^x du = x \quad (3.4.6)$$

Hence,  $F_Y(x) = F_U(x)$  for every  $x \in [0,1]$

The next step is to take the cumulative standard normal distribution of every sample shown in table 3-6. This would result to:

$\tilde{X}_1^*$	$\tilde{X}_2^*$
$\tilde{x}_{1,1}^* = cdf(\text{normal}, \tilde{x}_{1,1}, \mu = 0, \sigma = 1)$	$\tilde{x}_{2,1}^* = cdf(\text{normal}, \tilde{x}_{2,1}, \mu = 0, \sigma = 1)$
$\tilde{x}_{1,2}^* = cdf(\text{normal}, \tilde{x}_{1,2}, \mu = 0, \sigma = 1)$	$\tilde{x}_{2,2}^* = cdf(\text{normal}, \tilde{x}_{2,2}, \mu = 0, \sigma = 1)$
$\tilde{x}_{1,3}^* = cdf(\text{normal}, \tilde{x}_{1,3}, \mu = 0, \sigma = 1)$	$\tilde{x}_{2,3}^* = cdf(\text{normal}, \tilde{x}_{2,3}, \mu = 0, \sigma = 1)$
$\vdots$	$\vdots$
$\tilde{x}_{1,n}^* = cdf(\text{normal}, \tilde{x}_{1,n}, \mu = 0, \sigma = 1)$	$\tilde{x}_{2,n}^* = cdf(\text{normal}, \tilde{x}_{2,n}, \mu = 0, \sigma = 1)$

The random variables  $\tilde{X}_1^*$  and  $\tilde{X}_2^*$  are correlated and uniformly distributed. Their correlation matrix is still exactly the same as the target correlation matrix which resulted from the experiments, i.e.:

$$\begin{bmatrix} 1 & \rho(\tilde{X}_1^*, \tilde{X}_2^*) \\ \rho(\tilde{X}_1^*, \tilde{X}_2^*) & 1 \end{bmatrix} = Q = \begin{bmatrix} 1 & \rho(S_{11T}, E_1) \\ \rho(S_{11T}, E_1) & 1 \end{bmatrix} \quad (3.4.7)$$

for the case where the correlation between  $S_{11T}$  and  $E_1$  is to be considered.

The last step aims to transform these uniformly distributed random variables  $\tilde{X}_1^*, \tilde{X}_2^*$  to the inputs for the FEA model. Again, for the  $S_{11T}, E_1$  case and with the help of table 3-3 the inputs in the FEA model will be:

$S_{11T}^*$	$E_1^*$
$icdf(\text{Distribution}_1, \tilde{x}_{1,1}^*, 1^{st} \text{ parameter}, 2^{nd} \text{ parameter})$	$icdf(\text{Distribution}_2, \tilde{x}_{2,1}^*, 1^{st} \text{ parameter}, 2^{nd} \text{ parameter})$
$icdf(\text{Distribution}_1, \tilde{x}_{1,2}^*, 1^{st} \text{ parameter}, 2^{nd} \text{ parameter})$	$icdf(\text{Distribution}_2, \tilde{x}_{2,2}^*, 1^{st} \text{ parameter}, 2^{nd} \text{ parameter})$
$icdf(\text{Distribution}_1, \tilde{x}_{1,3}^*, 1^{st} \text{ parameter}, 2^{nd} \text{ parameter})$	$icdf(\text{Distribution}_2, \tilde{x}_{2,3}^*, 1^{st} \text{ parameter}, 2^{nd} \text{ parameter})$
$\vdots$	$\vdots$
$icdf(\text{Distribution}_1, \tilde{x}_{1,n}^*, 1^{st} \text{ parameter}, 2^{nd} \text{ parameter})$	$icdf(\text{Distribution}_2, \tilde{x}_{2,n}^*, 1^{st} \text{ parameter}, 2^{nd} \text{ parameter})$

Table 3-7: Input for FEA model

As it was mentioned at subchapter 3.3,  $\text{Distribution}_1$  represents the distribution that best fits the experimental data for the tensile strength,  $S_{11T}$ . Similarly,  $\text{Distribution}_2$  represents the distribution that best fits the experimental data for the elastic modulus,  $E_1$ . Due to the fact that these two distributions can be different, slight changes at the correlation matrix can be found, i.e.  $\rho(S_{11T}^*, E_1^*) \approx \rho(S_{11T}, E_1)$ . The exact values are shown at the main body of the thesis here and the small difference in the two correlation is small enough to be assumed negligible.

Prior to the next subchapter's presentation, a summary of the steps taken in subchapter 3.4.1 is considered appropriate:

- Generate samples with Latin Hypercube Sampling method (uncorrelated samples), result:  $x_{1,1}$  etc

- Find the values of the inverse standard normal cumulative function at each of the generated samples (uncorrelated values), result:  $x_{1,1}^*$  etc
- Correlate the values through Cholesky's decomposition (correlated values) result:  $\tilde{x}_{1,1}$  etc.
- Find the values of the standard normal cumulative function at each of the values extracted from the previous step (correlated values), result:  $\tilde{x}_{1,1}^*$  etc.
- Find the value of the inverse cumulative function that best describes the corresponding property (table 3-3) at each of the values found at the previous step (correlated values), result:  $S_{11T,i}^*, E_{1,i}^*$

## 3.5 Bootstrap Method

Prior to the presentation of the next chapter, it was decided that it could be beneficial to provide a different way of describing the material properties. In case that the reader is not interested in assigning distributions to each material property in order to avoid such a complex procedure that was mentioned above (subchapters 3.1-3.4), the bootstrap method was used to define the distribution of the mean values of the material properties. The simplest way of defining the strength and stiffness properties is to take into account only the average values derived from the experiments. However, this is unwise as the sample mean from the dataset  $x_1, x_2, \dots, x_n$  represents only one possible realization of the random sample  $X_1, X_2, \dots, X_n$ . To clarify that, let's consider the tensile strength  $S_{11T}$  and the experimental results which describe it:  $x_1, x_2, \dots, x_{15}$ . If a new testing plan is made with exactly the same conditions (constituent material, fibre volume, apparatus etc.) a different value of sample mean will be derived. Hence, in this subchapter a way to check the distribution of a sample statistic ( $\mu$  for example) is presented and it is based on the bootstrap principle.

The best way of explaining the bootstrap method is through an example which was found at Ref. [42]:

Example: Let's assume that a given sample has the values:  $x_1 = 1, x_2 = 2, x_3 = 4, x_4 = 4, x_5 = 10$ . We can make Bootstrap samples from the original sample by drawing  $n$  values with replacement where  $n$  is the size of the original sample. For example, the first Bootstrap sample can be made as:

- Draw a random value from the original sample, f.e.  $x_{1,1}^* = 2$ . We assume that each value has the same probability to be drawn, i.e.  $P(x_{i,j}^* = x_k) = 1/n$  where "i" takes values between 1 and  $N^*$  ( $N^*$  is the number of bootstrap samples)
- Put this value back into the original sample
- Draw the next random value of the first bootstrap sample, f.e.  $x_{1,2}^* = 1$
- Put this value back into the original sample
- Draw the next random value of the first bootstrap sample, f.e.  $x_{1,3}^* = 10$
- Put this value back into the original sample
- Draw the next random value of the first bootstrap sample, f.e.  $x_{1,4}^* = 4$
- Put this value back into the original sample
- Draw the next random value of the first bootstrap sample, f.e.  $x_{1,5}^* = 2$

Now the first bootstrap sample is ready, with values  $x_{1,j}^* = [2,1,10,4,2]$ . Then, this procedure is repeated  $N^*$  times, let's say 20 in this example. The bootstrap samples are shown below:

Bootstrap Samples			
2,1,10,4,2	4,10,10,2,4	1,4,1,4,4	4,1,1,4,10
4,4,1,4,2	4,10,10,10,4	2,4,4,2,1	2,4,1,10,4
1,10,2,10,10	4,1,10,1,10	4,4,4,4,1	1,2,4,4,2
4,4,10,10,2	4,2,1,4,4	4,4,4,4,4	4,2,4,1,1
4,4,4,2,4	10,4,1,4,4	4,2,1,1,2	10,2,2,1,1

Table 3-8: Bootstrap Samples, example

Then, the mean value for each bootstrap sample  $\bar{x}_i^*$  is calculated and put in ascending order: 2, 2.4, 2.6, 2.6, 2.8, 3, 3, 3.2, 3.4, 3.6, 3.8, 4, 4, 4.2, 4.6, 5.2, 6, 6, 6.6, 7.6. If we want to know in which interval the mean value lies with 90% confidence interval, one can just simply find the 5<sup>th</sup> and 95<sup>th</sup> percentile of the above matrix with the means in ascending order. Due to the fact that in this example  $N^* = 20$ , one can simply chose the second value as the one with 5% chance of not exceeding and the second to last value as the one with 95% of not exceeding, i.e. 2.4 and 6.6 respectively. Hence, we are 90% sure that the mean value lies between 2.4 and 6.6. This example was introduced in matlab in order to show the figure below where these confidence intervals are depicted.

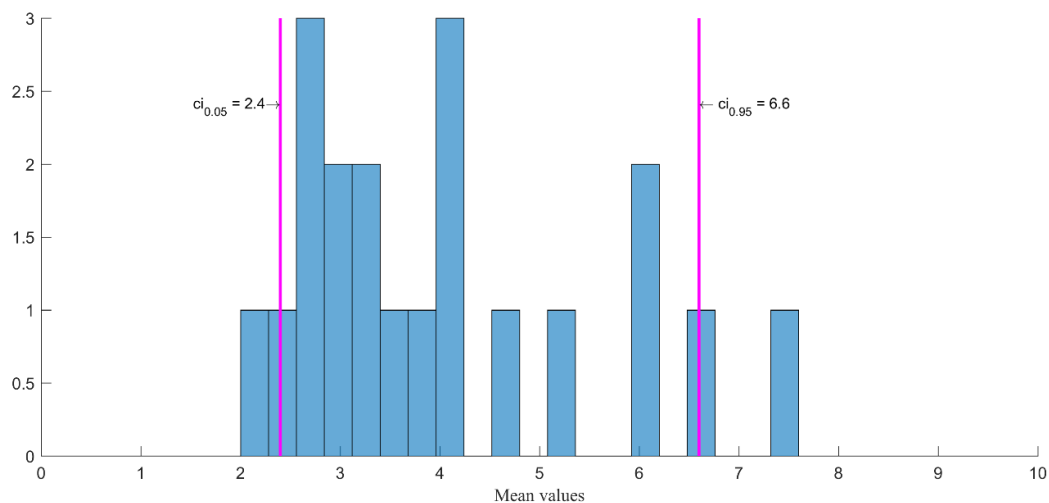


Figure 3-7: Histogram, mean values from Bootstrap samples, example

End of example.

For the experimental results, the same method was used to define the distribution of the material properties' mean values and the histograms are shown at the end of the main body's 3<sup>rd</sup> chapter. Now, let's consider the tensile strength  $S_{11T}$ ; if the reader is interested only to define a conservative value for the tensile strength, instead of implementing the statistical analysis shown in subchapters 3.1-3.4, he can just extract the respective value shown in fig. 3-7 as  $ci_{0.05}$ . However, it is worth-mentioning that for the experimental results, it was chosen to generate 10000 bootstrap samples and the confidence interval was increased to 95%. Also, instead of the simple percentile method, a matlab built-in algorithm was run which calculates the confidence interval with a bias corrected and accelerated percentile method. The description of this algorithm is way out of the scope of this thesis but interested readers can find information at the "bootci" matlab command. More information about the bootstrap method can be found in Ref. [13,43,44].

---

## 3.6 References

- [3.1] ASTM International, Standard Test Method for Tensile Properties of Polymer Matrix Composite Materials, D3039/D3039M-14, Approved: 15 May 2014, DOI: 10.1520/D3039\_D3039M-14
- [3.2] ASTM International, Standard Test Method for Compressive Properties of Polymer Matrix Composite Materials, with Unsupported Gage Section by shear Loading, D3410/D410M-03, Approved: 1 Sept 2008,, DOI: 10.1520/D3410\_D3410M-03R08.
- [3.3] ASTM Standard Test Method for Shear Properties of Composite materials by V-notched Rail Shear Method, D7078/D7078M-12, Approved: 15 June 2012,, DOI: 10.1520/D7078\_D7078M-12
- [3.4] D.J. Lekou, PhD thesis, Reliability determination for the design of structures made by composite materials”, 2010, [Greek]
- [3.5] Alfredo Hua-Sing. Ang, Wilson Hon-Chung. Tang, Probability concepts in engineering Planning and Design, vol.I, 1975, ISBN: 0-471-03200-X
- [3.6] The gamma distribution, University of Alabama in Huntsville, source: <http://www.math.uah.edu/stat/special/Gamma.html>
- [3.7] Nakagami Distribution (Nakagami-m): Definition, source: <http://www.statisticshowto.com/nakagami-distribution/>
- [3.8] Nakagami Distribution - MATLAB & Simulink - MathWorks United Kingdom, source: <https://uk.mathworks.com/help/stats/nakagami-distribution.html>
- [3.9] Krystyna Noga, Ryszard Studański, Estimation of Nakagami distribution parameters in describing a fading radio-communication channel, 2016, Zeszyty Naukowe Akademii Marynarki Wojennej, vol. 204, p.69-81
- [3.10] Logistic distribution, source: <http://www.statisticshowto.com/logistic-distribution/>
- [3.11] Logistic Distribution - MATLAB & Simulink - MathWorks United Kingdom, source: <https://uk.mathworks.com/help/stats/logistic-distribution.html>
- [3.12] Sheldon Ross, Probability and Statistics for Engineers and Scientists, 4<sup>th</sup> edition,2009, ISBN 13: 9780-12-370483-2
- [3.13] F.M. Dekking et al., Modern Introduction to Probability and Statistics, Understanding Why and how, 2005, ISBN 13: 978-1-85233-896-1
- [3.14] Normal Distributions: Definition, Word Problems, source: <http://www.statisticshowto.com/probability-and-statistics/normal-distributions/>
- [3.15] Kristina Zucchi, CFA, Lognormal and Normal Distribution, source: <http://www.investopedia.com/articles/investing/102014/lognormal-and-normal-distribution.asp>
- [3.16] Bessel Function of the First Kind, source: <http://mathworld.wolfram.com/BesselFunctionoftheFirstKind.html>
- [3.17] Theodore S. Rappaport, Rayleigh and Rician Distributions, 2015, source: <http://www.ni.com/white-paper/14912/en/>
- [3.18] Gregory D. Durgin, Georgia Institute of Technology, class notes, ECE 4370: Antenna Engineering, notes on Rician Fading , source: [http://propagation.ece.gatech.edu/ECE4370/notes/Notes\\_on\\_Rician\\_PDFs.pdf](http://propagation.ece.gatech.edu/ECE4370/notes/Notes_on_Rician_PDFs.pdf)
- [3.19] Extreme Value distributions, MathWave Technologies, source: <http://www.mathwave.com/articles/extreme-value-distributions.html>

- [3.20] Szilárd András, Árpád Baricz, Properties of the probability density function of the non-central chi-squared distribution, *J. Math. Anal. Appl.* 346 (2008), pp. 395–402, doi:10.1016/j.jmaa.2008.05.074
- [3.21] Christian Walck, Hand-book on statistical distributions for experimentalists, Particle Physics Group Fysikum University of Stockholm, 2007
- [3.22] H.J. Phillips, R.A. Sheno, S.M. Lewis, Effect of specimen size on the strength scaling of GFRP laminates, *Materials Letters* 21 (1994), pp. 229-238, SSI0167-577x(94)00173-1
- [3.23] Waloddi Weibull, A Statistical distribution function of Wide Applicability, *J. Appl. Mech.* 18 (1951) 293
- [3.24] M.R. Wisnom, Size effects in the testing of fibre-composite materials, *Composites Science and Technology* 59 (1999) 1937-1957, PII: S0266-3538(99)00053-6
- [3.25] Mihael Perman, Jon A. Wellner, An excursion approach to maxima of the Brownian bridge, *Stochastic Processes and their Applications* 124 (2014) 3106–3120, <http://dx.doi.org/10.1016/j.spa.2014.04.008> (LV: 10/ 11/ 2017)
- [3.26] Richard Serfozo, Basics of Applied Stochastic processes, 2009, ISBN: 978-3-540-89331-8
- [3.27] Dmitry Panchenko, MIT course: Statistics for Applications (2006), lecture notes, Kolmogorov-Smirnov test, section13, source: <https://ocw.mit.edu/courses/mathematics/18-443-statistics-for-applications-fall-2006/lecture-notes/lecture14.pdf> (LV: 10/ 11/ 2017)
- [3.28] Dallal, Gerard E. (2012). The Little Handbook of Statistical Practice. - Why 0.05? source: <http://www.jerrydallal.com/LHSP/p05.htm> (LV: 10/ 11/ 2017)
- [3.29] Stigler, Stephen, Fisher and the 5% level,(2008), *Chance* 21 (4): 12, source: <https://link.springer.com/content/pdf/10.1007%2Fs00144-008-0033-3.pdf> (LV: 10/ 11/ 2017)
- [3.30] Fisher, R.A., The arrangement of field experiments, *Journal of the Ministry of Agriculture*,(1926) p. 504
- [3.31] Kolmogorov-Smirnov Goodness of Fit Test, source: <http://www.statisticshowto.com/kolmogorov-smirnov-test/> (LV: 10/ 11/ 2017)
- [3.32] M. A. Stephens, Use of the Kolmogorov-Smirnov, Cramer-Von Mises and Related Statistics Without Extensive Tables, *Journal of the Royal Statistical Society. Series B (Methodological)*, Vol. 32, No. 1. (1970), pp. 115-122.
- [3.33] Nicolas Christou, Poisson, Gamma and Exponential distributions, Statistics University of California, Los Angeles Department of Statistics, Statistics 100A, source: [http://www.stat.ucla.edu/~nchristo/statistics100A/stat100a\\_poisson\\_gamma.pdf](http://www.stat.ucla.edu/~nchristo/statistics100A/stat100a_poisson_gamma.pdf) (LV: 10/ 11/ 2017)
- [3.34] Jared L. Deutsch, Clayton V. Deutsch, Latin hypercube sampling with multidimensional uniformity, *Journal of Statistical Planning and Inference* 142 (2012) 763–772, doi:10.1016/j.jspi.2011.09.016
- [3.35] M. D. McKay, R. J. Beckman & W. J. Conove, A Comparison of Three Methods for Selecting Values of Input Variables in the Analysis of Output From a Computer Code, 1979, *Technometrics*, 42:1, 55-61
- [3.36] Lonnie Chrisman, Latin Hypercube vs. Monte Carlo Sampling, 2014, source: <http://www.lumina.com/blog/latin-hypercube-vs.-monte-carlo-sampling> (LV: 10/ 11/ 2017)
- [3.37] Seung-Kyum Choi, Ramana V. Grandhi, Robert A. Canfield, Reliability-based Structural Design,2007, ISBN-13: 9781846284441
- [3.38] S.N.Jonkman et al., Probabilistic Design: Risk and Reliability Analysis in Civil Engineering, Lecture Notes CIE4130, Technical University of Delft, 2015

- 
- [3.39] Generating correlated random numbers: Why does Cholesky decomposition work?, June 2012, <https://math.stackexchange.com/questions/163470/generating-correlated-random-numbers-why-does-cholesky-decomposition-work> (LV: 10/ 11/ 2017)
- [3.40] Scheuer, E. M. and Stoller, D. S., On the Generation of Normal Random Vectors, (1962) *Technometrics*, 4, 278-281.
- [3.41] Ronald L. Iman & W. J. Conover, A distribution-free approach to inducing rank correlation among input variables, (1982), *Communications in Statistics - Simulation and Computation*, 11:3, 311-334, DOI: 10.1080/03610918208812265
- [3.42] Courtney Taylor, Example of Bootstrapping, 2017, source: <https://www.thoughtco.com/example-of-bootstrapping-3126155> (LV: 10/ 11/ 2017)
- [3.43] T.J. DiCiccio and B. Efron, "Bootstrap confidence intervals, (1996), "Statistical Science, v. 11, n. 3, pp. 189-228.
- [3.44] B. Efron and R.J. Tibshirani, *An Introduction to the Bootstrap*, (1993), Chapman & Hall, New York.

# Chapter 4: Mechanics

Throughout this chapter the theory that was used for the analysis of the composite materials is presented from a mechanics' perspective. According to Ref. [1]: "A laminate is two or more laminae bonded together to act as an integral structural element" where according to the same reference: "A lamina is a flat (sometimes curved as in a shell) arrangement of unidirectional fibers in a matrix". For the scope of this thesis, only unidirectional glass fibers will be examined in a XX matrix. The fibers' type is XX glass and the matrix(resin) used is XX which is a rubber modified based XX resin. More information about the fibers and the resin is presented at chapter 1.

## 4.1 Macromechanics of Laminae

The first step is to analyze the cornerstone of a laminate, i.e. the lamina. The direction of the unidirectional fibers can be arbitrary in a lamina and the way that the directions will be referred to is presented at fig. [4-1].  $X_1$  or simply "1" is the axis parallel to the fibers' direction (principal direction) and  $X_2$  or simply "2" will be the axis perpendicular to the "1" direction in such a way that the external vector  $X_1X_2$  represents the third direction  $X_3$  or simply "3" looking upwards. The angle " $\theta$ " of the fibers is measured counterclockwise starting from the positive " $x$ " axis.

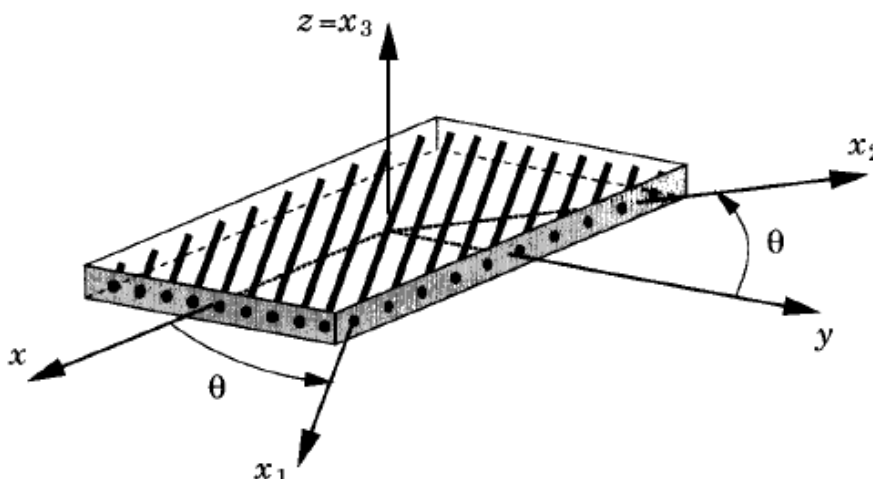


Figure 4-1: A lamina with its material coordinate system<sup>[2]</sup>

In most of the cases the loading direction is known at the material's body direction and the effect of these loads has to be found in the same direction. Ergo, the relation between stresses and strains for a unidirectional lamina is presented below.

For the analysis of the forces/stresses in a lamina with arbitrary fiber direction, the way that the stresses are transformed from a coordinate system to another, should be defined first. By following the procedure presented at Ref. [3], the aforementioned transformation is achieved.

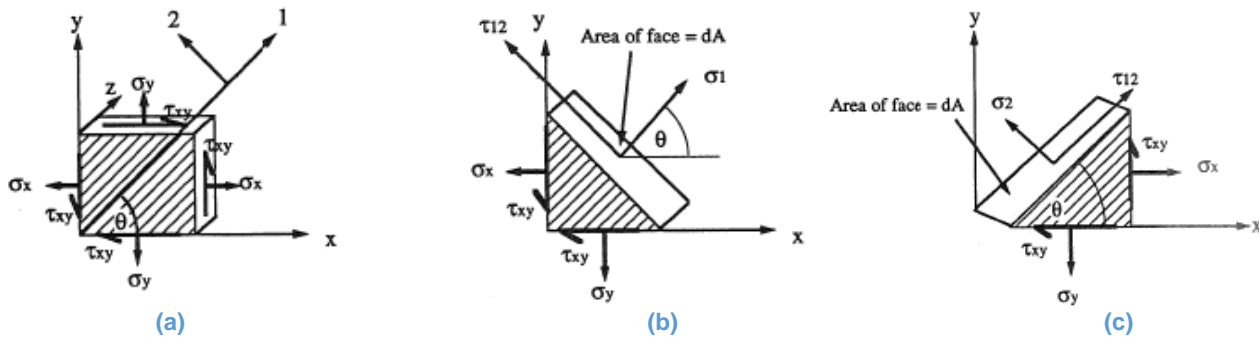


Figure 4-2: Generally Orthotropic Lamina

According to the “x” – “y” coordination system, the lamina can be assumed generally orthotropic for arbitrary fiber direction when the loading direction does not coincide with the principal material direction. At fig. [4-2], it is obvious that the loading direction is different than the principal material direction (“1”) and by implementing force equilibrium in “1” and “2” direction, under plane stress conditions:

Fig.4-2.(b)  $\Sigma F_1 = 0 = \sigma_1 \cdot dA - \sigma_x \cdot (dA \cdot \cos\theta) \cdot \cos\theta - \sigma_y \cdot (dA \cdot \sin\theta) \cdot \sin\theta - \tau_{xy} \cdot (dA \cdot \cos\theta) \cdot \sin\theta - \tau_{xy} \cdot (dA \cdot \sin\theta) \cdot \cos\theta$  (4.1.1)

Fig.4-2.(c)  $\Sigma F_2 = 0 = \sigma_2 \cdot dA - \sigma_x \cdot (dA \cdot \sin\theta) \cdot \sin\theta - \sigma_y \cdot (dA \cdot \cos\theta) \cdot \cos\theta + \tau_{xy} \cdot (dA \cdot \cos\theta) \cdot \sin\theta + \tau_{xy} \cdot (dA \cdot \sin\theta) \cdot \cos\theta$  (4.1.2)

Fig.4-2.(c)  $\Sigma F_1 = 0 = \tau_{12} \cdot dA + \sigma_x \cdot (dA \cdot \sin\theta) \cdot \cos\theta - \sigma_y \cdot (dA \cdot \cos\theta) \cdot \sin\theta - \tau_{xy} \cdot (dA \cdot \cos\theta) \cdot \cos\theta + \tau_{xy} \cdot (dA \cdot \sin\theta) \cdot \sin\theta$  (4.1.3)

If one simplifies the eq. (4.1.1), (4.1.2), (4.1.3) and solves them for  $\sigma_1, \sigma_2$  &  $\tau_{12}$ :

$$\begin{aligned} \sigma_1 &= \sigma_x \cdot \cos^2\theta + \sigma_y \cdot \sin^2\theta + 2 \cdot \tau_{xy} \cdot \sin\theta \cdot \cos\theta \\ \sigma_2 &= \sigma_x \cdot \sin^2\theta + \sigma_y \cdot \cos^2\theta - 2 \cdot \tau_{xy} \cdot \sin\theta \cdot \cos\theta \end{aligned} \tag{4.1.4}$$

$$\tau_{12} = -\sigma_x \cdot \sin\theta \cdot \cos\theta + \sigma_y \cdot \sin\theta \cdot \cos\theta + \tau_{xy} \cdot (\cos^2\theta - \sin^2\theta)$$

The results can be written in a matrix form, i.e.:

$$\begin{bmatrix} \sigma_1 \\ \sigma_2 \\ \tau_{12} \end{bmatrix} = \begin{bmatrix} \cos^2\theta & \sin^2\theta & 2 \cdot \sin\theta \cdot \cos\theta \\ \sin^2\theta & \cos^2\theta & -2 \cdot \sin\theta \cdot \cos\theta \\ -\sin\theta \cdot \cos\theta & \sin\theta \cdot \cos\theta & \cos^2\theta - \sin^2\theta \end{bmatrix} \cdot \begin{bmatrix} \sigma_x \\ \sigma_y \\ \tau_{xy} \end{bmatrix} \quad (4.1.5)$$

For the rest of the thesis, the transformation matrix  $[T]$ , will be defined as:

$$\begin{bmatrix} \sigma_1 \\ \sigma_2 \\ \tau_{12} \end{bmatrix} = [T] \cdot \begin{bmatrix} \sigma_x \\ \sigma_y \\ \tau_{xy} \end{bmatrix} \quad \text{and} \quad \begin{bmatrix} \sigma_x \\ \sigma_y \\ \tau_{xy} \end{bmatrix} = [T]^{-1} \cdot \begin{bmatrix} \sigma_1 \\ \sigma_2 \\ \tau_{12} \end{bmatrix} \quad (4.1.6)$$

where:

$$[T]^{-1} = \begin{bmatrix} \cos^2\theta & \sin^2\theta & -2 \cdot \sin\theta \cdot \cos\theta \\ \sin^2\theta & \cos^2\theta & 2 \cdot \sin\theta \cdot \cos\theta \\ \sin\theta \cdot \cos\theta & -\sin\theta \cdot \cos\theta & \cos^2\theta - \sin^2\theta \end{bmatrix} \quad (4.1.7)$$

By following the same rationale but including the out of plane stresses, the transformation matrix around the vertical axis is<sup>[2],[4]</sup>:

$$[T]_{3D} = \begin{bmatrix} \cos^2\theta & \sin^2\theta & 0 & 0 & 0 & 2 \cdot \sin\theta \cdot \cos\theta \\ \sin^2\theta & \cos^2\theta & 0 & 0 & 0 & -2 \cdot \sin\theta \cdot \cos\theta \\ 0 & 0 & 1 & 0 & 0 & 0 \\ 0 & 0 & 0 & \cos\theta & -\sin\theta & 0 \\ 0 & 0 & 0 & \sin\theta & \cos\theta & 0 \\ -\sin\theta \cdot \cos\theta & \sin\theta \cdot \cos\theta & 0 & 0 & 0 & \cos^2\theta - \sin^2\theta \end{bmatrix} \quad (4.1.8)$$

And its inverse is:

$$[T]_{3D}^{-1} = \begin{bmatrix} \cos^2\theta & \sin^2\theta & 0 & 0 & 0 & -2 \cdot \sin\theta \cdot \cos\theta \\ \sin^2\theta & \cos^2\theta & 0 & 0 & 0 & 2 \cdot \sin\theta \cdot \cos\theta \\ 0 & 0 & 1 & 0 & 0 & 0 \\ 0 & 0 & 0 & \cos\theta & \sin\theta & 0 \\ 0 & 0 & 0 & -\sin\theta & \cos\theta & 0 \\ \sin\theta \cdot \cos\theta & -\sin\theta \cdot \cos\theta & 0 & 0 & 0 & \cos^2\theta - \sin^2\theta \end{bmatrix} \quad (4.1.9)$$

where:

$$\begin{bmatrix} \sigma_1 \\ \sigma_2 \\ \sigma_3 \\ \tau_{23} \\ \tau_{13} \\ \tau_{12} \end{bmatrix} = [T]_{3D} \cdot \begin{bmatrix} \sigma_x \\ \sigma_y \\ \sigma_z \\ \tau_{yz} \\ \tau_{xz} \\ \tau_{xy} \end{bmatrix} \quad \text{and} \quad \begin{bmatrix} \sigma_x \\ \sigma_y \\ \sigma_z \\ \tau_{yz} \\ \tau_{xz} \\ \tau_{xy} \end{bmatrix} = [T]_{3D}^{-1} \cdot \begin{bmatrix} \sigma_1 \\ \sigma_2 \\ \sigma_3 \\ \tau_{23} \\ \tau_{13} \\ \tau_{12} \end{bmatrix} \quad (4.1.10)$$

As far as the strains are concerned, special attention should be given at the difference between engineering shear strain  $\gamma_{ij}$  and tensor shear strain  $\epsilon_{ij}$ <sup>[1]</sup>. These strains are related with the eq. (4.1.11):

$$\gamma_{ij} = 2 \cdot \epsilon_{ij} \quad (4.1.11)$$

For that reason, one should be careful before defining the relationship between the transformation matrix and the strain matrices in two different coordinate systems. One way that this relationship can be presented for plane stress conditions, is the following:

$$\begin{bmatrix} \epsilon_1 \\ \epsilon_2 \\ \epsilon_{12} \end{bmatrix} = \begin{bmatrix} \epsilon_1 \\ \epsilon_2 \\ \frac{\gamma_{12}}{2} \end{bmatrix} = [T] \cdot \begin{bmatrix} \epsilon_x \\ \epsilon_y \\ \frac{\gamma_{xy}}{2} \end{bmatrix} = [T] \cdot \begin{bmatrix} \epsilon_x \\ \epsilon_y \\ \epsilon_{xy} \end{bmatrix} \quad (4.1.12)$$

However, this notation can be confusing. Hence we will use the  $[R]$  matrix<sup>[5]</sup> (due to Reuter) to present the above relation in a more natural way:

$$[R] = \begin{bmatrix} 1 & 0 & 0 \\ 0 & 1 & 0 \\ 0 & 0 & 2 \end{bmatrix} \quad (4.1.13)$$

$$\begin{bmatrix} \varepsilon_1 \\ \varepsilon_2 \\ \gamma_{12} \end{bmatrix} = [R] \cdot \begin{bmatrix} \varepsilon_1 \\ \varepsilon_2 \\ \frac{\gamma_{12}}{2} \end{bmatrix} \quad \text{and} \quad \begin{bmatrix} \varepsilon_x \\ \varepsilon_y \\ \gamma_{xy} \end{bmatrix} = [R] \cdot \begin{bmatrix} \varepsilon_x \\ \varepsilon_y \\ \frac{\gamma_{xy}}{2} \end{bmatrix} \quad (4.1.14)$$

Now, by combining the eq. (4.1.14) with (4.1.12)

$$\begin{bmatrix} \varepsilon_1 \\ \varepsilon_2 \\ \gamma_{12} \end{bmatrix} = [R] \cdot \begin{bmatrix} \varepsilon_1 \\ \varepsilon_2 \\ \frac{\gamma_{12}}{2} \end{bmatrix} = [R] \cdot [T] \cdot \begin{bmatrix} \varepsilon_x \\ \varepsilon_y \\ \frac{\gamma_{xy}}{2} \end{bmatrix} = [R] \cdot [T] \cdot [R]^{-1} \begin{bmatrix} \varepsilon_x \\ \varepsilon_y \\ \gamma_{xy} \end{bmatrix} \Rightarrow \quad (4.1.15)$$

$$\begin{bmatrix} \varepsilon_1 \\ \varepsilon_2 \\ \gamma_{12} \end{bmatrix} = [R] \cdot [T] \cdot [R]^{-1} \begin{bmatrix} \varepsilon_x \\ \varepsilon_y \\ \gamma_{xy} \end{bmatrix}$$

The second step is to define how the stresses and the strains are related at the fibers' direction. The transformation of the stresses from the lamina's natural direction "x" to the principal material's direction "1" results in assuming the material as specially orthotropic. To further elaborate on this, a lamina with arbitrary fiber orientation is assumed generally orthotropic; but when it is looked from a coordination system at which one of the main axes coincide with the fibers' direction (other than the vertical axis which stays the same), the lamina can be assumed specially orthotropic and can be analyzed as such. The main characteristic of the specially orthotropic materials that simplifies the analysis is the fact that there is no coupling between the normal and the shear stresses. Later, it is shown that through the transformation matrix, there is coupling between normal and shear stresses for laminae with arbitrary fiber direction but for now, by looking the material from its principal material coordinates this is not the case. As a result, from the Hooke's Law, it is known that for an orthotropic material which is loaded at one of its principal directions (let's assume at "1" direction) the resultant strains are<sup>[6]</sup>:

$$\varepsilon_1 = \frac{\sigma_1}{E_1}, \quad \varepsilon_2 = -\frac{\nu_{12} \cdot \sigma_1}{E_1}, \quad \gamma_{12} = 0 \quad (4.1.16)$$

The strain-stress relations can be written in a matrix form for plane stress conditions as:

$$\begin{bmatrix} \varepsilon_1 \\ \varepsilon_2 \\ \gamma_{12} \end{bmatrix} = \begin{bmatrix} S_{11} & S_{12} & 0 \\ S_{21} & S_{22} & 0 \\ 0 & 0 & S_{66} \end{bmatrix} \cdot \begin{bmatrix} \sigma_1 \\ \sigma_2 \\ \tau_{12} \end{bmatrix} \quad (4.1.17)$$

where:

$$S_{11} = \frac{1}{E_1}, \quad S_{12} = S_{21} = -\frac{\nu_{12}}{E_1} = -\frac{\nu_{21}}{E_2}, \quad S_{22} = \frac{1}{E_2}, \quad S_{66} = \frac{1}{G_{12}} \quad (4.1.18)$$

The  $[S]$  is symmetric and as such  $S_{12} = S_{21}$ . The proof for that can be found at Ref. [1] at page 33.

If the strain in the out-of plane direction is to be defined:

$$\varepsilon_3 = S_{13} \cdot \sigma_1 + S_{23} \cdot \sigma_2 \quad (4.1.19)$$

But in order to define it, the out-of plane Poisson's ratios should be known, i.e.  $\nu_{23}, \nu_{13}$ . One can also define the stress-strain relation by inverting the relation in eq. (4.1.17) as:

$$\begin{bmatrix} \sigma_1 \\ \sigma_2 \\ \tau_{12} \end{bmatrix} = \begin{bmatrix} Q_{11} & Q_{12} & 0 \\ Q_{12} & Q_{22} & 0 \\ 0 & 0 & Q_{66} \end{bmatrix} \cdot \begin{bmatrix} \varepsilon_1 \\ \varepsilon_2 \\ \gamma_{12} \end{bmatrix} \quad \text{or} \quad \begin{bmatrix} \sigma_1 \\ \sigma_2 \\ \tau_{12} \end{bmatrix} = [Q] \cdot \begin{bmatrix} \varepsilon_1 \\ \varepsilon_2 \\ \gamma_{12} \end{bmatrix} \quad (4.1.20)$$

Where:

$$Q_{11} = \frac{S_{22}}{S_{11} \cdot S_{22} - S_{12}^2}, \quad Q_{12} = -\frac{S_{12}}{S_{11} \cdot S_{22} - S_{12}^2}, \quad Q_{22} = \frac{S_{11}}{S_{11} \cdot S_{22} - S_{12}^2}, \quad Q_{66} = \frac{1}{S_{66}} \quad (4.1.21)$$

The relations in eq. (4.1.21) adjusted according to the eq. (4.1.18) are presented below:

$$Q_{11} = \frac{E_1}{1 - \nu_{12} \cdot \nu_{21}}, \quad Q_{12} = \frac{\nu_{12} \cdot E_2}{1 - \nu_{12} \cdot \nu_{21}} = \frac{\nu_{21} \cdot E_1}{1 - \nu_{12} \cdot \nu_{21}}, \quad Q_{22} = \frac{E_2}{1 - \nu_{12} \cdot \nu_{21}}, \quad Q_{66} = G_{66} \quad (4.1.22)$$

To summarize, by combing eq. (4.1.6) with eq. (4.1.20) and eq. (4.1.15) the result is:

$$\begin{aligned}
 \begin{bmatrix} \sigma_x \\ \sigma_y \\ \tau_{xy} \end{bmatrix} &= [T]^{-1} \cdot \begin{bmatrix} \sigma_1 \\ \sigma_2 \\ \tau_{12} \end{bmatrix} \stackrel{\text{eq.(4.1.20)}}{=} [T]^{-1} \cdot [Q] \cdot \begin{bmatrix} \varepsilon_1 \\ \varepsilon_2 \\ \gamma_{12} \end{bmatrix} \stackrel{\text{eq.(4.1.15)}}{=} [T]^{-1} \cdot [Q] \cdot [R] \cdot [T] \cdot [R]^{-1} \begin{bmatrix} \varepsilon_x \\ \varepsilon_y \\ \gamma_{xy} \end{bmatrix}, \\
 \begin{bmatrix} \sigma_x \\ \sigma_y \\ \tau_{xy} \end{bmatrix} &= \begin{bmatrix} \bar{Q}_{11} & \bar{Q}_{12} & \bar{Q}_{16} \\ \bar{Q}_{12} & \bar{Q}_{22} & \bar{Q}_{26} \\ \bar{Q}_{16} & \bar{Q}_{26} & \bar{Q}_{66} \end{bmatrix} \cdot \begin{bmatrix} \varepsilon_x \\ \varepsilon_y \\ \gamma_{xy} \end{bmatrix} \quad \text{or} \quad \begin{bmatrix} \sigma_x \\ \sigma_y \\ \tau_{xy} \end{bmatrix} = [\bar{Q}] \cdot \begin{bmatrix} \varepsilon_x \\ \varepsilon_y \\ \gamma_{xy} \end{bmatrix}
 \end{aligned} \tag{4.1.23}$$

The matrix  $[\bar{Q}]$  is called the transformed reduced stiffness matrix and it relates the stresses at the body's directions which are usually the known quantities with the strains at the same direction. To describe what is shown in the eq. (4.1.23), the procedure starts by transforming the stresses from the body's direction to the principal material's directions, then the stresses are translated to strains at the same local coordinate system by taking into account the material as specially orthotropic and then the strains are transformed back to the original directions, i.e. the body's directions. Each individual term in the resultant relation (4.1.23) is shown in eq. (4.1.24):

$$\begin{aligned}
 \bar{Q}_{11} &= Q_{11} \cdot \cos^4 \theta + 2 \cdot (Q_{12} + 2 \cdot Q_{66}) \cdot \sin^2 \theta \cdot \cos^2 \theta + Q_{22} \cdot \sin^4 \theta \\
 \bar{Q}_{12} &= (Q_{11} + Q_{22} - 4 \cdot Q_{66}) \cdot \cos^2 \theta \cdot \sin^2 \theta + Q_{12} \cdot (\sin^4 \theta + \cos^4 \theta) \\
 \bar{Q}_{22} &= Q_{11} \cdot \sin^4 \theta + 2 \cdot (Q_{12} + 2 \cdot Q_{66}) \cdot \sin^2 \theta \cdot \cos^2 \theta + Q_{22} \cdot \cos^4 \theta \\
 \bar{Q}_{16} &= (Q_{11} - Q_{12} - 2 \cdot Q_{66}) \cdot \sin \theta \cdot \cos^3 \theta + (Q_{12} - Q_{22} + 2 \cdot Q_{66}) \cdot \sin^3 \theta \cdot \cos \theta \\
 \bar{Q}_{26} &= (Q_{11} - Q_{12} - 2 \cdot Q_{66}) \cdot \sin^3 \theta \cdot \cos \theta + (Q_{12} - Q_{22} + 2 \cdot Q_{66}) \cdot \sin \theta \cdot \cos^3 \theta \\
 \bar{Q}_{66} &= (Q_{11} + Q_{22} - 2 \cdot Q_{12} - 2 \cdot Q_{66}) \cdot \sin^2 \theta \cdot \cos^2 \theta + Q_{66} \cdot (\sin^4 \theta + \cos^4 \theta)
 \end{aligned} \tag{4.1.24}$$

As it was mentioned above, usually the stresses are known through which the strains can be calculated. Hence, by inverting the matrix  $[\bar{Q}]$  one can directly calculate the strains; this procedure is shown below (because it can be proven that<sup>[1]</sup>:  $[R] \cdot [T] \cdot [R]^{-1} = [T]^{-T}$ )

$$\begin{bmatrix} \varepsilon_x \\ \varepsilon_y \\ \gamma_{xy} \end{bmatrix} = [T]^T \cdot [S] \cdot [T] \cdot \begin{bmatrix} \sigma_x \\ \sigma_y \\ \tau_{xy} \end{bmatrix} = \begin{bmatrix} \bar{S}_{11} & \bar{S}_{12} & \bar{S}_{16} \\ \bar{S}_{12} & \bar{S}_{22} & \bar{S}_{26} \\ \bar{S}_{16} & \bar{S}_{26} & \bar{S}_{66} \end{bmatrix} \cdot \begin{bmatrix} \sigma_x \\ \sigma_y \\ \tau_{xy} \end{bmatrix} \tag{4.1.25}$$

Each individual term of the  $[\bar{S}]$  is presented below in eq. (4.1.26):

$$\begin{aligned}
\bar{S}_{11} &= S_{11} \cdot \cos^4 \theta + (2 \cdot S_{12} + S_{66}) \cdot \sin^2 \theta \cdot \cos^2 \theta + S_{22} \cdot \sin^4 \theta \\
\bar{S}_{12} &= (S_{11} + S_{22} - S_{66}) \cdot \cos^2 \theta \cdot \sin^2 \theta + S_{12} \cdot (\sin^4 \theta + \cos^4 \theta) \\
\bar{S}_{22} &= S_{11} \cdot \sin^4 \theta + (2 \cdot S_{12} + S_{66}) \cdot \sin^2 \theta \cdot \cos^2 \theta + S_{22} \cdot \cos^4 \theta \\
\bar{S}_{16} &= (2 \cdot S_{11} - 2 \cdot S_{12} - S_{66}) \cdot \sin \theta \cdot \cos^3 \theta - (2 \cdot S_{22} - 2 \cdot S_{12} - S_{66}) \cdot \sin^3 \theta \cdot \cos \theta \\
\bar{S}_{26} &= (2 \cdot S_{11} - 2 \cdot S_{12} - S_{66}) \cdot \sin^3 \theta \cdot \cos \theta - (2 \cdot S_{22} - 2 \cdot S_{12} - S_{66}) \cdot \sin \theta \cdot \cos^3 \theta \\
\bar{S}_{66} &= 2 \cdot (2 \cdot S_{11} + 2 \cdot S_{22} - 4 \cdot S_{12} - S_{66}) \cdot \sin^2 \theta \cdot \cos^2 \theta + S_{66} \cdot (\sin^4 \theta + \cos^4 \theta)
\end{aligned} \tag{4.1.26}$$

The values of  $S_{11}, S_{12}, S_{22}, S_{66}$  can be found through the equation (4.1.18)

**Note(4.1):** As it was mentioned earlier, a lamina with arbitrary orientation, i.e.  $\theta \neq 0^\circ$ , presents coupling between normal and shear stresses/strains. Mathematically, this is the case due to the non-zero terms of  $\bar{Q}_{16}, \bar{Q}_{26}$  or  $\bar{S}_{16}, \bar{S}_{26}$  respectively. From a physics perspective, the lamina is stronger at the direction at which the fibers lie whereas it is weaker at the perpendicular directions. When the lamina is stressed at the body's directions the diagonal that is stronger tends to deform less than the other diagonal leading the material to develop shear stresses. A graphical representation is given at fig. [4-3(a.)]; it is obvious that when the body is stressed in the "x" direction, the A – C side will elongate less than the B – D side according to the fibers' orientation given in the same figure. Hence, the body will deform in the way shown in fig. [4-3(b.)] leading to shear stresses. To conclude, even if the material is specially orthotropic when looked from its principal directions, in practice it behaves as generally orthotropic because frequently it is loaded in a direction different than its principal and after the transformation of stresses from one coordinate system to another, the results show a coupling between normal and shear stresses.

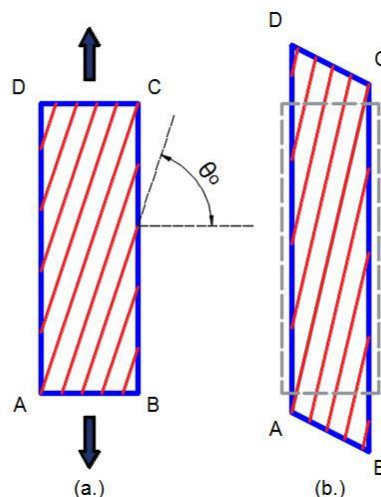


Figure 4-3: Lamina with arbitrary fiber orientation, axially loaded

By following the same rationale for the 3D case, the stress-strain relation is given below<sup>[2]</sup>:

$$\begin{bmatrix} \sigma_x \\ \sigma_y \\ \sigma_z \\ \tau_{yz} \\ \tau_{xz} \\ \tau_{xy} \end{bmatrix} = \begin{bmatrix} \bar{Q}_{11} & \bar{Q}_{12} & \bar{Q}_{13} & 0 & 0 & \bar{Q}_{16} \\ \bar{Q}_{12} & \bar{Q}_{22} & \bar{Q}_{23} & 0 & 0 & \bar{Q}_{26} \\ \bar{Q}_{13} & \bar{Q}_{23} & \bar{Q}_{33} & 0 & 0 & \bar{Q}_{36} \\ 0 & 0 & 0 & \bar{Q}_{44} & \bar{Q}_{45} & 0 \\ 0 & 0 & 0 & \bar{Q}_{45} & \bar{Q}_{55} & 0 \\ \bar{Q}_{16} & \bar{Q}_{26} & \bar{Q}_{36} & 0 & 0 & \bar{Q}_{66} \end{bmatrix} \cdot \begin{bmatrix} \varepsilon_x \\ \varepsilon_y \\ \varepsilon_z \\ \gamma_{yz} \\ \gamma_{xz} \\ \gamma_{xy} \end{bmatrix} \quad (4.1.27)$$

where the individual terms are:

$$\begin{aligned}
 \bar{Q}_{11} &= Q_{11} \cdot \cos^4 \theta + 2 \cdot (Q_{12} + 2 \cdot Q_{66}) \cdot \sin^2 \theta \cdot \cos^2 \theta + Q_{22} \cdot \sin^4 \theta \\
 \bar{Q}_{12} &= (Q_{11} + Q_{22} - 4 \cdot Q_{66}) \cdot \cos^2 \theta \cdot \sin^2 \theta + Q_{12} \cdot (\sin^4 \theta + \cos^4 \theta) \\
 \bar{Q}_{13} &= Q_{13} \cdot \cos^2 \theta + Q_{23} \cdot \sin^2 \theta \\
 \bar{Q}_{16} &= (Q_{11} - Q_{12} - 2 \cdot Q_{66}) \cdot \sin \theta \cdot \cos^3 \theta + (Q_{12} - Q_{22} + 2 \cdot Q_{66}) \cdot \sin^3 \theta \cdot \cos \theta \\
 \bar{Q}_{22} &= Q_{11} \cdot \sin^4 \theta + 2 \cdot (Q_{12} + 2 \cdot Q_{66}) \cdot \sin^2 \theta \cdot \cos^2 \theta + Q_{22} \cdot \cos^4 \theta \\
 \bar{Q}_{23} &= Q_{23} \cdot \cos^2 \theta + Q_{13} \cdot \sin^2 \theta \\
 \bar{Q}_{26} &= (Q_{11} - Q_{12} - 2 \cdot Q_{66}) \cdot \sin^3 \theta \cdot \cos \theta + (Q_{12} - Q_{22} + 2 \cdot Q_{66}) \cdot \sin \theta \cdot \cos^3 \theta \\
 \bar{Q}_{33} &= Q_{33} \\
 \bar{Q}_{44} &= Q_{44} \cdot \cos^2 \theta + Q_{55} \cdot \sin^2 \theta \\
 \bar{Q}_{45} &= (Q_{55} - Q_{44}) \cdot \cos \theta \cdot \sin \theta \\
 \bar{Q}_{55} &= Q_{55} \cdot \cos^2 \theta + Q_{44} \cdot \sin^2 \theta \\
 \bar{Q}_{66} &= (Q_{11} + Q_{22} - 2 \cdot Q_{12} - 2 \cdot Q_{66}) \cdot \sin^2 \theta \cdot \cos^2 \theta + Q_{66} \cdot (\sin^4 \theta + \cos^4 \theta)
 \end{aligned} \quad (4.1.28)$$

The terms appearing in the equation (4.1.28) can be found below as:

$$\begin{aligned}
 Q_{11} &= \frac{1 - \nu_{23} \cdot \nu_{32}}{E_2 \cdot E_3 \cdot \Delta} \\
 Q_{12} &= \frac{\nu_{21} + \nu_{31} \cdot \nu_{23}}{E_2 \cdot E_3 \cdot \Delta} = \frac{\nu_{12} + \nu_{32} \cdot \nu_{13}}{E_1 \cdot E_3 \cdot \Delta}
 \end{aligned} \quad (4.1.29)$$

$$Q_{13} = \frac{\nu_{31} + \nu_{21} \cdot \nu_{32}}{E_2 \cdot E_3 \cdot \Delta} = \frac{\nu_{13} + \nu_{12} \cdot \nu_{23}}{E_1 \cdot E_2 \cdot \Delta}$$

$$Q_{22} = \frac{1 - \nu_{13} \cdot \nu_{31}}{E_1 \cdot E_3 \cdot \Delta}$$

$$Q_{23} = \frac{\nu_{32} + \nu_{12} \cdot \nu_{31}}{E_1 \cdot E_3 \cdot \Delta} = \frac{\nu_{23} + \nu_{21} \cdot \nu_{13}}{E_1 \cdot E_2 \cdot \Delta}$$

$$Q_{33} = \frac{1 - \nu_{12} \cdot \nu_{21}}{E_1 \cdot E_2 \cdot \Delta}$$

$$Q_{44} = G_{23}$$

$$Q_{55} = G_{13}$$

$$Q_{66} = G_{12}$$

$$\Delta = \frac{1 - \nu_{12} \cdot \nu_{21} - \nu_{23} \cdot \nu_{32} - \nu_{31} \cdot \nu_{13} - 2 \cdot \nu_{21} \cdot \nu_{32} \cdot \nu_{13}}{E_1 \cdot E_2 \cdot E_3}$$

On the other hand, if the stresses have to be related with the strains for the 3D case, the resultant matrix is:

$$\begin{bmatrix} \varepsilon_x \\ \varepsilon_y \\ \varepsilon_z \\ \gamma_{yz} \\ \gamma_{xz} \\ \gamma_{xy} \end{bmatrix} = \begin{bmatrix} \bar{S}_{11} & \bar{S}_{12} & \bar{S}_{13} & 0 & 0 & \bar{S}_{16} \\ \bar{S}_{12} & \bar{S}_{22} & \bar{S}_{23} & 0 & 0 & \bar{S}_{26} \\ \bar{S}_{13} & \bar{S}_{23} & \bar{S}_{33} & 0 & 0 & \bar{S}_{36} \\ 0 & 0 & 0 & \bar{S}_{44} & \bar{S}_{45} & 0 \\ 0 & 0 & 0 & \bar{S}_{45} & \bar{S}_{55} & 0 \\ \bar{S}_{16} & \bar{S}_{26} & \bar{S}_{36} & 0 & 0 & \bar{S}_{66} \end{bmatrix} \cdot \begin{bmatrix} \sigma_x \\ \sigma_y \\ \sigma_z \\ \tau_{yz} \\ \tau_{xz} \\ \tau_{xy} \end{bmatrix} \quad (4.1.30)$$

where the individual terms are:

$$\bar{S}_{11} = S_{11} \cdot \cos^4 \theta + (2 \cdot S_{12} + S_{66}) \cdot \sin^2 \theta \cdot \cos^2 \theta + S_{22} \cdot \sin^4 \theta$$

$$\bar{S}_{12} = (S_{11} + S_{22} - S_{66}) \cdot \cos^2 \theta \cdot \sin^2 \theta + S_{12} \cdot (\sin^4 \theta + \cos^4 \theta)$$

$$\bar{S}_{13} = S_{13} \cdot \cos^2 \theta + S_{23} \cdot \sin^2 \theta$$

$$\bar{S}_{16} = (2 \cdot S_{11} - 2 \cdot S_{12} - S_{66}) \cdot \sin \theta \cdot \cos^3 \theta - (2 \cdot S_{22} - 2 \cdot S_{12} - S_{66}) \cdot \sin^3 \theta \cdot \cos \theta$$

$$\bar{S}_{22} = S_{11} \cdot \sin^4 \theta + (2 \cdot S_{12} + S_{66}) \cdot \sin^2 \theta \cdot \cos^2 \theta + S_{22} \cdot \cos^4 \theta$$

(4.1.31)

$$\begin{aligned}
\bar{S}_{23} &= S_{23} \cdot \cos^2 \theta + S_{13} \cdot \sin^2 \theta \\
\bar{S}_{26} &= (2 \cdot S_{11} - 2 \cdot S_{12} - S_{66}) \cdot \sin^3 \theta \cdot \cos \theta - (2 \cdot S_{22} - 2 \cdot S_{12} - S_{66}) \cdot \sin \theta \cdot \cos^3 \theta \\
\bar{S}_{33} &= S_{33} \\
\bar{S}_{44} &= S_{44} \cdot \cos^2 \theta + S_{55} \cdot \sin^2 \theta \\
\bar{S}_{45} &= (S_{55} - S_{44}) \cdot \cos \theta \cdot \sin \theta \\
\bar{S}_{55} &= S_{55} \cdot \cos^2 \theta + S_{44} \cdot \sin^2 \theta \\
\bar{S}_{66} &= 2 \cdot (2 \cdot S_{11} + 2 \cdot S_{22} - 4 \cdot S_{12} - S_{66}) \cdot \sin^2 \theta \cdot \cos^2 \theta + S_{66} \cdot (\sin^4 \theta + \cos^4 \theta)
\end{aligned}$$

The terms appearing in the equation (4.1.31) can be found below as:

$$\begin{aligned}
S_{11} &= \frac{1}{E_1}, & S_{33} &= \frac{1}{E_3} \\
S_{12} &= -\frac{\nu_{12}}{E_1} = -\frac{\nu_{21}}{E_2}, & S_{44} &= \frac{1}{G_{23}} \\
S_{13} &= -\frac{\nu_{31}}{E_3} = -\frac{\nu_{13}}{E_3}, & S_{55} &= \frac{1}{G_{13}} \\
S_{22} &= \frac{1}{E_2}, & S_{66} &= \frac{1}{G_{12}} \\
S_{23} &= -\frac{\nu_{32}}{E_3} = -\frac{\nu_{23}}{E_2}
\end{aligned} \tag{4.1.32}$$

## 4.2 Classical Lamination Theory

The previous chapter constitutes the basis for the analysis of the laminates. As it was mentioned in the introduction of this chapter, a laminate is nothing else than a sequence of laminae which are placed on top of each other. These laminae can be of different material, thickness and fiber orientation. During this thesis, the material will be assumed the same through the thickness of the laminated composite sections.

Prior to the analysis of the macromechanical behavior of the laminates, the assumptions that were made should be mentioned. One of the most prominent assumptions is that the laminates follow the Kirchhoff hypothesis. The latter defines that straight lines that are perpendicular to the midsurface of the section prior to the load, stay perpendicular after the loading as well as straight, thus  $\gamma_{xz} = \gamma_{yz} = 0$ . As a result, the straight line  $A - A'$  in fig. [4-4] only translates and rotates but it does not deform. The second assumption in Kirchhoff's hypothesis is that the length of the initially vertical line (for flat plates) that connects the top and bottom surfaces stays unchanged after the loading (distance  $t - t'$  in fig. [4-4]), thus  $\varepsilon_z = 0$ . Apart from the

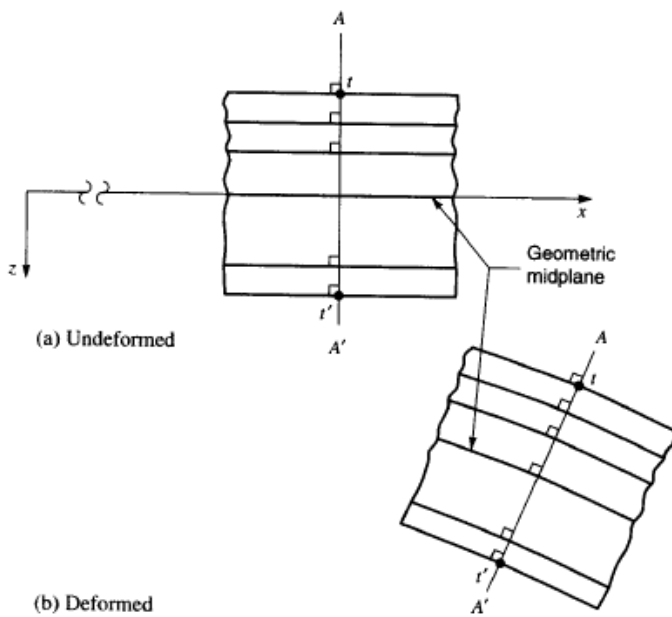


Figure 4-4: Kirchhoff's Hypothesis<sup>[7]</sup>

assumptions intrinsic in the Kirchhoff's hypothesis, there are also other assumptions that were made. For example, the strains and displacements are assumed small whereas the transverse shear strains at top and bottom surfaces of the laminate should be zero. Regarding the manufacturing procedure of the material, the layers are assumed to be perfectly bonded, without relative slippage between layers as well as that each layer is of uniform thickness. Finally, the laminates are considered thin.

The next step is to analyze how a random point  $P^0$  at the midsurface translates after the implication of loading. According to the aforementioned assumptions, in a "x" – "z" plane, the point  $P^0$  will translate horizontally  $u_0$  and vertically  $w_0$  as it is shown in fig. [4-5]. Every other point on the straight line  $A - A'$  will translate horizontally at a distance  $u_i$  according to its distance from the midplane and according to the rotation of the line  $A - A'$ .

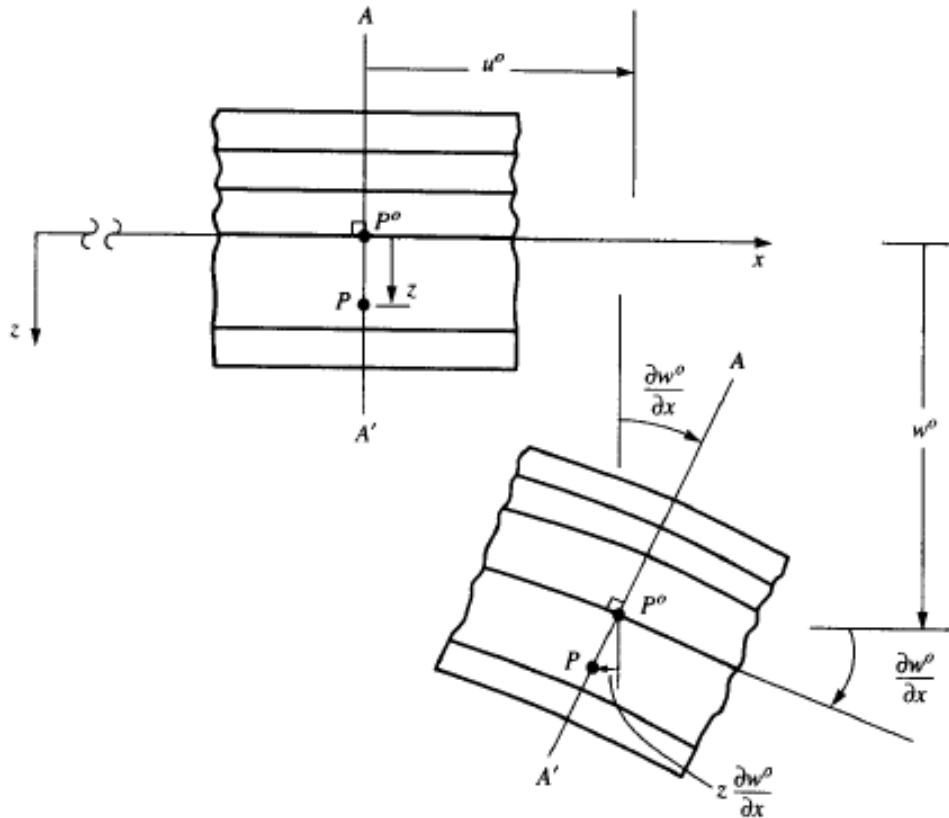


Figure 4-5: Kinematics of deformation as viewed in the "x" – "z" plane<sup>[7]</sup>

For example, for a random Point  $P$ , the horizontal translation in the "x" – "z" plane, will be:

$$u_P = u_0 - z_P \cdot \frac{\partial w^0}{\partial x} \quad (4.2.1)$$

By following the same rationale, in the "y" – "z" plane:

$$v_P = v_0 - z_P \cdot \frac{\partial w^0}{\partial y} \quad (4.2.2)$$

Their general form can be expressed as:

$$\begin{aligned} u &= u_0 - z \cdot \frac{\partial w^0}{\partial x} \\ v &= v_0 - z \cdot \frac{\partial w^0}{\partial y} \end{aligned} \quad (4.2.3)$$

It is also known that the strains expressed in displacements can be defined as (for small strains):

$$\begin{aligned} \varepsilon_x &= \frac{\partial u}{\partial x} \\ \varepsilon_y &= \frac{\partial v}{\partial y} \\ \gamma_{xy} &= \frac{\partial u}{\partial y} + \frac{\partial v}{\partial x} \end{aligned} \quad (4.2.4)$$

By combining the eq. (4.2.3eq2\_35) & eq. (4.2.4):

$$\begin{aligned} \varepsilon_x &= \frac{\partial}{\partial x} \left( u_0 - z \cdot \frac{\partial w^0}{\partial x} \right) = \frac{\partial u_0}{\partial x} - z \cdot \frac{\partial^2 w^0}{\partial x^2} \\ \varepsilon_y &= \frac{\partial}{\partial y} \left( v_0 - z \cdot \frac{\partial w^0}{\partial y} \right) = \frac{\partial v_0}{\partial y} - z \cdot \frac{\partial^2 w^0}{\partial y^2} \\ \gamma_{xy} &= \frac{\partial}{\partial y} \left( u_0 - z \cdot \frac{\partial w^0}{\partial x} \right) + \frac{\partial}{\partial x} \left( v_0 - z \cdot \frac{\partial w^0}{\partial y} \right) = \frac{\partial u_0}{\partial x} + \frac{\partial u_0}{\partial y} - 2 \cdot z \cdot \frac{\partial^2 w^0}{\partial x \cdot \partial y} \end{aligned} \quad (4.2.5)$$

In a matrix form the eq. (4.2.5) can be written as:

$$\begin{bmatrix} \varepsilon_x \\ \varepsilon_y \\ \gamma_{xy} \end{bmatrix} = \begin{bmatrix} \varepsilon_x^0 \\ \varepsilon_y^0 \\ \gamma_{xy}^0 \end{bmatrix} + z \cdot \begin{bmatrix} \kappa_x \\ \kappa_y \\ \kappa_{xy} \end{bmatrix} \quad (4.2.6)$$

where:

$$\begin{bmatrix} \varepsilon_x^0 \\ \varepsilon_y^0 \\ \gamma_{xy}^0 \end{bmatrix} = \begin{bmatrix} \frac{\partial u_0}{\partial x} \\ \frac{\partial v_0}{\partial y} \\ \frac{\partial u_0}{\partial y} + \frac{\partial v_0}{\partial x} \end{bmatrix} \quad (4.2.7)$$

$$\begin{bmatrix} \kappa_x \\ \kappa_y \\ \kappa_{xy} \end{bmatrix} = - \begin{bmatrix} \frac{\partial^2 w^0}{\partial x^2} \\ \frac{\partial^2 w^0}{\partial y^2} \\ 2 \cdot \frac{\partial^2 w^0}{\partial x \partial y} \end{bmatrix}$$

For a lamina "k", the eq. (4.2.6),(4.2.7) can be combined with the eq.(4.1.23) to get:

$$\begin{bmatrix} \sigma_x \\ \sigma_y \\ \tau_{xy} \end{bmatrix}_k = \begin{bmatrix} \bar{Q}_{11} & \bar{Q}_{12} & \bar{Q}_{16} \\ \bar{Q}_{12} & \bar{Q}_{22} & \bar{Q}_{26} \\ \bar{Q}_{16} & \bar{Q}_{26} & \bar{Q}_{66} \end{bmatrix}_k \cdot \left\{ \begin{bmatrix} \varepsilon_x^0 \\ \varepsilon_y^0 \\ \gamma_{xy}^0 \end{bmatrix} + z \cdot \begin{bmatrix} \kappa_x \\ \kappa_y \\ \kappa_{xy} \end{bmatrix} \right\} \quad (4.2.8)$$

The result of the equation (4.2.8) is that the stresses are not linear through the thickness of the section as the transformed reduced stiffness matrix  $[\bar{Q}]$  varies for laminae with different fiber orientation. In case of linear relation between stresses and strains in the lamina level (Hooke's Law), the stresses will have a multilinear form through the section even if the strain is linear through the thickness of the section; ergo, the stresses will be linear in a lamina level but with different inclination at each lamina in the laminate as shown in fig. [4-6fig12]. Nonetheless, if the stress strain relationship is not linear, the stresses even in a lamina will not be linear. For example, the stress-strain graph is not linear in compression and in shear which will result in a parabolic graph of stresses in a lamina for linear strains.

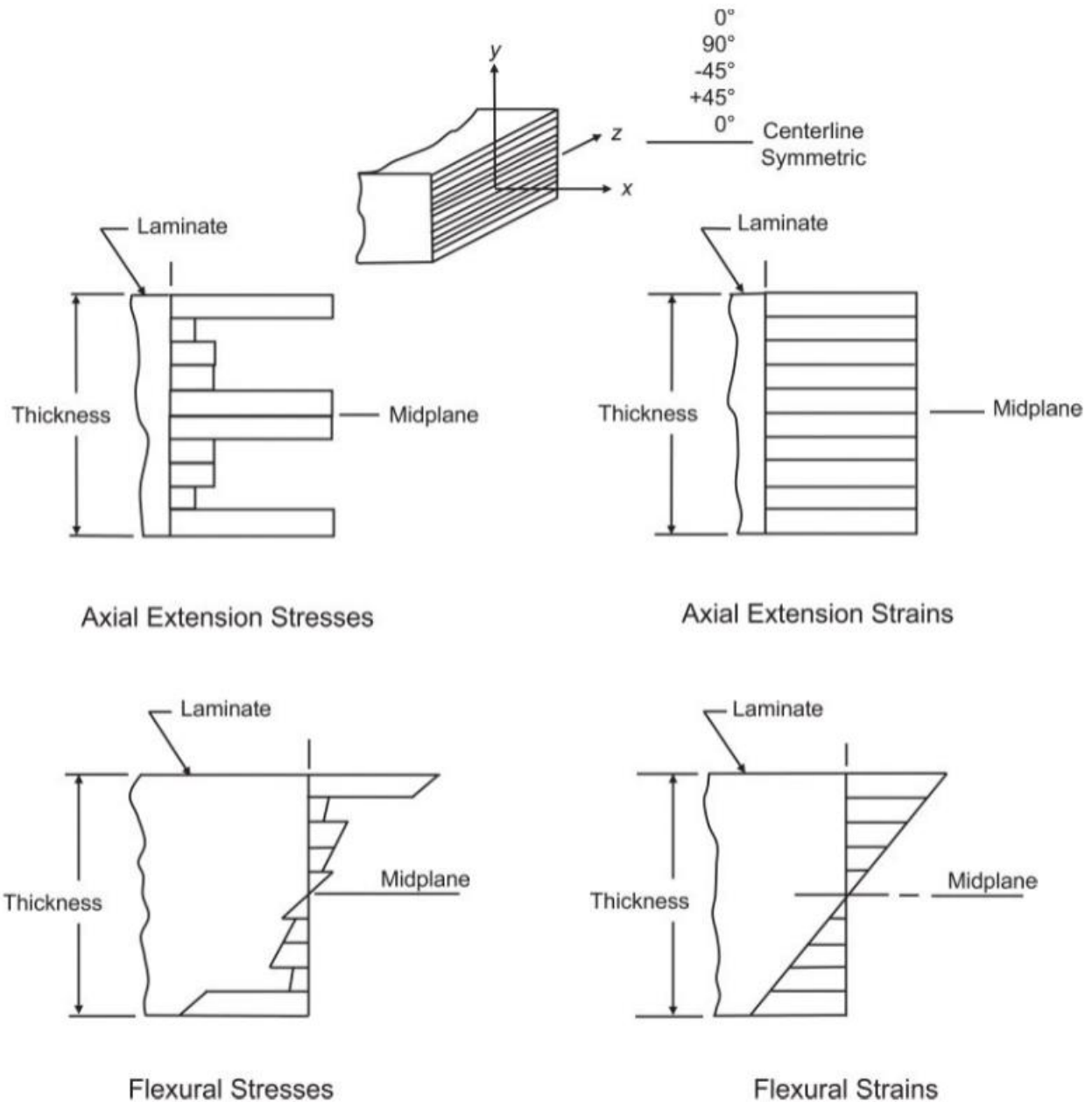


Figure 4-6: Variation of ply stresses and strains through the laminate thickness<sup>[8]</sup>

Frequently, the quantity that is given is not the stresses, but the forces. Thus, the relation that connects the forces with the strains/stresses has to be defined and this is done below.

From elementary structural mechanics, it is known that:

$$N_x = \int_{-\frac{t}{2}}^{\frac{t}{2}} \sigma_x dz \quad (4.2.9)$$

$$N_y = \int_{-\frac{t}{2}}^{\frac{t}{2}} \sigma_y dz$$

$$N_{xy} = N_s = \int_{-\frac{t}{2}}^{\frac{t}{2}} \tau_{xy} dz$$

$$M_x = \int_{-\frac{t}{2}}^{\frac{t}{2}} \sigma_x \cdot z dz$$

$$M_y = \int_{-\frac{t}{2}}^{\frac{t}{2}} \sigma_y \cdot z dz$$

$$M_{xy} = M_s = \int_{-\frac{t}{2}}^{\frac{t}{2}} \tau_{xy} \cdot z dz$$

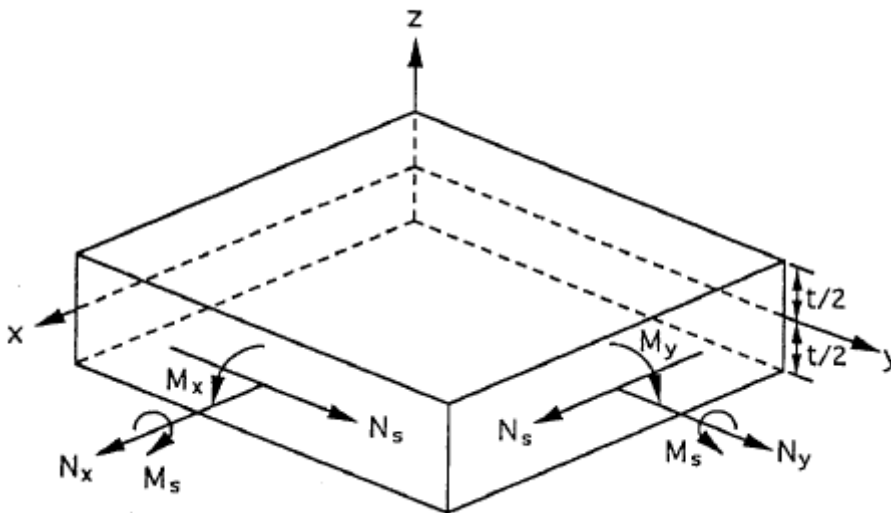


Figure 4-7: Element of single layer (lamina) with force and moment resultants<sup>[6]</sup>

In a matrix form, the eq. (4.2.9) can be written as:

$$\begin{bmatrix} N_x \\ N_y \\ N_{xy} \end{bmatrix} = \int_{-\frac{t}{2}}^{\frac{t}{2}} \begin{bmatrix} \sigma_x \\ \sigma_y \\ \tau_{xy} \end{bmatrix} dz = \sum_{k=1}^n \int_{h_{k-1}}^{h_k} \begin{bmatrix} \sigma_x \\ \sigma_y \\ \tau_{xy} \end{bmatrix} dz \quad (4.2.10)$$

$$\begin{bmatrix} M_x \\ M_y \\ M_{xy} \end{bmatrix} = \int_{-\frac{t}{2}}^{\frac{t}{2}} \begin{bmatrix} \sigma_x \\ \sigma_y \\ \tau_{xy} \end{bmatrix} \cdot z \, dz = \sum_{k=1}^n \int_{h_{k-1}}^{h_k} \begin{bmatrix} \sigma_x \\ \sigma_y \\ \tau_{xy} \end{bmatrix} \cdot z \, dz$$

By combining eq. (4.2.8) with eq. (4.2.10) and according to fig. [4-8]:

$$\begin{aligned} \begin{bmatrix} N_x \\ N_y \\ N_{xy} \end{bmatrix} &= \sum_{k=1}^n \left\{ \int_{h_{k-1}}^{h_k} \begin{bmatrix} \bar{Q}_{11} & \bar{Q}_{12} & \bar{Q}_{16} \\ \bar{Q}_{12} & \bar{Q}_{22} & \bar{Q}_{26} \\ \bar{Q}_{16} & \bar{Q}_{26} & \bar{Q}_{66} \end{bmatrix}_k \cdot \left\{ \begin{bmatrix} \varepsilon_x^0 \\ \varepsilon_y^0 \\ \gamma_{xy}^0 \end{bmatrix} + z \cdot \begin{bmatrix} \kappa_x \\ \kappa_y \\ \kappa_{xy} \end{bmatrix} \right\} dz \right\} \Rightarrow \\ \begin{bmatrix} N_x \\ N_y \\ N_{xy} \end{bmatrix} &= \sum_{k=1}^n \left\{ \begin{bmatrix} \bar{Q}_{11} & \bar{Q}_{12} & \bar{Q}_{16} \\ \bar{Q}_{12} & \bar{Q}_{22} & \bar{Q}_{26} \\ \bar{Q}_{16} & \bar{Q}_{26} & \bar{Q}_{66} \end{bmatrix}_k \cdot \left\{ \int_{h_{k-1}}^{h_k} \begin{bmatrix} \varepsilon_x^0 \\ \varepsilon_y^0 \\ \gamma_{xy}^0 \end{bmatrix} dz + \int_{h_{k-1}}^{h_k} \begin{bmatrix} \kappa_x \\ \kappa_y \\ \kappa_{xy} \end{bmatrix} \cdot z \, dz \right\} \right\} \\ \begin{bmatrix} M_x \\ M_y \\ M_{xy} \end{bmatrix} &= \sum_{k=1}^n \left\{ \int_{h_{k-1}}^{h_k} \begin{bmatrix} \bar{Q}_{11} & \bar{Q}_{12} & \bar{Q}_{16} \\ \bar{Q}_{12} & \bar{Q}_{22} & \bar{Q}_{26} \\ \bar{Q}_{16} & \bar{Q}_{26} & \bar{Q}_{66} \end{bmatrix}_k \cdot \left\{ \begin{bmatrix} \varepsilon_x^0 \\ \varepsilon_y^0 \\ \gamma_{xy}^0 \end{bmatrix} + z \cdot \begin{bmatrix} \kappa_x \\ \kappa_y \\ \kappa_{xy} \end{bmatrix} \right\} \cdot z \, dz \right\} \Rightarrow \\ \begin{bmatrix} M_x \\ M_y \\ M_{xy} \end{bmatrix} &= \sum_{k=1}^n \left\{ \begin{bmatrix} \bar{Q}_{11} & \bar{Q}_{12} & \bar{Q}_{16} \\ \bar{Q}_{12} & \bar{Q}_{22} & \bar{Q}_{26} \\ \bar{Q}_{16} & \bar{Q}_{26} & \bar{Q}_{66} \end{bmatrix}_k \cdot \left\{ \int_{h_{k-1}}^{h_k} \begin{bmatrix} \varepsilon_x^0 \\ \varepsilon_y^0 \\ \gamma_{xy}^0 \end{bmatrix} \cdot z \, dz + \int_{h_{k-1}}^{h_k} \begin{bmatrix} \kappa_x \\ \kappa_y \\ \kappa_{xy} \end{bmatrix} \cdot z^2 \, dz \right\} \right\} \end{aligned} \quad (4.2.11)$$

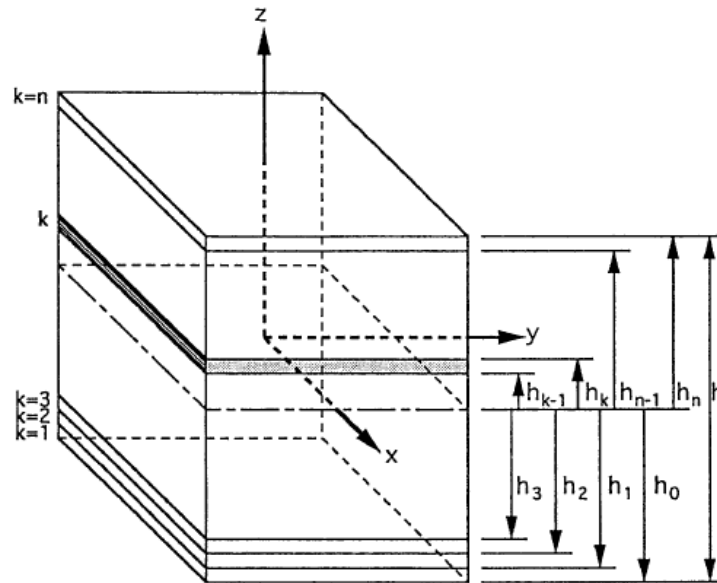


Figure 4-8: Multidirectional laminate with coordinate notation of individual plies<sup>[6]</sup>

In eq. (4.2.11), the transformed reduced stiffness matrix was put outside the integral as it is not dependent on the "z" coordinate. Also, according to the fig. [4-6fig12] which gives an example only for the axial stresses and strains, it is obvious that the strain  $\varepsilon_x^0$  (and in a similar way  $\varepsilon_y^0, \gamma_{xy}^0$ ) is independent of the "z" coordinate (and constant through the thickness) and can be put outside the integral too. Finally, the curvatures  $\kappa_x, \kappa_y, \kappa_{xy}$  are also independent of the "z" coordinate as the inclination of stresses stays constant through the thickness as it can be seen at the bottom right part of the same figure. Consequently, only the integrals  $\int_{h_{k-1}}^{h_k} dz, \int_{h_{k-1}}^{h_k} z dz, \int_{h_{k-1}}^{h_k} z^2 dz$  have to be calculated. The results from the eq. (4.2.11) can be written in the following form:

$$\begin{bmatrix} N_x \\ N_y \\ N_{xy} \end{bmatrix} = \begin{bmatrix} \bar{A}_{11} & \bar{A}_{12} & \bar{A}_{16} \\ \bar{A}_{12} & \bar{A}_{22} & \bar{A}_{26} \\ \bar{A}_{16} & \bar{A}_{26} & \bar{A}_{66} \end{bmatrix} \cdot \begin{bmatrix} \varepsilon_x^0 \\ \varepsilon_y^0 \\ \gamma_{xy}^0 \end{bmatrix} + \begin{bmatrix} \bar{B}_{11} & \bar{B}_{12} & \bar{B}_{16} \\ \bar{B}_{12} & \bar{B}_{22} & \bar{B}_{26} \\ \bar{B}_{16} & \bar{B}_{26} & \bar{B}_{66} \end{bmatrix} \cdot \begin{bmatrix} \kappa_x \\ \kappa_y \\ \kappa_{xy} \end{bmatrix} \quad (4.2.12)$$

$$\begin{bmatrix} M_x \\ M_y \\ M_{xy} \end{bmatrix} = \begin{bmatrix} \bar{B}_{11} & \bar{B}_{12} & \bar{B}_{16} \\ \bar{B}_{12} & \bar{B}_{22} & \bar{B}_{26} \\ \bar{B}_{16} & \bar{B}_{26} & \bar{B}_{66} \end{bmatrix} \cdot \begin{bmatrix} \varepsilon_x^0 \\ \varepsilon_y^0 \\ \gamma_{xy}^0 \end{bmatrix} + \begin{bmatrix} \bar{D}_{11} & \bar{D}_{12} & \bar{D}_{16} \\ \bar{D}_{12} & \bar{D}_{22} & \bar{D}_{26} \\ \bar{D}_{16} & \bar{D}_{26} & \bar{D}_{66} \end{bmatrix} \cdot \begin{bmatrix} \kappa_x \\ \kappa_y \\ \kappa_{xy} \end{bmatrix}$$

where:

$$A_{ij} = \sum_{k=1}^n (\bar{Q}_{ij})_k \cdot (h_k - h_{k-1}) \quad (4.2.13)$$

$$B_{ij} = \frac{1}{2} \cdot \sum_{k=1}^n (\bar{Q}_{ij})_k \cdot (h_k^2 - h_{k-1}^2)$$

$$D_{ij} = \frac{1}{3} \cdot \sum_{k=1}^n (\bar{Q}_{ij})_k \cdot (h_k^3 - h_{k-1}^3)$$

The terms  $A_{ij}, B_{ij}, D_{ij}$  in eq. (4.2.13) can be simplified in the following way:

$$\begin{aligned} (a.), \quad & (h_k - h_{k-1}) = t_k \\ (b.), \quad & (h_k^2 - h_{k-1}^2) = (h_k - h_{k-1}) \cdot (h_k + h_{k-1}) = t_k \cdot 2 \cdot \bar{z}_k \\ (c.), \quad & (h_k^3 - h_{k-1}^3) = [(h_k - h_{k-1})^3 + 3 \cdot h_k^2 \cdot h_{k-1} - 3 \cdot h_k \cdot h_{k-1}^2] = \\ & = [(h_k - h_{k-1})^3 + 3 \cdot (h_k - h_{k-1}) \cdot (h_k + h_{k-1})^2 - 3 \cdot (h_k^3 - h_{k-1}^3)] \Rightarrow \\ & 4 \cdot (h_k^3 - h_{k-1}^3) = (h_k - h_{k-1})^3 + 3 \cdot (h_k - h_{k-1}) \cdot (h_k + h_{k-1})^2 \Rightarrow \\ & (h_k^3 - h_{k-1}^3) = \frac{t_k^3}{4} + 3 \cdot t_k \cdot \bar{z}_k^2 \end{aligned} \quad (4.2.14)$$

where:

$t_k$ : ply thickness

$$\bar{z}_k = \frac{h_k + h_{k-1}}{2} = \text{distance from the geometric midsurface to the center of the } k^{\text{th}} \text{ ply}$$

As a result, by combining the eq. (4.2.13) with the eq. (4.2.14)

$$\begin{aligned} A_{ij} &= \sum_{k=1}^n (\bar{Q}_{ij})_k \cdot t_k \\ B_{ij} &= \sum_{k=1}^n (\bar{Q}_{ij})_k \cdot t_k \cdot \bar{z}_k \\ D_{ij} &= \sum_{k=1}^n \left[ (\bar{Q}_{ij})_k \cdot \frac{t_k^3}{12} + t_k \cdot \bar{z}_k^2 \right] \end{aligned} \quad (4.2.15)$$

In a matrix form, the eq. (4.2.15) can be written as:

$$\begin{bmatrix} N_x \\ N_y \\ N_{xy} \\ M_x \\ M_y \\ M_{xy} \end{bmatrix} = \begin{bmatrix} A_{11} & A_{12} & A_{16} & B_{11} & B_{12} & B_{16} \\ A_{12} & A_{22} & A_{26} & B_{12} & B_{22} & B_{26} \\ A_{16} & A_{26} & A_{66} & B_{16} & B_{26} & B_{66} \\ B_{11} & B_{12} & B_{16} & D_{11} & D_{12} & D_{16} \\ B_{12} & B_{22} & B_{26} & D_{12} & D_{22} & D_{26} \\ B_{16} & B_{26} & B_{66} & D_{16} & D_{26} & D_{66} \end{bmatrix} \cdot \begin{bmatrix} \varepsilon_x^0 \\ \varepsilon_y^0 \\ \gamma_{xy}^0 \\ \kappa_x \\ \kappa_y \\ \kappa_{xy} \end{bmatrix} \quad (4.2.16)$$

In a contracted form, the eq. (4.2.16) can be written as:

$$\begin{bmatrix} N \\ M \end{bmatrix} = \begin{bmatrix} A_{ij} & B_{ij} \\ B_{ij} & D_{ij} \end{bmatrix} \cdot \begin{bmatrix} \varepsilon^0 \\ \kappa \end{bmatrix} \quad (4.2.17)$$

But as it was mentioned above, usually the forces are known and the strains have to be found. For that reason, the  $ABD$  matrix should be inverted in the following way:

$$\begin{aligned} (a) \quad N &= A \cdot \varepsilon^0 + B \cdot \kappa \\ (b) \quad M &= B \cdot \varepsilon^0 + D \cdot \kappa \\ (a) \quad \Rightarrow \varepsilon^0 &= A^{-1} \cdot N - A^{-1} \cdot B \cdot \kappa, \quad (c) \\ (b),(c) \quad \Rightarrow M &= B \cdot A^{-1} \cdot N + (-B \cdot A^{-1} \cdot B + D) \cdot \kappa, \quad (d) \\ (c),(d) \quad \Rightarrow \begin{bmatrix} \varepsilon^0 \\ M \end{bmatrix} &= \begin{bmatrix} A^{-1} & -A^{-1} \cdot B \\ B \cdot A^{-1} & -B \cdot A^{-1} \cdot B + D \end{bmatrix} \cdot \begin{bmatrix} N \\ \kappa \end{bmatrix}, \quad (e) \\ \varepsilon^0 &= A^* \cdot N + B^* \cdot \kappa, \quad A^* = A^{-1}, \quad B^* = -A^{-1} \cdot B, \quad (f) \\ M &= H^* \cdot N + D^* \cdot \kappa, \quad H^* = B \cdot A^{-1}, \quad D^* = -B \cdot A^{-1} \cdot B + D, \quad (g) \\ (g) \quad \Rightarrow \kappa &= D^{*-1} \cdot M - D^{*-1} \cdot H^* \cdot N, \quad (h) \\ (f) \quad \Rightarrow \varepsilon^0 &= A^* \cdot N + B^* \cdot (D^{*-1} \cdot M - D^{*-1} \cdot H^* \cdot N) \Rightarrow \\ \varepsilon^0 &= B^* \cdot D^{*-1} \cdot M + (A^* - B^* \cdot D^{*-1} \cdot H^* \cdot N) \cdot N. \quad (i) \\ (f),(g),(h),(i) \quad \Rightarrow \begin{bmatrix} \varepsilon^0 \\ \kappa \end{bmatrix} &= \begin{bmatrix} A' & B' \\ H' & D' \end{bmatrix} \cdot \begin{bmatrix} N \\ M \end{bmatrix}, \quad (j), \end{aligned}$$

where:

$$A' = A^{-1} - (-A^{-1} \cdot B) \cdot (-B \cdot A^{-1} \cdot B + D)^{-1} \cdot B \cdot A^{-1}$$

$$B' = -A^{-1} \cdot B \cdot (-B \cdot A^{-1} \cdot B + D)^{-1}$$

$$H' = -(-B \cdot A^{-1} \cdot B + D)^{-1} \cdot B \cdot A^{-1},$$

$$D' = (-B \cdot A^{-1} \cdot B + D)^{-1}$$

By using the eq. (4.2.18.j), the strains can be found by directly introducing the applied forces and/or moments at the laminate section as shown in fig.[4-7].

Note(4.2): As it was expected, the matrix  $(B')^T$  is equal to the matrix  $H'$  because the matrix  $A'B'D'$  which is shown in eq. (4.2.18.j) should be symmetric as it was the matrix  $ABD$  at the equation (4.2.17)

## 4.3 Failure Criteria

Up to this point, the structural response of a laminate to a random applied loading condition has been defined. However, it is intuitive that if the loads get higher and higher, there should be a point that the laminate will fail. In case that an isotropic material was under investigation, the definition of the failure criteria would be straightforward. The strengths of the material would be extracted from experiments and then the principal stresses would be calculated for the given loading conditions at every point of the structure. Then, the principal stresses would be compared with the yield strength for ductile materials (if yielding is assumed as a failure) or the corresponding ultimate strength for brittle materials (fracture). On the other hand, the definition of a failure criterion for the case of laminated composites is much more complex. For example, even if we focus on an individual lamina, infinite number of strengths could be derived from an experiment by just changing the orientation of the fibres between each test. For that reason, it is desired to develop a failure criterion or failure theory that can predict the strength of a lamina under any loading condition (either axial or biaxial) where only the strength data from uniaxial tests are available. Below only the failure criteria used in this thesis are presented but readers that are interested to get a more spherical view on this important topic can visit the Ref. [1-2,6-17].

### 4.3.1 Maximum stress criterion

The maximum stress theory is probably the simplest theory which describes the failure of a lamina. It states that failure will be initiated when the stresses in the principal material's axes become equal or exceed the allowable stress of the material at the corresponding direction. To elaborate more, let's assume that a series of experiments is implemented (uniaxial tests) which results to the strength data:  $S_{11T}, S_{11C}, S_{22T}, S_{22C}, S_{12}$ . According to this theory, failure will be initiated when at least one of the following inequalities is satisfied:

$$\begin{aligned}
\sigma_1 &> S_{11T}, & \text{if } \sigma_1 \text{ is tensile} \\
\sigma_1 &< S_{11C}, & \text{if } \sigma_1 \text{ is compressive} \\
\sigma_2 &> S_{22T}, & \text{if } \sigma_2 \text{ is tensile} \\
\sigma_2 &< S_{22C}, & \text{if } \sigma_2 \text{ is compressive} \\
|\tau_{12}| &> S_{12}
\end{aligned} \tag{4.3.1}$$

Hence, for a given loading condition, i.e. with known  $N_x, N_y, N_{xy}, M_x, M_y, M_{xy}$ , the eq. (4.2.18.j) can be used to define  $\varepsilon^0, \kappa$ . Then, the eq. (4.2.8) can be used to define the stresses  $\sigma_x, \sigma_y, \tau_{xy}$  at various points along the height of the laminate. Usually, the stresses are calculated at the centre/midpoint of each ply (because it is simpler) but for better accuracy, especially for thick plies, the stresses can be calculated at both the top and bottom surface of each ply. Then, by using the eq. (4.1.5) the stresses  $\sigma_1, \sigma_2, \tau_{12}$  can be calculated which are compared to the allowable stresses as shown in eq. (4.3.1). If the given loading conditions is given in terms of  $\sigma_x, \sigma_y, \tau_{xy}$  then only the calculation of eq. (4.1.5) is necessary.

### 4.3.2 Puck failure criterion

The maximum stress criterion is maybe the easiest and most intuitive failure criterion, but when it is used to define the failure stress for laminae with fibre orientation different than the direction of the applied loading, discrepancies between experimental results and theory can be found which in some cases can be noticeable<sup>[1-2,6-17]</sup>. Especially, when interaction of stress states are to be accounted for, such as combined loading, i.e. a combination of  $\sigma_x, \sigma_y$  and  $\tau_{xy}$ , even more sophisticated failure criteria such as the Tsai-Hill and Tsai-Wu criteria<sup>[1-2,6-17]</sup> can be questionable and hard to prove<sup>[17]</sup>. For example, the latter criteria are based on ductile material while it is known that failure of composites is governed by brittle fracture in most of the cases<sup>[17]</sup>. Hence, an attempt was made by A. Puck, H. Schürmann<sup>[18]</sup> to combine phenomenological observations with thorough understanding of composite materials during fracture. The core of the theory is the Mohr/Coulomb<sup>[20-21]</sup> failure criterion which is used to define brittle material failures and in Puck's criterion is used for the determination of inter-fibre fracture criterion<sup>[19]</sup>. In Puck's criterion, the interactions curves at complex stress states are replaced by physically based reasoning regarding the way that stresses interact with each other. For example, tensile normal stresses on the failure plane tend to decrease the failure load whereas compressive stresses tend to increase the failure load.

Generally, an analysis of the background of this failure criterion is tedious and further explanation would lead to an extensive scrutiny of composites' mechanics which is not the aim of this supporting document. Of course, readers that are interested to learn more about Puck's criterion are suggested to visit Ref. [17-19, 22-23]. To conclude, a failure is initiated according to Puck's criterion when<sup>[24]</sup>:

$$\text{Fiber Failure: } \frac{\sigma_1}{S_{11T}} > 1 \ (\sigma_1 > 0) \ \text{or} \ \frac{-\sigma_1}{S_{11C}} > 1 \ (\sigma_1 < 0) \tag{4.3.2}$$

It is obvious that for the fibre failure, Puck’s criterion coincides with the maximum stress criterion. By using the classical lamination theory in combination with the Rule of Mixtures, the fibre failure in terms of strains can be defined as<sup>[18]</sup>:

$$\frac{1}{\varepsilon_{11T}} \left( \varepsilon_1 + \frac{\nu_{f12}}{E_{f1}} m_{\sigma f} \sigma_2 \right) > 1 \text{ for } (...) > 0$$

$$\frac{1}{\varepsilon_{11C}} \left( \varepsilon_1 + \frac{\nu_{f12}}{E_{f1}} m_{\sigma f} \sigma_2 \right) < -1 \text{ for } (...) < 0$$
(4.3.3)

where:

- $\nu_{f12}$  = fiber’s Poisson ratio
- $E_{f1}$  = fibers’ modulus of Elasticity
- $m_{\sigma f}$  = factor that accounts for a stress magnification effect,  $m_{\sigma f} = 1.3$ <sup>[18]</sup> for glass fibre

Concerning the matrix failure, Puck’s criterion discriminates three different modes. These modes represent different types of failure for the matrix and the choice of the correct mode depends on the sign of the transverse stress  $\sigma_2$  and the relationship between  $\sigma_2$  and  $\tau_{12}$ . For visual reasons, fig. 4-9 is shown below where the 3D stresses in an composite element are depicted along with the 3 matrix failure modes at fig. 4-10.

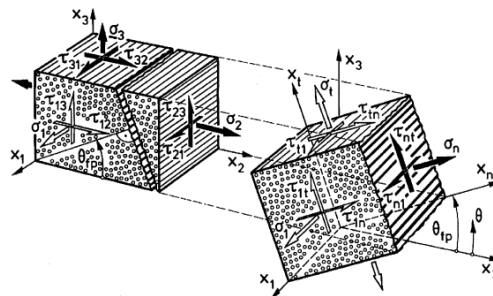


Figure 4-9: Three-dimensional stresses on a UD composite element<sup>[18]</sup>

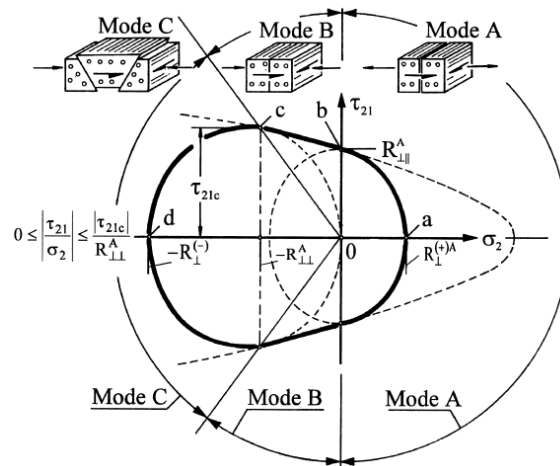


Figure 4-10:  $(\sigma_2, \tau_{21})$  fracture curve for  $\sigma_1 = 0$ , representing three different fracture modes A, B, C<sup>[18]</sup>. The curve is generated by two ellipses and one parabola

In a mathematical form, the 3 modes shown in fig. 4-10 can be expressed as<sup>[24]</sup>:

$$\text{Mode A: } I_{MF,A} = \sqrt{\left(\frac{\tau_{12}}{S_{12}}\right)^2 + \left(1 - p_{6t} \frac{S_{22T}}{S_{12}}\right)^2 \left(\frac{\sigma_2}{S_{22T}}\right)^2} + p_{6t} \frac{\sigma_2}{S_{12}}, \text{ if } \sigma_2 \geq 0 \quad (4.3.4)$$

$$\text{Mode B: } I_{MF,B} = \frac{1}{S_{12}} \left[ \sqrt{\tau_{12}^2 + (p_{6c} \sigma_2)^2} + p_{6c} \sigma_2 \right], \text{ if } \begin{cases} \sigma_2 < 0 \\ \left| \frac{\sigma_2}{\tau_{12}} \right| \leq \frac{F_{2A}}{F_{6A}} \end{cases} \quad (4.3.5)$$

$$\text{Mode C: } I_{MF,C} = \frac{S_{22C}}{\sigma_2} \left[ \left( \frac{\tau_{12}}{2(1 + p_{2c})S_{12}} \right)^2 + \left( \frac{\sigma_2}{S_{22C}} \right)^2 \right], \text{ if } \begin{cases} \sigma_2 < 0 \\ \left| \frac{\sigma_2}{\tau_{12}} \right| \geq \frac{F_{2A}}{F_{6A}} \end{cases} \quad (4.3.6)$$

where:

- $p_{6t}, p_{6c}, p_{2c} = \text{fitting parameters}$
- $F_{2A} = \frac{S_{12}}{2p_{6c}} \left[ \sqrt{1 + 2p_{6c} \frac{S_{22C}}{S_{12}}} - 1 \right]$
- $F_{6A} = S_{12} \sqrt{1 + 2p_{2c}}$
- $p_{2c} = p_{6c} \frac{F_{2A}}{S_{12}}$
- When  $I_{MF,i} = 1$  or higher, it is assumed that the failure has initiated. *MF* stands for Matrix Failure and the subscript “*i*” describes the mode

The values that were used for the fitting parameters  $p_{6t}, p_{6c}, p_{2c}$  were compliant with the recommendation specified in Ref. [23] for the glass fibers, i.e.  $p_{6t} = 0.3$ ,  $p_{6c} = 0.25$ ,  $p_{2c} = 0.2$

To sum up, the maximum stress criterion along with Puck’s criterion were used for the determination of the laminate’s structural response which is presented at chapter 3 of the main body of the thesis. The main reason of introducing such a complex criterion derives from the fact that the laminate is quasi-isotropic [0/45/90/−45] and the loading condition (3 point bending) will lead to a complex stress state due to the *A, B, D* matrices of such a lay-up.

#### Notes:

- There are several failure criteria in the literature but there is no optimal criterion that can fit to all the materials and loading conditions. A study of the optimum failure criterion for the given material and lay-up would require a thesis on its own.

- In the subchapter 4.3.2, Puck's criterion was explained briefly. But as it was mentioned before, the academic background of this criterion is complex and if the reader is interested to become familiar with the criterion in three dimensions instead of only two as it was described above, he is suggested to visit Ref. [17-19, 22-25].

### 4.3.3 Hashin failure criterion

Hashin failure criterion<sup>[31]</sup> is based on Tsai's failure criterion which in turn assumes that the failure of a unidirectional fibre composite has the same mathematical form as the yield criterion of an orthotropic ideally plastic material as given by Hill<sup>[32-33]</sup>. Basically, Hashin developed three dimensional failure criteria of unidirectional fibre composites in terms of quadratic stress polynomials which are expressed in terms of the transversely isotropic invariants of the applied average stress state. Quadratic polynomials are used because they fit better the experimental data when comparing with their linear counterparts. Similarly to the Puck's criterion presented above, Hashin distinguishes 4 different failure modes regarding the tension and compression for both the fibers and the matrix. In a mathematical form, the 3 – D Hashin criteria can be written as:

$$\text{Fiber Tension} \quad \left(\frac{\sigma_1}{S_{11T}}\right)^2 + \left(\frac{\tau_{12}}{S_{12}}\right)^2 + \left(\frac{\tau_{23}}{S_{23}}\right)^2 < 1, \quad \sigma_1 > 0 \quad (4.3.7)$$

$$\text{Fiber Compression} \quad -\frac{\sigma_1}{S_{11C}} < 1, \quad \sigma_1 < 0 \quad (4.3.8)$$

$$\text{Matrix Tension} \quad \left(\frac{\sigma_2}{S_{22T}}\right)^2 + \left(\frac{\tau_{23}}{S_{23}}\right)^2 + \left(\frac{\tau_{12}}{S_{12}}\right)^2 + \left(\frac{\tau_{13}}{S_{13}}\right)^2 < 1, \quad \sigma_2 > 0 \quad (4.3.9)$$

$$\text{Matrix Compression} \quad \left(\frac{\sigma_2}{2 \cdot S_{23}}\right)^2 + \left(\frac{\tau_{23}}{S_{23}}\right)^2 + \left(\frac{\tau_{12}}{S_{12}}\right)^2 + \left[\left(\frac{S_{22C}}{2 \cdot S_{23}}\right) - 1\right] \cdot \frac{\sigma_2}{S_{22C}} < 1, \quad \sigma_2 < 0 \quad (4.3.10)$$

$$\text{Delamination} \quad \left(\frac{\sigma_3}{S_3}\right)^2 + \left(\frac{\tau_{13}}{S_{13}}\right)^2 + \left(\frac{\tau_{23}}{S_{23}}\right)^2 < 1 \quad (4.3.11)$$

The result of the above equations is a piece-wise smooth criterion, i.e. a criterion which is smooth at each one of the failure modes and is being used by many researchers and finite element programs up to date. For example, as it is presented in the next subchapter, for this analysis a progressive damage model is used which is based on the instant ply discount method when a failure mode is initiated. For example, Ansys allows for the introduction of a progressive damage model based on the continuum damage mechanics (CDM) but only if it is assumed that the damage is initiated according to Hashin's criteria for all the damage modes. The CDM is a more sophisticated way to model the progressive damage of fibrous composites but it requires extra tests for the definition of fracture energies and more specifically, the values of  $G_I$  and  $G_{II}$ . Hence, due to the fact that these tests will increase significantly the cost and time of this thesis, these tests were not implemented and as a result, the instant ply discount method is used. Readers that are interested in this more sophisticated criterion are suggested to visit Ref. [24-25].

## 4.4 Progressive damage modelling

By the time that a specific ply fails either according to maximum stress criterion or according to Puck's or Hashin's criterion (subchapter 4.3), it does not mean that the whole structure has failed. Hence, a damage evolution law has to be defined here which determines the effect of a ply's failure. In Ansys v.17.1 there are two ways to model that. The first one is called continuum damage mechanics and it is based on the energy amounts that are dissipated for the various damage modes. However, this method would require specialized tests to define the energy dissipated per unit area from tensile fibre damage, compressive fibre damage as well as tensile matrix damage and compressive matrix damage. On top of that, the viscous damping coefficients for the same failure modes would have to be specified. Hence, the other method which is simpler is used in this thesis and which degrades the stiffness instantly when a failure mode is initiated. In Ansys, the following commands were used:

```
TB,DMGI,i,1,4,FCRT      ! Define damage initiation model, "i" material
TBDATA,1,4,2,3,3        ! Different failure criteria for different damage modes
                        ! Fiber Tension: Hashin criteria
                        ! Fiber Compression: Maximum Stress criterion
                        ! Matrix Tension: Puck's Criterion
                        ! Matrix Compression: Puck's Criterion

TB,DMGE,i,1,4,MPDG     ! Define damage evolution law specifications, last MPDG means
                        ! progressive damage evolution based on simple instant material stiffness
                        ! reduction, "i" material

TBDATA,1,0.93,0.89,0.8,0.6  ! Full loss of stiffness after failure when it is equal to 1
```

For the explanation of these commands the readers are suggested to visit Ref. [25] and the specific values that were introduced at the last TBDATA command are extracted from Ref. [26] and [34]. Lack of values for the damage variables in the literature led to the usage of values as shown in Ref. [34] where it is stated that these values lead to: *"a good agreement between experimental results and numerical predictions"*.

An explanation of what Ansys does internally when the above commands are issued has to be given. According to the theory presented in this chapter 4, Ansys calculates the stresses in the fibers' direction and at their transverse direction. Then, it separates 4 different damage modes and more specifically: fibre tensile damage, fibre compressive damage, matrix tensile damage and matrix compressive damage. For each of these modes and at each substep during the non-linear solution, a specified failure criterion is used to check if the damage is initiated or not for the corresponding modes. The failure criteria can be different for each mode as it is shown in the above commands. Then, when a failure mode is initiated, the ply that has failed replaces its undamaged elasticity matrix with the damaged one as (for general orthotropic material):

$$[Q]_d = \begin{bmatrix} \frac{S_{11}}{1-d_f} & S_{12} & S_{13} & 0 & 0 & 0 \\ S_{21} & \frac{S_{22}}{1-d_m} & S_{23} & 0 & 0 & 0 \\ S_{31} & S_{32} & \frac{S_{33}}{1-d_m} & 0 & 0 & 0 \\ 0 & 0 & 0 & \frac{S_{44}}{1-d_s} & 0 & 0 \\ 0 & 0 & 0 & 0 & \frac{S_{55}}{1-d_s} & 0 \\ 0 & 0 & 0 & 0 & 0 & \frac{S_{66}}{1-d_s} \end{bmatrix}^{-1} \quad (4.4.1)$$

Then, the material can be assumed transversely isotropic when it is looked from a coordination system where the fibres' orientation coincides with the coordination system's axis and I quote from Ref. [27]: *For a transversely isotropic material with plane stress state, primarily adopted for thin fibre-reinforced composite structures, the damaged elastic matrix can be expressed as:*

$$[Q]_d = \frac{1}{A} \begin{bmatrix} (1-d_f)E_f & (1-d_f)(1-d_m)v_{21}E_f & 0 \\ (1-d_f)(1-d_m)v_{21}E_f & (1-d_m)E_m & 0 \\ 0 & 0 & A(1-d_s)G_{fm} \end{bmatrix} \quad (4.4.2)$$

where:

- $A = 1 - v_{12}v_{21}(1-d_f)(1-d_m)$
- $E_f, E_m, G_{fm}$  = undamaged elastic and shear Moduli
- $v_{12}, v_{21}$  = Poisson's Ratios for the undamaged materials

The values of  $d_f, d_m, d_s$  are defined as:

$$d_f = \begin{cases} d_f^+, & \text{if } \lambda_f^+ > 0 \\ d_f^-, & \text{if } \lambda_f^- > 0 \end{cases} \quad (4.4.3)$$

$$d_m = \begin{cases} d_m^+, & \text{if } \lambda_m^+ > 0 \\ d_m^-, & \text{if } \lambda_m^- > 0 \end{cases}$$

$$d_s = (1-d_f^+)(1-d_f^-)(1-d_m^+)(1-d_m^-)$$

where:

- $\lambda_f^+, \lambda_f^-, \lambda_m^+, \lambda_m^-$  fiber tension, fiber compression, matrix tension, matrix compression failure

The above  $\lambda$  values are calculated from the effective Cauchy stress,  $\tilde{\sigma}$  (stress measured in the undamaged domain) as:

$$\tilde{\sigma} = [Q] \cdot \varepsilon \quad (4.4.4)$$

For this thesis, as it is shown above it was assumed that  $d_f^+ = 0.93, d_f^- = 0.86, d_m^+ = 0.8, d_m^- = 0.6$  [34].

An extensive investigation of the progressive damage model is a subject for which many dissertations and PhDs have been written for. It is in the knowledge of the writer that this method is an approximate one and that continuum damage mechanics can lead to improved results but an investigation for the correct variables that are necessary is not possible and for that reason it hasn't been implemented.

Readers that are interested to learn more about the progressive damage model in micro and meso scale are suggested to read Ref. [9,24,26,28-30].

---

## 4.5 References

- [4.1] Robert M. Jones, Mechanics of Composite materials, 1<sup>st</sup> edition, 1975, ISBN: 0-07-032790-4
- [4.2] J.N. Reddy, Mechanics of Laminated Composite plates and shells, Theory and Analysis, 2<sup>nd</sup> Edition, 2004, ISBN 0-8493-1592-1
- [4.3] Basic mechanics of Laminated Composite Plates, A.T. Nettles, NASA Reference publication 1351, 1994
- [4.4] Marco Siegl, Ingo Ehrlich, Transformation of the Mechanical Properties of Fiber-Reinforced Plastic Tubes from the Cartesian Coordinate System into the Cylindrical Coordinate System for the Application of Bending Models, Athens Journal of Technology & Engineering, pp. 47-62, March 2017
- [4.5] Robert C., Jr, Concise Property Transformation Relations for an Anisotropic Lamina, Reuter, J. Composite Materials, April, 1971, pp.270-272
- [4.6] M. Daniel, Ori Ishai, Engineering Mechanics of Composite Materials, Issaac, 1994, ISBN: 0-19-507506-4
- [4.7] Michael W. Hyer, Stress Analysis of Fiber-Reinforced Composite Materials, 1997, ISBN: 0-07-016700-1
- [4.8] F.C. Campell, Structural Composite materials, 2010, ISBN-10: 0-61503-037-9
- [4.9] Valery Vasiliev, Evgeny Morozov, Advanced Mechanics of Composite Materials and Structural Elements, 3<sup>rd</sup> Edition, (2013), ISBN: 978-0-08-098231-1
- [4.10] Bhagwan D. Agarwal, Lawrence J. Broutman, K. Chandrashekhara, Analysis and Performance of Fiber Composites 3<sup>rd</sup> Edition, (2006), ISBN-13: 978-0471268918
- [4.11] Marcal Pedro V., Yamagata Nobuki, Design and Analysis of Reinforced Fiber Composites, (2016), ISBN: 978-3-319-20006-4
- [4.12] Isaac M. Daniel, Ori Ishai, Engineering Mechanics of Composite Materials 2<sup>nd</sup> Edition, (2005), ISBN-13: 978-0195150971
- [4.13] Autar K. Kaw, Mechanics of Composite Materials, 2<sup>nd</sup> Edition, (2006), ISBN-13: 9780849313431
- [4.14] Huang Zheng-Ming, Zhou Ye-Xin, Strength of Fibrous Composites, (2012), ISBN: 978-3-642-22957-2
- [4.15] Vinson Jack R., Sierakowski Robert L., The Behavior of Structures Composed of Composite Materials, 2<sup>nd</sup> Edition, (2008), ISBN: 978-1-4020-0904-4
- [4.16] László P. Kollár, George S. Springer, Mechanics of Composite Structures, (2003), ISBN: 9780511547140
- [4.17] Kassapoglou Christos, Design and Analysis of composite structures with application to aerospace structures, 2010, DOI: 10.1002/9781118536933
- [4.18] A. Puck, H. Schürmann, Failure analysis of frp laminates by means of physically based phenomenological models, Volume 58, Issue 7, July 1998, Pages 1045-1067, PII: S0266-3538(96)00140-6
- [4.19] Alfred Puck, H. Matthias Deuschle, Progress in the Puck Failure Theory for Fibre Reinforced Composites: Analytical solutions for 3D-stress, source: [http://alfredpuck.de/download/Puck-Deuschle\\_Progress\\_in\\_the\\_Puck\\_Failure\\_Theory\\_for\\_Fibre\\_Reinforced\\_Composites-Analytical\\_solutions\\_for\\_3D-stress.pdf](http://alfredpuck.de/download/Puck-Deuschle_Progress_in_the_Puck_Failure_Theory_for_Fibre_Reinforced_Composites-Analytical_solutions_for_3D-stress.pdf) (LV: 10/ 11/ 2017)
- [4.20] Mohr, Welche Umstände bedingen die Elastizitätsgrenze und den Bruch eines Materials, Zeitschrift des VDI, vol.24 no.45&46, pp.1524-1541 & 1572-1577, 1900 [German].

- [4.21] C.A. Coulomb, Sur une Application des Règles de Maximis et Minimis a quelques, Problemes de Statique relatives a l'Architecture, in: Memoires de Mathematique et de Physique: Ann´e 1773, Academie Royal des Sciences par divers Savans, Paris, France, 1776 [French].
- [4.22] A. Puck, H. Schürmann, Failure analysis of FRP laminates by means of physically based phenomenological models, Composites Science and Technology 62 (2002) 1633–1662, PII: S0266-3538(01)00208-1
- [4.23] A. Puck, J. Kopp, M. Knops, Guidelines for the determination of the parameters in Puck's action plane strength criterion, Composites Science and Technology 62 (2002) 371–378, PII: S0266-3538(01)00202-0
- [4.24] Ever J. Barbero, finite element analysis of composite materials using Ansys®, 2nd Edition, (2014), ISBN-13: 978-1-4665-1690-8
- [4.25] Ansys Mechanical User's Guide, help manual v.17.1
- [4.26] Piotr Baszczynski, Sebastian Dziomdziora, Rafał Naze, Tomasz Kubiak, Numerical Model of CAI Test for Fibre–Reinforced Polymer Plate, (2016)
- [4.27] Shared Hierarchical Academic Research Computing Network, Ansys help, TB command, source: [https://www.sharcnet.ca/Software/Ansys/16.2.3/en-us/help/ans\\_cmd/Hlp\\_C\\_TB.html#TBdmge](https://www.sharcnet.ca/Software/Ansys/16.2.3/en-us/help/ans_cmd/Hlp_C_TB.html#TBdmge) (LV: 10/ 11/ 2017)
- [4.28] Ever J. Barbero, Mehdi Shahbazi, Determination of material properties for ANSYS progressive damage analysis of laminated composites, Composite Structures 176 (2017) 768–779
- [4.29] Theodore P Philippidis, Alexandros E Antoniou, A progressive damage FEA model for glass/epoxy shell structures, Journal of Composite Materials 47(5) 623–637,(2012), DOI: 10.1177/0021998312473678
- [4.30] R. Talreja and J. Varna, Modeling Damage, Fatigue and Failure of Composite Materials, Chapter 14, 2016, ISBN: 978-1-78242-286-0
- [4.31] Z. Hashin, Failure criteria for Unidirectional Composites, ASME Journal of Applied Mechanics, Vol. 47 (2), 1980, pp. 329-334
- [4.32] Tsai, S. W., "Strength Characteristics of Composite Materials," NASA, CR-224,1965
- [4.33] Hill, R., "A Theory of the Yielding and Plastic Flow of Anisotropic Materials," Proceedings of the Royal Society, Series A, Vol. 193, 1948, p. 281.
- [4.34] T. E. Tay, G. Liu, V. B. C. Tan, X. S. Sun and D. C. Pham, Progressive Failure Analysis of Composites, Journal of composite materials, Vol. 42, No. 18/2008, DOI: 10.1177/0021998308093912

